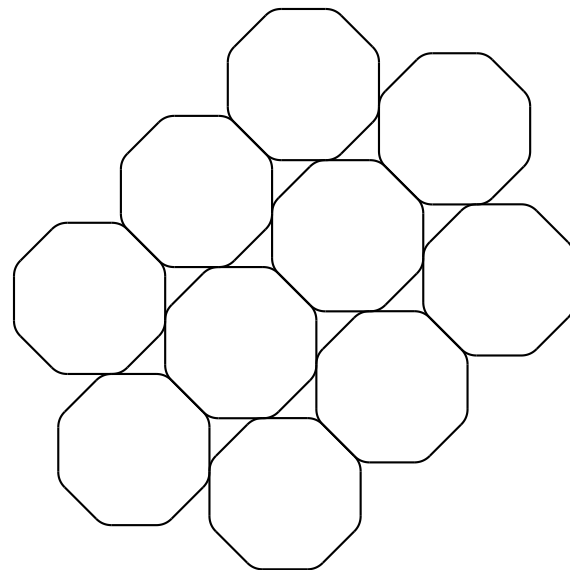


Packings of Smoothed Polygons

Thomas Hales and Koundinya Vajjha



Abstract

This book uses optimal control theory to prove that the most ununpackable centrally symmetric convex disk in the plane is a smoothed polygon. A smoothed polygon is a polygon whose corners have been rounded in a special way by arcs of hyperbolas. To be highly ununpackable means that even densest packing of that disk has low density.

Motivated by Minkowski’s geometry of numbers, which investigates lattice packings of convex bodies, researchers (notably Blaschke and Courant) began to search for the most ununpackable centrally symmetric convex disk (in brief, *the most ununpackable disk*) starting in the early 1920s. In 1934, Reinhardt conjectured that the most ununpackable disk is a smoothed octagon. Working independently of Reinhardt, but also motivated by Minkowski’s geometry of numbers, Mahler attempted without success in 1946 to prove that the most ununpackable disk must be a smoothed polygon. This book proves what Mahler set out to prove: *Mahler’s First conjecture* on smoothed polygons. His second conjecture is identical to the Reinhardt conjecture, which remains open.

This book explores the many remarkable structures of this packing problem, formulated as a problem in optimal control theory on a Lie group, with connections to hyperbolic geometry and Hamiltonian mechanics. Bang-bang Pontryagin extremals to the optimal control problem are smoothed polygons. Extreme difficulties arise in the proof because of chattering behavior in the optimal control problem, corresponding to possible smoothed “polygons with infinitely many sides” that need to be ruled out. To analyze and eliminate the possibility of chattering solutions, the book introduces a discrete dynamical system (the Poincaré first recurrence map) and gives a full description of its fixed points, stable and unstable manifolds, and basin of attraction on a blowup centered at a singular set. Some proofs in this book are computer-assisted using a computer algebra system.

Contents

I Preliminaries	11
1 Introduction	13
1.1 Karl Reinhardt's Problem	14
1.2 History of the Reinhardt Problem	16
1.3 Book Summary	17
2 Historical Results	27
2.1 A Statement of the Reinhardt Conjecture	27
2.2 Reinhardt's Approach	30
2.3 Mahler's Approach	37
2.4 Boundary Parameterization of Minimizer	40
2.4.1 Regularity Properties of Multi-Curves	41
2.4.2 Convexity of Multi-Curves	44
2.4.3 A Characterization of Balanced Disks	45
II Optimal Control	47
3 A Control Problem	49
3.1 State Dynamics in the Lie Group	49
3.2 The Cost Functional	55
3.3 Control Sets	57
3.4 Lie Algebra Dynamics	60
3.5 Initial and Terminal Conditions	62
3.6 Reinhardt Optimal Control Problem	62
4 The Upper Half-Plane	65
4.1 The Adjoint Orbit	65

4.2	Transfer of Dynamics to the Upper Half-Plane	66
4.3	The Cost Functional in Half-Plane Coordinates	68
4.4	The Star Domain in the Upper Half-Plane	69
4.5	Control Problem in the Half-Plane	70
4.6	Dihedral Symmetry	72
5	Compactification of the Star Domain	77
6	Hamiltonian and Maximum Principle	89
6.1	Existence of Optimal Control	89
6.2	The Pontryagin Maximum Principle	91
6.3	Left-invariance	94
6.4	Hamiltonian in the Lie Algebra	94
6.5	Costate Variables in Lie Algebra	96
6.6	Transversality Conditions	99
6.7	Summary of State and Costate Equations	100
6.8	Hamiltonian and Costate Equations in the Upper-half plane .	101
III	Solutions	103
7	Bang Bang Solutions	105
7.1	Solutions for Constant Control	105
7.2	Constant Control at the Vertices	108
7.3	Partition of the Cotangent Space	110
7.4	Constant Control Splines	111
7.5	Smoothed Polygons	113
7.6	Supplementary Remarks on Smoothed Polygons	120
7.7	Smoothed Octagon is an Isolated Extremal	121
8	Singular Locus	125
8.1	Edges of the Control Simplex	125
8.2	Singular Locus and Singular Subarcs	131
8.3	Non-chattering away from the Singular Locus	137
IV	Circular Control	141
9	Circular Control Set	143

9.1	Conserved Quantity for the Circular Control Set	145
9.2	Control Sets in the Special Unitary Group	148
9.3	Quadratic Equation for Optimal Control	150
10	Hyperboloid Coordinates	155
10.1	Coordinates	155
10.2	Hyperboloid ODE	157
10.3	Optimal Control	159
10.4	Application to Abnormal Solutions	161
11	The Fuller System	165
11.1	Trajectories near the Singular Locus	166
11.2	Hamiltonian Dynamics of the Truncated System	169
11.3	Log-Spiral Solutions	173
11.4	Literature on Fuller Systems	174
12	Global Dynamics of Fuller System	177
12.1	A Fiber Bundle	177
12.2	A Vector Field on the Base Space	181
12.3	Equilibrium Points	182
12.4	Global Behavior	183
12.5	A Special Trajectory	187
12.6	Proof	189
V	A Proof of Mahler's First Conjecture	191
13	Fuller System for Triangular Control	193
13.1	Introduction	193
13.2	Fuller system for Triangular Control	194
13.2.1	Hamiltonian	195
13.2.2	Switching Function	195
13.2.3	Symmetry	196
13.2.4	Walls	198
13.2.5	Switching Times	198
13.3	Singular Locus	200
13.4	Blowing up Fuller	202
13.5	Dynamical System and Equilibrium Points	203

14 Stable and Unstable Manifolds at Fixed Points	207
14.1 Lie Algebra Coordinates	207
14.2 Asymptotics	210
14.3 Analytic Extension of the Reinhardt system	213
14.4 A Computation of the Unstable Manifold	215
15 Geometry of the Fuller-Poincaré Map	219
15.1 Three-Cells	219
15.2 Smaller cells	222
15.3 Involution	224
16 Global Basin of Attraction and Mahler's First	229
16.1 Main result on Basin of Attraction	229
16.2 Classification of Outward Fuller Trajectories	233
16.3 Mahler's First: Bang-bang with Finitely Many Switches	235
16.4 Cluster Point Theorem	236
16.4.1 Coordinates	237
16.4.2 Reinhardt Switching functions as cubic polynomials . .	237
16.4.3 Proof	239
VI Appendices	241
A Background Material	243
A.1 Gronwall inequality	243
A.2 Functional derivative	244
A.3 Stable and Unstable Manifolds	244
A.4 Classical Lie Groups and Lie Algebras	245
A.5 Exceptional Isomorphisms in Rank One	246
A.6 Matrix Identities	247
A.7 Symplectic Geometry	248
A.8 Lie-Poisson Dynamics on the Lie Algebra	249
A.9 Poisson Reduction of the Extended State Space	251
A.10 Symplectic Structure of Coadjoint Orbits	252
A.11 Riemannian Metric on Coadjoint Orbits	253

B Extensions of the Theory	255
B.1 Hypotrochoids	255
B.2 Chaos in Numerical Experiments	257
B.3 Kuperberg's Area Formula	258
B.4 Research Problems	259

Part I

Preliminaries

Chapter 1

Introduction

This book shows how the still-unsolved Reinhardt conjecture in discrete geometry can be formulated as a problem in optimal control theory. A proof of Mahler’s First conjecture is presented, which is a weak form of the Reinhardt conjecture, asserting that the most unpackable centrally symmetric convex disk is a smoothed polygon.

Discrete geometers are interested in the class of problems which minimize or maximize the *packing density* $\delta(K, \mathcal{P})$ of a *convex body* $K \subset \mathbb{R}^n$; that is, a convex compact set with nonempty interior.¹ A convex body in \mathbb{R}^2 is called a *convex disk*. The packing density is roughly the fraction of space taken up by non-overlapping congruent copies of a convex body K when they are arranged according to the packing \mathcal{P} in Euclidean space \mathbb{R}^n . Since $\delta(K, \mathcal{P})$ is function of two variables, different flavors of this question may be posed: we may restrict the classes of convex bodies K under consideration, or we may restrict the type of packings \mathcal{P} .

For example, the *sphere packing problem* fixes the convex body K to be B^n (the unit ball in \mathbb{R}^n) and asks us to determine $\delta(K) := \sup_{\mathcal{P}} \delta(B^n, \mathcal{P})$, where the supremum ranges over all possible packings \mathcal{P} . Determining $\delta(K)$ for an arbitrary convex body K is an extremely hard optimization problem in general, even in low dimensions. In three dimensions, the sphere packing problem is the Kepler conjecture, which was asserted over 400 years ago, but not solved until 1998 [14]. In 2022, Maryna Viazovska received a Fields medal for the solution of the sphere packing problem in eight dimensions [6].

¹This and other terms are defined at the beginning of Chapter 2.

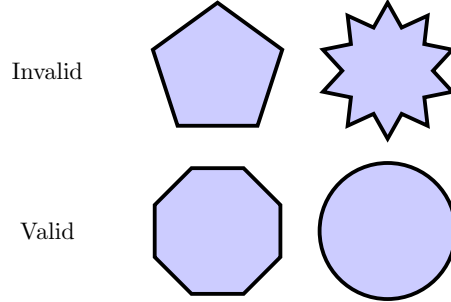


Figure 1.0.1: Valid and Invalid Convex Centrally Symmetric Disks.

1.1 Karl Reinhardt's Problem

Let \mathfrak{K} be the set of convex disks in the plane, and let $\mathfrak{K}_{ccs} \subset \mathfrak{K}$ be the set of centrally symmetric convex disks in the plane \mathbb{R}^2 . Examples of compact sets belonging to (and not belonging to) \mathfrak{K}_{ccs} are shown in Figure 1.0.1. The Reinhardt problem is to determine the infimum

$$\inf_{K \in \mathfrak{K}_{ccs}} \delta(K) = \inf_{K \in \mathfrak{K}_{ccs}} \sup_{\mathcal{P}} \delta(K, \mathcal{P})$$

and also that centrally symmetric convex disk which whose greatest packing density achieves this minimum. The Reinhardt problem is structured as a minimax problem: finding the infimum of a supremum (or to find that disk whose *greatest* packing density is the *least*). In our situation, a centrally symmetric convex disk achieving this minimum exists. We will see below that an affine transformation does not change the greatest packing density of a centrally symmetric convex disk. The minimizer is conjectured to be unique up to affine transformation.

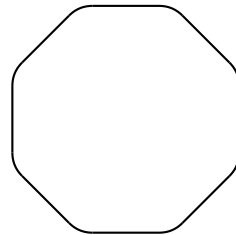


Figure 1.1.1: The Smoothed Octagon.

Although a plausible first guess for the minimizer is the circular disk in the plane, it turns out that there is a candidate which is slightly worse. (We say that one convex disk is *worse* than another if its greatest packing density is smaller. To be worse is to be less *packable* and more *unpackable*.) In 1934, Reinhardt conjectured that the minimum is achieved by the so-called *smoothed octagon* pictured in Figure 1.1.1 [40]. Independently, Kurt Mahler arrived at the same conjecture in 1947 [29].

Conjecture (Reinhardt [40], Mahler [29]). *The smoothed octagon achieves the least greatest packing density among all other centrally symmetric convex disks in the plane. Its density is given by*

$$\inf_{K \in \mathcal{K}_{ccs}} \delta(K) = \frac{8 - \sqrt{32 - \ln 2}}{\sqrt{8 - 1}} \approx 0.902414. \quad (1.1.1)$$

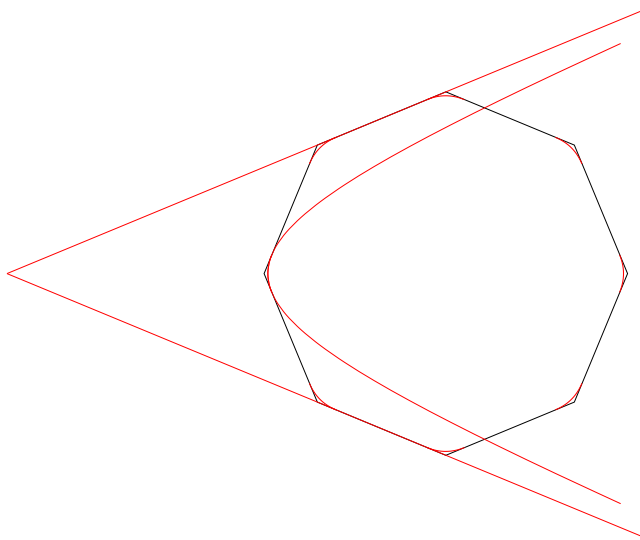


Figure 1.1.2: Construction of the Smoothed Octagon starting from a regular octagon. The hyperbolic arcs clipping each vertex are shown in red.

The smoothed octagon is constructed by clipping the vertices of a regular octagon by hyperbolic arcs which are tangent to the two edges at the vertex, and whose asymptotes pass through two further edges of the octagon, as shown in Figure 1.1.2. The density formula appears in Fejes Tóth [47, p.106]. A calculation of the density formula appears in an example before Theorem 7.5.6.

1.2 History of the Reinhardt Problem

The earliest mention of the Reinhardt problem is as Problem 17 in §27 of a 1923 book by Wilhelm Blaschke, where it is called *Courant's conjecture* [4], stating that the worst of all centrally symmetric convex disks is the circular disk (whose greatest packing density in the plane is $\pi/\sqrt{12}$).

Less than a decade later, Richard Courant's conjecture was shown to be false by Reinhardt in his 1934 article, by his construction of the smoothed octagon. In his article, Reinhardt also proved fundamental results on the existence, structure, and regularity of a minimizer. The title and motivation for Reinhardt's article came from Minkowski's work from 1904 on the lattice packings of convex bodies [32]. Reinhardt wrote,

“Bei unseren Bereichen kommt diejenige Figure in Betracht, welche aus einem regelmäßigen Achteck entsteht, wenn man jede Ecke durch diejenigen Hyperbel abschneidet, die die beiden austostenden Seiten berührt, und die beiden wieder an diese grenzenden Seiten zu Asymptoten hat” [40, p. 230].

Among our regions, that figure comes into consideration which arises from a regular octagon, if one cuts off each corner with that hyperbola which is tangent to the two outgoing sides, and again has the two sides bordering on these as asymptotes. (Compare Figure 1.1.2.)

More than a decade later, Kurt Mahler was also led to the smoothed octagon in a series of articles in 1946–47. Mahler's first article used the calculus of variations to refute Courant's conjecture by proving the existence of a convex disk whose packing density was worse than the circular disk [29]. In this paper, Mahler formulates the packing problem, considers a parameterized family of convex domains adapted to this problem, and writes down necessary conditions these domains should satisfy. Making the assumption that the boundary is sufficiently smooth, and by disregarding the convexity constraint, he shows that the only solution to the Euler-Lagrange equation is a circle, up to affine transformation. He then takes a second variation of the circle to show that it is not second-order optimal. In this way, he learns that the convexity condition cannot be disregarded. Our treatment of the circle is similar to his [15, §5.1, §5.2]. Like Mahler, we use parameterizations in $SL_2(\mathbb{R})$.

In the same article, Mahler makes the final remark:

It seems highly probable from the convexity condition, that the boundary of an extreme convex domain consists of line segments and arcs of hyperbolae. So far, however, I have not succeeded in proving this assertion.

We refer to this final remark as *Mahler's First conjecture*: the most unpackable centrally symmetric convex disk is a smoothed polygon.

In a follow-up article, Mahler gives an explicit construction of the smoothed octagon [28]. The term *smoothed octagon* appears explicitly in a later article by Mahler and Ledermann in 1949 [25]. Although we may tend to cite Mahler more frequently than Reinhardt, and although they worked from different perspectives, we wish to make it clear that priority for many early results belongs to Reinhardt.

Further progress was achieved by V. Ennola in 1961 and Paul Tammela in 1969 where they showed that $\inf_{K \in \mathcal{K}_{\text{ccs}}} \delta(K) \geq 0.8926\dots$ [9] [44]. Fedor Nazarov proved that the smoothed octagon is a local minimum in the space of convex disks equipped with the Hausdorff metric [36]. Discussions of the Reinhardt conjecture appear in the books by János Pach and Pankaj Agarwal and by L. Fejes Tóth [38] [46]. Hales's earlier work treats the Reinhardt problem as a problem in the calculus of variations [15].

As of 2024, the full Reinhardt conjecture is still beyond our immediate reach, having remained open since 1934. However, we firmly believe that optimal control theory is the proper framework for the study of this conjecture. This book uses optimal control theory to give a proof of Mahler's First conjecture.

1.3 Book Summary

This book is an extension of a 2017 preprint of Hales in which the Reinhardt problem is reduced to an optimal control problem on the tangent bundle of the Lie group $\text{SL}_2(\mathbb{R})$ [16]. The book also grows out of the 2022 PhD thesis of Vajjha, which considerably extends the theoretical framework [48]. We include all the results from that preprint and thesis, and we carry the program much further still.

As we show, the Reinhardt optimal control problem has a remarkable amount of structure with deep connections with hyperbolic geometry, Hamiltonian mechanics and the theory of chattering control. It is our belief that the

Reinhardt conjecture has now been transformed from an impossible problem to a difficult, but approachable one.

In Part I of the book, we recall Reinhardt's and Mahler's results, which will be essential for the construction of our control problem. In the formulation of the control problem, properties proved by Reinhardt himself in 1934 play an essential role. As an example, Reinhardt proved that the boundary of the minimizer is described by six points moving to generate six curves, which close up seamlessly into a single simple closed curve. The origin and any three of these consecutive points form a parallelogram whose area remains fixed as the three points move around the boundary. This is shown in Figure 1.3.1. The six curves (with centrally symmetric pairs colored similarly) form a *multi-curve*, in a sense made precise in Definition 2.4.1.

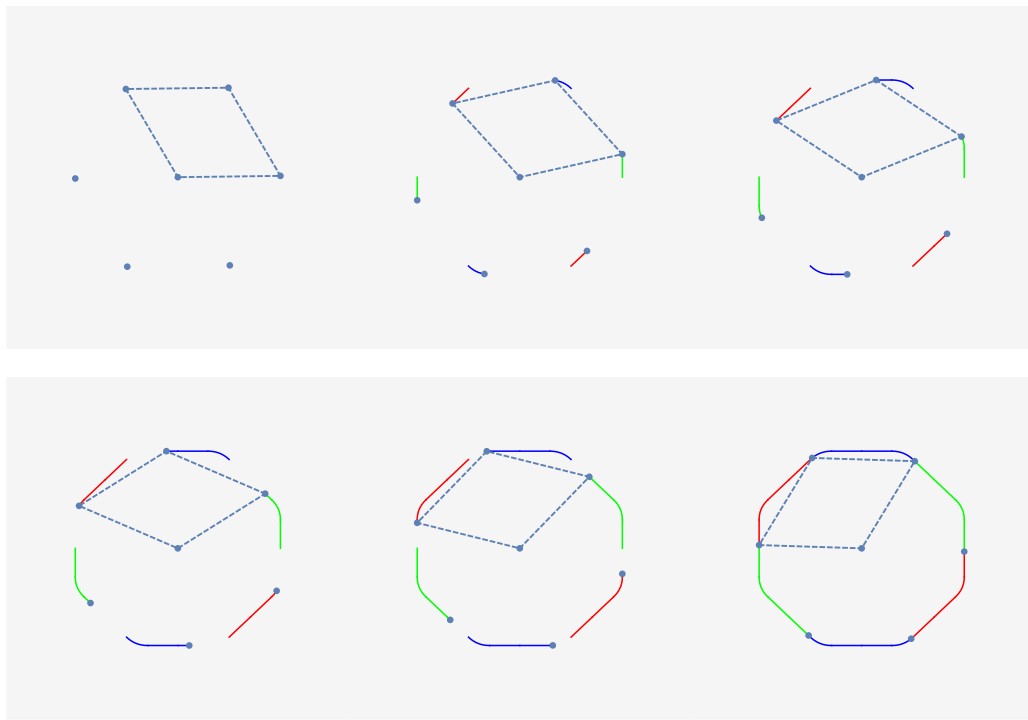


Figure 1.3.1: Multi-curves generating the smoothed octagon. The parallelograms all have the same area.

The points move along the boundary curves in a way that yields the convexity of the enclosed disk. Convexity is imposed *locally* via a local

curvature nonnegativity condition and *globally* via conditions on the tangents to the six curves. The curvatures of these curves play a role in determining the packing density of the resultant disk in the plane. The control problem reformulation takes all these conditions into account.

A noteworthy feature of our control problem is that the set of controls is the standard two-simplex in \mathbb{R}^3 . Each point in the control set can be viewed as a normalized ordered triple of curvatures, which are used to specify the planar curvatures of the six curves describing the boundary of a minimizer K . The bounding edges of the two-simplex constrain the planar curvatures to be nonnegative, enforcing the convexity of K . We prove an analogue of the Frenet-Serret formulas, showing that the six curves are determined from the curvature control function, by solving a second order ordinary differential equation with initial values. These differential equations appear in what we call the *state equations* of the Reinhardt control problem (equations (3.6.1) and (3.6.2) in problem 3.6.2).

The six curves describing the boundary of a minimizer K can be generated in a uniform way from a single curve, taking values in the Lie group $SL_2(\mathbb{R})$ of 2×2 matrices with real entries and determinant one. The control problem will occur naturally on a manifold that is closely related to this Lie group (its tangent bundle).

Symmetry is visible throughout this book and plays an important role. The control problem alluded to above is a left-invariant control problem on a Lie group, and it is well known that such problems admit a reduction in dynamics to coadjoint orbits in the corresponding Lie algebra [19]. The Poincaré upper-half plane (a well-known model of hyperbolic geometry) and its invariant metric also appear in a natural way – being symplectomorphic to this coadjoint orbit. Lemma 7.1.2 shows that many important trajectories of the control problem have constant speed with respect to the Riemannian metric on the upper-half plane.

Another prominent symmetry is the discrete dihedral symmetry of the equilateral triangle (expanded on in Section 4.6) arising from the standard two-simplex, which is our control set. Using the isomorphism between $SL_2(\mathbb{R})$ and the special unitary group $SU(1, 1)$, we transfer the dynamics to the hyperboloid model of the hyperbolic plane. In the hyperboloid model, the symmetries take a particularly nice form.

Part II of this book explores the *Reinhardt optimal control problem* 3.6.2, and highlights its remarkable structure and these connections with hyperbolic geometry and Hamiltonian mechanics.

The state space of the control problem is unbounded. In Chapter 5, the state space is compactified by cutting down the region of interest to a compact set containing the global minimizer K . This compactification is achieved by giving a geometric interpretation to trajectories that stray outside the compact set. In a sense that we make precise, such trajectories correspond to convex disks that are approximately parallelograms. Any such approximate parallelogram yields a packing in the plane with high density. In particular, it cannot have the worst greatest packing density, and thus it can be ruled out. Our motivation for compactifying the state space has been to make the Reinhardt control problem more amenable to numerical computer experiments and possibly also more amenable to computer-assisted proof.

First order necessary conditions for optimality of an optimal control problem are given by the Pontryagin Maximum Principle (PMP) which states that the optimal trajectory is given by a projection of the lifted controlled trajectory (living in the cotangent bundle of the underlying manifold) [49]. This means that our control problem is a *higher-order* variational problem since it involves the cotangent bundle of the tangent bundle of a Lie group [7]. The lifted controlled trajectory is the Hamiltonian flow of the *maximized Hamiltonian*, which is the pointwise maximum of a control-dependent Hamiltonian function on the control set.

A control function is said to be *bang-bang* if its range is contained in the set of extreme points of the control set, with discontinuous switching. In our setting, the extreme points of the control set are the vertices of the two-simplex. Critical points of control problems are frequently given by bang-bang controls. The smoothed octagon is an example of an explicit solution to the Reinhardt optimal control problem with bang-bang control. In earlier research, we viewed the Reinhardt conjecture as a problem in the calculus of variations [15]. However, one of our primary reasons to reformulate the conjecture as a problem in optimal control theory is the bang-bang behavior of the smoothed octagon. This behavior can be seen geometrically in the way its boundary switches suddenly between linear segments and segments that are as curved as possible at the rounded corners. This insight explains its shape. Lemma 3.1.8 shows that the rounded corners of the smoothed octagon are indeed as highly curved as possible, subject to the constraints of the problem.

In Part III, we construct explicit solutions to the Reinhardt optimal control problem 3.6.2. A bang-bang control function with finitely many switches always produces a smoothed polygon, and a smoothed polygon with the

corner-rounding of sort considered by Reinhardt and Mahler has a bang-bang control function with finitely many switches. In particular, in Section 7.5, the smoothed octagon is shown to be a critical point of the optimization problem (a Pontryagin extremal) given by a bang-bang control. More generally, for each $k = 1, 2, \dots$, Theorem 7.5.6 constructs a smoothed $6k + 2$ -gon that is a Pontryagin extremal of the Reinhardt optimal control problem. The associated control is bang-bang. As k tends to infinity, the smoothed $6k + 2$ -gon converges to the circle, which is also a Pontryagin extremal, but its control function is not bang-bang. Among this explicit list of extremals, the smoothed octagon has the worst greatest packing density.

If we examine the initial and terminal conditions of the optimal control problem, we find that the boundary conditions are periodic modulo a rotation by angle $\pi/3$. We can use the rotational symmetry of the boundary conditions to extend every extremal trajectory to a periodic orbit with a discrete rotational symmetry. In this way, the global minimizer of the Reinhardt control problem can be viewed as a periodic orbit of the dynamical system. Because of this, the research focus should be on the periodic Pontryagin extremals. For example, if we could classify the periodic extremals, then the global minimizer could be picked out from among them.

No other extremals have been found, but we have no proof that no other extremals exist. In light of our results, a proof that no other extremals exist would complete a proof of the Reinhardt conjecture. However, we do not hazard a guess about whether other extremals might exist.

Singular arcs in optimal control problems arise when the maximization condition in the Pontryagin maximum principle fails to determine a unique control over an interval of time. In such a case, a face of the control two-simplex can be found such that the entire face satisfies the maximization condition (by Lemma 7.3.1). When that face is an edge of the two-simplex, an anomalous situation occurs. Abnormal Pontryagin extremals exist, but those abnormal extremals are obviously spurious solutions. In this case, we modify the control problem slightly to form what we call the *edge control problem*. In the modified control problem, the spurious extremals disappear, and every Pontryagin extremal of the edge control problem has a bang-bang control with finitely many switches. This is Theorem 8.1.4.

As we have just mentioned, associated to each singular arc is a maximizing face of the control two-simplex. That face can be the entire control simplex. In this case, Theorem 8.2.6 gives a characterization of singular extremals. The result states that up to an affine transformation, the arc of a circle (generating

the circular disk K in the plane) is the unique such singular extremal of the Reinhardt optimal control problem. Although the arc of a circle is an extremal in the sense of Pontryagin, it does not satisfy the necessary second order conditions to be a global minimizer. Theorem 8.2.7 proves that the global minimizer contains no singular arcs.

The region of state space where singular behavior might appear is called the *singular locus*. As mentioned, the global minimizer does not remain in the singular locus during any positive time interval. Nevertheless, it is possible for trajectories to approach the singular locus, without remaining in the locus during a positive time interval. Extremals that completely avoid the singular locus have a simple form, as follows.

Theorem (8.3.2). *Every Pontryagin extremal of the Reinhardt control problem which does not meet the singular locus is given by a bang-bang control function with finitely many switches.*

In terms of the centrally symmetric convex domain K , this theorem implies that any such extremal is a smoothed polygon whose corners are rounded by hyperbolic arcs, according to Reinhardt's corner-smoothing procedure. Thus, if the global minimizer avoids the singular locus, then the global minimizer is a smoothed polygon. We eventually show that the global minimizer does indeed avoid the singular locus, and this yields a proof of Mahler's First conjecture, which is the main result of the book.

Theorem (Mahler's First 16.3.1). *The global minimizer of the Reinhardt optimal control problem is a bang-bang solution with finitely many switches. In particular, the minimizer K_{\min} of the Reinhardt problem is a finite-sided smoothed polygon with rounded hyperbolic arcs at each corner of the sort described by Reinhardt and Mahler.*

One of the most intriguing aspects of the Reinhardt problem is the behavior of trajectories near the singular locus. The only way for a Pontryagin extremal to approach the singular locus is through *chattering*, which is the term used to denote the phenomenon when the control function performs discontinuous and increasingly rapid transitions between extreme points of the control set in order to approach the singularity [50]. They were first studied in a problem of A. T. Fuller in 1963 [11] and were considered pathological for a time, but were eventually proven to be *ubiquitous* in a very precise sense by Ivan A. Kupka in the 1990s [24]. One of the main results of this book is the recovery

of the Fuller optimal control system in a neighborhood of the singular locus. To explain this precisely, we first discuss *circular control* sets.

An important strategy for us is to change the shape of the control set from the two-simplex to a circular disk. Part IV of this book is devoted to the study of the control problem for a circular control set. By changing the control set, the control problem changes, and we are no longer studying the Reinhardt problem in discrete geometry. However, there are good reasons to investigate the optimal control problem with a circular control set.

There are a few different ways to imagine the relationship between the original Reinhardt problem and the modified control problem with circular control. First, if we take the circular control set to be the circumscribing circle of the triangular control, then the modified optimal control problem is a *relaxation* of the original Reinhardt optimal control problem. This means that a lower bound on the cost in the modified problem should be a lower bound on the cost of the original problem.²

Second, the triangular control is a discretization of the circular control. We know that the optimal control function for trajectories that avoid the singular locus takes values in the set of extreme points of the control set. For circular control, each point on the circle is an extreme point, and the control function is continuous. For triangular control, the control function is discontinuous, taking values at the vertices of the two-simplex. Hence, the Reinhardt problem can be viewed as a three-point discretization of the continuous control.

Third, we can view the triangle as a continuous deformation of the circle. We can study the properties of the dynamical system for the circular control set. We can ask to what extent these properties are preserved as the circular control is deformed back into a triangular control set.

Finally, the triangular control is a symmetry breaking of the circular control problem. All data used to specify the Reinhardt control problem have a rotational symmetry except for the control set. The modification of the control set to make it circular allows us to construct a conserved quantity. This we do by appealing to a control-theoretic version of the classical Noether theorem, proved by Hector Sussmann [43].

²We do not claim this relaxation result as a theorem because of technicalities related to the fact that we have not extended the compactification result of Chapter 5 to the relaxed problem. The issue is that the relaxed problem is defined on a *smaller domain* than the original problem, and a global minimizer of a relaxed problem on the smaller domain is not *a priori* a lower bound to the unrelaxed problem on the full domain.

Theorem (9.1.6). *In the control problem with the circular disk control set, each Pontryagin extremal satisfies a conservation law (which we call the angular momentum).*

The symmetry is broken by the triangular control set, where the angular momentum is approximately but not exactly preserved. The circular control problem with its extra symmetry is a toy model for the original Reinhardt problem. We study the modified problem in the hope that it will lead to useful insights into the Reinhardt conjecture.

With this background about circular control sets, we return to examine the trajectories near the singular locus in greater detail. The conservation of angular momentum gives us valuable information about the optimal control.

Using this conservation law, we perform a truncation of the Pontryagin control system by estimating the magnitude of terms in the system of equations and then discarding all higher-order terms. We make the remarkable discovery that the truncation of our optimal control problem is precisely the Fuller optimal control problem for a chain of odd length. We find inward and outward logarithmic spiral solutions to the Fuller system, centered at the singular locus. (In a similar fashion, we construct triangular inward and outward spirals, when the control set is the two-simplex.)

We make a complete analysis of the global dynamics of this Fuller system. The dynamical system maps onto a simpler dynamical system in the plane. In the planar system, there are only two critical points. One is asymptotically stable and the other is unstable. Every point in the plane, except for the unstable equilibrium point, is in the basin of attraction of the stable critical point. Going from the planar system back to the full Fuller system, we find that the only trajectory that converges to the singular locus is an inward logarithmic spiral centered at the singular locus. The only trajectory that escapes from the singular locus is an outward spiral, which is unique up to rotational symmetry. The inward spiral is unstable, and the outward spiral is stable, so that a trajectory that is not exactly an inward spiral must necessarily swerve away from the singular locus, then reapproach an outward spiral.

We plot some solutions numerically and observe that the solutions appear to behave chaotically. We conjecture that for certain parameter values, the trajectories are indeed chaotic. For this and other research problems, we refer the reader to Appendix B.4.

In Part V, we return to the Reinhardt problem with triangular control set.

Several further ideas are introduced to give a proof of Mahler’s conjecture. Blowing up at the singular locus (in the sense of algebraic geometry) creates an exceptional divisor, which becomes the focus of attention. We make a detailed study of the Fuller system with a triangular control set on the exceptional divisor. By restricting the dynamical system to switching times, the Fuller system becomes a discrete dynamical system whose dynamics are given by a Poincaré first recurrence map.

We find that the discrete dynamical system has several features that are remarkably similar to features that were found in the toy system with circular control. There are exactly two fixed points. One is stable and the other is unstable. The two fixed points are related by a time-reversing symmetry. The stable fixed point has a global basin of attraction. The fixed points can be interpreted as self-similar spirals in a larger dynamical system that does not factor out by symmetries.

To prove that the stable fixed point has a global basin of attraction we introduce an explicit geometric partition of the exceptional divisor into finitely many compact pieces. On each piece, the discrete dynamical system is continuous. The dynamical system acquires a block upper triangular form with respect to the geometric partition. The strictly upper triangular blocks represent transient behavior of the dynamical system, and the diagonal terms are localized around the stable and unstable fixed points. In this way, the claim of global stability can be reduced to a statement about local stability. From a slightly different perspective, the upper triangular structure can be interpreted as a discrete Lyapunov function with respect to the geometric partition.

The stable and unstable fixed points for the discrete Fuller dynamical system are hyperbolic fixed points for the discrete Reinhardt dynamical system. On the blowup, the discrete Reinhardt dynamical system extends by analytic continuation to a neighborhood of the hyperbolic fixed points. We study the local stable and unstable manifolds near the fixed points. The global stability result (for the discrete Fuller system) is used to show that a chattering solution to the Reinhardt dynamical system must approach and depart the blown up singular locus through the stable and unstable manifolds of the hyperbolic fixed points. Explicit calculations show that trajectories on these stable and unstable manifolds cannot be periodic. However, the solution to the Reinhardt problem is necessarily periodic. We conclude that the solution to the Reinhardt problem is not a chattering solution and does not meet the singular locus. From this conclusion, it follows that the solution

to the Reinhardt problem is a smoothed polygon, affirming Mahler's First.

In many ways, the Reinhardt problem is a textbook control problem, because of the way it employs significant parts of the general theory in a single problem. Among other structures, we encounter Lax equations, control problems on Lie groups, the symplectic structure on coadjoint orbits, Poisson brackets, Lie-Poisson dynamics, Euler-Arnold equations, Lyapunov functions, a conserved quantity via the Noether-Sussmann theorem, singular arcs, chattering, the Fuller system, bang-bang solutions, and even an ODE without a Lipschitz condition.

Although this book does not succeed in resolving the Reinhardt conjecture, it is our firm belief that optimal control theory is the proper framework for understanding this problem. In particular, the Reinhardt conjecture is formulated as an entirely explicit control problem. This book brings us one step closer to a complete solution.

Acknowledgements

We would like to thank Velimir Jurdjevic and Greg Kuperberg for helpful discussions.

Vajjha would like to dedicate this book to his grandmother Saraswati Mokkapati.

Chapter 2

Historical Results

2.1 A Statement of the Reinhardt Conjecture

In this section, we state the Reinhardt conjecture and introduce terminology used throughout this book.

We will call a compact, convex set in \mathbb{R}^n with nonempty interior a *convex body*, and a convex body in \mathbb{R}^2 will be called a *convex disk*. By a *centrally symmetric* convex disk in the Euclidean plane, we mean a convex disk K in \mathbb{R}^2 such that if $\mathbf{v} \in K$ then $-\mathbf{v} \in K$. Here, and throughout this chapter, we assume the center of symmetry is the origin $\mathbf{0} := (0, 0)$. We denote by \mathcal{K}_{ccs} the set of all centrally symmetric convex disks in the plane \mathbb{R}^2 , which have the origin as the center of symmetry.

A family of convex disks in \mathbb{R}^2 is called a *packing* if any two distinct convex disks in the family *do not overlap*; that is, they have disjoint interiors. We can now define the *packing density* and *greatest packing density* of a packing in \mathbb{R}^2 . Intuitively the packing density corresponds to the proportion of the plane taken up by the packing.

Definition 2.1.1 (Greatest packing density). *Let B_r be a ball of radius r in \mathbb{R}^2 centered at the origin, and let area be the Lebesgue measure on \mathbb{R}^2 . The upper and lower density of a packing \mathcal{P} are defined to be*

$$\limsup_{r \rightarrow \infty} \frac{1}{\text{area}(B_r)} \sum_{K' \in \mathcal{P}} \text{area}(K' \cap B_r) \quad \text{and} \quad \liminf_{r \rightarrow \infty} \frac{1}{\text{area}(B_r)} \sum_{K' \in \mathcal{P}} \text{area}(K' \cap B_r)$$

respectively. If they both exist and coincide, the common number is called the density of the packing \mathcal{P} and is denoted $\delta(K, \mathcal{P})$. Given a convex body

K we define the greatest packing density as the packing density formed with congruent copies of K :

$$\delta(K) := \sup \{ \delta(K, \mathcal{P}) \mid \delta(K, \mathcal{P}) \text{ exists, and } \mathcal{P} \text{ is a packing with congruent copies of } K \}.$$

It can be proved that for a convex disk K , one can always find a packing \mathcal{P} such that $\delta(K, \mathcal{P})$ exists and is equal to $\delta(K)$ [38, Exercise 3.2].

A *lattice* is a discrete additive subgroup of \mathbb{R}^2 of full rank. An important class of packings are *lattice packings*, which consist of lattice translates of a convex disk K : If \mathbf{L} is a lattice in \mathbb{R}^2 and K is a fixed convex disk, then we consider the *packings of translates of K* under \mathbf{L} , provided the translates of K do not overlap (called the *lattice packing* of K). We write $K + \mathbf{L}$ for the packing and write $K + l$, for the lattice translate of the convex disk K , for $l \in \mathbf{L}$. We can now similarly define the lattice packing density and greatest lattice packing density.

Definition 2.1.2 (Greatest lattice packing density). *We define the upper and lower densities of a lattice packing $K + \mathbf{L}$ of congruent copies of a convex disk K to be respectively*

$$\limsup_{r \rightarrow +\infty} \frac{\sum_{l \in \mathbf{L}} \text{area}(B_r \cap (K + l))}{\text{area}(B_r)} \quad \text{and} \quad \liminf_{r \rightarrow +\infty} \frac{\sum_{l \in \mathbf{L}} \text{area}(B_r \cap (K + l))}{\text{area}(B_r)}.$$

It can be proved that given a convex disk K and a lattice \mathbf{L} , the upper and lower lattice packing densities of the packing $K + \mathbf{L}$ (provided that the \mathbf{L} -translates of K have disjoint interiors) coincide and are both equal to

$$\delta(K, \mathbf{L}) = \frac{\text{area}(K)}{\det(\mathbf{L})}$$

where $\det(\mathbf{L})$ is the determinant of the lattice \mathbf{L} (see Definition 2.3.2) [13, Corollary 30.1].

The common value $\delta(K, \mathbf{L})$ of the upper and lower densities is called the density of the lattice packing. The greatest lattice packing density is defined as

$$\delta_L(K) := \sup \{ \delta(K, \mathbf{L}) \mid \mathbf{L} \text{ a lattice in } \mathbb{R}^2 \text{ such that } K + \mathbf{L} \text{ is a packing} \}.$$

If K is a convex disk, let $K_{sym} := \{(\mathbf{v} - \mathbf{w})/2 \mid \mathbf{v}, \mathbf{w} \in K\}$ be its symmetrization. Then K_{sym} is a centrally symmetric convex disk. For a centrally

symmetric convex disk K , we have $K = K_{sym}$. Minkowski made the simple observation that $K + \mathbf{L}$ is a packing if and only if $K_{sym} + \mathbf{L}$ is a packing. In this way, questions about lattice packings for K can usually be reduced to corresponding questions for K_{sym} . This led early researchers to focus on centrally symmetric convex disks.

A key point is the following theorem of L. Fejes Tóth, which states that the greatest packing density and greatest lattice packing densities are actually equal for the class \mathfrak{K}_{ccs} [45],[46],[47].

Theorem 2.1.3 (Fejes Tóth). *If $K \subset \mathbb{R}^2$ is a centrally symmetric convex disk, then*

$$\delta(K) = \delta_L(K). \quad (2.1.1)$$

Many of the early research articles on the Reinhardt conjecture were restricted in scope to lattice packings. However, in view of Fejes Tóth's theorem, results about greatest lattice packing density actually imply results about greatest packing density (for the set \mathfrak{K}_{ccs}). In lattice form, packings of convex bodies were studied by multiple authors, beginning with Minkowski.

Now consider the infimum of densities:

$$\delta_{\min} := \inf_{K \in \mathfrak{K}_{ccs}} \delta(K).$$

So δ_{\min} is defined as a *minimax*: the least (or worst) greatest packing density among all centrally symmetric convex disks in \mathbb{R}^2 .

In 1904, Minkowski established a lower bound on this infimum [33]. In 1923, Blaschke called *Courant's conjecture* the statement that the ellipse minimizes the greatest packing density [4]. Later, Reinhardt proved that a minimizer exists, and proved several properties about it, including the fact that the ellipse is not the minimizer, refuting Courant's conjecture [40].

Reinhardt's problem now is to explicitly describe a $K_{\min} \in \mathfrak{K}_{ccs}$ for which $\delta(K_{\min}) = \delta_{\min}$, and also determine this worst greatest packing density. It is the problem of finding the *most unpackable shape* in \mathfrak{K}_{ccs} . As mentioned in the previous chapter, Reinhardt suggested a specific candidate, the *smoothed octagon*, to be the most unpackable; that is, to be the minimax optimizer. The smoothed octagon is a regular octagon whose vertices have been clipped by hyperbolic arcs (shown in Figure 1.1.1).

If \mathbf{L} gives a lattice packing of K , and if g is an affine transformation, then $g\mathbf{L}$ gives a lattice packing of gK of the same density. Because of this affine invariance, the set of worst disks is stable under the group of affine transformations.

Conjecture (Reinhardt [40], Mahler [29]). *The smoothed octagon achieves the least greatest packing density among all centrally symmetric convex disks in the plane. Its density is given by*

$$\frac{8 - \sqrt{32} - \ln 2}{\sqrt{8} - 1} \approx 0.902414.$$

The smoothed octagon is uniquely the worst, up to affine transformation.

This book investigates the Reinhardt conjecture by restating it as a problem in control theory. To do this, we rely on numerous geometric properties of the worst convex disk K_{\min} , which we collect in the following sections. These sections review the results contained in Reinhardt's article of 1934 and Mahler's articles written in the 1940s.

2.2 Reinhardt's Approach

In this section, we briefly review Reinhardt's article of 1934. The proofs that we give will be sketches, because the full details are available in Reinhardt's article. Let K be a centrally symmetric convex disk. Let $K + \mathbf{L}$ be a lattice packing of K .

Lemma 2.2.1. *The packing $K + \mathbf{L}$ is realized by placing K inside an appropriate parallelogram or centrally symmetric convex hexagon H_K , tiling the plane with translates of H_K , then placing a copy of K inside each translate of H_K .*

Proof. Homothetically expand K (to rK) and its translates by \mathbf{L} until two translates rK and $rK + l$ come in contact. Draw a separating line between these two translates (by the separating hyperplane theorem). Similarly separate other translates of rK using translates of the separating line. Continue to homothetically expand rK , but now cropping rK to $(rK)^{cr}$ so as to lie between its bounding separating lines, so that cropped translated regions $(rK)^{cr} + l$ do not overlap. Continue to expand until a new point of contact is formed. Repeat the process, adding new separating lines, cropping, and then continuing with cropped homothetic expansion. Eventually, after repeating the process a finite number of times, the plane is tiled by the translates of the cropped homothetic expansion H_K of K .

By construction H_K is a convex polygon, because it is bounded by the finitely many separating lines that were introduced. It is centrally symmetric by central symmetry of K and the symmetric placement of the separating lines. By considerations of Euler characteristic of a polygon tiling, the number of edges is at most six. Thus H_K is a parallelogram or centrally symmetric hexagon. \square

Every centrally symmetric hexagon tiles the plane. A parallelogram H_K never gives smaller area than that of the smallest centrally symmetric hexagon containing K , because its corners can be clipped to give a smaller hexagon containing K , except when K itself is a parallelogram. In this exceptional case, K itself tiles and has greatest packing density 1. We exclude this exception from our further discussions.

Theorem 2.2.2 (Reinhardt-Fejes-Tóth). *If $K \subset \mathbb{R}^2$ is a centrally symmetric convex disk that is not a parallelogram, then its packing density is*

$$\delta(K) = \frac{\text{area}(K)}{\text{area}(H_K)}, \quad (2.2.1)$$

where H_K is a centrally symmetric hexagon of least area circumscribing K .

We remark that the hexagon of smallest area circumscribing a centrally symmetric disk K can be realized as a centrally symmetric hexagon [38, Theorem 2.5].

Proof. By Fejes-Tóth (Equation 2.1.1), we have $\delta_L(K) = \delta(K)$. Let \mathbf{L} be a lattice that realizes this equality. By the previous lemma, the lattice packing $K + \mathbf{L}$ is obtained by tiling a centrally symmetric hexagon H_K . The density of this packing is given by (2.2.1). This hexagon has least area among centrally symmetric ones, because every centrally symmetric hexagon tiles, and one of smaller area circumscribing K would lead to a packing of greater density. \square

From now on, H_K will denote a centrally symmetric hexagon of smallest area circumscribing K . We call such a H_K a *critical hexagon*. This terminology is further explained in Definition 2.3.8 and Theorem 2.3.9.

The midpoints of the edges of H_K lie on the boundary of K . For otherwise, an edge of H_K can be rotated about some point on that edge to create a hexagon of smaller area. If we slide one edge of a convex polygon, where the movement is constrained to keep the area of the polygon fixed, then the

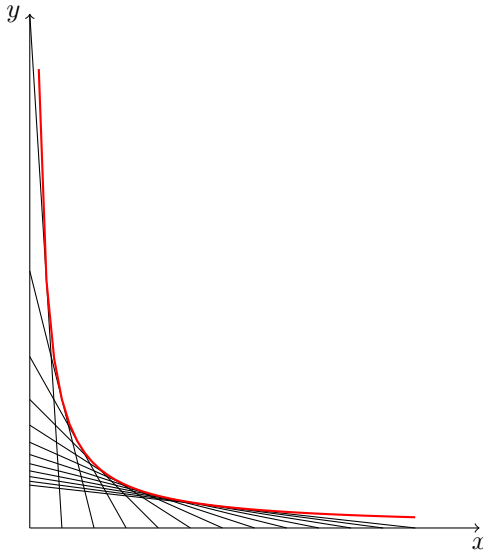


Figure 2.2.1: The hyperbola is the envelope of a pencil of lines the product of whose x and y -intercepts is constant.

envelope of the moving edge is a hyperbola whose asymptotes are the lines through the two adjacent edges. This observation follows from the fact that the hyperbola is the envelope of a pencil of lines the product of whose x and y -intercepts is constant. Additionally, every point on the hyperbolic envelope is the midpoint of a unique line segment formed by a line in the pencil and the x and y axes. See Figure 2.2.1.

Definition 2.2.3 (Support line). *For a convex disk K , a support line is a line containing at least one point of K but does not separate any points of K .*

From this observation about the hyperbola, it follows that the six edge midpoints of H_K on the boundary of K are not corners of K : the unique support line at each midpoint is the tangent to the hyperbolic envelope at that point. Otherwise the area of H_K is not minimal.

Remark 2.2.4. *We also observe that locally around each midpoint, K contains an arc of the hyperbola. It is here that we first see the significance of the hyperbola for the Reinhardt conjecture.*

The ratio $\text{area}(K)/\text{area}(H_K)$ in Theorem 2.2.2 is scale invariant and so there is no loss of generality in fixing the denominator $\text{area}(H_K)$. We choose

the normalization $\text{area}(H_K) = \sqrt{12}$, which is the area of a regular hexagon with inradius 1. This choice has the advantage of making the unit circular disk K satisfy the normalization condition.

Let $\det(\mathbf{v}_1, \mathbf{v}_2)$ denote the determinant of the 2×2 matrix with columns $\mathbf{v}_1, \mathbf{v}_2 \in \mathbb{R}^2$. If H_K is any critical hexagon of $K \in \mathcal{K}_{ccs}$, then the edge midpoints $\mathbf{s}_0, \mathbf{s}_1, \dots, \mathbf{s}_5$ give six points, ordered counterclockwise, around the boundary of K . The six points, by virtue of being the edge midpoints of a centrally symmetric convex hexagon, satisfy the following *multi-point* conditions

$$\mathbf{s}_0 + \mathbf{s}_2 + \mathbf{s}_4 = 0, \quad \mathbf{s}_{j+3} = -\mathbf{s}_j, \quad \det(\mathbf{s}_j, \mathbf{s}_{j+1}) = \text{constant}, \quad (2.2.2)$$

for all $j \in \mathbb{Z}/6\mathbb{Z}$, the constant being independent of j . Moreover, $\det(\mathbf{s}_j, \mathbf{s}_{j+1})$ is independent of the critical hexagon H_K , because it is a fixed fraction of the area of H_K . By fixing the area of H_K at $\sqrt{12}$, we have

$$\det(\mathbf{s}_j, \mathbf{s}_{j+1}) = \sqrt{3}/2. \quad (2.2.3)$$

Replacing K by its image under an affine transformation, we may assume that $\mathbf{s}_0, \mathbf{s}_1, \dots, \mathbf{s}_5$ are the sixth roots of unity \mathbf{s}_j^* in the plane, with complex coordinates $\mathbf{s}_j^* = \exp(2\pi ij/6)$, where $i = \sqrt{-1}$. The convex hull of the six points \mathbf{s}_j^* is a regular hexagon h_K contained in K . It follows from the convexity of K that the boundary of K is contained in the union of six equilateral triangles T_j , where triangle T_j has vertices $\mathbf{s}_j^*, \mathbf{s}_{j+1}^*, \mathbf{s}_j^* + \mathbf{s}_{j+1}^*$, for $j = 0, \dots, 5$. See Figure 2.2.2.

Lemma 2.2.5. *A disk K_{\min} with the worst greatest density lattice packing exists. K_{\min} has no corners. That is, there is a unique support line to K_{\min} at each boundary point. Moreover, the support line of each boundary point of K_{\min} contains an edge of some critical hexagon.*

Proof. Reinhardt uses the Blaschke selection theorem to prove the existence of a centrally symmetric K with a worst greatest density lattice packing. We fix one such $K = K_{\min}$. The set of critical hexagons of K is closed: a convergent limit of critical hexagons is again critical. Moreover, every point on the boundary of $K = K_{\min}$ lies on some edge of a critical hexagon. Otherwise, if the point \mathbf{u} is not on the edge of any critical hexagon, then by closedness, the same holds for all nearby boundary points, and a small area can be shaved in a centrally symmetric manner from K at $\pm \mathbf{u}$ to decrease the area of K .

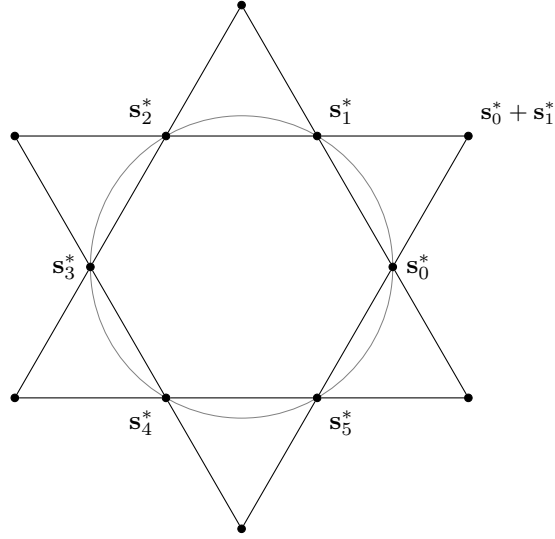


Figure 2.2.2: Hexagon formed by the sixth roots of unity along with triangles T_j formed by the vertices s_j^* , s_{j+1}^* , $s_j^* + s_{j+1}^*$.

without changing the minimal area of the critical hexagons. This contradicts the density minimax property of K_{\min} . If a boundary point \mathbf{u} is a midpoint of a critical hexagon H_K , then as seen above with the hyperbolic envelope, \mathbf{u} is not a corner.

If a boundary point \mathbf{u} lies on some edge of a critical hexagon without being its midpoint, then an entire segment containing \mathbf{u} of the edge lies along the boundary of K . The segment determines the unique support line for points in the relative interior of the segment. Each endpoint of the segment is the midpoint of an edge of a critical hexagons and hence not a corner, for otherwise it can be shaved as above. \square

Lemma 2.2.6. *Assume that the boundary of K_{\min} has critical hexagon with edge midpoints s_j^* . Consider a second critical hexagon of K_{\min} with edge midpoints s_0, \dots, s_5 , indexed so that $s_0 \in T_0 \setminus \{s_0^*, s_1^*\}$. Then for all j , we have that s_j lies in the interior of T_j .*

Reinhardt calls this property *monotonicity*. As the midpoint s_0 advances counterclockwise beyond s_0^* , the other midpoints s_j advance counterclockwise beyond s_j^* into the interior of T_j . See Figure 2.2.3. Note that if $\{s_j \mid j\} \neq \{s_j^* \mid j\}$, we can always assume without generality that the subscripts are

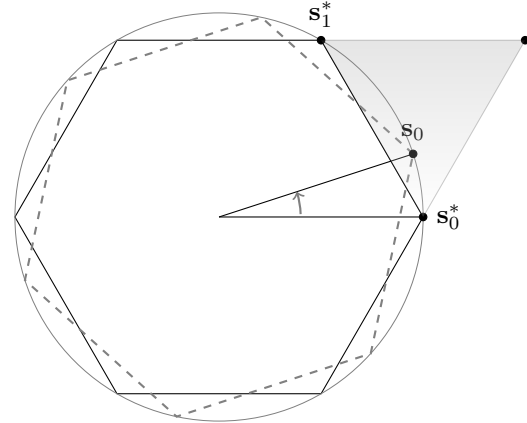


Figure 2.2.3: This figure shows *monotonicity*. The points \mathbf{s}_j of the rotated hexagons lie in triangles T_j .

indexed such that

$$\mathbf{s}_0 \in T_0 \setminus \{\mathbf{s}_j^* \mid j\} = T_0 \setminus \{\mathbf{s}_0^*, \mathbf{s}_1^*\},$$

to satisfy the assumption of the lemma.

Proof. Assume $\mathbf{s}_0 \in T_0$. For some j and k , we have $\mathbf{s}_1 \in T_j$ and $\mathbf{s}_2 \in T_k$. As above, we have $\mathbf{s}_1 = \mathbf{s}_0 + \mathbf{s}_2$, which gives a system of constraints

$$\mathbf{s}_1 \in T_j \cap (T_0 + T_k),$$

expressed using the *Minkowski sum*

$$T_0 + T_k := \{\mathbf{u}_0 + \mathbf{u}_k \mid \mathbf{u}_0 \in T_0, \mathbf{u}_k \in T_k\}.$$

Also, for fixed \mathbf{s}_0 , the inequality $\det(\mathbf{s}_0, \mathbf{s}_1) > 0$ places a half-plane constraint on \mathbf{s}_1 . These constraints imply that $\mathbf{s}_1 \in T_1$ and $\mathbf{s}_2 \in T_2$. Using $\mathbf{s}_{j+3} = -\mathbf{s}_j$ and rotational symmetry, we have a weak form of monotonicity: if for some j , we have $\mathbf{s}_j \in T_j \setminus \{\mathbf{s}_j^*, \mathbf{s}_{j+1}^*\}$, then for all k , we have $\mathbf{s}_k \in T_k$.

Now suppose for a contradiction that \mathbf{s}_0 lies on the relative interior of the edge $(\mathbf{s}_0^*, \mathbf{s}_1^*)$ of T_0 . By the convexity of K , the entire edge $[\mathbf{s}_0^*, \mathbf{s}_1^*]$ lies on the boundary of K . Let $\mathbf{u}_1 \in \partial K$ be any midpoint of a critical hexagon in the interior of T_1 such that its support line is different from the support lines at \mathbf{s}_1^* and \mathbf{s}_2^* . The point \mathbf{u}_1 exists because there are no corners, by Lemma 2.2.5. Let \mathbf{u}_j be the other midpoints. By the weak form of monotonicity in the

previous paragraph, the point \mathbf{u}_0 lies in T_0 , hence along the edge of T_0 . The multi-point conditions (2.2.2) now imply that for some $t_0, t_1 \in \mathbb{R}$, we have

$$\mathbf{u}_0 = \mathbf{s}_0^* + t_0 \mathbf{s}_2^*, \quad \mathbf{u}_1 = \mathbf{s}_2^* + t_1 \mathbf{u}_0 \quad \mathbf{u}_2 = \mathbf{s}_2^* + (t_1 - 1) \mathbf{u}_0.$$

The condition that \mathbf{u}_1 is an interior point of T_1 gives $0 < t_1 < 1$. Thus, $\mathbf{u}_1, \mathbf{s}_2^*, \mathbf{u}_2$ are distinct collinear points on ∂K so that the entire segment from \mathbf{u}_1 to \mathbf{u}_2 lies on the boundary of K . This shows that \mathbf{s}_2^* and \mathbf{u}_1 have the same support line, which is contrary to the construction of \mathbf{u}_1 . Thus \mathbf{u}_0 does not lie on the relative interior of the edge. Repeating this argument for each j , we find that no \mathbf{s}_j lies on the relative interior of the edge $(\mathbf{s}_j^*, \mathbf{s}_{j+1}^*)$ of T_j .

Now assume that $\mathbf{s}_0 \in T_0 \setminus [\mathbf{s}_0^*, \mathbf{s}_1^*]$. We claim that $\mathbf{s}_1 \neq \mathbf{s}_1^*$. Otherwise, the multi-point condition $\mathbf{s}_5 = \mathbf{s}_0 - \mathbf{s}_1^*$ forces \mathbf{s}_5 to lie along the relative interior of the edge $(\mathbf{s}_5^*, \mathbf{s}_0^*)$, which we have shown to be impossible. Similarly, we claim that $\mathbf{s}_1 \neq \mathbf{s}_2^*$. Otherwise, the multi-point condition gives $\mathbf{s}_0 = \mathbf{s}_2^* - \mathbf{s}_2$, which forces \mathbf{s}_0 to lie on the forbidden edge $[\mathbf{s}_0^*, \mathbf{s}_1^*]$.

Thus, \mathbf{s}_1 satisfies the hypotheses of the previous paragraph (shifting indices by one): $\mathbf{s}_1 \in T_1 \setminus [\mathbf{s}_1^*, \mathbf{s}_2^*]$. Iterating the argument of the previous paragraph for consecutive j , we find that for all j , we have $\mathbf{s}_j \in T_j \setminus [\mathbf{s}_j^*, \mathbf{s}_{j+1}^*]$. Furthermore, no \mathbf{s}_j is on the boundary of T_j . Otherwise, the convexity of K forces \mathbf{s}_{j+1} or \mathbf{s}_{j-1} to lie on the forbidden edge. This completes the proof. \square

Lemma 2.2.7. *Let $K = K_{\min}$ have worst greatest packing density. Then every point of the boundary of K is the midpoint of an edge of a unique critical hexagon. As \mathbf{s}_0 advances around the boundary of K in a counterclockwise direction, the five other midpoints $\mathbf{s}_1, \dots, \mathbf{s}_5$ advance strictly monotonically and continuously in a counterclockwise direction.*

Proof. Strict monotonicity is established in the previous lemma. In particular, each point on the boundary is the edge midpoint of at most one critical hexagon. Continuity follows from monotonicity if we show that there are no jumps. We show that every open interval along the boundary of K contains the edge midpoint of a critical hexagon.

Suppose for a contradiction that an open interval exists without a such a midpoint. Then picking the interval to be as large as possible, there exist critical hexagons and edge midpoints $\mathbf{s}_0, \mathbf{u}_0$ marking the endpoints. Let $\mathbf{s}_0, \dots, \mathbf{s}_5$ and $\mathbf{u}_0, \dots, \mathbf{u}_5$ be the corresponding midpoints of the six edges of these two critical hexagons. For each j , we claim that no point on ∂K between \mathbf{s}_j and \mathbf{u}_j is an edge midpoint of a critical hexagon. For otherwise,

by monotonicity the same critical hexagon has an edge midpoint between \mathbf{s}_0 and \mathbf{u}_0 . By Lemma 2.2.5, the boundary segments of ∂K between \mathbf{s}_j and \mathbf{u}_j are straight lines, included in edges of critical hexagons. This forces the critical hexagon for \mathbf{s}_j and \mathbf{u}_j to be equal (both hexagons having their edges along these straight lines), and since these are the edge midpoints $\mathbf{s}_j = \mathbf{u}_j$ for all j . Thus, no such open interval exists. \square

Thus, in summary, excluding the degenerate case when K is a parallelogram, Reinhardt constructed the hexagon H_K as the centrally symmetric hexagon of least area containing K . He showed that the midpoints of the edges of H_K lie on the boundary of K . He constructed h_K as the centrally symmetric polygon joining these midpoints and showed that to achieve the densest lattice packing of K , the plane is tiled by copies of H_K . Reinhardt also proved the existence of a disk K_{\min} which has the worst greatest lattice packing density, and proved properties about its boundary.

2.3 Mahler's Approach

In the previous chapter, we have mentioned Minkowski's discovery of the connection between centrally symmetric convex disks and lattices, which resulted in the famous Minkowski theorem on lattice points [34]. These results initiated the *geometry of numbers*. Kurt Mahler rediscovered the Reinhardt conjecture while attempting to extend Minkowski's results. These results were published in a series of papers in the 1940s. We review his approach in this section.

Definition 2.3.1 (Admissible lattice). *For a $K \in \mathfrak{K}_{ccs}$ centered at the origin, a lattice \mathbf{L} is called K -admissible if no point of \mathbf{L} other than $\mathbf{0} = (0, 0)$ lies in the interior of K .*

The lattice \mathbf{L} of a centrally symmetric convex disk K is K -admissible if and only if $K/2 + \mathbf{L}$ is a lattice packing of $K/2$. Thus, results about admissible lattices translate readily into results about lattice packings.

Definition 2.3.2 (Determinant of a Lattice). *For any lattice \mathbf{L} with basis $\mathbf{u}_0, \mathbf{u}_1 \in \mathbb{R}^2$, the determinant $\det(\mathbf{L})$ is equal to the absolute value $|\det(\mathbf{u}_0, \mathbf{u}_1)|$. This is also sometimes called the covolume of the lattice \mathbf{L} .*

Definition 2.3.3 (Minimal determinant). *For $K \in \mathfrak{K}_{ccs}$, the minimizer*

$$\Delta(K) := \inf_{K\text{-admissible}} \det(\mathbf{L}),$$

where the infimum runs over all K -admissible lattices, is called the minimal determinant of the convex disk K .

Definition 2.3.4 (Critical lattice). *A lattice is called critical for a convex disk K if its determinant is equal to the minimal determinant of K .*

Definition 2.3.5 (Irreducible disk). *A convex disk $K \in \mathfrak{K}_{ccs}$ is called irreducible if every boundary point of K lies on a critical lattice of K .*

We remark that this is not the original definition of irreducibility of a convex disk. We choose our definition based on [29, Lemma 3], which shows that this definition is equivalent to the original definition. We reiterate that the most significant results of this section were known to Reinhardt in 1934, without using the language of critical lattices, minimal determinants, and irreducibility.

Minkowski proved the following theorem which gives conditions under which points on K give rise to critical lattices.

Theorem 2.3.6 (Minkowski [33], Mahler [27]). *Let \mathbf{L} be a critical lattice of a convex disk $K \in \mathfrak{K}_{ccs}$. Then \mathbf{L} contains three points $\mathbf{s}_0, \mathbf{s}_1, \mathbf{s}_2$ on the boundary of K such that (i) $\mathbf{s}_0, \mathbf{s}_1$ is a basis of the lattice \mathbf{L} , and (ii) $\mathbf{0s}_0\mathbf{s}_1\mathbf{s}_2$ is a parallelogram of area $\det(\mathbf{L}) = |\det(\mathbf{s}_0, \mathbf{s}_1)| = \Delta(K)$, the minimal determinant of K . Conversely, if $\mathbf{s}_0, \mathbf{s}_1, \mathbf{s}_2$ are three points on the boundary of K such that $\mathbf{0s}_0\mathbf{s}_1\mathbf{s}_2$ is a parallelogram, then the area of this parallelogram is not less than $\Delta(K)$ and is equal to $\Delta(K)$ if and only if the lattice with basis $\mathbf{s}_0, \mathbf{s}_1$ is critical.*

The parallelogram of the theorem above is shown in Figure 1.3.1.

Since centrally symmetric hexagons can be decomposed into three parallelograms, the above result shows that a critical lattice of a convex disk $K \in \mathfrak{K}_{ccs}$ gives rise to an *inscribed centrally symmetric hexagon* h_K within our convex disk K so that $\Delta(K) = \text{area}(h_K)/3$ which is *minimal* in the sense that

$$\text{area}(h_K) = \inf_h \text{area}(h),$$

where the infimum is taken over all hexagons h with vertices $\mathbf{s}_0, \mathbf{s}_1, \mathbf{s}_2$ (and their reflections about $\mathbf{0}$) on the boundary of K and with $\mathbf{s}_0 - \mathbf{s}_1 + \mathbf{s}_2 = \mathbf{0}$. In

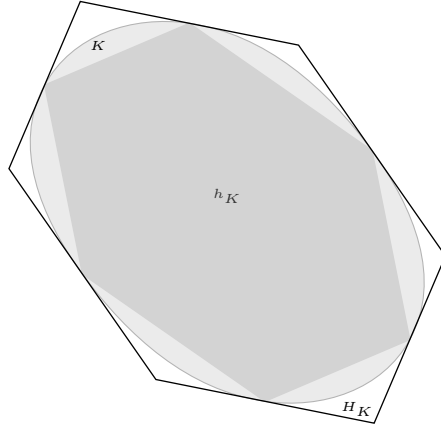


Figure 2.3.1: Critical hexagons for an ellipse.

1947, Mahler [29] proved an analogous result for *circumscribed hexagons* of K :

Theorem 2.3.7 (Mahler [29]). *Let $K \in \mathfrak{K}_{ccs}$ be a convex disk which is not a parallelogram. Let \mathbf{L} be a critical lattice of K with lattice point $\mathbf{s}_0, \dots, \mathbf{s}_5$ on the boundary of K satisfying $\mathbf{s}_0 - \mathbf{s}_1 + \mathbf{s}_2 = 0$ and $\mathbf{s}_{j+3} = -\mathbf{s}_j$. Then there are unique symmetric support lines ℓ_j of K at these points, such that*

1. *no two of these lines coincide;*
2. *the area of the centrally symmetric hexagon H_K bounded by the support lines is given by $\text{area}(H_K) = 4\Delta(K)$;*
3. *each side of H_K is bisected at the lattice point \mathbf{s}_j where it touches the boundary of K ;*
4. *the hexagon H_K is minimal in the sense that*

$$\text{area}(H_K) = \inf_H \text{area}(H),$$

where the infimum is taken over the set of all hexagons H bounded by symmetric support lines of the convex disk K .

By construction, $h_K, H_K \in \mathfrak{K}_{ccs}$. The hexagons H_K and h_K for an ellipse are shown in Figure 2.3.1. The critical lattice of any $K \in \mathfrak{K}_{ccs}$ gives rise to hexagons h_K and H_K whose areas are related as

$$\Delta(K) = \frac{1}{3} \text{area}(h_K) = \frac{1}{4} \text{area}(H_K). \quad (2.3.1)$$

Definition 2.3.8 (Critical Hexagon). *For a convex disk $K \in \mathfrak{K}_{ccs}$, a hexagon H_K given by the construction of Theorem 2.3.7 is called a critical hexagon.*

In the section on Reinhardt's approach, we defined critical hexagons differently. The following theorem shows that the definitions are compatible.

Theorem 2.3.9. *Let $K \in \mathfrak{K}_{ccs}$. Let H_K be a centrally symmetric hexagon of least area circumscribing K . Then H_K is a critical hexagon in the sense of Definition 2.3.8.*

Proof. Let \mathbf{s}_j be the edge midpoints of H_K . These points lie on the boundary of K . Since H_K is centrally symmetric, the points \mathbf{s}_j satisfy the multi-point conditions (2.2.2).

Tile the plane with translates of H_K . Let \mathbf{L} be the lattice generated by \mathbf{s}_0 and \mathbf{s}_1 . The centers of the tiles form the sublattice $2\mathbf{L}$ generated by $2\mathbf{s}_0$ and $2\mathbf{s}_1$. A lattice point with one or two odd coordinates is the midpoint of an edge of a translate of H_K centered at an adjacent even lattice point. Thus, none of the nonzero lattice points of \mathbf{L} lie in the interior of K . That is, \mathbf{L} is K -admissible. Note that H_K is a fundamental domain for the lattice $2\mathbf{L}$. Thus, $4\Delta(K) = \det(2\mathbf{L}) = \text{area}(H_K)$.

We claim that \mathbf{L} is critical. Let $\tilde{\mathbf{L}}$ be a critical lattice with critical hexagon \tilde{H}_K . Since H_K and the critical hexagon \tilde{H}_K both have smallest area among centrally symmetric circumscribing hexagons, their areas must be equal. They are both fundamental domains for the corresponding even sublattices $2\mathbf{L}$ and $2\tilde{\mathbf{L}}$. Hence the determinants of the lattices are equal. This implies that \mathbf{L} is a critical lattice.

It is now easy to see that the properties of Theorem 2.3.7 all hold for H_K , if we take ℓ_j to be the line through the j th edge of H_K . \square

Corollary 2.3.10. *Let $K = K_{\min}$ have worst greatest packing density. Then K is irreducible.*

Proof. By Reinhardt, every boundary point of K is a midpoint of an edge of an area-minimizing centrally symmetric circumscribing hexagon H_K . By Theorem 2.3.9 and its proof, the boundary point is a lattice point of a critical lattice \mathbf{L} . \square

2.4 Boundary Parameterization of Minimizer

We return to Reinhardt's setup from Section 2.2. Let $K = K_{\min}$ be a centrally symmetric convex disk that gives the worst greatest density.

We have seen that each point \mathbf{s}_0 on the boundary of K is associated with other points $\mathbf{s}_1, \dots, \mathbf{s}_5$ that satisfy the multi-point conditions (2.2.2), with area normalization (2.2.3).

Since the boundary of K does not contain any corners, we can parameterize the boundary by a regular C^1 curve $t \mapsto \sigma_0(t)$, traversing the boundary in the *counter-clockwise direction*. We will call this the *positive orientation*. Then by the above discussion, the point $\sigma_0(t)$ gives rise to other points $\sigma_1(t), \dots, \sigma_5(t)$ which are subject to the multi-point conditions at each time t :

$$\sigma_j(t) + \sigma_{j+2}(t) + \sigma_{j+4}(t) = 0, \quad \sigma_{j+3}(t) = -\sigma_j(t), \quad \det(\sigma_j(t), \sigma_{j+1}(t)) = \frac{\sqrt{3}}{2}. \quad (2.4.1)$$

Definition 2.4.1 (Multi-point and multi-curve). *A function $\mathbf{s} : \mathbb{Z}/6\mathbb{Z} \rightarrow \mathbb{R}^2$ such that is called a multi-point if it satisfies the multi-point conditions (2.2.2) with normalization (2.2.3). An indexed set of C^k curves $\sigma : \mathbb{Z}/6\mathbb{Z} \times [0, t_f] \rightarrow \mathbb{R}^2$ is a C^k multi-curve if for all $t \in [0, t_f]$, $j \mapsto \sigma_j(t)$ is a multi-point.*

If the differentiability class C^k is not specified, then C^1 is assumed. The regularity of the curves will be established in the next section.

Example.

- The collection of sixth roots of unity $\mathbf{s}_j^* = \exp\left(\frac{2\pi i j}{6}\right) \in \mathbb{C}$, viewed as points in \mathbb{R}^2 , is an example of a multi-point.
- If $\theta : [0, t_f] \rightarrow \mathbb{R}$ is a C^1 curve, then the rotation

$$\sigma_j(t) = \begin{pmatrix} \cos(\theta(t)) & -\sin(\theta(t)) \\ \sin(\theta(t)) & \cos(\theta(t)) \end{pmatrix} \mathbf{s}_j^*$$

of a multi-point is an example of a multi-curve.

- Section B.1 in the Appendix gives an example of a hypotrochoid curve in \mathbb{R}^2 which satisfies the multi-curve properties in Equation (2.4.1).

2.4.1 Regularity Properties of Multi-Curves

Lemma 2.4.2 (Hales [15]). *Let $K = K_{\min} \in \mathcal{K}_{ccs}$ be a centrally symmetric convex disk that has the worst greatest packing density. Consider a C^0 multi-curve σ parameterization of its boundary. If $t \mapsto \sigma_0(t)$ is a positively oriented*

C^1 regular curve parameterizing the boundary of K , then so is $\sigma_j(t)$ for $j = 1, \dots, 5$.

Positively-oriented regular C^1 parameterizations σ_0 exist for the boundary of K . For example, the arclength parameterization has this property. By Lemma 2.2.7, the curves $\sigma_j(t)$ are continuous.

Proof. Given that $\sigma'_0(t)$ is continuous, we show that $\sigma'_2(t)$ exists and is continuous [15, Lemma 11]. Since K has no corners, the unit tangent $\mathbf{u}(t)$ to $\sigma_2(t)$, with the orientation given by σ_0 , is a continuous function of t . It is enough to check that the speed s_2 of σ_2 is continuous in t . We know that $\det(\sigma_0(t), \sigma_2(t))$ does not depend on t .

We claim that $\det(\sigma_0(t), \mathbf{u}(t)) \neq 0$. Let $h_K(t)$ be the hexagon given by the convex hull of $\{\sigma_j(t)\}$. If $\det(\sigma_0(t), \mathbf{u}(t)) = 0$, then the tangent line to σ_2 at t contains the edge of $h_K(t)$ through $\sigma_2(t)$ and $\sigma_1(t)$. This is contrary to Lemma 2.2.6. In fact, $\det(\sigma_0(t), \mathbf{u}(t)) < 0$. Similarly, we claim that $\det(\sigma'_0(t), \sigma_2(t)) \neq 0$. Otherwise the tangent line to σ_0 at t lies along another edge of $h_K(t)$, which is contrary to Lemma 2.2.6. In fact, $\det(\sigma'_0(t), \sigma_2(t)) < 0$.

Define a positive continuous function $s_2 : \mathbb{R} \rightarrow (0, \infty)$ by the equation

$$\det(\sigma'_0(t), \sigma_2(t)) + \det(\sigma_0(t), \mathbf{u}(t))s_2(t) = 0. \quad (2.4.2)$$

The curve

$$\tilde{\sigma}_2(t) := \int_{t_0}^t \mathbf{u}(t)s_2(t)dt + \sigma_2(t_0),$$

has the same initial value at $t = t_0$ as σ_2 , the same tangent direction for all t , and satisfies the same area relation

$$\det(\sigma_0(t), \tilde{\sigma}_2(t)) = \det(\sigma_0(t), \sigma_2(t)) = \sqrt{3}/2$$

by (2.4.2). We conclude that $\sigma_2 = \tilde{\sigma}_2$ and that $\sigma'_2(t) = \mathbf{u}(t)s_2(t)$. The regularity condition is $s_2(t) \neq 0$. (Compare the proof of Lemma 2.4.5.)

Similar statements for other curves σ_j follow by iteration over j . \square

Lemma 2.4.3. *Let $\sigma(t)$ denote a C^1 multi-curve parameterization of the boundary of $K = K_{\min} \in \mathfrak{K}_{ccs}$, giving worst greatest packing density. Assume that the curve σ_0 is parameterized according to arclength. Then, the tangents σ'_j are Lipschitz continuous for all j .*

Proof. This is Hales [15, Lemmas 17,18]. We recall the proof. We start by establishing the Lipschitz continuity of σ'_0 . We parameterize the curve σ_0 according to arclength s . Then σ'_0 is a unit tangent vector. The vector σ'_0 is continuous, because the convex region K has no corners, and the support lines are unique.

For each value s of arclength, let γ_s be the hyperbola through $\sigma_0(s)$ tangent to the curve σ_0 at s , whose asymptotes are the lines in direction $\sigma'_j(s)$ through $\sigma_j(s)$, for $j = \pm 1$. By Remark 2.2.4, locally near $\sigma_0(s)$, the arc γ_s lies inside K . As s varies, by continuity over the compact boundary, the curvatures of the hyperbolas γ_s at $\sigma_0(s)$ are bounded above by some $\kappa \in \mathbb{R}$. (The curvature of the hyperbola depends analytically on the parameters defining the asymptotes and tangent lines. These parameters vary continuously along the boundary of K . Thus, the curvature of the hyperbola varies continuously along the boundary of K , even when the second derivative of σ_0 and the curvature of σ_0 do not exist.) This means that an osculating circle of fixed curvature κ can be placed locally in K at each point $\sigma_0(s)$ so that $\sigma'_0(s)$ is tangent to the circle. By convexity, the curve σ_0 near s is constrained to pass between the tangent line at $\sigma_0(s)$ and the osculating circle of curvature κ . If we parameterize the curve by arclength, then $\sigma'_0(s)$ has unit length. Lipschitz continuity now follows from this bound κ on the curvature.

Now consider the Lipschitz continuity for $j \neq 0$. By evident symmetries, it is enough to consider $j = 2$. Let t be the arclength parameter for the curve σ_0 and let s be the arclength parameter for the curve σ_2 . Write $s = s(t)$ and $t = t(s)$ for the reparameterizations. By Lemma 2.4.2, the functions $s(t), t(s)$ are C^1 . Set $\tilde{\sigma}_2(s) = \sigma_2(t(s))$. The derivative of $\det(\sigma_0(t), \sigma_2(t)) = \sqrt{3}/2$ gives

$$\det(\sigma'_0(t), \sigma_2(t)) + \det(\sigma_0(t), \frac{d\tilde{\sigma}_2(s(t))}{ds}) \frac{ds}{dt} = 0.$$

The Lipschitz continuity of ds/dt (and of dt/ds) follows from the Lipschitz continuity of the other functions σ'_0 , σ_2 , σ_0 , and $d\tilde{\sigma}_2/ds$ in that equation. Then we also have the Lipschitz continuity of

$$\sigma'_2(t) = \frac{d\tilde{\sigma}_2}{ds} \frac{ds}{dt}.$$

□

Corollary 2.4.4. *The functions $\sigma'_j(t)$ are differentiable almost-everywhere.*

Proof. This follows by Rademacher's theorem and Lemma 2.4.3. □

Until further notice, we assume that the curve $t \mapsto \sigma_0(t)$ is parameterized according to arclength. See Proposition 3.1.9.

2.4.2 Convexity of Multi-Curves

This subsection investigates the convexity conditions on the curves σ .

Lemma 2.4.5 (Star conditions). *Let $K \in \mathfrak{K}_{ccs}$ be a convex disk with boundary parameterized by the C^1 regular multi-curve σ . At a given time t , let $j \mapsto \mathbf{s}_j = \sigma_j(t)$ be a multi-point on the boundary of the convex disk K . Then for each j and time t , the tangent $\sigma'_j(t)$ points into the open cone with apex \mathbf{s}_j and bounding rays through \mathbf{s}_{j+1} and $\mathbf{s}_j + \mathbf{s}_{j+1}$.*

Proof. This situation is depicted in Figure 2.4.1. This is asserted in Hales [15, 16] and is called the *star condition*. By convexity of the disk K , at any time t the hexagon $h_K(t)$ is a subset of K (as h_K is the convex hull of the points $\{\mathbf{s}_j\}$). Now, the vector $\sigma'_j(t)$ cannot point into the hexagon, because continuity would then create a non-convex piece of the curve σ_j . Dually, it cannot point beyond the ray from \mathbf{s}_j through $\mathbf{s}_j + \mathbf{s}_{j+1}$, as that would force $\sigma'_{j+2}(t)$ to point into h_K . Thus, the tangent vector points into the closed cone.

If the vector $\sigma'_j(t)$ points along the edge $\mathbf{s}_j\mathbf{s}_{j+1}$ of the triangle, then it would have to remain pointing in that same direction until reaching \mathbf{s}_{j+1} , as it cannot point inward (by the above argument) or outward (as then it would not be convex). This implies that $\sigma'_j(t)$, $\sigma'_{j+1}(t)$, $\sigma'_{j+3}(t)$, and $\sigma'_{j+4}(t)$ are all parallel. The relation $\sigma'_0(t) + \sigma'_2(t) + \sigma'_4(t) = 0$ implies that $\sigma'_{j+2}(t)$ and $\sigma'_{j+5}(t)$ are parallel as well. However, the star domain of $\sigma'_{j+2}(t)$ contains no vectors in that direction, forcing $\sigma'_{j+2}(t) = 0$. This contradicts the regularity of the curve σ_{j+2} .

Finally, if $\sigma'_j(t)$ points along the edge $\mathbf{s}_j(\mathbf{s}_j + \mathbf{s}_{j+1})$, then $\sigma'_{j-1}(t)$ points along $\mathbf{s}_{j-1}\mathbf{s}_j$, and the argument can be repeated with $j - 1$ in place of j . \square

Apart from the star conditions, there is another condition on the curvature of the boundary curve which needs to be imposed:

Lemma 2.4.6 (Curvature constraint). *Consider a convex disk $K \in \mathfrak{K}_{ccs}$ with boundary parameterized by a C^1 regular multi-curve σ with Lipschitz continuous derivative. Then we have the following condition almost everywhere:*

$$\det(\sigma'_j(t), \sigma''_j(t)) \geq 0 \quad j \in \mathbb{Z}/6\mathbb{Z}. \quad (2.4.3)$$

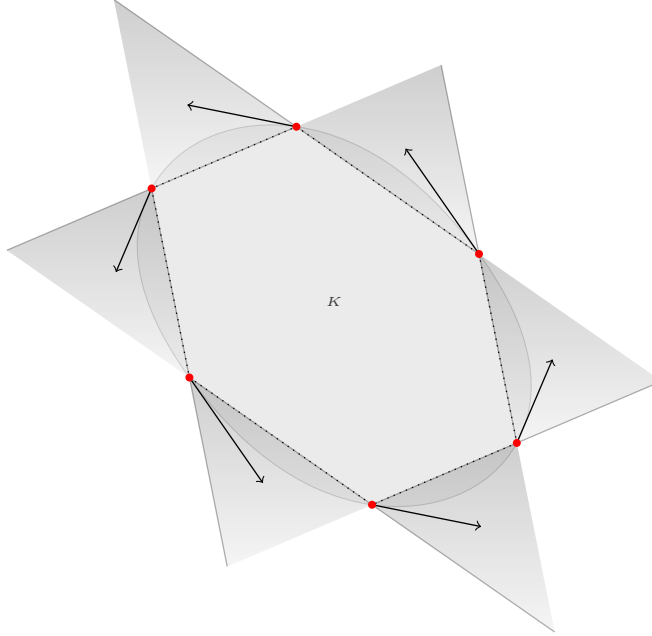


Figure 2.4.1: Global convexity condition for the ellipse.

Proof. The derivatives exist almost everywhere by the Lipschitz assumption. A well-known theorem (see Proposition 3.8 of Shifrin [42]) states that a simple closed regular plane curve is convex if and only if its orientation can be chosen in such a way so that its signed planar curvature is everywhere nonnegative. The left-hand side of (2.4.3) is the planar curvature

$$\frac{\det(\sigma'_j(t), \sigma''_j(t))}{|\sigma'(t)|^3}.$$

up to a positive factor depending on the parameterization. The assertion follows. \square

2.4.3 A Characterization of Balanced Disks

Summarizing, we define a class $\mathfrak{K}_{bal} \subset \mathfrak{K}_{ccs}$ (the class of balanced disks) of centrally symmetric disks K as those satisfying the properties that we have established.

Definition 2.4.7. *A centrally symmetric convex disk $K \in \mathfrak{K}_{ccs}$ is balanced if the following conditions hold.*

1. The boundary of K is parameterized counterclockwise by six regular C^1 curves $\sigma_j : \mathbb{R} \rightarrow \mathbb{R}^2$.
2. The derivatives σ'_j are Lipschitz.
3. For each t , $j \mapsto \sigma_j(t)$ is a multi-point with normalization convention (2.2.3).
4. For almost all t , we have the curvature constraint $\det(\sigma'_j(t), \sigma''_j(t)) \geq 0$.
5. For each t , the vector $\sigma'_j(t)$ points into the open cone with apex $\sigma_j(t)$ and rays passing through $\sigma_{j+1}(t)$ and $\sigma_j(t) + \sigma_{j+1}(t)$.
6. The image of each curve $\sigma_j : \mathbb{R}/(6t_f \mathbb{Z}) \rightarrow \mathbb{R}^2$ is the same simple closed curve in \mathbb{R}^2 , where $6t_f$ is the common period of the functions σ_j .

Let $\mathfrak{K}_{\text{bal}}$ denote the set of all balanced disks. A balanced pair (K, σ) consists of a balanced disk K and a boundary parameterization by a multi-curve σ satisfying the foregoing enumerated properties.

By convention, the area of the hexagon H_K has area normalized to $\sqrt{12}$. By the results of this section, every minimizer K_{\min} following this convention belongs to $\mathfrak{K}_{\text{bal}}$.

By affine invariance, there is no loss of generality in assuming that the sixth roots of unity $\{\mathbf{s}_j^* \mid j\}$ lie on the boundary of the convex disk K . We make this multi-point the *initial* position of the multi-curve σ . Following Hales [15], we call this representation the *circle representation of the convex disk K* .

Problem 2.4.8 (Balanced Reinhardt Problem in Circle Representation). *Describe those $K_{\min} \in \mathfrak{K}_{\text{bal}}$ in circle representation for which*

$$\text{area}(K_{\min}) = \inf_{\{K \in \mathfrak{K}_{\text{bal}} \mid K \text{ in circle representation}\}} \text{area}(K),$$

where $\mathfrak{K}_{\text{bal}}$ is the class of balanced disks.

Part II

Optimal Control

Chapter 3

A Control Problem

Now that we have a description of the set \mathfrak{K}_{bal} of balanced disks, we can use this to restate the Reinhardt conjecture as an optimal control problem. Optimal control problems solve for a policy that drives an agent in an environment over a period of time such that a cost function is optimized. We pin down our reformulation in three steps:

1. Recast the system as a dynamical system on a *state space* (which, in our case, will be a manifold).
2. Introduce a well-defined *cost functional*.
3. Determine a well-defined *control parameter*.

This will be our focus in this section.

3.1 State Dynamics in the Lie Group

Let $\text{SL}_2(\mathbb{R})$ be the Lie group consisting of all 2×2 matrices with real entries and determinant 1. The multi-curve conditions give rise to a curve in $\text{SL}_2(\mathbb{R})$ in the following sense.

Theorem 3.1.1 (Mahler [28], Hales [15]). *Let σ be a C^k multi-curve, and let \mathbf{s} be any multi-point. Then σ determines a C^k curve $g : [0, t_f] \rightarrow \text{SL}_2(\mathbb{R})$, by the conditions*

$$\sigma_j(t) = g(t)\mathbf{s}_j \tag{3.1.1}$$

for all j and all $t \in [0, t_f]$.

Proof. Given a multi-curve σ and $t \in [0, t_f]$, the value $\sigma(t)$ is a multi-point. It is enough to construct a 2×2 real matrix $g(t)$ so that

$$\sigma_j(t) = g(t)\mathbf{s}_j, \quad j = 0, 2,$$

because the multi-point conditions then imply by linearity that $\sigma_j(t) = g(t)\mathbf{s}_j$ for all $j \in \mathbb{Z}/6\mathbb{Z}$. A unique such matrix $g(t)$ can always be found by linear independence:

$$\det(\mathbf{s}_0, \mathbf{s}_1) = \det(\mathbf{s}_0, \mathbf{s}_2) \neq 0.$$

The identity

$$\det(\sigma_0(t), \sigma_2(t)) = \det(g(t)\mathbf{s}_0, g(t)\mathbf{s}_2) = \det(g(t)) \det(\mathbf{s}_0, \mathbf{s}_2)$$

gives $\det(g(t)) = 1$, and $g(t) \in \mathrm{SL}_2(\mathbb{R})$. Thus, if we have a C^k curve of multi-points $\sigma(t)$, we obtain a unique induced C^k curve $g : [0, t_f] \rightarrow \mathrm{SL}_2(\mathbb{R})$. \square

Remark 3.1.2.

- If t_0, t_1, t_2 are three time instants, and $\sigma_k(t_i) = g(t_i, t_j)\sigma_k(t_j)$, then $g(t_2, t_0) = g(t_2, t_1)g(t_1, t_0)$.
- Later in the book, the multi-point is \mathbf{s}_j^* , and the multi-curves σ_j are given by $\sigma_j(t) = g(t)\mathbf{s}_j^*$, where $g(t) \in \mathrm{SL}_2(\mathbb{R})$.

Let $\mathfrak{sl}_2(\mathbb{R})$ be the Lie algebra of 2×2 matrices with real entries and trace 0. Let $\mathrm{Ad}_g(X) = gXg^{-1}$ be the *adjoint representation* of $\mathrm{SL}_2(\mathbb{R})$ on its Lie algebra.

Similarly, the tangents $\{\sigma'_j(t)\}$ give rise to a corresponding curve in the Lie algebra $\mathfrak{sl}_2(\mathbb{R})$ as follows.

Definition 3.1.3. *For a C^1 curve $g : [0, t_f] \rightarrow \mathrm{SL}_2(\mathbb{R})$ as above, define $X : [0, t_f] \rightarrow \mathfrak{sl}_2(\mathbb{R})$ by $g'(t) = g(t)X(t)$.*

Theorem 3.1.4. *Assume that we have a convex disk K boundary parameterized by a regular C^1 multi-curve σ . Let g be the induced curve in $\mathrm{SL}_2(\mathbb{R})$ for some multi-point \mathbf{s} given by Equation (3.1.1), and define X by $g' = gX$. Then*

1. $X(t) \in \mathfrak{sl}_2(\mathbb{R})$.
2. $\sigma'_j(t) = \mathrm{Ad}_{g(t)}(X(t))\sigma_j(t) = g(t)X(t)g(t)^{-1}\sigma_j(t)$ for all $j \in \mathbb{Z}/6\mathbb{Z}$.

3. $X : [0, t_f] \rightarrow \mathfrak{sl}_2(\mathbb{R})$ is Lipschitz continuous.

Proof. First of all, the matrix $X(t)$ belongs to $\mathfrak{sl}_2(\mathbb{R})$ because if $g : [0, t_f] \rightarrow \mathrm{SL}_2(\mathbb{R})$ is any differentiable curve, then $X = g^{-1}g' \in \mathfrak{sl}_2(\mathbb{R})$. Let $\sigma_j(t) = g(t)\mathbf{s}_j$, for some multi-point \mathbf{s}_j . We then have

$$\sigma'_j(t) = g'(t)\mathbf{s}_j = g(t)X(t)\mathbf{s}_j = g(t)X(t)g(t)^{-1}g(t)\mathbf{s}_j = \mathrm{Ad}_{g(t)}(X(t))\sigma_j(t).$$

To see that $X(t)$ is Lipschitz, it is enough to show that $X(t)\mathbf{s}_j = g(t)^{-1}\sigma'_j(t)$ is Lipschitz for each j , which follows because σ'_j is Lipschitz by Lemma 2.4.3, and g is a C^1 curve on a compact interval. \square

Definition 3.1.5. Let

$$J := \begin{pmatrix} 0 & -1 \\ 1 & 0 \end{pmatrix} \in \mathfrak{sl}_2(\mathbb{R}).$$

J is the infinitesimal generator of the rotation group $\mathrm{SO}_2(\mathbb{R})$. This infinitesimal generator gives rotations $\exp(Jt) \in \mathrm{SO}_2(\mathbb{R})$. In particular,

$$R := \exp(J\pi/3) \tag{3.1.2}$$

is counterclockwise rotation by angle $\pi/3$. The matrices J and R are global notations throughout.

Corollary 3.1.6. For a balanced disk $K \in \mathfrak{K}_{bal}$, with C^1 boundary parameterization $\sigma_j(t) = g(t)\mathbf{s}_j^*$, we have the following properties for $X = X(t)$ defined in Definition 3.1.3 for all times t .

- We have $\rho_i(X) > 0$, for $i = 0, 1, 2$, where

$$\rho_0(X) := \frac{c + \sqrt{3}a}{\sqrt{3}}, \tag{3.1.3}$$

$$\rho_1(X) := \frac{c - \sqrt{3}a}{\sqrt{3}}, \tag{3.1.4}$$

$$\rho_2(X) := \frac{-(3b + c)}{2\sqrt{3}} \tag{3.1.5}$$

and

$$X = \begin{pmatrix} a & b \\ c & -a \end{pmatrix}.$$

In particular, $\sqrt{3}|a| < c$, $3b + c < 0$, $0 < c$, and $\mathrm{trace}(JX) = b - c < 0$.

- $\det(X(t)) > 0$ for all t .

We call the inequalities $\rho_i(X) > 0$ the *star inequalities* for $X \in \mathfrak{sl}_2(\mathbb{R})$.

Proof. At time t , the multi-point is given by $g(t)\mathbf{s}_j^*$. The star conditions in Lemma 2.4.5 imply that the tangent vector $\sigma'_j(t) = g(t)X(t)\mathbf{s}_j^*$ lies in the open cone with apex at the origin bounded by the rays through the points $g(t)\mathbf{s}_{j+1}^*$ and $g(t)\mathbf{s}_{j+2}^*$. After cancelling a factor of $g(t)$ from both sides, and writing X for $X(t)$, these open cone conditions become

$$X\mathbf{s}_j^* = \rho_j(X)\mathbf{s}_{j+1}^* + \tilde{\rho}_{j+1}(X)\mathbf{s}_{j+2}^*, \quad (3.1.6)$$

for some unknowns $\rho_j(X), \tilde{\rho}_j(X) > 0$, for $j \in \mathbb{Z}/6\mathbb{Z}$ and $X \in \mathfrak{sl}_2(\mathbb{R})$. By central symmetry, $\rho_{j+3} = \rho_j$ and $\tilde{\rho}_{j+3} = \tilde{\rho}_j$. Solving this systems of linear equations for $\rho_j, \tilde{\rho}_j$ in terms of the matrix entries a, b, c of X , we obtain for all j that ρ_j is given by the statement of the lemma. Also, $\tilde{\rho}_j = \rho_j$. It follows that

$$\sqrt{3}|a| < c \quad 3b + c < 0.$$

In particular, $c > 0$. Using these values, we have by direct calculation that

$$\det(X) = \rho_0\rho_1 + \rho_1\rho_2 + \rho_2\rho_0 > 0. \quad (3.1.7)$$

□

Remark 3.1.7 (Reconstructing the hexagon). *Given $X \in \mathfrak{sl}_2(\mathbb{R})$ satisfying the star inequalities in the conclusion of the corollary, we can reconstruct a centrally symmetric hexagon whose edge midpoints are the points \mathbf{s}_j^* and such that the hexagon satisfies the star conditions. The edge direction at \mathbf{s}_j^* is $X\mathbf{s}_j^*$. Two elements in the Lie algebra give the same hexagon if one element is a positive multiple of the other.*

The vertices of the hexagon are constructed as the solutions to linear equations; each vertex is the point of intersection between the line through \mathbf{s}_j^ in direction $X\mathbf{s}_j^*$ and the line through \mathbf{s}_{j+1}^* in the direction $X\mathbf{s}_{j+1}^*$. Explicitly, by solving the equations, the vertex is*

$$\mathbf{s}_j^* + \frac{\rho_{j+2}(X)}{\det(X)}X\mathbf{s}_j^* = \mathbf{s}_{j+1}^* - \frac{\rho_j(X)}{\det(X)}X\mathbf{s}_{j+1}^*. \quad (3.1.8)$$

Each \mathbf{s}_j^ is manifestly an edge midpoint, given as the midpoint of vertices $\mathbf{s}_j^* \pm \rho_{j+2}(X)X\mathbf{s}_j^*/\det(X)$.*

The following fact is an easy corollary of Reinhardt's observations about the significance of hyperbolic arcs.

Lemma 3.1.8. *Suppose that $K \in \mathfrak{K}_{ccs}$. Assume the boundary is parameterized by a C^1 multi-curve σ . If two curves σ_{i-1} and σ_{i+1} move along straight lines during some time interval, then the third curve σ_i moves along a hyperbolic arc, whose asymptotes are the lines determined by σ_{i-1} and σ_{i+1} .*

Proof. For simplicity and without loss of generality, take $i = 0$. The curves $\pm\sigma_1$ and $\pm\sigma_{-1}$ trace out lines that form four of the edges (forming a fixed parallelogram P_K) of the time dependent critical hexagon $H_K(t)$. The tangent lines to $\pm\sigma_0(t)$ form the final two edges of the critical hexagon, and $\pm\sigma_0(t)$ are the midpoints of those edges. As t varies, the area cut off by these two tangent lines from the parallelogram P_K is constant, because the areas of P_K and $H_K(t)$ are both constant. As Reinhardt observed, the pencil of lines cutting a constant area from (two adjacent edges of) a parallelogram has an envelope that is a hyperbola whose asymptotes are the lines extending the edges of the parallelogram. The midpoints $\sigma_0(t)$ must lie on that envelope, a hyperbola with the required properties. \square

If $K \in \mathfrak{K}_{bal}$ has boundary parameterization $\sigma_j(t) = g(t)\mathbf{s}_j^*$, then the midpoint hexagon H_K of K at the multi-point $g(t_0)\mathbf{s}_j^*$ is the left translate by $g(t_0)$ of the hexagon constructed in the Remark 3.1.7 using $X = X(t_0) = g^{-1}g'(t_0)$.

We have one equation for our state space dynamics viz., equation $g' = gX$. Before deriving dynamics in the Lie algebra, we shift to a more convenient choice of parameterization.

Proposition 3.1.9. *Let s denote the arclength parameter of σ_0 , and let $\tilde{X}(t)$ denote the reparameterization of the matrix-valued curve X , using the reparameterization of g to a time variable t such that $\det(\tilde{X}(t)) = 1$. Then we have that $t \mapsto \tilde{X}(t)$ is a Lipschitz continuous function.*

Proof. Reparameterize $\tilde{g}(t) := g(s(t))$. In this new parameterization, we define \tilde{X} by the differential relation $d\tilde{g}(t)/dt = \tilde{g}(t)\tilde{X}(t)$. We have by the chain rule:

$$\begin{aligned} \frac{d\tilde{g}(t)}{dt} &= \frac{d}{dt}g(s(t)) = \frac{d}{ds}g(s(t))\frac{ds}{dt} \\ &= g(s)X(s)\frac{ds}{dt}. \end{aligned}$$

So that $\tilde{X}(t) = X(s(t)) \frac{ds}{dt}$. Now we require $\det(\tilde{X}(t)) = 1$, which forces

$$\frac{ds}{dt} = \frac{1}{\det(X(s))^{1/2}},$$

which gives us the reparameterization equation. By Corollary 3.1.6 we have $\det(X(s)) > 0$ so that the right-hand side is real and finite. Recall that we have that $X(s)$ is Lipschitz by Theorem 3.1.4 and $\det(X(s))$ is bounded away from zero since it is a continuous function on a compact interval. Then ds/dt is Lipschitz. This proves that \tilde{X} is Lipschitz as well. \square

By abuse of notation, we let t denote the new parameter, so that $\det(X(t)) = 1$.

Corollary 3.1.10. *With respect to the parameterization making $\det(X(t)) = 1$, the curve X is differentiable almost everywhere.*

Proof. This follows from Rademacher's theorem and Proposition 3.1.9. \square

Corollary 3.1.11. *A parameterization which makes $\det(X(t))$ a constant also makes $X + X^{-1}X' \in \mathfrak{sl}_2(\mathbb{R})$ almost everywhere, and conversely.*

Proof. This is immediate from the Jacobi's formula for the derivative of a determinant (Lemma 3.1.12):

$$\frac{\det(X)'}{\det(X)} = \text{trace}(X^{-1}X'), \quad (3.1.9)$$

and from $\text{trace}(X) = 0$. \square

Lemma 3.1.12 (Jacobi's formula). *Let A be a differentiable function taking values in $\text{GL}_n(\mathbb{C})$. Then*

$$\det(A)' = \det(A)\text{trace}(A^{-1}A').$$

(The same formula holds without the assumption that A is invertible, if $\det(A)A^{-1}$ is replaced with the adjugate of A .)

Proof. Both sides of the Jacobi formula are polynomials in the matrix coefficients of A and A' . It is therefore sufficient to verify the polynomial identity on the dense subset where the eigenvalues of A are distinct and nonzero.

If A factors differentiably as $A = A_1 A_2$, then

$$\mathrm{tr}(A^{-1}A') = \mathrm{tr}(A_1^{-1}A'_1) + \mathrm{tr}(A_2^{-1}A'_2).$$

In particular, if L is invertible, then $I = L^{-1}L$ and

$$0 = \mathrm{tr}(I^{-1}I') = \mathrm{tr}(L(L^{-1})') + \mathrm{tr}(L^{-1}L').$$

Since A has distinct eigenvalues, there exists a differentiable complex invertible matrix L such that $A = L^{-1}DL$ and D is diagonal. Then

$$\mathrm{tr}(A^{-1}A') = \mathrm{tr}(L(L^{-1})') + \mathrm{tr}(D^{-1}D') + \mathrm{tr}(L^{-1}L') = \mathrm{tr}(D^{-1}D').$$

Let λ_i , $i = 1, \dots, n$ be the eigenvalues of A . Then

$$\frac{\det(A)'}{\det(A)} = \sum_{i=1}^n \lambda'_i / \lambda_i = \mathrm{tr}(D^{-1}D') = \mathrm{tr}(A^{-1}A'),$$

which is the Jacobi formula for matrices A with distinct nonzero eigenvalues. □

3.2 The Cost Functional

We now compute the cost functional in terms of the matrix-valued curve X parameterized as above. From the balanced Reinhardt problem 2.4.8 in circle representation, we see that the quantity to be minimized is the area of a convex disk in \mathfrak{K}_{bal} . Our strategy is to compute this area using Green's theorem, by using the pullback of the one-form $xdy - ydx$ on \mathbb{R}^2 . We let \cdot^{tr} denote the transpose of a matrix.

Lemma 3.2.1. *Let $g : [0, t_f] \rightarrow \mathrm{SL}_2(\mathbb{R})$ be a path so that $g' = gX$ as above and let $\mathbf{u} \in \mathbb{R}^2$. Define $\gamma : [0, t_f] \rightarrow \mathbb{R}^2$ by $\gamma(t) := g(t)\mathbf{u}$. Consider the one-form $\theta = xdy - ydx$ on \mathbb{R}^2 . Then we have the following formula for the pullback of θ to $[0, t_f]$:*

$$\gamma^* \theta = -\mathbf{u}^{tr} J X \mathbf{u} dt.$$

Proof. If we write $\gamma(t) = (\gamma_1(t), \gamma_2(t))$, then

$$\begin{aligned}\gamma^* \theta &= \theta(\gamma(t)) \\ &= (\gamma_1(t)\gamma'_2(t) - \gamma_2(t)\gamma'_1(t)) dt \\ &= (\det(\gamma, \gamma')) dt \\ &= (\det(g\mathbf{u}, gX\mathbf{u})) dt \\ &= (\det(\mathbf{u}, X\mathbf{u})) dt \\ &= -\mathbf{u}^{tr} JX\mathbf{u} dt,\end{aligned}$$

since $\det(g) = 1$ and

$$\det(\mathbf{u}, X\mathbf{v}) = -\mathbf{u}^{tr} JX\mathbf{v}, \quad (3.2.1)$$

for all $X \in \mathfrak{sl}_2(\mathbb{R})$ and $\mathbf{u}, \mathbf{v} \in \mathbb{R}^2$. \square

The lemma above enables us to compute pullbacks of θ by the multi-curves σ_j . Indeed, the boundary ∂K of an arbitrary balanced convex disk $K \in \mathfrak{K}_{bal}$ is a simple closed curve parameterized by the curves σ , given by $\sigma_j(t) = g(t)\mathbf{s}_j^* = g(t)(R^j\mathbf{s}_0^*)$.

Lemma 3.2.2. *Let $Y \in \mathfrak{sl}_2(\mathbb{R})$. Then we have*

$$JY + (R^2)^{tr} JY R^2 + (R^4)^{tr} JY R^4 = \frac{3\text{trace}(JY)}{2} I_2,$$

where I_2 is the 2×2 identity matrix.

Proof. This is a simple computation. \square

We now derive a formula for the area of $K \in \mathfrak{K}_{bal}$. By Green's theorem

and the lemmas from above, we have

$$\begin{aligned}
\text{area}(K) &= \frac{1}{2} \oint_{\partial K} \theta \\
&= \frac{1}{2} \int_0^{t_f} \gamma^* \theta dt \\
&= \int_0^{t_f} \sigma_0^* \theta + \sigma_2^* \theta + \sigma_4^* \theta dt \quad (\text{by Lemma 3.2.1}) \\
&= \int_0^{t_f} -\mathbf{u}^{tr} JX \mathbf{u} - (R^2 \mathbf{u})^{tr} JX (R^2 \mathbf{u}) - (R^4 \mathbf{u})^{tr} JX (R^4 \mathbf{u}) dt \\
&= - \int_0^{t_f} \mathbf{u}^{tr} (JX + (R^2)^{tr} JX R^2 + (R^4)^{tr} JX R^4) \mathbf{u} dt \\
&= - \int_0^{t_f} |\mathbf{u}|^2 \frac{3\text{trace}(JX)}{2} dt \quad (\text{by Lemma 3.2.2}).
\end{aligned}$$

The parameterization of convex disk K is of the form $\sigma_0(t) = g(t)\mathbf{s}_0^*$, which means that $\mathbf{u} = \mathbf{s}_0^* = (1, 0)$. So $|\mathbf{u}| = 1$ and

$$\text{area}(K) = -\frac{3}{2} \int_0^{t_f} \text{trace}(JX) dt, \quad (3.2.2)$$

which is the quantity to be minimized.

Example. We show that the area of a unit disk K is π , as expected, by using (3.2.2). In this case,

$$g(t) = \exp(Jt), \quad X(t) = J, \quad t_f = \pi/3 \quad (\text{one-sixth the circumference}),$$

where $\exp(-)$ is the matrix exponential. Note that X is a constant curve in this case. Then

$$\text{area}(K) = -\frac{3}{2} \int_0^{t_f} \text{trace}(JX) dt = -\frac{3}{2} \text{trace}(J^2) \int_0^{\pi/3} dt = -\frac{3}{2} (-2) \frac{\pi}{3} = \pi.$$

3.3 Control Sets

We now investigate the *control* parameters which affect this cost. It is intuitively obvious that the curvature of the curves making up the boundary

of the convex disk $K \in \mathcal{K}_{bal}$ affect its area. So, it makes sense to allow the curvatures to play the role of the controls. Problems in which curvature plays the role of a control are well-studied in the literature, the Dubins-Delauney problem being one a prominent such example [20]. Other examples, such as Kirchoff's problem and the elastic problem are discussed in [21].

To begin, recall that Lemma 2.4.6 says that $\det(\sigma'_j(t), \sigma''_j(t)) \geq 0$ almost everywhere in t . Now since our convex disk is in circle representation, we have $\sigma_j(t) = g(t)\mathbf{s}_j^*$. Then we have, for $j = 0, 1, 2$,

$$\begin{aligned}\kappa_j(t) := \det(\sigma'_{2j}(t), \sigma''_{2j}(t)) &= \det(g'(t)\mathbf{s}_{2j}^*, g''(t)\mathbf{s}_{2j}^*) \\ &= \det(gX\mathbf{s}_{2j}^*, (gX^2 + gX')\mathbf{s}_{2j}^*) \\ &= \det(X\mathbf{s}_{2j}^*, (X^2 + X')\mathbf{s}_{2j}^*) \\ &= \det(\mathbf{s}_{2j}^*, (X + X^{-1}X')\mathbf{s}_{2j}^*) \geq 0,\end{aligned}\quad (3.3.1)$$

almost everywhere in t . Here we used Proposition 3.1.9 and Corollaries 3.1.6 and 3.1.10. We call $\kappa_j(t)$ the *state-dependent curvature* as it depends on where we are in the state space. Note the indexing conventions $j \leftrightarrow 2j$ relating κ_j and σ_{2j} .

Lemma 3.3.1. *Let $g : [0, t_f] \rightarrow \text{SL}_2(\mathbb{R})$ be C^1 with Lipschitz derivative satisfying the star and curvature conditions (3.3.1). Then almost everywhere, there exists an index j so that $\kappa_j(t) > 0$.*

Proof. Take $X = g^{-1}g'$. Assuming $\kappa_0, \kappa_1 = 0$, a short calculation shows almost everywhere that

$$\kappa_2(t) = \det(\mathbf{s}_4^*, (X + X^{-1}X')\mathbf{s}_4^*) = \frac{\sqrt{3}\det(X)}{\rho_0(X)}.$$

This is strictly positive by the star inequalities in Corollary 3.1.6. (This gives a second interpretation of the functions ρ_i in terms of state-dependent curvatures.)

A second proof can be obtained from Lemma 3.1.8: if two of the state-dependent curvatures are zero, then the third curvature is such that associated curve is an arc of a hyperbola. Hence the third curvature is positive.

A third proof appears at the end of the proof of Theorem 3.4.2, which gives a formula for $\kappa_0 + \kappa_1 + \kappa_2$ as a ratio of negative numbers. \square

Since the state-dependent curvatures $\kappa_j(t)$ depend on X and X' in general, they are not suitable as control variables for our control problem. To this end, we introduce normalizations of the state-dependent curvatures as follows.

Definition 3.3.2 (control variables). *For each $j = 0, 1, 2$, define control variables given by the normalized state-dependent curvatures as*

$$u_j := \frac{\kappa_j}{\kappa_0 + \kappa_1 + \kappa_2}.$$

Note that the denominator is positive by Lemma 3.3.1. The control variables u_i evidently satisfy $0 \leq u_i \leq 1$ and $u_0 + u_1 + u_2 = 1$. Note also that the control variables are functions of time.

Definition 3.3.3 (Triangular control set). *The triangular or simplex control set is the set*

$$U_T := \{(u_0, u_1, u_2) \mid 0 \leq u_i \leq 1, u_0 + u_1 + u_2 = 1\},$$

which is just the two-simplex in \mathbb{R}^3 .

We map the control set U_T into the Lie algebra $\mathfrak{sl}_2(\mathbb{R})$ using the following transformation:

$$Z_u = \begin{pmatrix} \frac{u_1 - u_2}{\sqrt{3}} & \frac{u_0 - 2u_1 - 2u_2}{3} \\ u_0 & \frac{u_2 - u_1}{\sqrt{3}} \end{pmatrix} \in \mathfrak{sl}_2(\mathbb{R}), \quad u = (u_0, u_1, u_2) \in U_T. \quad (3.3.2)$$

This *control matrix* $Z_u \in \mathfrak{sl}_2(\mathbb{R})$ is uniquely determined by the equations

$$u_j = \det(\mathbf{s}_{2j}^*, Z_u \mathbf{s}_{2j}^*) \quad j = 0, 1, 2. \quad (3.3.3)$$

In summary, the optimal control function of the control problem takes values in the two-simplex U_T . The values in U_T specify the values of curvature functions, which determine the boundary curves of a convex disk $K \in \mathcal{K}_{bal}$. The optimal control function minimizes the area of K .

Henceforth, we adopt the notation $\langle X, Y \rangle := \text{trace}(XY)$, for any two matrices $X, Y \in \mathfrak{sl}_2(\mathbb{R})$. This form is a nondegenerate invariant bilinear form on $\mathfrak{sl}_2(\mathbb{R})$.

We can now prove an equivalent star condition.

Lemma 3.3.4. *The star inequalities on X hold if and only if $\langle Z_u, X \rangle < 0$ for all controls $u \in U_T$.*

Proof. An easy calculation gives the following identity.

$$\langle Z_u, X \rangle = -\frac{2}{\sqrt{3}}(\rho_2(X)u_0 + \rho_1(X)u_1 + \rho_0(X)u_2).$$

The right-hand side is everywhere negative on U_T if and only if $\rho_j(X) > 0$, for $j = 0, 1, 2$. These are the star inequalities on X . \square

3.4 Lie Algebra Dynamics

Let us first collect a number of results about matrices in $\mathfrak{sl}_2(\mathbb{R})$ which we will need. All of these are elementary and so we admit them without proofs. Let $[X, Y] = XY - YX$ be the Lie algebra commutator of two matrices $X, Y \in \mathfrak{sl}_2(\mathbb{R})$.

Lemma 3.4.1. *We have the following results about matrices in $\mathfrak{sl}_2(\mathbb{R})$.*

1. *If $X \in \mathfrak{sl}_2(\mathbb{R})$, $\langle X, X \rangle = -2 \det(X)$.*
2. *If X, Y are any two matrices in $\mathfrak{sl}_2(\mathbb{R})$, and \mathbf{s} is a multi-point*

$$\det(\mathbf{s}_j, X\mathbf{s}_j) = \det(\mathbf{s}_j, Y\mathbf{s}_j), \quad j = 0, 1, 2,$$

then $X = Y$.

3. *If $X, Y \in \mathfrak{sl}_2(\mathbb{R})$ then $XY + YX = \langle X, Y \rangle I_2$.*
4. *For any matrices $X, Y, Z \in \mathfrak{sl}_2(\mathbb{R})$ we have $\langle X, [Y, Z] \rangle = \langle [X, Y], Z \rangle$.*

We return to X as the trajectory defined by $g' = gX$. Let us now derive the control-dependent dynamics for X .

Theorem 3.4.2 (Dynamics for X). *The dynamics for X (which is control-dependent) is given by*

$$X' = \frac{[Z_u, X]}{\langle Z_u, X \rangle}.$$

It is shown in Lemma 3.3.4 that the star conditions imply $\langle Z_u, X \rangle < 0$, for all controls $u \in U_T$. The denominator $\langle Z_u, X \rangle$ appearing in the theorem is therefore nonzero.

Proof. By Corollary 3.1.11, we find $X + X^{-1}X' \in \mathfrak{sl}_2(\mathbb{R})$. From Equations (3.3.1) and (3.3.3) we find

$$\begin{aligned} u_j &= \det(\mathbf{s}_{2j}^*, Z_u \mathbf{s}_{2j}^*) \\ \kappa_j &= \det(\mathbf{s}_{2j}^*, (X + X^{-1}X') \mathbf{s}_{2j}^*), \end{aligned}$$

for each j . Let $\kappa = \kappa_1 + \kappa_2 + \kappa_3$. Since, by Definition 3.3.2, we have $\kappa u_j = \kappa_j$, by Lemma 3.4.1,(2) we obtain that

$$X + X^{-1}X' = \kappa Z_u,$$

from which we obtain

$$X' = X(\kappa Z_u - X). \quad (3.4.1)$$

Taking traces and using $\text{trace}(X') = 0$, we obtain $\kappa = \langle X, X \rangle / \langle X, Z_u \rangle = -2 / \langle X, Z_u \rangle$, where the last equality uses Lemma 3.4.1,(1). Let $P = Z_u / \langle X, Z_u \rangle$. We have $\langle P, X \rangle = 1$ and

$$\begin{aligned} [P, X] &= PX - XP = -2XP + (PX + XP) \\ &= -2XP + \langle P, X \rangle I_2 \quad \text{from Lemma 3.4.1, (3)} \\ &= -2XP + I_2 \\ &= \kappa XZ_u - X^2 \quad \text{from Lemma 3.4.1, (1, 3)} \\ &= X', \end{aligned}$$

which proves the claimed differential equation. \square

Remark 3.4.3.

1. The equation $X' = [P, X]$ where P, X are time-dependent matrices is called the *Lax equation* and X, P so related are called a *Lax equation*. Lax equations are well-studied in the theory of integrable systems (see Perelomov [39], Jurdjevic [21], Babelon et al. [3]). Lax representations of integrable systems are quite desirable since the evolution of a Lax equation is *isospectral*, meaning that the spectrum of the matrix X is an invariant of motion.
2. The dynamics for X is Hamiltonian for a particular Hamiltonian defined on $\mathfrak{sl}_2(\mathbb{R})$, with respect to a Poisson structure on $\mathfrak{sl}_2(\mathbb{R})$ called the *Lie-Poisson structure*. See Appendix A.8 for more details.
3. As explained in Perelomov [39, p. 52], the spectral invariants guaranteed by the dynamics for X are *trivial* integrals, and so it is more accurate to consider the dynamics for X as giving a control-dependent infinitesimal generator for the (co)adjoint action of $\text{SL}_2(\mathbb{R})$ on $\mathfrak{sl}_2(\mathbb{R})$, rather than to regard it as describing the dynamics of an integrable system.
4. The equation (3.4.1) appears in [16], where its Lax equation reformulation was not explicitly recognized.

3.5 Initial and Terminal Conditions

We now have dynamics for g and X in the Lie group and Lie algebra respectively. We also have an associated cost objective. The only thing remaining is to specify initial and terminal conditions. Since our convex disk is in circle representation, this means that $\sigma_j(0) = \mathbf{s}_j^*$ so that we start out at the sixth roots of unity, and so we set $g(0) = I_2$. The initial condition $X(0) = X_0$ may be an arbitrary matrix in $\mathfrak{sl}_2(\mathbb{R})$ of determinant 1, provided it satisfies the star conditions in Corollary 3.1.6.

The terminal conditions $g(t_f)$ should be such that the curves σ_j close up seamlessly to form a simple closed curve:

$$g(t_f)\mathbf{s}_j^* = g(0)\mathbf{s}_{j+1}^* \Leftrightarrow g(t_f) = R, \quad (3.5.1)$$

where R is the usual rotation matrix. For terminal conditions on X , note that we have the following conditions on g which we obtain by the remark following Theorem 3.1.1 (and setting $t_0 = 0$ there):

$$g(t + t_f)\mathbf{s}_j^* = g(s(t))\mathbf{s}_{j+1}^* = g(s(t))R\mathbf{s}_j^*; \quad g(t + t_f) = g(s(t))R,$$

for some orientation-preserving reparameterization $s(t)$ such that $s(0) = 0$. Differentiating, we obtain

$$X(t + t_f) = R^{-1}X(s(t))R \frac{ds}{dt},$$

which gives us $X(t_f) = R^{-1}X_0Rds/dt$. Using $\det(X) = 1$ and $ds/dt > 0$, we get $ds/dt = 1$, $s(t) = t$, and

$$X(t_f) = R^{-1}X_0R.$$

3.6 Reinhardt Optimal Control Problem

Summarizing the discussion so far, we are finally ready to state the Reinhardt conjecture as an optimal control problem. Let us begin with a well-known proposition on the trivialization of the tangent and cotangent bundles of a Lie group.

Proposition 3.6.1. *Let G be any real Lie group and let \mathfrak{g} be its Lie algebra. Then we have $T^*G \cong G \times \mathfrak{g}^*$ and $TG \cong G \times \mathfrak{g}$, where \mathfrak{g}^* is the linear dual of \mathfrak{g} .*

Proof. The Lie algebra \mathfrak{g} is the tangent space of G at the neutral element $e \in G$. Let $L_g : G \rightarrow G$ be left-multiplication by g , given by $L_g(h) := gh$, The tangent map

$$TL_g : T_e G \rightarrow T_{gh} G,$$

at $h = e$ is an isomorphism from $T_e G$ to $T_g G$, the tangent spaces at e and g . This isomorphism gives the trivialization of the tangent bundle $TG \cong G \times \mathfrak{g}$. Dually, each fiber $T_g^* G$ of the cotangent bundle is canonically isomorphic to the dual $T_e^* G = \mathfrak{g}^*$. This trivializes the cotangent bundle. \square

The above proposition and remark apply to $\mathrm{SL}_2(\mathbb{R})$. Using this, we group together the state equations, controls and cost functional to give a well-defined control problem.

Problem 3.6.2 (Reinhardt Control Problem). *The convex disks in \mathfrak{K}_{bal} in circle representation arise via the following optimal control problem. On the manifold $\mathrm{SL}_2(\mathbb{R}) \times \mathfrak{sl}_2(\mathbb{R}) \cong T\mathrm{SL}_2(\mathbb{R})$, consider the following optimal control problem with free-terminal time.*

$$g' = gX, \quad g : [0, t_f] \rightarrow \mathrm{SL}_2(\mathbb{R}); \quad (3.6.1)$$

$$X' = \frac{[Z_u, X]}{\langle Z_u, X \rangle}, \quad X : [0, t_f] \rightarrow \mathfrak{sl}_2(\mathbb{R}); \quad (3.6.2)$$

$$-\frac{3}{2} \int_0^{t_f} \langle J, X \rangle dt \rightarrow \min, \quad J = \begin{pmatrix} 0 & -1 \\ 1 & 0 \end{pmatrix}, \quad (3.6.3)$$

where the set of controls for this problem is the image of the two-simplex U_T in \mathbb{R}^3 inside the Lie algebra $\mathfrak{sl}_2(\mathbb{R})$ via the affine map Z_u .

$$Z : U_T = \left\{ (u_0, u_1, u_2) \mid \sum_i u_i = 1, u_i \geq 0 \right\} \rightarrow \mathfrak{sl}_2(\mathbb{R}) \quad (3.6.4)$$

$$Z_u = \begin{pmatrix} \frac{u_1 - u_2}{\sqrt{3}} & \frac{u_0 - 2u_1 - 2u_2}{3} \\ u_0 & \frac{u_2 - u_1}{\sqrt{3}} \end{pmatrix}. \quad (3.6.5)$$

The initial conditions are $g(0) = I_2 \in \mathrm{SL}_2(\mathbb{R})$ and $X(0) = X_0 \in \mathfrak{sl}_2(\mathbb{R})$ satisfying the star conditions. Also, the terminal conditions are $g(t_f) = R$ and $X(t_f) = RX_0R^{-1}$ where R is the usual rotation matrix (3.1.2).

Chapter 4

The Upper Half-Plane

Now that we have the optimal control problem fully stated, a natural next step would be to write down the necessary conditions for optimality of trajectories. But before we do that, we will first cut down the state space of the problem.

4.1 The Adjoint Orbit

Recall that the star conditions (Corollary 3.1.6) on the matrix X imply that $\langle J, X \rangle$ is negative. We have also imposed the condition $\det(X) = 1$. We begin with a characterization of such matrices.

Lemma 4.1.1. *The set of matrices $X \in \mathfrak{sl}_2(\mathbb{R})$ with $\det(X) = 1$ and $\langle J, X \rangle < 0$ is the adjoint orbit $\mathcal{O}_J := \{\text{Ad}_g J \mid g \in \text{SL}_2(\mathbb{R})\}$ in $\mathfrak{sl}_2(\mathbb{R})$ of the infinitesimal generator J .*

Proof. The adjoint orbit \mathcal{O}_J of J in $\mathfrak{sl}_2(\mathbb{R})$ consists of elements gJg^{-1} for $g \in \text{SL}_2(\mathbb{R})$. The Iwasawa decomposition of $\text{SL}_2(\mathbb{R})$ implies that g belongs to a left coset $h \text{SO}_2(\mathbb{R})$ where

$$h = \begin{pmatrix} 1 & x \\ 0 & 1 \end{pmatrix} \begin{pmatrix} \sqrt{y} & 0 \\ 0 & 1/\sqrt{y} \end{pmatrix}, \quad y > 0.$$

Since $\text{SO}_2(\mathbb{R})$ centralizes J , the orbit consists of elements

$$gJg^{-1} = hJh^{-1} = \begin{pmatrix} x/y & -(x^2 + y^2)/y \\ 1/y & -x/y \end{pmatrix} =: \Phi(z), \quad z = x+iy \in \mathfrak{h}. \quad (4.1.1)$$

This is precisely the form of a general element X satisfying the conditions of the lemma. Hence, the result follows. \square

Remark 4.1.2. Since $\mathfrak{sl}_2(\mathbb{R})$ admits a nondegenerate invariant symmetric bilinear form $\langle \cdot, \cdot \rangle$, the Lie algebra can be identified with its linear dual, by identifying $X \in \mathfrak{sl}_2(\mathbb{R})$ with the linear functional

$$Y \mapsto \langle Y, X \rangle$$

on $\mathfrak{sl}_2(\mathbb{R})$. Under this identification, the coadjoint orbits and adjoint orbits become identified. See Appendix A.10 and also Chapter 5 of Jurdjevic [19].

4.2 Transfer of Dynamics to the Upper Half-Plane

The group $\mathrm{SL}_2(\mathbb{R})$ acts on the upper-half plane

$$\mathfrak{h} = \{x + iy \mid y > 0\}$$

by linear fractional transformations (or Möbius transformations).

$$\mathrm{SL}_2(\mathbb{R}) \times \mathfrak{h} \rightarrow \mathfrak{h}, \quad \begin{pmatrix} a & b \\ c & d \end{pmatrix} \cdot z = \frac{az + b}{cz + d}. \quad (4.2.1)$$

We denote the action by (\cdot) .

By the orbit-stabilizer theorem, we have $\mathcal{O}_J \cong \mathrm{SL}_2(\mathbb{R})/\mathrm{SO}_2(\mathbb{R})$, since the stabilizer of J in $\mathrm{SL}_2(\mathbb{R})$ under the conjugation action (the centralizer) is $\mathrm{SO}_2(\mathbb{R})$. Viewing this in a different way, the group $\mathrm{SL}_2(\mathbb{R})$ acts on the upper half-plane \mathfrak{h} by linear fractional transformations, with stabilizer of $i \in \mathfrak{h}$ being given by $\mathrm{SO}_2(\mathbb{R})$. Thus, the quotient is isomorphic to the Poincaré upper half-plane \mathfrak{h} . Putting all of this together, we have

Lemma 4.2.1. *The following map Φ is a isomorphism.*

$$\Phi : \mathfrak{h} \rightarrow \mathcal{O}_J$$

$$z = x + iy \mapsto \Phi(z) := \begin{pmatrix} x/y & -(x^2 + y^2)/y \\ 1/y & -x/y \end{pmatrix}.$$

Remark 4.2.2.

- Note that $\mathcal{O}_J = \mathcal{O}_{\Phi(z)}$ as $\Phi(z) \in \mathcal{O}_J$.
- We write X in place of $\Phi(z)$ for simplicity, bearing in mind that Φ is surjective onto \mathcal{O}_J .
- Note that $\Phi(z)$ is a regular semisimple element of the Lie algebra $\mathfrak{sl}_2(\mathbb{R})$ because the element J is.
- The map Φ is $\mathrm{SL}_2(\mathbb{R})$ -equivariant for the action by linear fractional transformations on \mathfrak{h} . That is, for every $g \in \mathrm{SL}_2(\mathbb{R})$,

$$g\Phi(z)g^{-1} = \Phi(g \cdot z).$$

This map Φ allows us to move back and forth between the upper half-planes and the adjoint orbit in the Lie algebra $\mathfrak{sl}_2(\mathbb{R})$. Also, the map Φ is more than just a bijection — we show later that this map is actually an anti-symplectomorphism and use this to transfer the state and costate dynamics from the Lie algebra to the upper half-plane. But first, we compute the tangent map $T\Phi$ at a $z \in \mathfrak{h}$.

Lemma 4.2.3. *For any $X \in \mathfrak{sl}_2(\mathbb{R})$, we have*

$$T_X \mathcal{O}_X = \{[Y, X] \mid Y \in \mathfrak{sl}_2(\mathbb{R})\} \cong \mathfrak{sl}_2(\mathbb{R})/\mathbb{R}X,$$

where $\mathbb{R}X$ is the span of the element X and $T_X \mathcal{O}_X$ denotes the tangent space to \mathcal{O}_X at X .

Explicitly, the first equality views the tangent space at X of the manifold \mathcal{O}_X as a subspace of $\mathfrak{sl}_2(\mathbb{R}) \cong T_X \mathfrak{sl}_2(\mathbb{R})$, the tangent space at X of the ambient space $\mathfrak{sl}_2(\mathbb{R})$. The isomorphism on the right is given by $[Y, X] \mapsto Y + \mathbb{R}X$.

Proof. Note that $\mathcal{O}_X = \{\mathrm{Ad}_g X \mid g \in \mathrm{SL}_2(\mathbb{R})\}$. We have to describe tangent vectors to \mathcal{O}_X . For any $Y \in \mathfrak{sl}_2(\mathbb{R})$, $\mathrm{Ad}_{\exp(tY)} X$ is a curve in \mathcal{O}_X . Thus, the tangent vector to this curve is computed as

$$\frac{d}{dt} \mathrm{Ad}_{\exp(tY)} X \Big|_{t=0} = \mathrm{ad}_Y X := [Y, X] \in T_X \mathcal{O}_X.$$

This calculation is actually finding infinitesimal generators of the adjoint action. There is an isomorphism

$$\mathfrak{sl}_2(\mathbb{R})/\mathfrak{sl}_2(\mathbb{R})_X \cong \{[Y, X] \mid Y \in \mathfrak{sl}_2(\mathbb{R})\}, \quad Y \mapsto [Y, X],$$

where $\mathfrak{sl}_2(\mathbb{R})_X$ is the isotropy algebra (the centralizer) of the element X . The element X is regular in the rank one algebra $\mathfrak{sl}_2(\mathbb{R})$, so that its centralizer $\mathfrak{sl}_2(\mathbb{R})_X$ is the span $\mathbb{R}X$ of X . \square

We write $[Y]$ for the coset $Y + \mathbb{R}X$ in $\mathfrak{sl}_2(\mathbb{R})/\mathbb{R}X$.

Lemma 4.2.4. *We have the following expression for the tangent map $T\Phi$.*

$$T\Phi : T_z\mathfrak{h} \rightarrow T_X\mathcal{O}_X \cong \mathfrak{sl}_2(\mathbb{R})/\mathbb{R}X \quad (4.2.2)$$

$$(r_1 \frac{\partial}{\partial x} + r_2 \frac{\partial}{\partial y}) \mapsto \begin{pmatrix} r_2/2y & (yr_1 - r_2x)/y \\ 0 & -r_2/2y \end{pmatrix} \pmod{\mathbb{R}X}. \quad (4.2.3)$$

Proof. We have, at $z = x + iy$ and $X = \Phi(z)$:

$$T_z\Phi(r_1, r_2) = \frac{d}{dt}\Phi(x + tr_1, y + tr_2)\Big|_{t=0} \quad (4.2.4)$$

$$= r_1 \frac{\partial\Phi}{\partial x} + r_2 \frac{\partial\Phi}{\partial y} \in T_X\mathcal{O}_X. \quad (4.2.5)$$

We know by the previous lemma that there exists a matrix Y_z such that

$$T_z\Phi(r_1, r_2) = r_1 \frac{\partial\Phi}{\partial x} + r_2 \frac{\partial\Phi}{\partial y} = [Y_z(r_1, r_2), X].$$

Using this equation to solve for this matrix Y_z gives us the following.

$$Y_z \equiv \begin{pmatrix} r_2/2y & (yr_1 - r_2x)/y \\ 0 & -r_2/2y \end{pmatrix} \pmod{\mathbb{R}X}. \quad (4.2.6)$$

So, for any arbitrary vector $(r_1, r_2) \in T_z\mathfrak{h}$ we obtain its image inside the quotient space $\mathfrak{sl}_2(\mathbb{R})/\mathbb{R}X$. \square

4.3 The Cost Functional in Half-Plane Coordinates

We can also compute the cost functional that we derived in Section 3.2 in half-plane coordinates. From equation (3.2.2), we have

$$-\frac{3}{2} \int_0^{t_f} \langle J, X \rangle dt = \frac{3}{2} \int_0^{t_f} \frac{x^2 + y^2 + 1}{y} dt \rightarrow \min. \quad (4.3.1)$$

The cost functional is $\text{SO}_2(\mathbb{R})$ -invariant, because if A is any rotation matrix, then

$$\langle J, \text{Ad}_A X \rangle = \langle \text{Ad}_{A^{-1}} J, X \rangle = \langle J, X \rangle.$$

The circular symmetry is also apparent in this reinterpretation. The level sets of $(x^2 + y^2 + 1)/y$ are concentric circles (with respect to the hyperbolic metric) centered at the point i in the upper half-plane. Thus, the cost is $\text{SO}_2(\mathbb{R})$ -invariant.

Lemma 4.3.1. *The global minimizer of the Reinhardt control problem has terminal time $t_f < \pi/3$.*

Proof. The global minimizer has area less than the area π of the unit circle K . We have $(x^2 + y^2 + 1)/y \geq (y + 1/y) \geq 2$, so that

$$\pi > \text{area}(K_{\min}) = \frac{3}{2} \int_0^{t_f} \frac{x^2 + y^2 + 1}{y} dt \geq \frac{3}{2} \int_0^{t_f} 2 dt = 3t_f.$$

□

Remark 4.3.2. The Poincaré upper half-plane is conformally equivalent to other models of hyperbolic geometry such as the Poincaré disk and the hyperboloid model. The cost functional derived above can also be derived in these models. In the disk model, $\mathbb{D} = \{w \in \mathbb{C} \mid |w| < 1\}$, for example, the cost of a path $w : [0, t_f] \rightarrow \mathbb{D}$ becomes

$$3 \int_0^{t_f} \frac{1 + |w|^2}{1 - |w|^2} dt \rightarrow \min.$$

In the hyperboloid model of hyperbolic geometry, the model is the upper sheet of the two-sheeted hyperboloid. In that model, the cost functional becomes the integral of the height function on the hyperboloid sheet. See [16].

4.4 The Star Domain in the Upper Half-Plane

We can now prove our first state space reduction result.

Theorem 4.4.1. *The dynamics of the Reinhardt control problem is constrained to an ideal triangle in the upper half-plane.*

$$\mathfrak{h}^* := \left\{ x + iy \in \mathfrak{h} \mid -\frac{1}{\sqrt{3}} < x < \frac{1}{\sqrt{3}}, \quad \frac{1}{3} < x^2 + y^2 \right\}. \quad (4.4.1)$$

Thus, the new state-space of the control problem is $\text{SL}_2(\mathbb{R}) \times \mathfrak{h}^*$.

Proof. The star conditions on X in Corollary 3.1.6 applied to $X = \Phi(z) = \Phi(x + iy)$ give us the conditions on x and y which an *admissible trajectory* should satisfy.

This region, called the *star domain*, is the interior of an ideal triangle in the upper half-plane. The vertices of this triangle are the points $z = \pm \frac{1}{\sqrt{3}}$ and $z = \infty$. A picture of the star domain is shown in Figure 4.4.1. \square

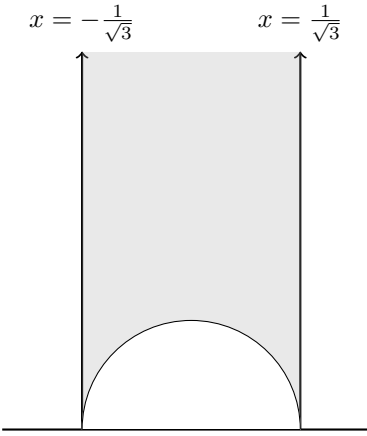


Figure 4.4.1: The star domain in the upper half-plane.

Summarizing the results so far, we have parameterized the boundary of convex disks in \mathfrak{K}_{bal} as U_T -controlled paths $(g(t), z(t)) \in \mathrm{SL}_2(\mathbb{R}) \times \mathfrak{h}^*$ subject to the terminal conditions. Our task is to find a *control function* $u(t) \in U_T$ which minimizes the area enclosed by the resulting curve, given in hyperbolic coordinates by equation (4.3.1).

4.5 Control Problem in the Half-Plane

Evolution of $X(t) = h(t)Jh(t)^{-1}$ by adjoint action in \mathcal{O}_J corresponds to evolution by linear fractional transformations of the corresponding element z_0 in the upper half-plane picture. If $\Phi(z_0) = X_0$ and $\Phi(z(t)) = X(t)$, then by the $\mathrm{SL}_2(\mathbb{R})$ -equivariance of Φ , the initial and terminal conditions derived in Section 3.5 are transformed as

$$\begin{aligned} X(0) = X_0 &\iff z(0) = z_0, \\ X(t_f) = R^{-1}X_0R &\iff z(t_f) = R^{-1} \cdot z_0, \end{aligned}$$

where R is the usual rotation matrix (3.1.2).

Thus, we obtain the following reformulation of the Reinhardt conjecture from the coadjoint orbit of the Lie algebra to the Poincaré upper half-plane.

Problem 4.5.1 (Half-Plane Control Problem). *On the set $\mathrm{SL}_2(\mathbb{R}) \times \mathfrak{h}^* \subset \mathrm{TSL}_2(\mathbb{R})$, consider the following free-terminal time optimal control problem.*

$$g' = gX, \quad X = \begin{pmatrix} x/y & -(x^2 + y^2)/y \\ 1/y & -x/y \end{pmatrix} = \Phi(x + iy),$$

$$x' = f_1(x, y; u) := \frac{y(2ax + b - cx^2 + cy^2)}{2ax + b - cx^2 - cy^2},$$

$$y' = f_2(x, y; u) := \frac{2y^2(a - cx)}{2ax + b - cx^2 - cy^2},$$

$$\frac{3}{2} \int_0^{t_f} \frac{x^2 + y^2 + 1}{y} dt \rightarrow \min,$$

$$g : [0, t_f] \rightarrow \mathrm{SL}_2(\mathbb{R}), \quad x, y : [0, t_f] \rightarrow \mathfrak{h}^*,$$

where the coefficients a, b, c are the following affine functions of the control (3.6.5).

$$a = a(u) = \frac{u_2 - u_1}{\sqrt{3}}, \quad b = b(u) = \frac{u_0 - 2u_1 - 2u_2}{3}, \quad c = c(u) = u_0,$$

with $u = (u_0, u_1, u_2) \in U_T$, which is the two-simplex in \mathbb{R}^3 . This problem has initial conditions $g(0) = I_2 \in \mathrm{SL}_2(\mathbb{R})$ and $z(0) = z_0 \in \mathfrak{h}^*$ and terminal conditions $g(t_f) = R$ and $z(t_f) = R^{-1} \cdot z_0$ where R is the usual rotation.

Lemma 4.5.2. *The ODE (3.6.2) for X implies the system of ODEs for x', y' in the half-plane optimal control problem 4.5.1.*

Proof. We compute

$$\begin{pmatrix} (yx' - xy')/y^2 & * \\ -y'/y^2 & * \end{pmatrix} = \Phi(z(t))' = \frac{[Z_u, \Phi(z)]}{\langle Z_u, \Phi(z) \rangle} = \begin{pmatrix} (yf_1 - xf_2)/y^2 & * \\ -f_2/y^2 & * \end{pmatrix}.$$

Comparing the left and right-hand sides of this equation, find that $x' = f_1$ and $y' = f_2$. This also shows that

$$T\Phi(f_1, f_2) = \left[\frac{Z_u}{\langle Z_u, X \rangle} \right] \in T_X \mathcal{O}_X. \quad (4.5.1)$$

□

Thus, we have transferred the Lie algebra dynamics to the upper half-plane. In Appendix A.10, we also prove that the map Φ is actually an anti-symplectomorphism onto the upper half-plane. Thus, it is entirely equivalent to study the control problem in the Lie algebra picture or the half-plane picture. We may also transfer the dynamics to other models of hyperbolic geometry: for example, the Poincaré disk model or the hyperboloid model. Each picture has its advantages, with some simplifying equations while others are better since the symmetries are more apparent.

We have finally reached the end of the reduction chain and have transformed a problem in discrete geometry to an optimal control problem on $T\mathrm{SL}_2(\mathbb{R})$. Already, we see that this problem is remarkably rich, with connections to Hamiltonian mechanics and hyperbolic geometry.

4.6 Dihedral Symmetry

The dihedral group Dih_6 of order 12 of the hexagon acts on the sixth roots of unity through orthogonal transformations. This action of the dihedral group extends to many of the constructions throughout this book.

Let σ be a multi-curve parameterizing the boundary of $K \in \mathfrak{K}_{bal}$. We assume that K is in the circle representation, and that $\sigma_j(0) = \mathbf{s}_j^*$. Let A be an element of the dihedral group of the hexagon, considered as an element of the orthogonal group $O_2(\mathbb{R})$. Let $\epsilon_A = \det(A) \in \{\pm 1\}$ be the determinant. Let $\sigma_j(t) = g(t)\mathbf{s}_j^*$ as usual, with $g(0) = I_2$. Then $\tilde{g}(t) = Ag(\epsilon_A t)A^{-1}$ determines a multi-curve

$$\tilde{\sigma}_j(t) = Ag(\epsilon_A t)A^{-1}\mathbf{s}_j^*,$$

parameterizing the boundary of a convex disk $AK \in \mathfrak{K}_{bal}$ with the same area as K . The sign ϵ_A is chosen to make the multi-curve parameterize the boundary of AK in a counterclockwise direction. Then the action extends to the Lie algebra

$$(\tilde{g}^{-1}\tilde{g}')(t) = \tilde{X}(t) = \epsilon_A AX(\epsilon_A t)A^{-1}.$$

Generators of the dihedral group are the rotation R and the reflection across the vertical axis:

$$S = \begin{pmatrix} -1 & 0 \\ 0 & 1 \end{pmatrix},$$

with $\epsilon_S = \det(S) = -1$. Writing $X = \Phi(z)$, the reflection acts by $z \mapsto -\bar{z}$, where \bar{z} is complex conjugation:

$$\epsilon_S S \Phi(z) S^{-1} = \Phi(-\bar{z}).$$

This preserves the upper-half plane, but is not orientation preserving. The rotation R (with $\epsilon_R = 1$) acts by linear fractional transformation

$$R \Phi(z) R^{-1} = \Phi(R \cdot z).$$

The actions of the dihedral group \mathbf{Dih}_6 on the multi-point \mathbf{s}_j , on multi-curves, on the control set, on the star conditions, on the ideal triangle, and on the upper half plane through Möbius transformation are all compatible. That is, many of our maps are equivariant with respect to the dihedral group. Recall that the linear fractional action of $\exp(J\theta)$ on \mathfrak{h} acts on the tangent space $T_i \mathfrak{h}$ at $i = \sqrt{-1}$ by a *clockwise* rotation by angle 2θ . $R^3 = -I_2$ acts trivially, so that the action of the dihedral group of the hexagon factors through the dihedral group of an equilateral triangle – the symmetric group on three letters.

The action of the dihedral group permutes the star inequalities. In terms of the linear functions $\rho_j : \mathfrak{sl}_2(\mathbb{R}) \rightarrow \mathbb{R}$ defined in Corollary 3.1.6, we have

$$\begin{aligned} \rho_j(\epsilon_S S X S^{-1}) &= \rho_{1-j}(X), \\ \rho_j(R X R^{-1}) &= \rho_{j-1}(X), \quad j \in \mathbb{Z}/6\mathbb{Z}. \end{aligned}$$

It follows that the dihedral group acts on the star domain \mathfrak{h}^* . The group permutes the ideal vertices of \mathfrak{h}^* . The action on the ideal vertices $\pm 1/\sqrt{3}$ and $+\infty$ is by linear fractional transformations on \mathbb{RP}^1 . Here we are viewing the boundary of the upper-half plane, consisting of the real axis and the point at infinity, as a real projective line. We have

$$\begin{aligned} R \cdot (+\infty) &= 1/\sqrt{3}, \quad R \cdot (1/\sqrt{3}) = -1/\sqrt{3}, \quad R \cdot (-1/\sqrt{3}) = +\infty, \\ S \cdot (\pm 1/\sqrt{3}) &= \mp 1/\sqrt{3}. \end{aligned}$$

We describe a fundamental domain for the action of the dihedral group (the symmetric group on three letters) on \mathfrak{h}^* . The positive imaginary axis is a geodesic in the upper-half plane. Under the action, the orbit of this geodesic is a set of three geodesics. The other two geodesics are the circles of radius $2/\sqrt{3}$ centered at the two cusps $(0, \pm 1/\sqrt{3})$ on the real axis. These three geodesics meet at $z = 0 + i \in \mathfrak{h}^*$ and partition \mathfrak{h}^* into six sectors. Each of these sectors is a fundamental domain for the action. See Figure 4.6.1. Specifically, one such fundamental domain is given by

$$\{z = x + iy \in \mathfrak{h}^* \mid x \geq 0, \quad (x - 1/\sqrt{3})^2 + y^2 \leq 4/3\}.$$

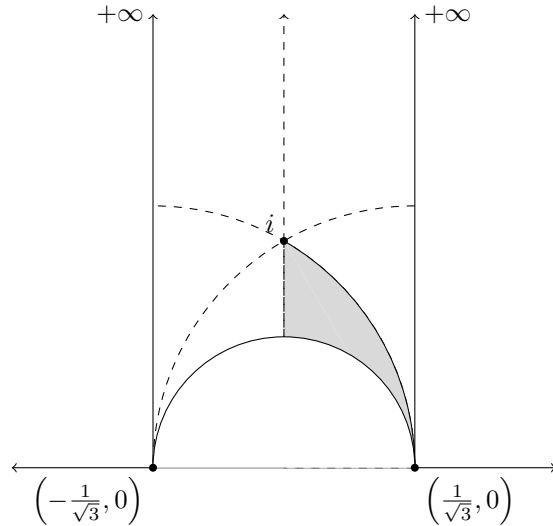


Figure 4.6.1: A fundamental domain for the dihedral action on \mathfrak{h}^* is shaded in gray. The generators of the dihedral group R and S take the shaded domain to the other unshaded ones.

The dihedral group acts on *everything in sight*, such as the control set U_T , and so forth. The dihedral group acts on the control by the rule

$$\epsilon_A A Z_u A^{-1} = Z_{A \cdot u}, \quad A \in \mathbf{Dih}_6, \quad u \in U_T.$$

Explicitly,

$$\begin{aligned} R \cdot (0, 0, 1) &= (0, 1, 0) & R \cdot (0, 1, 0) &= (1, 0, 0), & R \cdot (1, 0, 0) &= (0, 0, 1) \in U_T. \\ RZ_{(0,0,1)}R^{-1} &= Z_{(0,1,0)}, & RZ_{(0,1,0)}R^{-1} &= Z_{(1,0,0)}, & RZ_{(1,0,0)}R^{-1} &= Z_{(0,0,1)}. \\ -SZ_{(0,1,0)}S^{-1} &= Z_{(0,0,1)}, & -SZ_{(1,0,0)}S^{-1} &= Z_{(1,0,0)}. \end{aligned}$$

The action on U_T is such that if X is a solution to the Lie algebra state equation with constant control u , then the transform \tilde{X} by A is a solution to the state equation with constant control $\tilde{u} = A \cdot u$, as can be checked directly from the ODE $X' = [Z_u, X]/\langle Z_u, X \rangle$.

For example, the trajectory with control $(0, 0, 1)$ has state-dependent curvatures $\kappa_0 = 0$ and $\kappa_1 = 0$, so that $g(t)\mathbf{s}_0^*$ and $g(t)\mathbf{s}_2^*$ are straight lines, while $g(t)\mathbf{s}_4^*$ moves in a hyperbolic arc. Taking $A = R$, we see that $\tilde{\sigma}_2(t) = Rg(t)R^{-1}\mathbf{s}_2^* = -Rg(t)\mathbf{s}_3^*$ also moves in a hyperbolic arc, and its control is $\tilde{u} = (0, 1, 0) = R \cdot (0, 0, 1)$.

Chapter 5

Compactification of the Star Domain

While the star domain is a reduction of the state space, it is an ideal triangle with one vertex at infinity. Thus, it is open and unbounded in the upper half-plane. Our task in this section will be to explore a further reduction of this admissible region.

Empirical observations show that if $z \in \mathfrak{h}^*$ is close to the boundary curves of the star domain, then the corresponding critical hexagon (constructed in Lemma 5.0.3) is close to a parallelogram. Classical results of Mahler and Reinhardt state that the only convex disks in \mathfrak{K}_{ccs} with a parallelogram for a (degenerate) critical hexagon are parallelograms themselves. This suggests that there is a neighborhood of the boundary of the star domain which gives rise to convex disks in \mathfrak{K}_{ccs} whose packing density is close to one and so these convex disks can be excluded from consideration, since they are never optimal for our control problem. We make this intuition precise presently.

Our hope is that if we can cut down the state space to a compact region, eventually computer numerical solutions of the dynamics will become feasible. We have obtained the following compactification. In this chapter, by *compactification*, we mean an explicit compact subset of the star domain \mathfrak{h}^* , such that all trajectories of interest must lie inside that compact set. We have not optimized parameters to obtain the smallest possible compact region. We leave that for future work.

We define a *horocycle* in the upper-half plane to be a horizontal line, or a Euclidean circle in the upper half-plane that is tangent to the real axis. We define a *horoball* to be the region in the upper-half plane that is bounded by

the horocycle: either the region above the horizontal line or the interior of the circle. In general the image of the horocycle $y = y_0 \in \mathfrak{h}^*$ under a linear fractional transformation

$$A = \begin{pmatrix} a & b \\ c & d \end{pmatrix}$$

is a Euclidean circle tangent to the real axis, with center $(A \cdot \infty) + ir = a/c + ir$ and radius $r = \det A / (2y_0 c^2)$.

Definition 5.0.1 (compactification). *Let $\mathfrak{h}^{**} \subset \mathfrak{h}^*$ be the compact set defined by the following inequalities. The inequality $y > 4.5$ defines an open horoball $B(i\infty)$ around the cusp of \mathfrak{h}^* at $z = +i\infty$. By linear fractional transformations $R, R^2 \in \mathrm{SL}_2(\mathbb{R})$ acting on \mathfrak{h} , we obtain open horoballs $B(1/\sqrt{3})$ and $B(-1/\sqrt{3})$ at the other cusps (that is, at the ideal vertices) $z = \pm 1/\sqrt{3}$ of \mathfrak{h} . If the linear fractional transformation is $A = R^{\pm 1}$ and $y_0 = 4.5$, the radius r is $4/27$, and the center is $(A \cdot \infty) = (R^{\pm} \cdot \infty) = \pm 1/\sqrt{3}$.*

The open half-plane Π_0^+ defined by $y > 15(1/\sqrt{3} - x)$ includes the boundary curve $x = 1/\sqrt{3}$, $y > 0$ of \mathfrak{h}^ . By linear fractional transformations R, R^2 , we obtain transformed regions Π_1^+ and Π_2^+ around the other boundary curves. Set*

$$\mathfrak{h}^{**} = \mathfrak{h}^* \setminus (B(i\infty) \cup B(1/\sqrt{3}) \cup B(-1/\sqrt{3}) \cup \Pi_0^+ \cup \Pi_1^+ \cup \Pi_2^+).$$

The set $\mathfrak{h}^{**} \subset \mathfrak{h}^*$ is compact. See Figure 5.0.1. The shape of the compactification \mathfrak{h}^{**} has been chosen to be invariant under the action of the dihedral group. The entire chapter is devoted to the proof of the following theorem.

Theorem 5.0.2. *Let K be a convex disk in \mathfrak{K}_{bal} , with corresponding boundary trajectory (g, X) . Define a trajectory z in \mathfrak{h}^* by $\Phi \circ z = X$. If any point of the trajectory z is not in \mathfrak{h}^{**} , then the cost of the trajectory is strictly greater than the area of the smoothed octagon. Hence K is not a global minimizer.*

Given a convex disk K in \mathfrak{K}_{bal} in the circle representation, we parameterize the boundary multi-curve $\sigma_j(t) = g(t)\mathbf{s}_j^*$, with $g(0) = I_2$. At $t = 0$, we obtain an element $z \in \mathfrak{h}^*$ such that $\Phi(z) = X(0) = g^{-1}(0)g'(0)$. Also associated with K is a critical hexagon H_K with midpoints at the points $\{\mathbf{s}_j^*\}$. Conversely, an element $z \in \mathfrak{h}^*$ can be used to reconstruct a centrally symmetric hexagon H_K with midpoints $\{\mathbf{s}_j^*\}$ as follows.

Lemma 5.0.3. *Every $z \in \mathfrak{h}^*$ gives rise to a centrally symmetric hexagon $H_K(z)$ whose midpoints are at $\{\mathbf{s}_j^*\}$ and whose oriented directions along the*

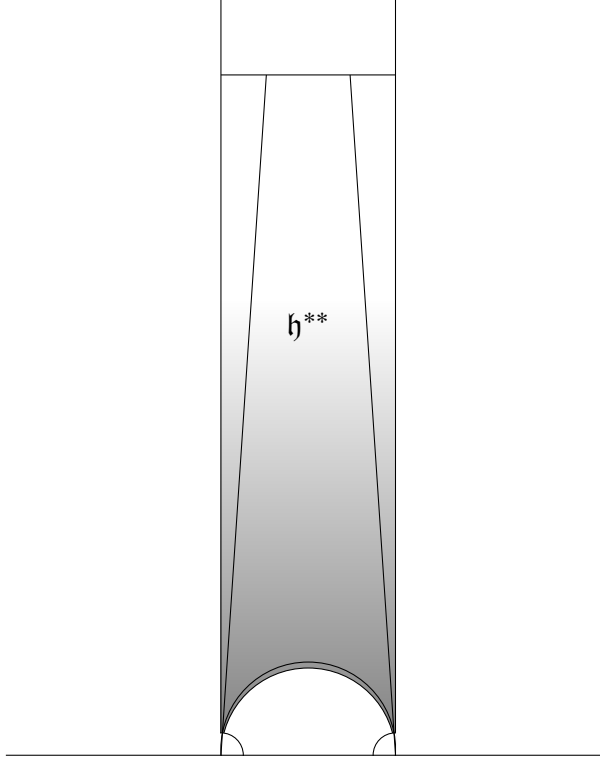


Figure 5.0.1: The central region away from the boundary of the star domain is the compactification h^{**} of the star domain.

edges point into the star domain. If z is constructed from the boundary parameterization of a convex disk $K \in \mathfrak{K}_{bal}$ in the circle representation as described above at multi-point $\{\mathbf{s}_j^*\}$, then $H_K(z)$ is the critical hexagon at the multi-point $\{\mathbf{s}_j^*\}$ of K .

Proof. The element z in the upper half-plane determines a matrix $\Phi(z)$ in the adjoint orbit of J in the Lie algebra \mathfrak{sl}_2 . The centrally symmetric hexagon $H_K(z)$ is then reconstructed from $\Phi(z)$ according to Remark 3.1.7. \square

Lower case bold letters will denote points $\mathbf{p}_i, \mathbf{q}_i, \mathbf{r}_i, \mathbf{s}_i$. Upper case will denote triangles T_i, T_i^{ext} in the plane and convex regions H, K . We often use the same upper case letter for a triangle and its area with respect to Lebesgue measure. The correct interpretation can be inferred by context.

We consider subscripts modulo 6, as we do elsewhere in the book, with the understanding that when it comes to area computations, the area is preserved

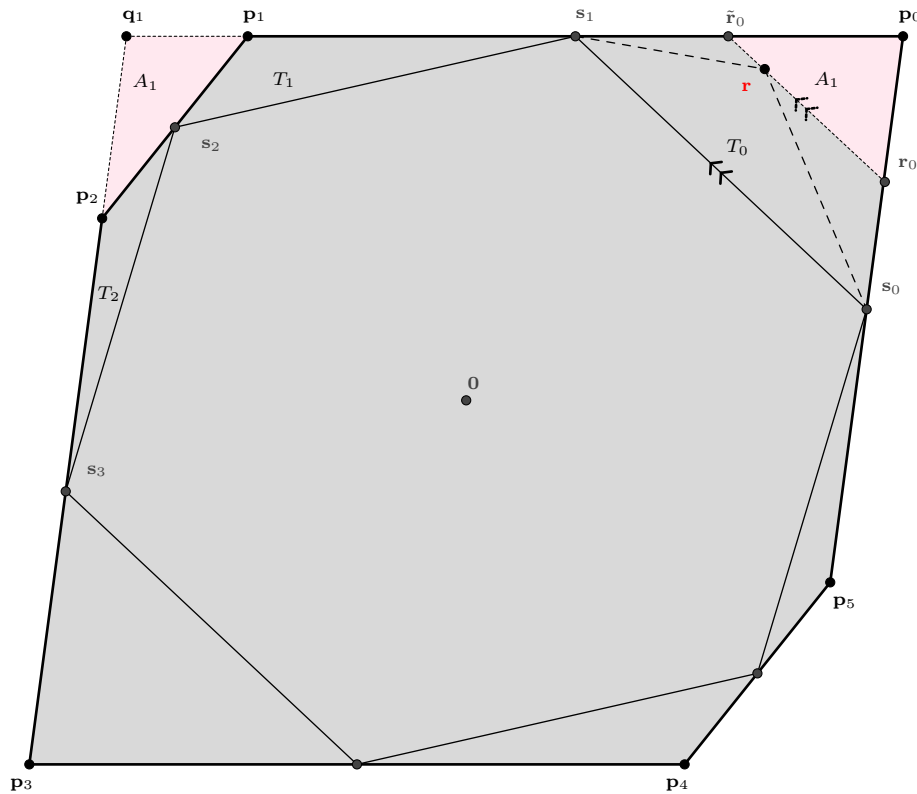


Figure 5.0.2: Critical Hexagon. (The figure has been rotated to make p_0p_1 horizontal, so that the sixth roots of unity s_i are also in a rotated position.) The triangles shown in pink are a result of the construction in Lemma 5.0.5.

under central reflection, so that area calculations have a smaller period of 3.

The situation is depicted in Figure 5.0.2. Recall that our convex disk is in circle representation, having the sixth roots of unity on its boundary. Let $\mathbf{p}_0, \mathbf{p}_1, \mathbf{p}_2, \mathbf{p}_3, \mathbf{p}_4, \mathbf{p}_5$ be the vertices of the critical hexagon with midpoints at $\mathbf{s}_j = \mathbf{s}_j^*$. We define (interior) triangles $T_0 = \Delta \mathbf{s}_0 \mathbf{p}_0 \mathbf{s}_1$, $T_1 = \Delta \mathbf{s}_1 \mathbf{p}_1 \mathbf{s}_2$, $T_2 = \Delta \mathbf{s}_2 \mathbf{p}_2 \mathbf{s}_3$. Let \mathbf{q}_1 denote the point of intersection of the lines $\mathbf{p}_3 \mathbf{p}_2$ and $\mathbf{p}_0 \mathbf{p}_1$ through nonadjacent edges of the hexagon. Similarly for \mathbf{q}_0 and \mathbf{q}_2 . This now determines the exterior triangles $T_0^{ext} = \Delta \mathbf{p}_1 \mathbf{q}_1 \mathbf{p}_2$, $T_1^{ext} = \Delta \mathbf{p}_2 \mathbf{q}_2 \mathbf{p}_3$, and $T_2^{ext} = \Delta \mathbf{p}_0 \mathbf{q}_0 \mathbf{p}_1$. (The latter two triangles are not depicted in the figure.) For our compactification result, we will need the areas of these triangles in terms of $z = x + iy$.

The functions ρ_0, ρ_1, ρ_2 of Equation (3.1.3) are linear functions of $X \in \mathfrak{sl}_2(\mathbb{R})$. Considering them as a function of $z \in \mathfrak{h}$ through the map $X = \Phi(z)$, we abuse notation slightly by writing $\rho_j(z)$ for $\rho_j(\Phi(z))$, where now $\rho_j : \mathfrak{h} \rightarrow \mathbb{R}$. The star domain \mathfrak{h}^* is defined in \mathfrak{h} by the star inequalities $\rho_j(z) > 0$ for $j = 0, 1, 2$.

Lemma 5.0.4. *We have*

$$\text{area}(T_0) = \frac{\sqrt{3}}{4} \rho_0 \rho_2, \quad \text{area}(T_1) = \frac{\sqrt{3}}{4} \rho_0 \rho_1, \quad \text{area}(T_2) = \frac{\sqrt{3}}{4} \rho_1 \rho_2,$$

and

$$\text{area}(T_0^{ext}) = \sqrt{3} \rho_1^2, \quad \text{area}(T_1^{ext}) = \sqrt{3} \rho_2^2, \quad \text{area}(T_2^{ext}) = \sqrt{3} \rho_0^2,$$

where area is the Lebesgue measure on \mathbb{R}^2 . Furthermore, we have

$$\text{area}(T_0) + \text{area}(T_1) + \text{area}(T_2) = \frac{\sqrt{3}}{4}.$$

Proof. Lemma 5.0.3 leads to an explicit construction of the coordinates of the points \mathbf{p}_i and \mathbf{q}_i for $i = 0, 1, 2$. Once we have coordinates of all these points, finding the areas of the associated triangles is straightforward from Equations (3.1.3), (3.1.6) and (3.1.8), with $\det(X) = 1$. For example,

$$\mathbf{p}_0 = \mathbf{s}_0 + \rho_2 X \mathbf{s}_0 = \mathbf{s}_0 + \rho_2 (\rho_0 \mathbf{s}_1 + \rho_1 \mathbf{s}_2)$$

gives

$$\text{area}(T_0) = \frac{1}{2} \det((\mathbf{p}_0 - \mathbf{s}_0), \mathbf{s}_2) = \frac{1}{2} \rho_2 \det(X \mathbf{s}_0, \mathbf{s}_2) = \frac{1}{2} \rho_2 \rho_0 \det(\mathbf{s}_1, \mathbf{s}_2) = \frac{\sqrt{3}}{4} \rho_0 \rho_2.$$

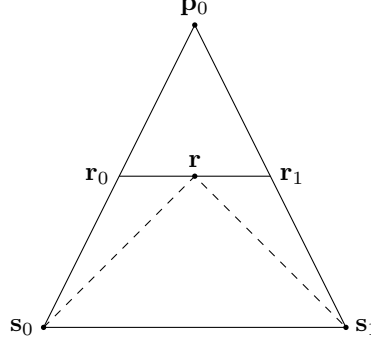


Figure 5.0.3: Area of cutoff triangles.

We have $\mathbf{q}_1 = \mathbf{p}_1 + 2\rho_1 X \mathbf{s}_1 = \mathbf{p}_2 - 2\rho_1 X \mathbf{s}_3$, and

$$\begin{aligned} \text{area}(T_0^{ext}) &= \frac{1}{2} \det((\mathbf{p}_2 - \mathbf{q}_1), (\mathbf{p}_1 - \mathbf{q}_1)) \\ &= -2\rho_1^2 \det(X \mathbf{s}_3, X \mathbf{s}_1) = -2\rho_1^2 \det(\mathbf{s}_3, \mathbf{s}_1) = \sqrt{3}\rho_1^2. \end{aligned}$$

The other cases are similar, by shift of indices.

The sum of the areas T_i is obtained by Equation (3.1.7).

$$\frac{\sqrt{3}}{4}(\rho_0\rho_2 + \rho_1\rho_2 + \rho_0\rho_1) = \frac{\sqrt{3}}{4} \det(X) = \frac{\sqrt{3}}{4}.$$

To give a second proof that the sum of the areas of T_i is $\sqrt{3}/4$, an equilateral triangle of edge length 1 can be dissected into three triangles congruent to T_1, T_2, T_3 . \square

Lemma 5.0.5. *As shown in Figure 5.0.3, in triangle $\Delta s_0 s_1 p_0$, let \tilde{r}_0 and r_0 be points on $s_1 p_0$ and $s_0 p_0$ respectively such that $r_0 \tilde{r}_0$ is parallel to $s_0 s_1$. If r is any point on $\tilde{r}_0 r_0$, then*

$$\Delta s_0 s_1 r = \Delta s_0 p_0 s_1 - \sqrt{\Delta r_0 p_0 \tilde{r}_0 \Delta s_0 p_0 s_1}.$$

Proof. By an affine transformation, we may assume the angle at s_1 is a right angle, $s_0 s_1 = 1$, $s_1 p_0 = 1$, $s_1 \tilde{r}_0 = r$ where $r \in (0, 1)$. Then the identity to be proved is

$$\frac{r}{2} = \frac{1 - \sqrt{(1-r)^2}}{2},$$

which is immediate. \square

We now prove a lower bound on area. Let us denote by

$$\mathfrak{h}_i := \{z \in \mathfrak{h}^* \mid T_i(z) \geq T_i^{ext}(z)\}, \quad i = 0, 1, 2.$$

Here and below, we consider the indices modulo 6, but \mathfrak{h}_i has period three: $\mathfrak{h}_i = \mathfrak{h}_{i+3}$. We derive a lower bound for all convex disks K having $H_K(z)$ as a minimal midpoint hexagon, where z belongs to the regions $\mathfrak{h}_0, \mathfrak{h}_1$ or \mathfrak{h}_2 . For $i = 0, 1, 2$ define

$$\text{area}_i(z) := T_i(z) - \sqrt{T_i^{ext}(z) T_i(z)}.$$

Let $\mathbf{I}_i : \mathfrak{h} \rightarrow \{0, 1\}$ be the indicator function of the set \mathfrak{h}_i .

Theorem 5.0.6. *If $K \in \mathfrak{K}_{bal}$ is in circle representation and has $H_K(z)$ as a critical hexagon, where $z \in \mathfrak{h}^*$, then we have that*

$$\text{area}(K) \geq \frac{3\sqrt{3}}{2} + 2 \sum_{i=0}^2 \mathbf{I}_i(z) \text{area}_i(z).$$

Proof. As in the Figure 5.0.2 above, let $\mathbf{p}_0 \mathbf{p}_1 \mathbf{p}_2 \mathbf{p}_3 \mathbf{p}_4 \mathbf{p}_5$ be the critical hexagon of an undepicted convex disk K . The convex disk K is inscribed in this hexagon and passes through the points $\mathbf{s}_j^* = \mathbf{s}_j$ which are midpoints of its sides.

We may assume that $z \in \mathfrak{h}^*$ lies in the set

$$\mathfrak{h}_0 \cup \mathfrak{h}_1 \cup \mathfrak{h}_2 = \{z \in \mathfrak{h}^* \mid T_0(z) \geq T_0^{ext}(z) \text{ or } T_1(z) \geq T_1^{ext}(z) \text{ or } T_2(z) \geq T_2^{ext}(z)\}.$$

Otherwise, the inequality to be shown reduces to $\text{area}(K) \geq \text{area}(h_K) = 3\sqrt{3}/2$, where h_K is the convex hull of the points \mathbf{s}_i . This area inequality holds because $K \supset h_K$. (This area inequality appears in Reinhardt's 1934 article and was used in his proof of the existence of a minimizer.)

We show that the set $\mathfrak{h}_0 \cap \mathfrak{h}_1 \cap \mathfrak{h}_2$ is empty. By the Cauchy-Schwarz inequality and the area formulas of Lemma 5.0.4, we have

$$\sum_{i=1}^3 T_i = \frac{\sqrt{3}}{4}(\rho_0 \rho_2 + \rho_0 \rho_1 + \rho_1 \rho_2) \leq \frac{\sqrt{3}}{4}(\rho_0^2 + \rho_1^2 + \rho_2^2) = \frac{1}{4} \sum_{i=1}^3 T_i^{ext} < \sum_{i=1}^3 T_i^{ext}.$$

This shows we cannot have $T_i(z) \geq T_i^{ext}(z)$ for all $i = 0, 1, 2$. So the inequalities defining \mathfrak{h}_i must hold individually or pairwise. The regions \mathfrak{h}_i and the other data have a three-fold symmetry given by shifting indices i modulo 3. This gives us two cases.

Case 1: Without loss of generality, by symmetry, assume that $z \in \mathfrak{h}_0$ and $z \notin \mathfrak{h}_1 \cup \mathfrak{h}_2$. That means $T_0(z) \geq T_0^{ext}(z)$. In Figure 5.0.2 above, this gives an inequality between areas $\Delta s_0 p_0 s_1 \geq \Delta p_1 q_1 p_2$. Construct a triangle $\Delta r_0 p_0 \tilde{r}_0$ such that $\text{area}(\Delta r_0 p_0 \tilde{r}_0) = \text{area}(\Delta p_1 q_1 p_2)$ and such that the line segment $r_0 \tilde{r}_0$ is parallel to $s_0 s_1$. The triangles with equal area are shown in pink.

We claim that there is at least one point r on the line segment $r_0 \tilde{r}_0$ which also lies on the boundary of the undepicted convex disk K . Otherwise, if there were no such point, then the convex disk K would be contained in the centrally symmetric hexagon with vertices r_0, \tilde{r}_0, q_1 , and their reflections. This hexagon has the same area as the hexagon of $p_0 p_1 p_2 p_3 p_4 p_5$, which has minimal area. We reach a contradiction by constructing a centrally symmetric hexagon containing K of even smaller area: make an inward parallel shift of the line through the edge $r_0 \tilde{r}_0$ (and its reflection) until it meets K .

The above argument exhibits the point r on $r_0 \tilde{r}_0$ and its reflection $-r$ on the reflected edge respectively, which are also on the boundary of the convex disk K . Since K is convex, it contains the convex hull H of the points s_0, s_1, s_2, r and their reflections. Thus, we have

$$\begin{aligned} \text{area}(K) &\geq \text{area}(H) \\ &= \text{area}(s_0 s_1 s_2 s_3 s_4 s_5) + 2\Delta s_0 r s_1 \\ &= \frac{3\sqrt{3}}{2} + 2\Delta s_0 r s_1 \\ &= \frac{3\sqrt{3}}{2} + 2\left(T_0 - \sqrt{T_0^{ext} T_0}\right) \quad (\text{using Lemma 5.0.5}). \end{aligned}$$

Case 2: Assume without loss of generality that $z \in \mathfrak{h}_0 \cap \mathfrak{h}_1$. We have $T_0(z) \geq T_0^{ext}(z)$ and $T_1(z) \geq T_1^{ext}(z)$. The above argument can also be adapted here again to exhibit four points (two new points inside the triangles $\Delta s_0 p_0 s_1$ and $\Delta s_1 p_1 s_2$ respectively, along with their reflections) also on the boundary of the convex disk K , so that we have

$$\text{area}(K) \geq \frac{3\sqrt{3}}{2} + 2\left(T_0 - \sqrt{T_0^{ext} T_0}\right) + 2\left(T_1 - \sqrt{T_1^{ext} T_1}\right).$$

Accounting for all cases, we have

$$\text{area}(K) \geq \frac{3\sqrt{3}}{2} + 2 \sum_{z \in \mathfrak{h}_i} \mathbf{I}_i(z) \text{area}_i(z).$$

□

The regions $\mathfrak{h}_0, \mathfrak{h}_1, \mathfrak{h}_2$ are shown in Figure 5.0.4. The boundaries of \mathfrak{h}_0 and \mathfrak{h}_2 meet along the imaginary axis at $(x, y) = (0, \sqrt{3})$.

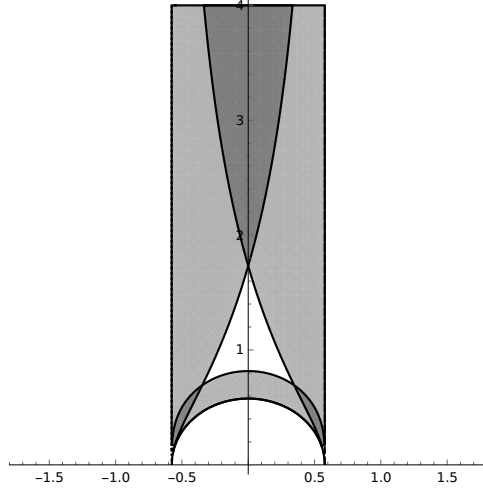


Figure 5.0.4: Covered boundary of the star domain. The shaded region along the right edge is \mathfrak{h}_0 . The shaded region along the left edge is \mathfrak{h}_2 , and the shaded region along the lower bounding circle is \mathfrak{h}_1 .

Recall that $\text{area}(H_K(z)) = \sqrt{12}$. Let us write

$$\delta(z) := \frac{1}{\sqrt{12}} \left(\frac{3\sqrt{3}}{2} + 2 \sum_{z \in \mathfrak{h}_i} \mathbf{I}_i(z) \text{area}_i(z) \right) = \frac{3}{4} + \sum_{z \in \mathfrak{h}_i} \frac{\mathbf{I}_i(z) \text{area}_i(z)}{\sqrt{3}},$$

for the lower bound of the packing density for convex disks $K \in \mathfrak{K}_{bal}$ having $H_K(z)$ as a critical hexagon. Also, let δ_{oct} denote the packing density of the smoothed octagon. If $z \in \mathfrak{h}^*$ is such that $\delta(z) > \delta_{oct}$, then by the above theorem, the density of every convex disk K having $H_K(z)$ as a critical hexagon is greater than δ_{oct} and is not a global minimizer. Such K can be dropped from consideration. The next result shows that all but a compact subset of \mathfrak{h}^* can be excluded in this way. In the next lemma, we write \mathbf{I}_2 , area_i , and δ as functions of (x, y) instead of $z = x + iy$.

Lemma 5.0.7.

1. For all $y \geq 1$, the function $\text{area}_0(x, y)$ is monotonically increasing in x on $0 < x < 1/\sqrt{3}$.

2. For all $y \geq \sqrt{3}$, the function $\text{area}_0(x, y) + \text{area}_2(x, y)$ is monotonically increasing in x on $0 < x < 1/\sqrt{3}$.
3. For all fixed $y \geq \sqrt{3}$, the function $\mathbf{I}_0(x, y)\text{area}_0(x, y) + \mathbf{I}_2(x, y)\text{area}_2(x, y)$ is minimized at $x = 0$ on the domain $x \in (-1/\sqrt{3}, 1/\sqrt{3})$.
4. For all $x \in (-1/\sqrt{3}, 1/\sqrt{3})$ and all $y \geq 4.5$, we have

$$\delta(x, y) > \delta_{\text{oct}}.$$

Proof. The functions ρ_j are positive on \mathfrak{h}^* . Write $(\cdot)_x$ for the partial derivative with respect to x . Then, $\rho_{0,x} > 0$ and $\rho_{1,x} < 0$ on \mathfrak{h}^* . The sign of $\rho_{2,x} = \sqrt{3}x/y$ is the same as the sign of x .

(1) We compute the partial derivative with respect to x of

$$\text{area}_0(x, y) = \frac{\sqrt{3}}{4} \left(\rho_0 \rho_2 - 2\sqrt{\rho_0 \rho_1^2 \rho_2} \right).$$

The partial derivative is positive on the given domain $y \geq 1$ and $0 < x < 1/\sqrt{3}$ because $\rho_{0,x} \rho_2 > 0$, $\rho_0 \rho_{2,x} > 0$, and $-(\rho_0 \rho_1^2 \rho_2)_x > 0$, the final inequality being a polynomial inequality in x and y , which is easily checked.

(2) We consider the domain $\mathfrak{h}^* \cap \{x > 0, y \geq \sqrt{3}\}$. We compute the partial derivative with respect to x of

$$\text{area}_0(x, y) + \text{area}_2(x, y) = \frac{\sqrt{3}}{4} \left((\rho_0 + \rho_1) \rho_2 - 2\sqrt{\rho_0 \rho_1^2 \rho_2} - 2\sqrt{\rho_0^2 \rho_1 \rho_2} \right)$$

and show that this partial derivative is positive. The first term $(\rho_0 + \rho_1) \rho_2$ in the numerator has positive partial derivative $2x/y^2 > 0$ on the given domain. It remains to show that

$$0 > \frac{(\rho_0 \rho_1^2 \rho_2)_x}{\sqrt{\rho_1}} + \frac{(\rho_0^2 \rho_1 \rho_2)_x}{\sqrt{\rho_0}}.$$

The two polynomial numerators on the right are separately negative when $x \geq 1/4$. When $0 \leq x \leq 1/4$, the two terms on the right are separately decreasing functions in x , and their sum is 0 at $x = 0$. (This too is a polynomial verification.) These routine checks prove the result.

(3) Along the boundary of \mathfrak{h}_i , where \mathbf{I}_i jumps, we have $\text{area}_i(x, y) = 0$. Thus,

$$\sum_i \mathbf{I}_i(x, y) \text{area}_i(x, y) \tag{5.0.1}$$

is continuous on \mathfrak{h}^* . Since it is monotonic increasing in $x \in (0, 1/\sqrt{3})$ on each of $\mathfrak{h}_0 \setminus \mathfrak{h}_2$ and $\mathfrak{h}_0 \cap \mathfrak{h}_2$, it is also monotonic increasing in x on $\mathfrak{h}_0 \cap \{x > 0, y \geq \sqrt{3}\}$.

Note that $\text{area}_2(x, y) = \text{area}_0(-x, y)$, because $\rho_0(-x, y) = \rho_1(x, y)$. Since the function (5.0.1) is even, it must be monotonic decreasing in x on $\mathfrak{h}_0 \cap \{x < 0, y \geq \sqrt{3}\}$. Thus, the critical point at $x = 0$ is a minimum.

(4) Along the imaginary axis, for $y \geq \sqrt{3}$, we have

$$\text{area}_0(0, y) = \text{area}_2(0, y) = \frac{\sqrt{3}}{4} (\sqrt{\rho_0 \rho_2} (\sqrt{\rho_0 \rho_2} - 2\rho_1)).$$

Both $\rho_0 \rho_2 = (y^2 - 1/3)/(2y^2)$ and $\sqrt{\rho_0 \rho_2} - 2\rho_1$ are increasing functions of y . Hence $\text{area}_0(0, y)$ is increasing. If $x \in (-1/\sqrt{3}, 1/\sqrt{3})$ and $y \geq 4.5$,

$$\delta(x, y) \geq \delta(0, y) \geq \delta(0, 4.5) = 0.9059 \dots > \delta_{\text{oct}}.$$

□

Proof of Theorem 5.0.2. Everything in this subsection up until this point has been equivariant with respect to the action of the dihedral group on \mathfrak{h}^* . The region \mathfrak{h}^{**} described in the statement of the theorem is likewise stable under the action of the dihedral group. Thus, it is enough to prove the theorem for all points z in a fundamental domain for the action of the dihedral group on \mathfrak{h}^* . One such fundamental domain is given in subsection 4.6 as

$$\{z = x + iy \in \mathfrak{h}^* \mid x \geq 0, (x - 1/\sqrt{3})^2 + y^2 = 4/3\}.$$

We work on the slightly larger subset of \mathfrak{h}^* defined by the inequalities $x \geq 0$ and $y \geq 1$. The only horoball (among the three) meeting this set is $B(i\infty)$, and the only half-plane meeting this set is Π_0^+ .

If any point of the trajectory (g, X) passes through a point $X = \Phi(z)$ with $z = x + iy$, where $y > 4.5$, then the previous lemma shows that $\delta(x, y) > \delta_{\text{oct}}$. This shows that we may exclude all trajectories that enter the horoball $B(i\infty)$.

Next we show that we can exclude all trajectories that meet the half-plane Π_0^+ defined by $y > 15(1/\sqrt{3} - x)$. We show that

$$\delta(z) \geq \delta_0(z) := \frac{3}{4} + \frac{\text{area}_0(z)}{\sqrt{3}} > \delta_{\text{oct}},$$

for all $z \in \mathfrak{h}^* \cap \Pi_0^+ \cap \{1 \leq y \leq 4.5\} \subset \mathfrak{h}_0$. Proving this inequality will complete the proof of the theorem, because the regions Π_1^+ and Π_2^+ do not meet the fundamental domain.

By the first part of the lemma, we have monotonicity of area_0 in x along each horizontal slice $y = y_0$ such that $y \geq 1$. Thus, it is enough to prove the inequality along the graph of the affine map $y(x) = 15(1/\sqrt{3}-x)$. Furthermore, we may assume that $y \leq 4.5$. The preimage of $[1, 4.5]$ under the map y is contained in $[0.277, 0.511]$. On this domain, we have $\delta_0(x, y(x)) > \delta_{\text{oct}}$. \square

Chapter 6

Hamiltonian and Maximum Principle

6.1 Existence of Optimal Control

The existence of optimal solutions to problems such as the Reinhardt control problem (Problem 3.6.2) is based on Filippov's theorem which gives conditions under which the corresponding *attainable set* of the control system in question is compact. In informal terms, the attainable set corresponds to all the points in the manifold which are reachable provided one is only allowed to move according to the control. The compactness of attainable sets implies the existence of optimal control. The optimal control function is a *measurable function*.

Theorem 6.1.1 (Filippov). *On a smooth manifold M , let $q' = f(q, u)$ be an optimal control system with an associated cost objective $\int_0^t \phi(q, u) dt \rightarrow \min$. Here $u \in U \subset \mathbb{R}^m$ which is a compact set (the control set). Assume that the velocity set $f(q, U) = \{f(q, u) \mid u \in U\}$ is convex for each $q \in M$ and that the support of f is a compact subset of $M \times U$. Then, the attainable sets are compact and an optimal control exists.*

For the Reinhardt control problem, all assumptions of the Filippov theorem are shown to hold as follows.

- The control set is the simplex U_T defined in Definition 3.3.3, which is obviously compact.

- The velocity sets are convex; in fact, each velocity set is the convex hull of the velocities at the three vertices the control set, as shown in Lemma 6.1.2 for the simplex U_T .
- Recall that Reinhardt has proved the existence of a optimal solution to the Reinhardt problem. We claim that the velocity sets can be assumed to be compactly supported. By Definition 3.1.3 and Lemma 4.5.2, the relevant vectors fields are

$$[Z_u, \Phi(z)]/\langle Z_u, \Phi(z) \rangle \quad \text{and} \quad g\Phi(z), \quad z \in \mathfrak{h}^*. \quad (6.1.1)$$

By Theorem 5.0.2, we may assume that z lies in the compact set \mathfrak{h}^{**} . Then $\Phi(z)$ is also confined to a compact set, as well as the first vector field in (6.1.1). The second vector field $g\Phi(z)$ lies in a compact set if $g \in \text{SL}_2(\mathbb{R})$ can be shown to be bounded. We have an upper bound $t_f \leq \pi/3$ on the terminal time by Lemma 4.3.1. Gronwall's inequality applied to the ODE $g' = gX$ gives a bound on g (Appendix A.1). This shows that the vector fields are confined to a compact subset.

To make the vector field smooth, we can multiply the vector fields in the star domain in the Reinhardt control problem 4.5.1 by a smooth cutoff function of compact support $\psi : \mathfrak{h}^* \rightarrow \mathbb{R}$ with $\psi|_{\mathfrak{h}^{**}} = 1$, to obtain smooth vector fields of compact support.

We can apply Filippov's theorem to these smoothed vector fields of compact support. Thus, the optimal control exists for the optimal control system. The proof used the following lemma.

Lemma 6.1.2. *Let $f(x, y; u) = (f_1(x, y; u), f_2(x, y; u))$ be the control-dependent vector field on \mathfrak{h}^* defined by the half-plane control problem 4.5.1. For each $z = x + iy \in \mathfrak{h}^*$, the image $f(x, y; U_T)$ of U_T in \mathbb{R}^2 is a convex set. Moreover, the affine hull of the image $f(x, y; U_T)$ is all of \mathbb{R}^2 .*

Proof. Let ρ_j be the positive functions of $z \in \mathfrak{h}^*$ from Lemma 5.0.4. Fix $z = x + iy \in \mathfrak{h}^*$ and let $\mathbf{e}_1, \mathbf{e}_2, \mathbf{e}_3$ be the standard basis of \mathbb{R}^3 , giving the vertices of U_T . We prove that the image $f(x, y; U_T)$ is in fact the convex hull of

$$\{f(x, y; \mathbf{e}_j) \mid j = 1, 2, 3\}.$$

By explicit calculation, the basis vectors map to distinct points in the velocity set. For example,

$$f(x, y, \mathbf{e}_3) - f(x, y, \mathbf{e}_2) = \left(0, \frac{2}{\sqrt{3}\rho_0\rho_1}\right) \neq (0, 0),$$

which is finite and nonzero by the star inequalities. Let $L : \mathbb{R}^2 \rightarrow \mathbb{R}$ be the nonzero affine function that vanishes at $f(x, y; \mathbf{e}_i)$ and $f(x, y; \mathbf{e}_j) \in \mathbb{R}^2$ and takes value 1 at $f(x, y; \mathbf{e}_k)$, where (i, j, k) is any chosen permutation of $(1, 2, 3)$. Computing, we find that $L(f(x, y; u))$ is the ratio of two affine functions of U_T (depending on the parameters x, y), where the denominator is positive on U_T . For example, if $u = (u_0, u_1, u_2)$ and $(i, j, k) = (1, 2, 3)$, we compute that

$$L(f(x, y; u)) = \frac{u_2 \rho_0(z)}{u_0 \rho_2(z) + u_1 \rho_1(z) + u_2 \rho_0(z)}.$$

We observe that the numerator of L vanishes along the segment $[\mathbf{e}_1, \mathbf{e}_2] \subset U_T$ and that the numerator is nonnegative on U_T (in fact strictly positive, except on the edge segment). Similarly, for each permutation (i, j, k) of the vertices of U_T , the corresponding line $L = 0$ defines a boundary segment of $f(x, y; U_T)$. We conclude that the image $f(x, y; U_T)$ is the convex hull of three points as claimed. Since the image is a triangle, its affine hull is all of \mathbb{R}^2 . \square

6.2 The Pontryagin Maximum Principle

The Pontryagin Maximum Principle (PMP) is a powerful first-order necessary condition for optimality of solutions to an optimal control problem on a smooth manifold M with *closed* control set $U \subseteq \mathbb{R}^m$ and free-terminal time. We summarize the basic ideas below. For full details and a proof of the PMP, we refer to [49].

Given a control system

$$q' = f(q, u) \in T_q M \tag{6.2.1}$$

$$q(0) = q_0 \in M \tag{6.2.2}$$

on a manifold M with an associated cost objective

$$\min_{u \in U} \int_0^{t_f} \phi(q, u) dt,$$

we assume that the control-dependent vector field $f(q, u)$ satisfies

1. $q \mapsto f(q, u)$ is a smooth vector field on M for any fixed $u \in U$.
2. $(q, u) \mapsto f(q, u)$ is a continuous mapping for $q \in M, u \in U$,

This optimal control system is denoted by the tuple (M, U, f, ϕ) . We sometimes denote the vector field $f(u, q)$ for $u \in U$ by $f_u(q)$. The PMP relies on the following *control-dependent Hamiltonian* which is *cost-extended* on T^*M :

$$\mathcal{H}(q, p, u) = \langle p, f(q, u) \rangle_* + \lambda_{cost} \phi(q, u) \quad p \in T_q^*M \quad \lambda_{cost} \in \mathbb{R}_{\leq 0},$$

where $\langle \cdot, \cdot \rangle_*$ is the natural pairing between a vector space and its dual and λ_{cost} , Pontryagin multiplier is a constant nonpositive scalar. Note that \mathcal{H} is linear in p .

Let $u^* = u^*(p, q)$ denote a function defined implicitly as a function of $(q, p) \in T^*M$ by

$$\mathcal{H}^+(q, p) := \mathcal{H}(q, p, u^*) = \max_{u \in U} \mathcal{H}(q, p, u). \quad (6.2.3)$$

\mathcal{H}^+ is called the *maximized Hamiltonian*. Note that it is quite possible that u^* might not be uniquely determined by the maximization condition. This is related to *singular* subarcs, discussed later. See Definition 6.2.1. Regardless, the value of the maximized Hamiltonian \mathcal{H}^+ is independent of the choice of u^* .

The PMP says that the extremals of the optimal control problem are projections (from T^*M to M) of the flow-trajectory of $\vec{\mathcal{H}}^+$, which is the Hamiltonian vector field corresponding to \mathcal{H}^+ with respect to the canonical symplectic structure on the cotangent bundle T^*M . Integral curves of the vector field $\vec{\mathcal{H}}^+$ satisfy

$$q' = \frac{\partial \mathcal{H}^+}{\partial p} = f(x, u^*), \quad p' = -\frac{\partial \mathcal{H}^+}{\partial q}. \quad (6.2.4)$$

This trajectory $(u^*(t), q(t), p(t))$ in T^*M is called the *lifted controlled trajectory*.

The PMP (for free terminal time periodic problems) also guarantees the following of lifted trajectories.

1. Transversality conditions (endpoint conditions for the co-state trajectories) hold.
2. The Hamiltonian $\mathcal{H}(q, p, u^*)$ vanishes identically along the lifted controlled trajectory.
3. The cotangent vector $(\lambda_{cost}, p(t)) \in \mathbb{R}_{\leq 0} \times T_{q(t)}^*M$ is nonzero for all $t \in [0, t_f]$.

4. The scalar λ_{cost} is constant, and when it is non-zero, may be taken to be $\lambda_{cost} = -1$ by rescaling the covector, using the linearity of the ODE for p .

The lifted curves which satisfy the conditions of the PMP are called *Pontryagin extremals* or simply *extremals*.

Definition 6.2.1 (Normal, Abnormal and Singular extremals).

1. *An extremal for which $\lambda_{cost} = 0$ is called an abnormal extremal.*
2. *An extremal for which $\lambda_{cost} \neq 0$ is called a normal extremal. Recall that in the normal case a renormalization allows us to take $\lambda_{cost} = -1$.*
3. *If there is an open time interval on which equation (6.2.3) fails to uniquely determine the function $u^*(t)$, the trajectory during that interval is called a singular subarc.*

Our strategy is to apply the maximum principle to our problem with the hope that these necessary conditions will provide us more information about the structure of the extremals. Recall the framework of the Reinhardt control problem 3.6.2, where we have dynamics occurring in the Lie group $SL_2(\mathbb{R})$ and the Lie algebra $\mathfrak{sl}_2(\mathbb{R})$. If we apply the PMP to this problem, the lifted trajectories live in

$$T^*(SL_2(\mathbb{R}) \times \mathfrak{sl}_2(\mathbb{R})) \cong (SL_2(\mathbb{R}) \times \mathfrak{sl}_2(\mathbb{R})) \times (\mathfrak{sl}_2(\mathbb{R}) \times \mathfrak{sl}_2(\mathbb{R})),$$

where we have used the cotangent bundle trivialization of Proposition 3.6.1 making $T^*SL_2(\mathbb{R}) \cong SL_2(\mathbb{R}) \times \mathfrak{sl}_2(\mathbb{R})^*$ and the identification $\mathfrak{sl}_2(\mathbb{R})^* \cong \mathfrak{sl}_2(\mathbb{R})$ via the nondegenerate trace form as in Appendix A.8. So, for the state variables $q = (g, X) \in SL_2(\mathbb{R}) \times \mathfrak{sl}_2(\mathbb{R})$ the PMP gives corresponding costate variables $p = (\Lambda_1, \Lambda_2) \in \mathfrak{sl}_2(\mathbb{R}) \times \mathfrak{sl}_2(\mathbb{R})$.

Note that the PMP system is a Hamiltonian system on $T^*TSL_2(\mathbb{R})$ and is an instance of a *higher-order variational system on a Lie group*. Similar problems and the background theory is described in Gay-Balmaz et. al. [12] and Colombo and de Deigo [7].

We now derive expressions for the Hamiltonian and the costate equations in both the Lie algebra coordinates and the upper half-plane coordinates via the isomorphism described in Lemma 4.2.1.

6.3 Left-invariance

Definition 6.3.1 (Jurdjevic [19]). *An arbitrary optimal problem with control system $dg/dt = f(g, u)$ defined on a real Lie group G with control functions $u(t) \in U \subseteq \mathbb{R}^m$ is said to be left-invariant if $TL_h f(g, u) = f(hg, u)$ for each $g, h \in G$. Here $L_h(g) = hg$ is the left-multiplication map, and $TL_h : T_g G \rightarrow T_{hg} G$ is its tangent map.*

Also, we require the associated cost function $\phi(g, u)$ to be left-invariant: $\phi(g, u) = \phi(e, u)$ for all g and u , where $e \in G$ is the neutral element.

The dynamical system breaks into the ordinary differential equation (ODE) for the group (3.6.1) and the ODE for the Lie algebra (3.6.2). We refer to these two subsystems as the dynamics *at the Lie group level* and the dynamics *at the Lie algebra level*. The dynamics are coupled through X , which appears in both levels.

The dynamics of the Reinhardt optimal problem at the Lie group level is clearly left-invariant in the sense that the cost function depends on X but not g and in the sense that the ODE for g can be left-multiplied by a constant $h \in \text{SL}_2(\mathbb{R})$. Left-invariance of a dynamical system on a Lie group implies that we can reduce its dynamics to co-adjoint orbits of the associated Lie algebra.

Since the cost and dynamics for X are independent of g , we note that the only purpose served by the Lie group dynamics for g is to describe an endpoint (transversality) condition $g(t_f) = R$. Because of the minor purpose served by the Lie group dynamics, we can often focus on the control problem exclusively at the Lie algebra level, and postpone the endpoint condition on g until the very last step. In later sections, we will drop the group dynamics and exclusively focus on state/costate dynamics in the Lie algebra.

6.4 Hamiltonian in the Lie Algebra

Following the Reinhardt optimal control problem 3.6.2, the Hamiltonian is the sum of the Hamiltonians for the Lie group part and the Lie algebra part.

The costate variable corresponding to the Lie group element $g \in \text{SL}_2(\mathbb{R})$ is denoted $\Lambda_1 \in \mathfrak{sl}_2(\mathbb{R})$. Ignoring the Lie algebra dynamics for a moment, we derive the Hamiltonian corresponding to the group element g . As pointed

out earlier, the control problem is left-invariant (see Definition 6.3.1) and Hamiltonians of left-invariant systems are functions of $\mathfrak{sl}_2(\mathbb{R})^*$ only.

Proposition 6.4.1 (Jurdjevic [19]). *Consider an arbitrary left-invariant control system $dg/dt = f(g, u)$ on a real Lie group G , with control $u \in U \subseteq \mathbb{R}^m$. Let us also assume that the Lie algebra \mathfrak{g} of G is equipped with a nondegenerate invariant symmetric bilinear form $\langle \cdot, \cdot \rangle$. Then the Hamiltonian function corresponding to this system is*

$$\mathcal{H}(g, p) = \langle p, f(e, u) \rangle, \quad p \in \mathfrak{g},$$

where $e \in G$ is the group identity.

Proof. Let $\langle \cdot, \cdot \rangle_*$ be the canonical pairing between a vector space and its dual. Let $\tilde{p} \in T_g^*G$. Using the trivialization $T^*G \cong G \times \mathfrak{g}^*$ of Proposition 3.6.1, we write $\tilde{p} = T^*L_{g^{-1}}(p)$ for some $p \in \mathfrak{g}^*$. Then we have by the definition of the Hamiltonian for a control system,

$$\begin{aligned} \mathcal{H}(g, \tilde{p}) &= \langle \tilde{p}, f(g, u) \rangle_* \\ &= \langle p, TL_{g^{-1}}(f(g, u)) \rangle_* = \langle p, TL_{g^{-1}}(TL_g f(e, u)) \rangle_* \\ &= \langle p, f(e, u) \rangle_*, \end{aligned}$$

since the control system is left-invariant. Since \mathfrak{g} is equipped with a nondegenerate invariant form $\langle \cdot, \cdot \rangle$, we have that $\mathfrak{g} \cong \mathfrak{g}^*$. Using this identification, we have $\mathcal{H}(g, p) = \langle p, f(e, u) \rangle$, where p is now identified with an element of \mathfrak{g} . \square

We need a slight extension of this result, where the control system has the form

$$dg/dt = f(g, TL_g X, u), \quad u \in U, \quad X \in \mathfrak{g}.$$

Left-invariance is expressed as $TL_h f(g, TL_g X, u) = f(hg, TL_{hg} X, u)$, and the corresponding Hamiltonian in the proposition becomes $\langle p, f(e, X, u) \rangle$.

In our case, taking $p = \Lambda_1$ and $f(e, X, u) = X$, this means that the term the Hamiltonian corresponding to the group is $\langle \Lambda_1, X \rangle$. The cost extended term of the Hamiltonian is

$$\mathcal{H}_1(\Lambda_1, X) := \langle \Lambda_1, X \rangle - \frac{3}{2} \lambda_{cost} \langle J, X \rangle.$$

The Lie algebra part of the Hamiltonian, corresponding to the costate variable Λ_2 , is

$$\mathcal{H}_2(\Lambda_2, X; Z_u) := \frac{\langle \Lambda_2, [Z_u, X] \rangle}{\langle X, Z_u \rangle} = -\frac{\langle [\Lambda_2, X], Z_u \rangle}{\langle X, Z_u \rangle}.$$

The form of the Hamiltonian suggests introducing a new variable $\Lambda_R := [\Lambda_2, X]$. The full Hamiltonian of the problem is now

$$\begin{aligned} \mathcal{H}(\Lambda_1, \Lambda_R, X; Z_u) &:= \mathcal{H}_1(\Lambda_1, X) + \mathcal{H}_2(\Lambda_2, X; Z_u) \\ &= \left\langle \Lambda_1 - \frac{3}{2} \lambda_{cost} J, X \right\rangle - \frac{\langle [\Lambda_2, X], Z_u \rangle}{\langle X, Z_u \rangle} \\ &= \left\langle \Lambda_1 - \frac{3}{2} \lambda_{cost} J, X \right\rangle - \frac{\langle \Lambda_R, Z_u \rangle}{\langle X, Z_u \rangle}. \end{aligned} \quad (6.4.1)$$

The maximum principle states that the extremals of the control problem are integral curves of the maximized Hamiltonian, which is the pointwise maximum of the control-dependent Hamiltonian over the control set. For our immediate application, we take the control set to be the simplex U_T (see Definition 3.3.3).

$$\begin{aligned} \mathcal{H}^+(\Lambda_1, \Lambda_2, X) &:= \max_{u \in U_T} \mathcal{H}(\Lambda_1, \Lambda_R, X; Z_u) \\ &= \left\langle \Lambda_1 - \frac{3}{2} \lambda_{cost} J, X \right\rangle + \max_{u \in U_T} \frac{\langle -\Lambda_R, Z_u \rangle}{\langle X, Z_u \rangle}. \end{aligned} \quad (6.4.2)$$

6.5 Costate Variables in Lie Algebra

Proposition 6.5.1 (Lie algebra costate variables). *The costate variables evolve as*

$$\Lambda'_1 = [\Lambda_1, X] \quad (6.5.1)$$

$$\Lambda'_R = ([P, \Lambda_R] - \langle \Lambda_R, P \rangle [P, X]) + \left[-\Lambda_1 + \frac{3}{2} \lambda_{cost} J, X \right], \quad (6.5.2)$$

where $P = Z_u / \langle X, Z_u \rangle$ and $\Lambda_R := [\Lambda_2, X]$.

Proof. Let \mathcal{H}^+ denote the maximized Hamiltonian in equation (6.4.2). Let

$$(g, X, \Lambda_1, \Lambda_2) \in \mathrm{SL}_2(\mathbb{R}) \times \mathfrak{sl}_2(\mathbb{R}) \times \mathfrak{sl}_2(\mathbb{R}) \times \mathfrak{sl}_2(\mathbb{R}) \cong T^*(\mathrm{SL}_2(\mathbb{R}) \times \mathfrak{sl}_2(\mathbb{R}))$$

denote the state and costate variables in the trivialized bundles. Since the Hamiltonian is independent of $\mathrm{SL}_2(\mathbb{R})$, it is left-invariant.

By the maximum principle, we have that the state and costate equations are Hamilton's equations in the cotangent bundle with respect to an appropriate symplectic form. For the (g, Λ_1) pair, the dynamics is Hamiltonian with respect to the pullback of the canonical symplectic form on $T^*(\mathrm{SL}_2(\mathbb{R}))$ to $\mathrm{SL}_2(\mathbb{R}) \times \mathfrak{sl}_2^*(\mathbb{R})$. These equations are called the Euler-Arnold equations for a left-invariant Hamiltonian (see [8, pp. 285]) and are given by

$$\begin{aligned} g' &= g \frac{\delta \mathcal{H}^+}{\delta \Lambda_1} = gX \\ \Lambda'_1 &= \mathrm{ad}_{\delta \mathcal{H}^+ / \delta \Lambda_1}^* \Lambda_1 = -\mathrm{ad}_X \Lambda_1 = [\Lambda_1, X], \end{aligned}$$

where we identify $\mathfrak{sl}_2(\mathbb{R})^*$ with $\mathfrak{sl}_2(\mathbb{R})$ as usual, sending the ad^* -operator to ad -operator, as described in Appendix A.4. The expression $\delta \mathcal{H}^+ / \delta \Lambda_1$ denotes the functional derivative of \mathcal{H}^+ with respect to Λ_1 and is defined in Appendix A.8 in equation (A.2.1). For the pair $(X, \Lambda_2) \in \mathfrak{sl}_2(\mathbb{R}) \times \mathfrak{sl}_2(\mathbb{R})^*$, the dynamics is Hamiltonian with respect to the canonical symplectic structure on the trivial cotangent bundle $T^*(\mathfrak{sl}_2(\mathbb{R}))$ which gives us Hamilton's equations in the usual form.

$$\begin{aligned} X' &= \frac{\delta \mathcal{H}^+}{\delta \Lambda_2} = [P, X] \\ \Lambda'_2 &= -\frac{\delta \mathcal{H}^+}{\delta X} = -\Lambda_1 + \frac{3}{2} \lambda_{\mathrm{cost}} J - [\Lambda_2, P] + \langle [\Lambda_2, P], X \rangle P. \end{aligned}$$

Using this, we can derive

$$\begin{aligned} \Lambda'_R &= [\Lambda_2, X]' = [\Lambda'_2, X] + [\Lambda_2, X'] \\ &= \left[-\Lambda_1 + \frac{3}{2} \lambda_{\mathrm{cost}} J, X \right] + \langle [\Lambda_2, P], X \rangle [P, X] - [[\Lambda_2, P], X] + [\Lambda_2, [P, X]] \\ &= \left[-\Lambda_1 + \frac{3}{2} \lambda_{\mathrm{cost}} J, X \right] + \langle [\Lambda_2, P], X \rangle [P, X] + [P, [\Lambda_2, X]] \\ &= \left[-\Lambda_1 + \frac{3}{2} \lambda_{\mathrm{cost}} J, X \right] - \langle \Lambda_R, P \rangle [P, X] + [P, \Lambda_R] \\ &= \left([P, \Lambda_R] - \frac{\langle \Lambda_R, Z_u \rangle}{\langle X, Z_u \rangle} [P, X] \right) + \left[-\Lambda_1 + \frac{3}{2} \lambda_{\mathrm{cost}} J, X \right]. \end{aligned}$$

□

Remark 6.5.2.

- Note that the variable Λ_R is constrained to lie in the two-dimensional subspace $\{A \in \mathfrak{sl}_2(\mathbb{R}) \mid \langle A, X \rangle = 0\}$. Thus, we can consider Λ_R to be the *reduced* costate variable. (The subscript R stands for *reduced*.)
- In Appendix A.9, we show that there is a Poisson bracket with respect to which the Reinhardt control system admits a Poisson bracket representation.

Corollary 6.5.3 (Jurdjevic [19, 21]). *The costate variable Λ_1 , whose dynamics is given by a Lax equation, evolves in an adjoint orbit of $\mathfrak{sl}_2(\mathbb{R})$ through the initial value $\Lambda_1(0)$ and its general solution is given by*

$$\Lambda_1(t) = \text{Ad}_{g(t)^{-1}}(\Lambda_1(0)) = g(t)^{-1} \Lambda_1(0) g(t).$$

Moreover, the determinant $\det(\Lambda_1(t))$ is a constant of motion.

Proof. This can be verified by differentiating. We immediately find the determinant is constant. If the identification of the Lie algebra with its dual is not made, the evolution is in a coadjoint orbit through the representation Ad^* . \square

Corollary 6.5.4. *In the ODE for Λ_R in equation (6.5.2), the control dependent term has the following expression.*

$$\left([P, \Lambda_R] - \frac{\langle \Lambda_R, Z_u \rangle}{\langle X, Z_u \rangle} [P, X] \right) = \text{ad}_{Z_u} \frac{\delta}{\delta Z_u} \frac{\langle \Lambda_R, Z_u \rangle}{\langle X, Z_u \rangle} = \text{ad}_{Z_u} \frac{\delta \mathcal{H}_2}{\delta Z_u}, \quad (6.5.3)$$

where $\frac{\delta}{\delta Z_u}$ denotes the functional derivative (defined in Section A.8).

Proof. The proof is by computation.

$$\begin{aligned} \text{ad}_{Z_u} \frac{\delta}{\delta Z_u} \left(\frac{\langle \Lambda_R, Z_u \rangle}{\langle X, Z_u \rangle} \right) &= \left[Z_u, \frac{\delta}{\delta Z_u} \left(\frac{\langle \Lambda_R, Z_u \rangle}{\langle X, Z_u \rangle} \right) \right] \\ &= \left[Z_u, \frac{\Lambda_R \langle X, Z_u \rangle - \langle \Lambda_R, Z_u \rangle X}{\langle X, Z_u \rangle^2} \right] \\ &= \frac{[Z_u, \Lambda_R]}{\langle X, Z_u \rangle} - \frac{\langle \Lambda_R, Z_u \rangle}{\langle X, Z_u \rangle^2} [Z_u, X] \\ &= [P, \Lambda_R] - \frac{\langle \Lambda_R, Z_u \rangle}{\langle X, Z_u \rangle} [P, X]. \end{aligned}$$

\square

6.6 Transversality Conditions

For free terminal time optimal control problems, the Pontryagin Maximum Principle specifies *transversality* conditions which are endpoint conditions which the extremals need to satisfy.

On a manifold M , if $(q(t), u(t))$ is the projection of the lifted extremal trajectory $p(t) \in T_{q(t)}^* M$ in the cotangent bundle, then transversality requires that

$$\langle p(t_f), v \rangle_* = 0 \quad v \in T_{q(t_f)} M_f,$$

where $T_{q(t_f)} M_f$ is the tangent space at $q(t_f)$ of the *final submanifold* M_f (which is the submanifold in which the terminal point $q(t_f)$ is allowed to vary).

More generally, if the initial point $q(0)$ is also allowed to vary in an *initial submanifold* M_0 , then transversality requires that the lifted extremal trajectory $p(t)$ in the cotangent bundle annihilates the vectors in the tangent spaces of the initial and terminal manifolds at the initial and terminal times.

$$\begin{aligned} \langle p(0), \mathbf{v} \rangle_* &= 0, & \mathbf{v} \in T_{q(0)} M_0; \\ \langle p(t_f), \mathbf{v} \rangle_* &= 0, & \mathbf{v} \in T_{q(t_f)} M_f. \end{aligned}$$

Letting R be the usual rotation matrix, we have that our system is periodic up to a rotation by R . In this case, the initial and terminal submanifolds coincide after rotation by R and so, transversality simply means that the lifted extremal trajectories are periodic functions modulo rotation by R . Rotations act through the adjoint action $Y \mapsto \text{Ad}_R Y = RYR^{-1}$ on the Lie algebra $\mathfrak{sl}_2(\mathbb{R})$.

For our system, we have $p(t) = (g(t), X(t), \Lambda_1(t), \Lambda_R(t))$. We have already seen endpoint conditions for g and X in Section 3.5. Collecting everything we obtain

$$\begin{aligned} g(t_f) &= R \\ X(t_f) &= R^{-1} X(0) R \\ \Lambda_1(t_f) &= R^{-1} \Lambda_1(0) R \\ \Lambda_R(t_f) &= R^{-1} \Lambda_R(0) R. \end{aligned} \tag{6.6.1}$$

Remark 6.6.1.

- The transversality conditions in the Reinhardt problem require the terminal time to satisfy

$$X(t_f) = R^{-1}X_0R,$$

where R is the usual rotation matrix. Thus, if we extend time, every optimal solution can be made into a periodic one.

$$X(3t_f) = X_0.$$

The same requirement also holds of g, Λ_1 and Λ_R , except that the period for g is larger: $g(6t_f) = I_2$. Thus, every transversal trajectory determines a periodic solution (with discrete rotational symmetry) of the lifted trajectories in the cotangent bundle.

- The transversality condition for Λ_1 is a consequence of the transversality condition for g . In fact, we know the general solution for Λ_1 in terms of g . See Corollary 6.5.3.

6.7 Summary of State and Costate Equations

At this point, we have the state and costate equations fully stated in both the coadjoint orbit picture and the upper half-plane picture. We also have the transversality conditions stated. We collect them as

Problem 6.7.1 (State-Costate Equations). *The Reinhardt control problem 3.6.2 is an optimal control problem on the manifold $M = \mathrm{SL}_2(\mathbb{R}) \times \mathfrak{sl}_2(\mathbb{R})$. This problem has the Hamiltonian*

$$\mathcal{H}(\Lambda_1, \Lambda_R, X; Z_u) = \left\langle \Lambda_1 - \frac{3}{2}\lambda_{cost}J, X \right\rangle - \frac{\langle \Lambda_R, Z_u \rangle}{\langle X, Z_u \rangle}.$$

We lift the state trajectories described by (g, X) in the Reinhardt control problem 3.6.2 to the following Hamiltonian system on the cotangent bundle of M :

$$\begin{aligned} g' &= gX \\ X' &= [P, X] \\ \Lambda'_1 &= [\Lambda_1, X] \\ \Lambda'_R &= ([P, \Lambda_R] - \langle \Lambda_R, P \rangle [P, X]) + \left[-\Lambda_1 + \frac{3}{2}\lambda_{cost}J, X \right], \end{aligned}$$

where $P = Z_u/\langle Z_u, X \rangle$. The transversality conditions described in Section 6.6 hold and the pair (X, Λ_R) have equivalent dynamics in the upper half-plane described in Lemma 4.5.2 and Theorem 6.8.3. The control dependent part of the Hamiltonian also has an expression in the upper half-plane picture as Theorem 6.8.2.

6.8 Hamiltonian and Costate Equations in the Upper-half plane

An earlier preprint expressed the Hamiltonian and the maximum principle in terms of the cotangent variables $\nu = \nu_1 dx + \nu_2 dy \in T_z^* \mathfrak{h}$ [16]. It turns out that it is significantly simpler to express the costate differential equations in terms of the coordinate $\Lambda_R \in \mathfrak{sl}_2(\mathbb{R})$ instead of (ν_1, ν_2) . In this book we use Λ_R , rather than ν . However, for reasons of compatibility with the earlier preprint, this section briefly reviews the correspondence between the two coordinate system. This section will not be used elsewhere in the book.

With this aim in mind, we now proceed to transport the Hamiltonian from Lie algebra coordinates to upper half-plane coordinates. Recall that we have an isomorphism $\Phi : \mathfrak{h} \rightarrow \mathcal{O}_X \subset \mathfrak{sl}_2(\mathbb{R})$ defined in Lemma 4.2.1. This induces the tangent map $T\Phi : T_z \mathfrak{h} \rightarrow T_X \mathcal{O}_X$ as described in Lemma 4.2.4. This also induces the dual (cotangent) map: $T^*\Phi : T_X^* \mathcal{O}_X \rightarrow T_z^* \mathfrak{h}$.

Lemma 6.8.1.

$$T_X^* \mathcal{O}_X \cong X^\perp = \{[W, X] \mid W \in \mathfrak{sl}_2(\mathbb{R})\},$$

where $X^\perp = \{Y \in \mathfrak{sl}_2(\mathbb{R}) \mid \langle Y, X \rangle = 0\}$.

Explicitly, the isomorphism identifies the cotangent space with the dual of the tangent space, under the identification of the tangent space with the quotient $\mathfrak{sl}_2(\mathbb{R})/\mathbb{R}X$ of Lemma 4.2.3.

Proof. By a general fact in elementary linear algebra we have

$$T_X^* \mathcal{O}_X \cong (\mathfrak{sl}_2(\mathbb{R})/\mathbb{R}X)^* \cong \mathbb{R}X^\circ = X^\perp,$$

where

$$\mathbb{R}X^\circ = \{Y \in \mathfrak{sl}_2(\mathbb{R}) \mid \langle Y, W \rangle = 0 \text{ for all } W \in \mathbb{R}X\}$$

is the annihilator of the span of X . Here the annihilator, which is defined as a subspace of the dual vector space, is identified with a subspace of the Lie algebra itself via the nondegenerate trace form.

It is clear that any Lie algebra element of the form $[W, X]$ is orthogonal to X since $\langle [W, X], X \rangle = \langle W, [X, X] \rangle = 0$. Dimension counting again gives us that $T_X^* \mathcal{O}_X = \{[W, X] \mid W \in \mathfrak{sl}_2(\mathbb{R})\}$. \square

We define

$$\nu := T^* \Phi(-\Lambda_R) = \nu_1 dx + \nu_2 dy \in T_z^* \mathfrak{h}. \quad (6.8.1)$$

The covector $\nu \in T_z^* \mathfrak{h}$ is well-defined since $\Lambda_R \in X^\perp$ by Lemma 6.8.1.

Theorem 6.8.2 (Hamiltonian in Upper Half-Plane). *Let Φ be as in Lemma 4.2.1 and let Λ_R be as above. Then we have that the Hamiltonian $\mathcal{H}(\Lambda_1, \Lambda_R, X; Z_u)$ in equation (6.4.1) in upper half-plane coordinates becomes*

$$\mathcal{H}(\Lambda_1, x, y, \nu_1, \nu_2; u) = \left\langle \Lambda_1 - \frac{3}{2} \lambda_{cost} J, X \right\rangle + \nu_1 f_1 + \nu_2 f_2.$$

Proof. The only part of the Hamiltonian in equation (6.4.1) which will change is $\mathcal{H}_2(\Lambda_2, X; Z_u)$.

$$\begin{aligned} \mathcal{H}_2(\Lambda_R, X; Z_u) &= \frac{\langle -\Lambda_R, Z_u \rangle}{\langle Z_u, X \rangle} = \left\langle -\Lambda_R, \frac{Z_u}{\langle Z_u, X \rangle} \right\rangle \\ &= \left\langle -\Lambda_R, \frac{Z_u}{\langle Z_u, X \rangle} + \mathbb{R}X \right\rangle \\ &= \langle -\Lambda_R, T\Phi(f_1, f_2) \rangle \quad \text{by (4.5.1)} \\ &= \langle T^* \Phi(-\Lambda_R), (f_1, f_2) \rangle_* \\ &= \langle \nu, (f_1, f_2) \rangle_* \\ &= \nu_1 f_1 + \nu_2 f_2, \end{aligned}$$

where we have used the definition of the cotangent map and the fact that $\Lambda_R \in X^\perp$, the annihilator subspace of X in $\mathfrak{sl}_2(\mathbb{R})$. \square

Theorem 6.8.3. *The ODE for Λ_R is transformed to the ODE*

$$\nu' = -d\mathcal{H} = -\frac{\partial \mathcal{H}}{\partial x} dx - \frac{\partial \mathcal{H}}{\partial y} dy,$$

where \mathcal{H} is the Hamiltonian derived in equation (6.4.1).

Proof. We note that this equation is Hamilton's equation for the costate. We omit the long direct calculation that this equation is equivalent to the ODE for Λ_R . Details can be found in [48]. \square

Part III

Solutions

Chapter 7

Bang Bang Solutions

We have a well-defined control problem on the cotangent bundle, and we now turn to describing special solutions of this system. We start with the easiest case, where the control is constant.

7.1 Solutions for Constant Control

Lemma 7.1.1. *The quantity $\langle X, Z_u \rangle$ for a fixed control matrix Z_u is a constant of motion along X .*

Proof. The quantity in question is constant since

$$\langle X, Z_u \rangle' = \langle X', Z_u \rangle = \frac{\langle [Z_u, X], Z_u \rangle}{\langle X, Z_u \rangle} = 0, \quad (7.1.1)$$

where we have used the fact that $\langle [X, Y], Z \rangle = \langle X, [Y, Z] \rangle$. □

Lemma 7.1.2. *Assume that the control $u \in U_T$ is constant. Then the speed $\langle X', X' \rangle^{1/2}$ of X is constant. Moreover, the trajectory z in \mathfrak{h} , defined by $X = \Phi \circ z$, has constant speed with respect to the invariant Riemannian metric on \mathfrak{h} .*

Proof. Let $P = Z_u / \langle X, Z_u \rangle$ with constant control $u \in U_T$. By the previous lemma, P is constant. To show that the speed is constant, we differentiate

$$\begin{aligned} \langle X', X' \rangle' &= 2 \langle X'', X' \rangle = 2 \langle [P, X]', X' \rangle = 2 \langle [P, X'], X' \rangle \\ &= 2 \langle P, [X', X'] \rangle = 0. \end{aligned}$$

The trajectory z also has constant speed because of the compatibility of the invariant metric on the upper half plane with the trace form on $\mathfrak{sl}_2(\mathbb{R})$, by Lemma A.11.1. \square

In this section, we keep the control matrix Z_u constant and derive general solutions to the state and costate equations. This means that $\langle Z_u, X \rangle$ is a constant of motion (by equation (7.1.1)), and hence $P = Z_u/\langle Z_u, X \rangle$ is also constant. So, for $g(0) = I_2$ and $X(0) = X_0$ (or, equivalently $z(0) = z_0$), write $P_0 := Z_u/\langle Z_u, X_0 \rangle$. The general solutions for (g, X) are

$$g(t) = \exp(t(X_0 + P_0)) \exp(-tP_0), \quad (7.1.2)$$

$$z(t) = \exp(tP_0) \cdot z_0, \quad (7.1.3)$$

$$X(t) = \exp(tP_0)X_0 \exp(-tP_0) = \text{Ad}_{\exp(tP_0)}X_0. \quad (7.1.4)$$

As previously noted in Corollary 6.5.3, the general solution for Λ_1 is

$$\Lambda_1(t) = \text{Ad}_{g(t)^{-1}}\Lambda_1(0) = g(t)^{-1}\Lambda_1(0)g(t).$$

We also have a rather complicated (but ultimately elementary) expression for the general solution for Λ_R .

$$\Lambda_R(t) = \text{Ad}_{\exp(tP_0)}\tilde{\Lambda}_R(t),$$

where

$$\begin{aligned} \tilde{\Lambda}_R(t) &:= \Lambda_R(0) - [\Psi(t) + \psi(t)P_0, X_0], \\ \psi(t) &:= \int_0^t \langle P_0, \Lambda_R(0) - [\Psi(s), X_0] \rangle ds, \\ \Psi(t) &:= \int_0^t \text{Ad}_{\exp(-(X_0 + P_0)s)}\Lambda_1(0) - \frac{3}{2}\lambda_{cost}\text{Ad}_{\exp(-P_0s)}J ds. \end{aligned}$$

The two quadratures can be carried out explicitly for any given matrices X_0 and $X_0 + P_0$. The exponentials of these matrices are expressed in terms of the exponentials $\exp(\lambda s)$ of the eigenvalues λ of these matrices. The integrands are exponentials (possibly multiplied by polynomials), and the integrals are easily computed. In computing the solution Λ_R , we first compute Ψ , then ψ , then $\tilde{\Lambda}_R$, and finally Λ_R .

By inspection of the formula for ψ , we note that if $\tilde{\Lambda}_{R,0}(t)$ is the specialization of $\tilde{\Lambda}_R(t)$ to the initial condition $\Lambda_R(0) = 0$, then the general solution adds an affine term

$$\tilde{\Lambda}_R(t) = \tilde{\Lambda}_{R,0}(t) + \Lambda_R(0) - t \langle P_0, \Lambda_R(0) \rangle [P_0, X_0].$$

Lemma 7.1.3. *The matrices P_0 and $X_0 + P_0$ have the same characteristic polynomial (and hence the same eigenvalues). If $\det(Z_u) < 0$, the eigenvalues are real: $\pm\sqrt{-\det(Z_u)}/\langle X_0, Z_u \rangle$.*

The most important case occurs when u is a vertex of the control set U_T , where $\det(Z_u) = -1/3 < 0$.

Proof. The characteristic polynomial of matrices $P_0, X_0 + P_0 \in \mathfrak{sl}_2$ is determined by the determinant. We have $\det(X_0) = 1$, and $\langle X_0, P_0 \rangle = 1$. Then by Lemma 3.4.1, we have

$$\begin{aligned} -2\det(X_0 + P_0) &= \langle X_0 + P_0, X_0 + P_0 \rangle \\ &= \langle X_0, X_0 \rangle + 2\langle X_0, P_0 \rangle + \langle P_0, P_0 \rangle \\ &= -2\det(P_0). \end{aligned}$$

Recall that $\text{trace}(Z_u) = 0$ and that Z_u and P_0 are scalar multiples of each other. When $\det(Z_u) < 0$, the control matrix P_0 has two real eigenvalues. \square

We analyze the solution $z(t) = \exp(tP_0) \cdot z_0$ in greater detail. Let Z_0 be the value of Z_u at $t = 0$. If $\det(Z_0) < 0$, let $\pm\lambda$ be the real eigenvalues of P_0 , chosen so that $\lambda > 0$. The matrix P_0 can be diagonalized over \mathbb{R} :

$$\exp(tP_0) = A \text{diag}(\exp(t\lambda), \exp(-t\lambda))A^{-1},$$

for some $A \in \text{SL}_2(\mathbb{R})$. The columns of $A = (\mathbf{v}_+, \mathbf{v}_-)$ are the column eigenvectors \mathbf{v}_\pm of Z_0 , associated to the positive and negative eigenvectors, respectively. The matrix P_0 has the same eigenvectors. The solution is then

$$z(t) = A \cdot (\exp(2t\lambda)\tilde{z}_0), \quad \tilde{z}_0 := A^{-1} \cdot z_0.$$

The image of the trajectory $t \mapsto \exp(2t\lambda)\tilde{z}_0$ is a Euclidean line through $0 + 0i$ and $\tilde{z}_0 \in \mathfrak{h}$. By adopting the convention that $\lambda > 0$, this linear trajectory tends to 0 as time t tends to $-\infty$, reaches \tilde{z}_0 at $t = 0$, and tends to infinity as t tends to infinity. Linear fractional transformations send generalized circles (that is Euclidean circles or lines) to generalized circles. Thus, the image of z is the unique generalized circle through $A \cdot 0$, $z_0 = A \cdot \tilde{z}_0$, and $A \cdot \infty$.

The boundary of \mathfrak{h} can be identified with the real projective line $\mathbb{R} \cup \{\infty\}$. From the description of A as the column of eigenvectors, we have $A \cdot 0 = [\mathbf{v}_-]$ and $A \cdot \infty = [\mathbf{v}_+]$, where $[\mathbf{v}_-]$ and $[\mathbf{v}_+]$ are the lines through the origin spanned by the eigenvectors, viewed as points in the real projective line.

Thus, the trajectories are arcs of generalized circles, from $[\mathbf{v}_-]$ to $[\mathbf{v}_+]$ on the boundary of \mathfrak{h} .

If $\det(Z_0) > 0$, then the eigenvalues are pure imaginary. The solutions $z(t)$ in \mathfrak{h} are then periodic. In fact, the solutions are circles whose center (with respect to the hyperbolic metric) is the point $z_0 \in \mathfrak{h}$, defined by the fixed point condition $Z_0 \cdot z_0 = z_0$. (Equivalently, $(z_0, 1)$ is a complex eigenvector of Z_0 , chosen so that $z_0 \in \mathfrak{h}$.) Each trajectory moves at constant speed with respect to the hyperbolic metric on \mathfrak{h} . When $u = (1/3, 1/3, 1/3)$ (the center of U_T), $Z_0 = J/3$, and the fixed point is $i \in \mathfrak{h}$.

If $\det(Z_0) = 0$, then the eigenvalues are 0 (but Z_0 has rank 1). (For example, take control $u = (2/3, 1/6, 1/6)$.) The solutions $z(t)$ in \mathfrak{h} move along horocycles centered at an ideal point in the real projective line (viewed as the boundary of \mathfrak{h}). That ideal point is the line formed by the kernel of Z_0 .

7.2 Constant Control at the Vertices

As we will see in Lemma 7.3.1, the constant controls at the vertices of the control triangle have particular significance, because they often maximize the Hamiltonian. Assume that the control remains at a vertex u of the control triangle U_T during some time interval $t \in [t_1, t_2]$. By the construction of the control from state-dependent curvatures, two of the state-dependent curvatures κ_j, κ_{j+1} are zero. Thus the corresponding trajectories

$$\sigma_i(t) = g(t)\mathbf{s}_i^*, \quad i = 2j, 2j+2,$$

move along straight lines. According to Lemma 3.1.8, the third curve $\sigma_{2j+1}(t)$ moves along an arc of a hyperbola. The solution (7.1.2) gives explicit parameterizations of these straight lines and hyperbolic arcs.

If u is a vertex of the control triangle U_T , then $\det(Z_u) = -1/3 < 0$, and the eigenvalues of $-Z_u$ are $\pm 1/\sqrt{3}$. Let \mathbf{v}_\pm be eigenvectors for $1/\sqrt{3}$ and $-1/\sqrt{3}$ respectively. The remarks of the earlier paragraph apply, to show that the trajectories in \mathfrak{h} are generalized circles moving from $[\mathbf{v}_-]$ toward $[\mathbf{v}_+]$ on the boundary of \mathfrak{h} . The explicit parameterization is in terms of exponentials, as described above.

If $u = (0, 0, 1)$, the eigenvectors of $-Z_u$ are computed to be

$$\mathbf{v}_- = (-1/\sqrt{3}, 1), \quad \mathbf{v}_+ = (1, 0).$$

Trajectories z are straight lines moving from the ideal vertex $[\mathbf{v}_-] = -1/\sqrt{3}$ toward the ideal vertex $[\mathbf{v}_+] = +\infty$. Explicitly, we have

$$x(t) = [\mathbf{v}_-] + C_0 \exp(rt), \quad y(t) = C_0 r \exp(rt),$$

where the constants of integration $r, C_0 > 0$ are uniquely determined at $t = 0$.

$$x_0 = x(0) = [\mathbf{v}_-] + C_0, \quad y_0 = y(0) = C_0 r.$$

If $u = (0, 1, 0)$, the eigenvectors of $-Z_u$ are computed to be

$$\mathbf{v}_- = (1, 0), \quad \mathbf{v}_+ = (1/\sqrt{3}, 1).$$

The trajectories z are straight lines moving from the ideal vertex $[\mathbf{v}_-] = +\infty$ toward the ideal vertex $[\mathbf{v}_+] = +1/\sqrt{3}$. The trajectory is

$$x(t) = [\mathbf{v}_+] + C_0 \exp(rt), \quad y(t) = C_0 r \exp(rt),$$

where now $C_0, r < 0$. Note that when $u = (0, *, *)$, the matrix Z_u is upper triangular, so that the eigenvectors and $\exp(Pt)$ are trivial to compute.

If $u = (1, 0, 0)$, the eigenvectors of $-Z_u$ are computed to be

$$\mathbf{v}_- = (1/\sqrt{3}, 1), \quad \mathbf{v}_+ = (-1/\sqrt{3}, 1).$$

The trajectories z are Euclidean circles moving from the ideal vertex $[\mathbf{v}_-] = 1/\sqrt{3}$ toward the ideal vertex $[\mathbf{v}_+] = -1/\sqrt{3}$.

Note that the solutions at the different vertices are related by linear fractional transformations R , which rotates the star domain \mathfrak{h}^* , and permutes the ideal vertices.

We record the preceding discussion in the form of a lemma.

Lemma 7.2.1. *If the control function is a constant at one of the vertices of U_T , then the trajectories in the star domain are arcs generalized circles. If the control is $(0, 0, 1)$ or $(0, 1, 0)$, then each trajectory moves along a Euclidean straight line.*

Proof.

□

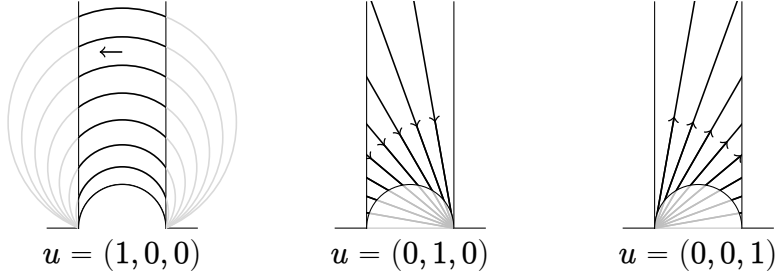


Figure 7.2.1: The trajectories with constant control u are generalized circles, shown here in the star domain of the upper half-plane.

7.3 Partition of the Cotangent Space

Let K be a compact convex set in \mathbb{R}^n . A nonempty convex subset F of K is called a *face* if and only if for all $x, y \in K$ and all $t \in (0, 1)$, the membership $tx + (1 - t)y \in F$ implies endpoint membership: $x, y \in F$.

Lemma 7.3.1. *Assume that the control set is U a compact convex set in the affine plane $\{(u_0, u_1, u_2) \mid \sum u_i = 1\}$. For each point in the cotangent space $(g, X, \Lambda_1, \Lambda_R)$, the set of controls $u \in U$ maximizing the Hamiltonian $\mathcal{H}(\Lambda_1, \Lambda_R, X, Z_u)$ in equation (6.4.2) is equal to a face of the control set.*

Proof. Fix $(g, X, \Lambda_1, \Lambda_R)$. We consider the dependence of the control-dependent part (denoted \mathcal{H}_2) of the Hamiltonian in equation (6.4.2). As a function of $u \in U$, the Hamiltonian is a ratio of two affine functions. Fixing $u, v \in U$, the dependence on t along the segment $tu + (1 - t)v \in U$, for $0 \leq t \leq 1$, of the control-dependent part of the Hamiltonian takes the general form

$$\mathcal{H}_2(t) = \frac{at + b}{ct + d}$$

with nonzero denominator. The derivative $(ad - bc)/(ct + d)^2$ of this expression has fixed sign. Thus, Hamiltonian is monotonic along the segment. If an internal point of the segment is a maximizer, then both endpoints are also maximizers. According to the definition of face, the set of maximizers must be a face. \square

Thus, if we consider the control set U_T , the set of maximizers are either the entire control set U_T , or one of its edges or vertices.

The control-dependent part of the Hamiltonian depends on state and costate variables through (X, Λ_R) . Such pairs can be identified with the cotangent space of \mathcal{O}_J :

$$T^*\mathcal{O}_J \cong \{(X, \Lambda_R) \in \mathcal{O}_J \times \mathfrak{sl}_2(\mathbb{R}) \mid \Lambda_R \in X^\perp\}.$$

For each nonempty subset $\emptyset \neq I \subseteq \{1, 2, 3\}$, we have a face $(U_T)_I \subseteq U_T$ defined by the convex hull of $\{\mathbf{e}_i \mid i \in I\}$, where $\mathbf{e}_1 = (1, 0, 0)$, $\mathbf{e}_2 = (0, 1, 0)$, $\mathbf{e}_3 = (0, 0, 1)$ is the standard basis of \mathbb{R}^3 . These subsets classify faces of U_T . For each I , there is a corresponding region of $T^*\mathcal{O}_J$.

$$(T^*\mathcal{O}_J)_I := \{(X, \Lambda_R) \in T^*\mathcal{O}_J \mid \operatorname{argmax}_{u \in U_T} \mathcal{H}_2(\cdot, \Lambda_R, X, Z_u) = (U_T)_I\}.$$

As I runs over nonempty subsets of $\{1, 2, 3\}$, the sets $(T^*\mathcal{O}_J)_I$ partition $T^*\mathcal{O}_J$ into locally closed subsets.

The union of the three sets $(T^*\mathcal{O}_J)_I$, for $|I| = 1$ is a dense open subset of $(T^*\mathcal{O}_J)$. On this dense open subset, the Hamiltonian is maximized at a uniquely determined vertex. In general, the control function $u : [0, t_f] \rightarrow U_T$ is allowed to be any measurable function. The solutions of the control system ODEs do not change by modifying the control u on a set of zero measure in $[0, t_f]$. If the control u remains in the dense open subset for all $t \in [0, t_f]$, (that is, if the image of the control function u is contained in the set of vertices of U_T), we will call the solution a *bang-bang* solution. Note that the control function is necessarily discontinuous where it jumps from one vertex to another. This chapter is concerned with bang-bang solutions, but later chapters will extend the investigation to solutions that are not bang-bang.

Definition 7.3.2 (Bang-bang control). *A control function is said to be bang-bang if its range is contained in the set of extreme points of the control set, with discontinuous switching.*

We call the three sets $(T^*\mathcal{O}_J)_I$, for $|I| = 2$ the *walls* in $T^*\mathcal{O}_J$. The walls have codimension 1 in $T^*\mathcal{O}_J$. The wall $\{i, j\}$ is contained in boundary between the open regions with indices $I = \{i\}$ and $\{j\}$. Finally, there is a set $(T^*\mathcal{O}_J)_{\{1, 2, 3\}}$, where the three walls meet.

7.4 Constant Control Splines

By a *spline* we mean a trajectory that has been pieced together from constant control trajectories, by matching the endpoints of one trajectory on

one subinterval with the initial conditions on the next subinterval. In this section, we give explicit constructions of splines. In this section, we do not assume that the curves satisfy the Pontryagin Maximum Principle conditions in the cotangent space. However, the trajectories are assumed to satisfy the state space ODEs (for (g, X)) and controls at the vertices of U_T .

Fix a vertex $u_0 = \mathbf{e}_j \in U_T$ in the control simplex. For $t \geq 0$ and initial position $z = z_0 \in \mathfrak{h}$, let $g_0(z, t) \in \mathrm{SL}_2(\mathbb{R})$ be the trajectory with solving the state ODE for g with constant control u_0 and initial conditions

$$g_0(z, 0) = I_2, \quad g'_0(z, 0) = \Phi(z).$$

(As always, prime denotes the derivative with respect to t .) Let $g_i(z, t) \in \mathrm{SL}_2(\mathbb{R})$, for $t \geq 0$, $i \in \mathbb{Z}$, and $z \in \mathfrak{h}$ be the trajectory

$$g_i(z, t) := R^i g_0(z, t) R^{-i}.$$

We have

$$g_i(z, 0) = I_2, \quad g'_i(z, 0) = \Phi(R^i \cdot z),$$

with constant control $u_i = R^i \cdot u_0$, using the action of the cyclic subgroup $\langle R \rangle$ of the dihedral group \mathbf{Dih}_6 on the control simplex U_T .

We define a continuous (shifted) extension of g_i that is non-constant only for $t \in [\tilde{t}_1, \tilde{t}_2]$:

$$g_i(z, \tilde{t}_1, \tilde{t}_2, t) := \begin{cases} I_2, & \text{if } t \leq \tilde{t}_1; \\ g_i(z, t - \tilde{t}_1), & \text{if } \tilde{t}_1 \leq t \leq \tilde{t}_2; \\ g_i(z, \tilde{t}_2 - \tilde{t}_1), & \text{if } \tilde{t}_2 \leq t. \end{cases}$$

The derivative g'_i has jump discontinuities at \tilde{t}_1 and \tilde{t}_2 . Let $z(z_0, t)$ be the solution to the ODE (4.5.1) with constant control u_0 and initial condition z_0 . For any tuple

$$\mathcal{I} = ((k_1, t_1), (k_2, t_2), \dots, (k_n, t_n)),$$

with $k_i \in \mathbb{Z}$ and $t_i \geq 0$, and for any $z_0 \in \mathfrak{h}^*$, let

$$\begin{aligned} \tilde{t}_0 &= 0; \\ \tilde{t}_{i+1} &= \tilde{t}_i + t_{i+1}; \\ z_i &= R^{k_i - k_{i+1}} \cdot z(z_{i-1}, t_i); \\ g(\mathcal{I}, z_0, t) &= g_{k_1}(z_0, \tilde{t}_0, \tilde{t}_1, t) g_{k_2}(z_1, \tilde{t}_1, \tilde{t}_2, t) \cdots g_{k_n}(z_{n-1}, \tilde{t}_{n-1}, \tilde{t}_n, t). \end{aligned} \tag{7.4.1}$$

Note that on the right-hand side of the last equation, only one factor at a time is non-constant. Then $g(\mathcal{I}, z, t)$ is continuous in t and has unit speed parametrization. Set $X(\mathcal{I}, z, t) := g(\mathcal{I}, z, t)^{-1}g'(\mathcal{I}, z, t)$. Note that for $t \in [\tilde{t}_{i-1}, \tilde{t}_i]$, when the i th factor is active, we have

$$\begin{aligned} X(\mathcal{I}, z_0, t) &= g_{k_i}(z_{i-1}, \tilde{t}_{i-1}, \tilde{t}_i, t)^{-1}g'_{k_i}(z_{i-1}, \tilde{t}_{i-1}, \tilde{t}_i, t) \\ &= g_{k_i}(z_{i-1}, t - \tilde{t}_{i-1})^{-1}g'_{k_i}(z_{i-1}, t - \tilde{t}_{i-1}) \\ &= R^{k_i}X(z_{i-1}, t - \tilde{t}_{i-1})R^{-k_i}, \end{aligned}$$

where $X(z, t) = g_0(z, t)^{-1}g'_0(z, t)$. Comparing left and right limits of $X(\mathcal{I}, z_0, t)$ at the boundary value $t = \tilde{t}_i$, we find that $X(\mathcal{I}, z_0)$ is continuous in t .

$$\begin{aligned} X(\mathcal{I}, z_0, \tilde{t}_i^-) &= \Phi(R^{k_i} \cdot z(z_{i-1}, t_i)) = \Phi(R^{k_{i+1}} \cdot z_i); \\ X(\mathcal{I}, z_0, \tilde{t}_i^+) &= \Phi(R^{k_{i+1}} \cdot z_i). \end{aligned}$$

From this, it is easy to see that $g(\mathcal{I}, z_0)$ is the general bang-bang trajectory with finitely many switches (at times $\tilde{t}_0, \dots, \tilde{t}_n$), as we vary \mathcal{I} and z_0 . The control on the interval $[\tilde{t}_{i-1}, \tilde{t}_i]$ is $u = R^{k_i} \cdot u_0 \in U$.

The total cost($z_0, [0, t]$) of the trajectory (7.4.1) with initial condition z_0 up to time t is an easy (freshman calculus) integral to compute from Equation (4.3.1), which we do not display here. The total cost of $g(\mathcal{I}, z_0, t)$ from time 0 to \tilde{t}_n is the sum of the costs on each constant control segment.

$$\sum_{i=0}^{n-1} \text{cost}(z_i, [0, t_{i+1}]). \quad (7.4.2)$$

7.5 Smoothed Polygons

In this section, we construct a family of Pontryagin extremals of the control problem, all given by a bang-bang control. Reinhardt conjectured that the smoothed octagon is the solution to his problem. The smoothed octagon belongs to a family of smoothed $(6k + 2)$ -gons, which are all given by bang-bang controls. The X -component of the trajectory of the smoothed 8-gon and the 14-gon are shown in Figure 7.5.1. These are periodic solutions in \mathfrak{h} , repeatedly retracing the edges of equilateral triangles in \mathfrak{h} (with edges formed by generalized circular arcs). The triangle has full dihedral group symmetry about the center $i \in \mathfrak{h}$ with respect to the hyperbolic metric. The

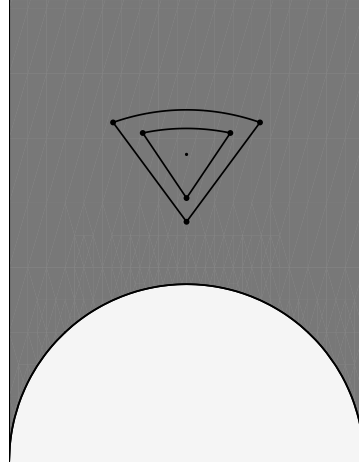


Figure 7.5.1: Periodic trajectories of the smoothed 8-gon and 14-gon in \mathfrak{h}^* . The larger triangle is the orbit of the 8-gon, and the smaller is that of 14-gon.

triangles shrink toward the central point $i \in \mathfrak{h}^*$ as $k \rightarrow \infty$. In \mathfrak{K}_{bal} , the smoothed polygons are converging to the circle as k grows.

The smoothed octagon comes from a periodic bang-bang control to the state equations with three modes, corresponding to the three vertices of the control simplex U_T and the three edges of the triangle in \mathfrak{h} . The trajectory moves in a counterclockwise direction around the triangle in \mathfrak{h} , at constant speed in the hyperbolic metric, completing the four-step mode sequence one vertex counterclockwise from the starting vertex. The smoothed octagon itself can be visualized in 24 segments: 8 smoothed corners and 16 straight half-edges. These 24 segments are arranged into four groups, each consisting of a multi-curve of 6 arcs. The four groups are congruent to one another, under the rotational symmetry R . These six arcs are shown in Figure 1.3.1.

Now we turn to the rigorous specification of these smoothed polygons, generalizing the smoothed octagon as follows. Let k be a positive integer. We consider a trajectory $t \mapsto g(\mathcal{I}, z_0, t)$ with a control mode sequence \mathcal{I} of $3k + 1$ parts of the same switching time t_{sw} , taking the form

$$\mathcal{I} = ((0, t_{sw}), (-1, t_{sw}), (-2, t_{sw}), \dots, (-3k, t_{sw})), \quad (7.5.1)$$

where $t_{sw} > 0$ and $z_0 \in \mathfrak{h}$ are to be determined as functions of $k \geq 1$ in Lemma 7.5.5. We use the initial control $u_0 = \mathbf{e}_3 = (0, 0, 1) \in U_T$.

We impose the strong boundary condition

$$z(z_0, t_{sw}) = R^{-1} \cdot z_0, \quad \text{where } z_0 = 0 + iy_0, \quad y_0 \in (1/\sqrt{3}, 1). \quad (7.5.2)$$

This boundary condition imposes the congruence of the sides of the triangle in \mathfrak{h} . The endpoints $1/\sqrt{3}$ and 1 for y_0 are natural; one endpoint is the boundary of the star domain, and the other endpoint center i of the triangles. Solving (7.5.2) for t_{sw} (the switching time), we obtain

$$t_{sw} = \frac{\ln(4/(3y_0^2 + 1))}{\sqrt{3}y_0} \in (0, \ln 2). \quad (7.5.3)$$

We view t_{sw} as a function of a real variable $y_0 \in (1/\sqrt{3}, 1)$. It is useful to delay imposing the transversality condition $g(t_f) = R$ for as long as possible, which discretizes the problem using the parameter k , and to leave y_0 as a continuous variable for now.

The proof that the smoothed $6k+2$ -gon are extremals has been broken into steps. Theorem 7.5.1 constructs one edge of the triangle in \mathfrak{h} . Lemma 7.5.3 shows the Hamiltonian maximizing property. Lemma 7.5.5 shows how the terminal condition $g(t_f) = R$ places a discreteness condition on the size of the triangle in \mathfrak{h} to give $6k+2$ -gons. Finally Theorem 7.5.6 proves extremality of the $6k+2$ -gons.

We define the switching functions χ_{ij} by

$$\begin{aligned} \chi_{ij}(t) &:= \langle \Lambda_R(t), P_{i,j}(t) - P_{i,i} \rangle \\ P_{i,j}(t) &:= Z_{\mathbf{e}_j} / \langle Z_{\mathbf{e}_j}, X(t) \rangle, \quad (X, \Lambda_R \text{ with constant control } u = \mathbf{e}_i) \end{aligned} \quad (7.5.4)$$

where X and Λ_R are both computed with respect to the constant control $u = \mathbf{e}_i$. By (7.1.1), the matrix $P_{i,i}$ is a constant $Z_{\mathbf{e}_i} / \langle Z_{\mathbf{e}_i}, X_0 \rangle$.

Theorem 7.5.1. *Let $y_0 \in (1/\sqrt{3}, 1)$, $z_0 = 0 + iy_0$, and let $t_{sw} > 0$ be given by (7.5.3). Let $z(z_0, t)$ and $g(t) = g_0(z_0, t)$ be the solutions to the state equations with constant control $u = \mathbf{e}_3 = (0, 0, 1)$ on $[0, t_{sw}]$. Then these solutions lift uniquely (up to scalar factor) to a costate trajectory $(\Lambda_1, \Lambda_R, \lambda_{cost})$ satisfying*

$$\Lambda_R(0) \in X(0)^\perp, \quad \chi_{23}(0) = 0, \quad (7.5.5)$$

and

$$\mathcal{H}_{u=\mathbf{e}_3} = 0, \quad \chi_{31}(t_{sw}) = 0, \quad (7.5.6)$$

and strong transversality conditions

$$\Lambda_R(t_{sw}) = R^{-1}\Lambda_R(0)R, \quad \Lambda_1(t_{sw}) = R^{-1}\Lambda_1(0)R.$$

The trajectory is normal: $\lambda_{cost} \neq 0$.

Proof. We start with the endpoint condition for Λ_1 . Using (6.5.3), we have the condition

$$g(t_{sw})^{-1}\Lambda_1(0)g(t_{sw}) = \Lambda_1(t_{sw}) = R^{-1}\Lambda_1(0)R. \quad (7.5.7)$$

In other words, $\Lambda_1(0) \in \mathfrak{sl}_2(\mathbb{R})$ centralizes the element $h := g(t_{sw})R^{-1} \in \mathrm{SL}_2(\mathbb{R})$. A calculation using the explicit solution for $g(t_{sw})$ shows that the trace of h is $r := 4/(1 + 3y_0^2) \in (1, 2)$. This implies that h is a regular elliptic element. Its centralizer in $\mathfrak{sl}_2(\mathbb{R})$ is $\mathbb{R}\Lambda_{10}$, where

$$\Lambda_{10} := h - rI_2/2 = \frac{1}{2y_0^2(1 + 3y_0^2)} \begin{pmatrix} 0 & 4\sqrt{3}y_0^4 \\ -\sqrt{3}(1 + y_0^2)(3y_0^2 - 1) & 0 \end{pmatrix} \in \mathfrak{sl}_2(\mathbb{R}).$$

Thus $\Lambda_1(0) = \lambda_1\Lambda_{10}$, for some $\lambda_1 \in \mathbb{R}$ to be determined.

Next, we turn to the choice of $\Lambda_R(0) \in \mathfrak{sl}_2(\mathbb{R})$. The two initial conditions (7.5.5) force $\Lambda_R(0)$ to have the form

$$\Lambda_R(0) = \lambda_R \begin{pmatrix} 0 & y_0^2 \\ 1 & 0 \end{pmatrix},$$

for some $\lambda_R \in \mathbb{R}$. At this point, the initial state $(\Lambda_1(0), \Lambda_R(0), \lambda_{cost})$ is determined by three scalars: $\lambda_1, \lambda_R, \lambda_{cost}$, where y_0 is held fixed. Equations (7.5.6) place two independent homogenous linear relations on these three variables, determining them up to a single scalar multiple. To avoid the zero solution, we set $\lambda_{cost} = -1$. A calculation, using the explicit solutions for Λ_R gives

$$\begin{aligned} \lambda_1 &= -((1 + 3y_0^2)(-3 - 6y_0^2 + (1 + 3y_0^2)\ell(y_0)))/(12\sqrt{3}y_0^4), \\ \lambda_R &= -(3 - 12y_0^2 - 9y_0^4 + 18y_0^6 + (-1 + 3y_0^2 + 21y_0^4 + 9y_0^6)\ell(y_0))/(24y_0^6), \end{aligned}$$

where $\ell(y_0) = \ln(4/(3y_0^2 + 1))$.

Finally, we have the transversality conditions at t_{sw} . Remarkably, a calculation shows that the transversality conditions hold for the calculated values of parameters λ_1, λ_R .

Lemma 7.5.3 supplements the proof, which shows that the maximum property is met for the Hamiltonian. \square

Remark 7.5.2. *We have a constant of motion*

$$\begin{aligned} d = d(y_0) &:= \det(\Lambda_1(t)) = \lambda_1^2 \det(\Lambda_{10}) \\ &= (-1 + 2y_0^2 + 3y_0^4)(3 + 6y_0^2 - (1 + 3y_0^2)\ell(y_0))^2 / (144y_0^8). \end{aligned}$$

The function d is monotonic increasing in $y_0 \in (1/\sqrt{3}, 1)$ with range $(0, 9/4)$. Thus, the determinant uniquely determines the parameter y_0 of the triangle.

Lemma 7.5.3. *Fix $y_0 \in (1/\sqrt{3}, 1)$ and corresponding time t_{sw} . Let χ_{ij} be the switching functions, defined for the costate trajectory constructed in Theorem 7.5.1 with constant control $\mathbf{e}_3 = (0, 0, 1)$. Then the PMP conditions hold:*

$$\chi_{31}(t) \geq 0, \quad \chi_{32}(t) \geq 0, \quad \text{for } t \in [0, t_{sw}].$$

The functions are zero only when $\chi_{32}(0) = \chi_{31}(t_{sw}) = 0$.

Proof. An easy substitution gives

$$\chi_{31}(t_{sw} - t) = \chi_{32}(t), \quad t \in [0, t_{sw}].$$

Thus, it is enough to show that $\chi_{32}(t) \geq 0$ with equality only at $t = 0$.

We define new variables (y, r) :

$$y = 1 + 3y_0^2, \quad r = y \exp(\sqrt{3}y_0 t).$$

The region defined by $y_0 \in (1/\sqrt{3}, 1)$ and $t \in [0, t_{sw}]$ transforms to the triangle

$$T = \{(y, r) \in [2, 4]^2 \mid y \leq r\}.$$

Note that $t = 0$ is transformed to the diagonal $y = r$ of T . Discarding obviously positive multiplicative factors, the inequality to be proved is $f(y, r) \geq 0$ on T , where

$$\begin{aligned} f(y, r) &:= 2r(-1 + y)y \ln(r) \\ &\quad - (r - y)(r(-1 + y) + y(-5 + 2y) + y^2 \ln(4/y)) \\ &\quad - 2r(-1 + y)y \ln(y). \end{aligned}$$

We show that f is nonnegative on the triangle T as follows. (These calculations appear in the accompanying Mathematica code. There are several thousand lines of Mathematica code that are used to support the

claims in this book.) First, an easy substitution gives $f(y, y) = 0$. (This was already verified above in a different manner, when we showed that $t = 0$ is a switching time.) Second, the derivative is negative on the diagonal.

$$\frac{\partial f}{\partial y}|_{r=y} = y((y-4) + y \ln(4/y)) \leq 0. \quad (7.5.8)$$

Finally, the second derivative is positive on T .

$$\frac{\partial^2 f}{\partial y^2} = -10 - 5r + (2r)/y + 7y + 4r \ln(r) - 2(r-3y) \ln(4/y) - 4r \ln(y) \geq 0.$$

(We leave this last inequality as a tedious but elementary exercise for the reader.) Nonnegativity follows. \square

Remark 7.5.4. *Looking more closely at the cases of equality, we see that the only zero of the switching function on $[0, t_{sw}]$ occurs at $t = 0$, and that the derivative is strictly positive at $t = 0$. (The derivative is zero in (7.5.8) at the corner $r = y = 4$ of the disk, but this corresponds to the unrealizable limiting case $y_0 = 1$.)*

The following lemma uses transversality conditions to place an integrality condition k on the size of the triangles in \mathfrak{h} .

Lemma 7.5.5. *Consider a trajectory $g : [0, t_f] \rightarrow \mathrm{SL}_2(\mathbb{R})$, with $g(0) = I_2$ following the dynamical system (7.5.1). The trajectory reaches $g(t_f) = R$ after a sequence of $3k+1$ control mode parts $t_f = (3k+1)t_{sw}$ of equal duration t_{sw} , provided*

$$\frac{4}{3y_0^2 + 1} = 2 \cos \theta_k, \quad \text{where } \theta_k = \frac{\pi k}{3k+1}. \quad (7.5.9)$$

Proof. Let $g_{sw} = g(z_0, t_{sw}) \in \mathrm{SL}_2(\mathbb{R})$ be the position at the switching time. By the spline equations, the condition $g(t_f) = R$ for (7.5.1) is

$$R = g_{sw}(R^{-1}g_{sw}R^1)(R^{-2}g_{sw}R^2) \cdots (R^{-3k}g_{sw}R^{3k}),$$

or equivalently,

$$(R^{-1}g_{sw})^{3k+1} = R^{-3k} = (-I_2)^k. \quad (7.5.10)$$

Let λ, λ^{-1} be the eigenvalues of $R^{-1}g_{sw} \in \mathrm{SL}_2(\mathbb{R})$. Comparing eigenvalues on the two sides of (7.5.10), we obtain $\lambda^{3k+1} = (-1)^k$, and

$$\lambda = \exp(\pi i k / (3k+1) + 2\pi i \ell / (3k+1)), \quad \ell \in \mathbb{Z}.$$

We pick the eigenvalues $\lambda^{\pm 1}$ that place g_{sw} in the smallest neighborhood of 1; that is, we take $\ell = 0, -k$. (Other pairs of eigenvalues will produce the right boundary conditions, but the corresponding multi-curves σ_i will have the wrong winding number around the origin.) Then

$$\text{trace}(R^{-1}g_{sw}) = \lambda + \lambda^{-1} = 2 \cos \theta_k.$$

The trace $r = 4/(1 + 3y_0^2)$ of $R^{-1}g_{sw} = R^{-1}hR$ is computed in the proof of Theorem 7.5.1. \square

Example (Smoothed Octagon). *For example, $k = 1$ for the smoothed octagon K_{oct} , and $\theta_k = \pi/4$. The trace is $\sqrt{2}$, and*

$$y_0 = \sqrt{(\sqrt{8} - 1)/3} \approx 0.781, \quad t_{sw} = \ln 2 / \left(2\sqrt{\sqrt{8} - 1} \right) \approx 0.256.$$

If we initialize $X_0 = \Phi(0 + iy_0)$ according to this value, then we can compute the density of a packing of smoothed octagons in the plane using the cost (3.2.2), terminal time $t_f = 4t_{sw}$, and explicit ODE solution with constant control (7.1.4).

$$\begin{aligned} \delta &= \text{area}(K_{oct})/\sqrt{12}, \\ \text{area}(K_{oct}) &= -6 \int_0^{t_{sw}} \langle J, X \rangle dt \\ &= \sqrt{12} \frac{8 - \sqrt{32 - \ln 2}}{\sqrt{8} - 1} \\ &\approx 3.126 < \pi. \end{aligned}$$

This value appears as (1.1.1).

Theorem 7.5.6. *For each positive integer k , the smoothed $6k + 2$ -gon is a Pontryagin extremal given by a bang-bang control.*

Proof. From (7.5.2), it follows that transversality for z from the half-plane control problem (4.5.1) holds with $t_f = (3k + 1)t_{sw}$:

$$z(z_0, t_f) = R^{-(3k+1)} \cdot z_0 = R^{-1} \cdot z_0.$$

The strong transversality conditions for Λ_1, Λ_R imply the transversality conditions at time $t_f = (3k + 1)t_{sw}$. \square

7.6 Supplementary Remarks on Smoothed Polygons

Remark 7.6.1. *A discreteness condition on y_0 comes from the transversality condition $g(t_f) = R$, described in Lemma 7.5.5. We have solved the nonlinear equations (7.5.9) and (7.5.3) explicitly for t_{sw} and y_0 in the accompanying code, but we do not display the solution here. For each positive integer k , the trajectory for the smoothed $6k + 2$ -gon is now completely determined by these values of t_{sw} and y_0 , given as solutions to nonlinear equations.*

We can use Equation (7.5.9) and the lemma to define k as a continuous function of y_0 . The cost function can then be interpolated to a function of a real variable y_0 (or k). Figure 7.6.3 graphs the area of the smoothed $6k + 2$ -gon as a function of k . It appears that the area function is increasing in k and tends to the area π of the circular disk.

Remark 7.6.2. *A related construction gives a trajectory with $3k - 1$ parts in the control mode sequence – the smoothed $6k - 2$ -gon, for $k \geq 2$. The changes are minor. We replace equation (7.5.1) with*

$$\mathcal{I} = ((1, t_{sw}), (2, t_{sw}), (3, t_{sw}), \dots, (3k - 1, t_{sw})). \quad (7.6.1)$$

The parameters are

$$z_0 = 0 + iy_0, \quad t_{sw} = -\frac{\ln(4/(3y_0^2 + 1))}{\sqrt{3}y_0}, \quad y_0 > 1.$$

The initial control mode is $u = \mathbf{e}_2$.

Remark 7.6.3. *It seems that the smoothed $6k - 2$ -gon is not a Pontryagin extremal trajectory. Specifically, all of the conditions seem to hold, except that the Pontryagin multiplier $\lambda_{cost} > 0$ has the wrong sign. This suggests that these smoothed polygons are Pontryagin extremal trajectories for the problem of maximizing the area.*

Remark 7.6.4. *When $k = 1$, the smoothed $6k - 2$ -gon degenerates to a rectangle with corners (Figure 7.6.1) and area $\sqrt{12}$. Allowing k to be non-integral, for small values of $k > 1$, we obtained smoothed rectangles (that do not quite satisfy the boundary conditions).*

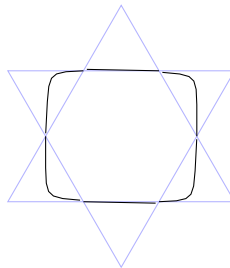


Figure 7.6.1: By taking a smoothed $6k - 2$ -gon and interpolating formulas to a fractional number of sides (here $k = 1.03$), we see that the shape appears to be tending to a rectangle of area $\sqrt{12}$ as $k \rightarrow 1$.

The trajectory X in \mathfrak{h} for the $6k + 2$ -gon follows a triangle (with edges following the arcs of Figure 7.2.1) centered at $z = i \in \mathfrak{h}$. It moves counterclockwise around i , traversing one edge for each control mode (Figure 7.6.2). The trajectory X in \mathfrak{h} for the $6k - 2$ -gon also follows an inverted triangle centered at $z = i \in \mathfrak{h}$. It moves clockwise.



Figure 7.6.2: The trajectory in the upper-half plane of a smoothed $6k + 2$ -gon follows $3k + 1$ edges moving counterclockwise on a triangular path centered at $i \in \mathfrak{h}$ (left). The trajectory for the smoothed $6k - 2$ -gon follows $3k - 1$ edges moving clockwise on an inverted triangle centered at $i \in \mathfrak{h}$ (right).

The cost increases with k for the $6k + 2$ -gon and decreases with k for $6k - 2$ -gon. In both cases, the limit of the cost is π as $k \rightarrow \infty$. We show a graph of the costs of the smoothed polygons as a function of the number $n = 6k \pm 2$ of sides (Figure 7.6.3).

7.7 Smoothed Octagon is an Isolated Extremal

The previous section showed that the smoothed octagon is an extremal trajectory. In this section we show that it is an isolated extremal.

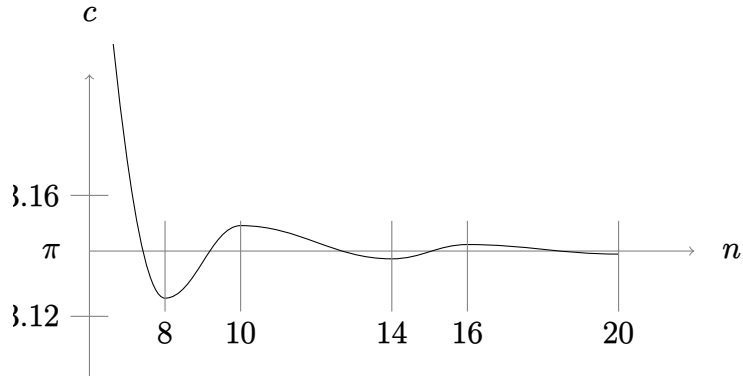


Figure 7.6.3: The graph interpolates the cost c of known critical points as a function of the number $n = 6k \pm 2$ of straight edge segments in the corresponding smoothed polygon. The cost tends to π as n increases. The data is consistent with Reinhardt's conjecture.

Theorem 7.7.1. *The lifted trajectory of the smoothed octagon is an isolated extremal. That is, in some neighborhood of the set of initial conditions in the cotangent space, the only extremal trajectory satisfying the transversality conditions at the endpoints is that of the smoothed octagon.*

Proof sketch. Fix $d > 0$ close to the value $d_{oct} = \det(\Lambda_1)$ obtained for a smoothed octagon. In the proof, we ignore the transversality on the group element $g \in G$, and the discreteness parameter k it produces, until the final lines of the proof. Instead, we let d run over a small interval containing d_{oct} .

We consider the five dimensional manifold $M = M_d$ given by $q = (X, \Lambda_1, \Lambda_R) \in \mathfrak{sl}_2(\mathbb{R})^3$ in a neighborhood of the smoothed octagon parameters subject to four constraints:

$$\det(X) = 1, \quad \langle X, \Lambda_R \rangle = 0, \quad \det(\Lambda_1) = d, \quad \mathcal{H} = 0.$$

Fix two vertices i, j of the control simplex U_T . We consider the four-dimensional *Poincaré section* N_d obtained by requiring the vanishing of a switching function $\chi_{ij} = \langle \Lambda_R, P_i - P_j \rangle = 0$. For each $q_0 \in N_d$, let $q(t, q_0)$ be the extremal trajectory in M , starting at initial condition q_0 .

Fixing d , we let $y_0(d)$ be the real number constructed in Section 7.5. Associated with y_0 and d , we have constructed an extremal lifted periodic trajectory $q(t, q_{fix}(d)) = (X(t), \Lambda_R(t), \Lambda_1(t))$ in M_d starting at the appropriate initial condition $q_{fix}(d) \in N_d$.

Let $t_{sw}(q_{fix}(d)) > 0$ be the first positive switching time of the trajectory $q(t, q_{fix}(d))$. By transversality of switching times (justified in the remark following Lemma 7.5.3), there is a unique first switching time $t_{sw}(q_0)$ near $t_{sw}(q_{fix}(d))$ for the extremal trajectory $q(t, q_0)$, when q_0 is near $q_{fix}(d)$.

Define a Poincaré map $f_d : N_d \rightarrow N_d$ by

$$f_d(q_0) = \text{Ad}(R)q(t_{sw}(q_0), q_0),$$

where Ad acts componentwise on $N_d \subset \mathfrak{sl}_2(\mathbb{R})^3$. By the strong transversality conditions for the trajectories in Section 7.5, f_d has a fixed point at $q_{fix}(d)$. If q_0 is a nearby initial condition that gives an extremal satisfying transversality, then setting $q_{i+1} = f_d(q_i)$, we have

$$\text{Ad}(R^{-4})q_4 = \text{Ad}(R^{-1})q_0, \quad \text{or } f^4 q_0 = q_0. \quad (7.7.1)$$

The *four* is half the number of edges of the smoothed octagon; that is, the terminal time is $t_f = 4t_{sw}(q_{oct})$.

Let $A_d := T_f d : T_q N_d \rightarrow T_q N_d$ be the tangent map of f_d at the fixed point $q = q_{fix}(d)$. Direct calculation shows that the fixed point $q_{oct} := q_{fix}(d_{oct})$ is hyperbolic; that is, $A_{d_{oct}}$ has no eigenvalues of absolute value 1. Then the fixed point $q_{fix}(d)$ is also hyperbolic for the map f_d^4 for sufficiently nearby parameters d . By the implicit function theorem, for each d near d_{oct} , the function $f_d^4 - I$ can be inverted in an open neighborhood of the fixed point $q_{fix}(d)$, forcing the fixed point to be isolated (where I is the identity map). Thus, the only fixed points near q_{oct} are the fixed points $q_{fix}(d)$. For d near d_{oct} , the only fixed point $q_{fix}(d)$ satisfying the final transversality conditions (7.5.9) is q_{oct} . \square

Remark 7.7.2. *A different proof that the smoothed octagon is isolated appears in the preprint [16].*

Chapter 8

Singular Locus

8.1 Edges of the Control Simplex

At the end of this section, Remark 8.1.6 shows that abnormal extremals can be constructed to the Reinhardt control problem with an arbitrary measurable control function, taking values in a fixed edge of the control set U_T . These anomalous abnormal extremals seem to be an artifact of way we have chosen to encode the convexity conditions of the convex disk K into the control problem. These abnormal solutions indicate that the Reinhardt control problem has unnecessarily many extremals.

In this section, we consider a modified control problem (8.1.3), which we call the *edge control problem*. As we will see, in this modified control problem, these particular abnormal extremals disappear. We will then consider trajectories that are extremal in two respects: with respect to the Reinhardt optimal control problem, but also with respect to the edge control problem.

Definition 8.1.1 (Edge Control Problem). *The edge control system on an interval $[t_0, t_1]$ with free terminal time t_1 is the control problem with state equations (8.1.3), control set $[-1/2, 1/2]$, endpoint conditions (8.1.4), cost functional (8.1.5), and Hamiltonian (8.1.6). The state variables $x, y, s : [t_0, t_1] \rightarrow \mathbb{R}$ have range restrictions $y > 0$ and $-1/\sqrt{3} < x < 1/\sqrt{3}$.*

Let $(g, X) : [t_0, t_1] \rightarrow \text{SL}_2(\mathbb{R}) \times \mathfrak{h}^*$ be a trajectory of the Reinhardt state equations whose control is restricted to the edge $u = (0, u_1, u_2)$ of the control set U_T . We show how to define state variables s, x, y and an edge control

problem. We write the control in this edge as

$$u(t) \in \left\{ \left(0, \frac{1}{2} + u_{edge}, \frac{1}{2} - u_{edge} \right) \in U_T \mid -1/2 \leq u_{edge} \leq 1/2 \right\}.$$

Thus the control function on an interval $[t_0, t_1]$ is determined by a measurable function $u_{edge} : [t_0, t_1] \rightarrow [-1/2, 1/2]$.

The variables x, y are the same as in the Reinhardt problem: $z = x + iy \in \mathfrak{h}^*$. The vector field on \mathfrak{h}^* controlling the Reinhardt state equations (Lemma 4.5.2) is

$$(x', y') = (f_1, f_2) = (y, f_2(x, y, u_{edge})) = \left(y, \frac{2\sqrt{3}y^2u_{edge}}{-1 + 2\sqrt{3}xu_{edge}} \right).$$

In particular, $x' = y > 0$, so that x is monotonically increasing. In this setting, we can solve the state ODE $g' = gX$ with initial condition $g(t_0) = g_0$ explicitly.

$$g(t) = g_0 h(t_0)^{-1} h(t), \quad \text{where} \quad (8.1.1)$$

$$h(t) = \begin{pmatrix} 1 & -x(t) \\ s(t) & 1 - s(t)x(t) \end{pmatrix}, \quad \text{and} \quad s(t) := \int_{t_0}^t \frac{dt}{y(t)}. \quad (8.1.2)$$

The state equations for the edge control problem take the form

$$s' = 1/y, \quad x' = y, \quad y' = f_2(x, y, u_{edge}) \quad (8.1.3)$$

subject to boundary conditions

$$(s(t_0), s(t_1), x(t_0), x(t_1), y(t_0), y(t_1)) = (s_0, s_1, x_0, x_1, y_0, y_1) \quad (8.1.4)$$

that are chosen to agree with the boundary conditions of the Reinhardt trajectory (g, X) . We can take $s_0 = 0$. (If a constant of integration is added to s , the path $g(t) \in \text{SL}_2(\mathbb{R})$ is unchanged.)

Up to a positive constant, the cost is given by Equation (4.3.1).

$$\begin{aligned} \int_{t_0}^{t_1} \frac{1 + y^2 + x^2}{y} dt &= \int_{t_0}^{t_1} (s'(t) + x'(t)) dt + \int_{t_0}^{t_1} \phi_{edge}(x, y) dt \\ &= (s_1 + x_1) - (s_0 + x_0) + \int \phi_{edge}(x, y) dt. \end{aligned}$$

where $\phi_{edge}(x, y) = x^2/y$. Subtracting a constant determined by the boundary conditions, we can take the cost to be

$$\int \phi_{edge}(x, y) dt. \quad (8.1.5)$$

This data specifies a control problem with fixed initial time t_0 and free terminal time t_1 . The state variables are x, y, s , satisfying the ODE (8.1.3). The control is measurable control $u_{edge} : [t_0, t_1] \rightarrow [-1/2, 1/2]$.

The state variables (x, y, s) take values in an open subset of \mathbb{R}^3 . The cotangent space is therefore $T^*\mathbb{R}^3 = \mathbb{R}^6$ with variables $x, y, s, \lambda_1, \lambda_2, \lambda_3$. The Hamiltonian is

$$\mathcal{H} = \sum_i \lambda_i f_i + \lambda_{cost} \phi_{edge} = \lambda_1 y + \lambda_2 f_2(x, y, u_{edge}) + \lambda_3/y + \lambda_{cost} \phi_{edge}(x, y). \quad (8.1.6)$$

The term λ_{cost} is constant and is nonpositive. This completes our description of the edge control system and its relation to the Reinhardt control problem with edge-constrained control. By rotational symmetry, we obtain edge control systems likewise for the other edges of U_T .

Definition 8.1.2. *We say that a trajectory (g, X) is edge extremal, if on every subinterval of the domain on which one of the components of the control function $u = (u_0, u_1, u_2)$ is zero a.e. (say $u_j = 0$ a.e.), the trajectory is extremal with respect to the corresponding edge control problem.*

Proposition 8.1.3. *The global solution of the Reinhardt problem is an extremal for the Reinhardt control problem, and it is also edge extremal.*

Proof. We have seen that the global minimizer must be extremal for the Reinhardt optimal control problem for some optimal control function u taking values in U_T . On any subinterval of the domain where the optimal control function takes values in an edge of U_T , then the globally minimizing trajectory must minimize cost among all trajectories with the same endpoint conditions on the subinterval and that have their control function similarly restricted to the edge. Thus, the global minimizer is also edge extremal. \square

The purpose of this section is to prove the following bang-bang behavior on edges with finite switching.

Theorem 8.1.4. *Consider an extremal lifted trajectory in the edge control system on a closed interval $[t_0, t_1]$. Then the optimal control function u_{edge} is bang-bang with finitely many switches. That is, the control function is equal a.e. to a piecewise constant function*

$$u_{edge}(t) = \pm 1/2, \quad \text{for all } t \in [t_0, t_1],$$

with finitely many switches on $[t_0, t_1]$.

Proof. The costate equations of the Hamiltonian (8.1.6) are

$$\begin{aligned}\lambda'_1 &= -\frac{\partial \mathcal{H}}{\partial x} = \frac{\lambda_2 12y^2 u_{edge}^2}{(1 - 2\sqrt{3}xu_{edge})^2} - \frac{2\lambda_{cost}x}{y}, \\ \lambda'_2 &= -\frac{\partial \mathcal{H}}{\partial y} = \frac{\lambda_3}{y^2} - \lambda_1 - \frac{\lambda_2 4\sqrt{3}yu_{edge}}{-1 + 2\sqrt{3}xu_{edge}} + \frac{\lambda_{cost}x^2}{y^2}, \\ \lambda'_3 &= -\frac{\partial \mathcal{H}}{\partial s} = 0.\end{aligned}\quad (8.1.7)$$

We note that λ_3 is constant.

The only term of the Hamiltonian depending on the control is $\lambda_2 f_2$. The function f_2 is monotonic decreasing in u_{edge} . Maximizing the Hamiltonian, when $\lambda_2 \neq 0$, the control is $u_{edge} = \mp 1/2$ depending on the sign of λ_2 . Thus, λ_2 is a switching function for the control.

The functions $x, y, s, \lambda_1, \lambda_2, \lambda_3$ are continuous by construction. The function λ'_2 is also continuous by the form of the ODE it satisfies. (Although the ODE depends a measurable control function u_{edge} , when λ_2 has fixed nonzero sign, the control function is constant and hence continuous. Also, $\lambda_2 f_2(x, y, u_{edge})$ tends to zero with λ_2 . Thus, λ'_2 is continuous.)

We claim that at any point $t_2 \in [t_0, t_1]$ where $\lambda_2(t_2) = \lambda'_2(t_2) = 0$, the costate is given by

$$\lambda_3 = -x(t_2)^2 \lambda_{cost}, \quad \lambda_1(t_2) = 0, \quad \lambda_2(t_2) = 0, \quad \lambda_{cost} \neq 0. \quad (8.1.8)$$

(In particular, $-\lambda_3/\lambda_{cost} \geq 0$ and $x(t_2) = \pm\sqrt{-\lambda_3/\lambda_{cost}}$.) In fact, under these vanishing conditions on λ_2 and λ'_2 , we obtain a nonsingular linear system of two equations and two unknowns

$$\mathcal{H} = \frac{\partial \mathcal{H}}{\partial y} = 0$$

for λ_3 and $\lambda_1(t_2)$. The unique solution to this linear system is as given. If $\lambda_{cost} = 0$, then all of the costate variables are zero at t_2 , which is contrary to the Pontryagin extremality conditions. Thus, $\lambda_{cost} \neq 0$ and the solution is normal.

In (8.1.8), since x is monotonic increasing, along any extremal lifted trajectory, there are at most two times $t \in [t_0, t_1]$ such that $x(t) = \pm\sqrt{-\lambda_3/\lambda_{cost}}$. At any other switching time t with $\lambda_2(t) = 0$, the trajectory passes transversally through the wall $\lambda_2 = 0$ (that is, $\lambda'_2(t) \neq 0$). In such a case the zero of the switching function λ_2 is isolated.

The next lemma shows that even at times when the conditions of (8.1.8) are met, the zeros of the switching function λ_2 are isolated. By translation in time, we may assume without loss of generality that $t_2 = 0$ in the lemma.

In conclusion, all the zeros of the switching function λ_2 are isolated and there are at most finitely many switches on any finite time interval. Adjusting the control u_{edge} on a set of measure zero, we may assume that u_{edge} is piecewise constant, taking values $\pm 1/2$. \square

In the next lemma, we write $f_1 = O(f_2)$ to mean that there exist $t_1 > 0$ and $C_1 > 0$ such that f_1, f_2 are defined on $(-t_1, t_1)$ and

$$|f_1(t)| \leq C_1 |f_2(t)|, \quad \text{for all } t \in (-t_1, t_1).$$

Lemma 8.1.5. *Fix constants $\lambda_{\text{cost}} = -1$, $\lambda_3 = -\lambda_{\text{cost}}x_0^2$, where $|x_0| < 1/\sqrt{3}$, and $y_0 > 0$. Let $t_1 > 0$ and choose any measurable function $u_{\text{edge}} : (-t_1, t_1) \rightarrow [-1/2, 1/2]$. Let $x, y, \lambda_1, \lambda_2$ be solutions to the state (8.1.3) and costate equations (8.1.7) on $(-t_1, t_1)$ with initial conditions $(x(0), y(0)) = (x_0, y_0)$, $(\lambda_1(0), \lambda_2(0)) = (0, 0)$, and control function u_{edge} . Then there exist an integer $n \geq 2$ and a real nonzero constant $C \neq 0$ (both n and C depending on the initial data x_0, y_0 but not on the choice of control function u_{edge}) such that*

$$\lambda_2(t) = Ct^n + O(t^{n+1}).$$

In particular, having this form, the switching function λ_2 has an isolated zero at $t = 0$ with multiplicity n .

Proof. If $x_0 \neq 0$, set $n = 2$. Otherwise, set $n = 3$. If $x_0 \neq 0$, set $C = -x_0(1 + y_0)/y_0^2$. Otherwise set $C = -2/3$. We approximate the functions λ_1, λ_2 by the functions $\tilde{\lambda}_1, \tilde{\lambda}_2$, where

$$\tilde{\lambda}_1(t) := \int_0^t \frac{2x(\tau)}{y(\tau)} d\tau, \quad \tilde{\lambda}_2(t) := - \int_0^t \left(\frac{x(\tau)^2 - x_0^2}{y(\tau)^2} + \tilde{\lambda}_1(\tau) \right) d\tau.$$

Then it is enough to show that $\tilde{\lambda}_2(t) = Ct^n + O(t^{n+1})$ and $\lambda_2(t) = \tilde{\lambda}_2(t) + O(t^{n+1})$. Consider the error term $\mathbf{v} = (v_1, v_2)$, where $v_i := \lambda_i - \tilde{\lambda}_i$. The costate equations for λ_1 and λ_2 , when expressed in terms of \mathbf{v} , become $\mathbf{v}' = -A\mathbf{v} - \tilde{\lambda}_2 \mathbf{b}$, where

$$A = \begin{pmatrix} 0 & f_{2x} \\ 1 & f_{2y} \end{pmatrix}, \quad \mathbf{v} = \begin{pmatrix} v_1 \\ v_2 \end{pmatrix}, \quad \mathbf{b} = \begin{pmatrix} f_{2x} \\ f_{2y} \end{pmatrix}.$$

Here f_{2x} and f_{2y} are the partial derivatives of f_2 evaluated at $(x(t), y(t), u_{edge}(t))$.

If $x_0 \neq 0$, we compute

$$\begin{aligned} y &= y_0 + O(t), \\ x &= x_0 + y_0 t + O(t^2), \\ \frac{x^2 - x_0^2}{y^2} &= \frac{2x_0 y_0 t}{y_0^2} + O(t^2), \\ \tilde{\lambda}_1 &= \frac{2x_0 t}{y_0} + O(t^2), \\ \tilde{\lambda}_2 &= - \int_0^t \frac{2x_0(1 + y_0)}{y_0^2} \tau + O(\tau^2) d\tau = Ct^n + O(t^{n+1}). \end{aligned}$$

If $x_0 = 0$, we compute

$$\begin{aligned} y &= y_0 + O(t), \\ x &= y_0 t + O(t^2), \\ \tilde{\lambda}_1 &= t^2 + O(t^3), \\ \tilde{\lambda}_2 &= -\frac{2t^3}{3} + O(t^4) = Ct^n + O(t^{n+1}). \end{aligned}$$

We use the Euclidean norm on \mathbb{R}^2 and the natural matrix norm on the vector space of 2×2 matrices. By the Cauchy-Schwarz inequality, we have $\|\mathbf{v}'\| \leq \|\mathbf{v}'\|$. Pick $0 < t_2 < t_1$ such that the denominator of $f_2(x(t), y(t), u_{edge}(t))$ is bounded away from zero on $(-t_2, t_2)$. Then there exists $C_0 > 0$ such that $\|A(x(t), y(t), u_{edge}(t))\| \leq C_0$ for all $t \in (-t_2, t_2)$. We have for some $C_1 > 0$,

$$\|\mathbf{v}'\| \leq \|\mathbf{v}'\| = \|\tilde{\lambda}_2 \mathbf{b} + A\mathbf{v}\| \leq |\tilde{\lambda}_2| \|\mathbf{b}\| + C_0 \|\mathbf{v}\| \leq C_1 |t|^n + C_0 \|\mathbf{v}\|.$$

In integral form,

$$\|\mathbf{v}\| \leq \frac{C_1 |t|^{n+1}}{n+1} + C_0 \int_0^t \|\mathbf{v}\| dt.$$

By the Gronwall inequality (Corollary A.1.3), we have $\|\mathbf{v}\| = O(t^{n+1})$. Then

$$|\lambda_2 - Ct^n| = |v_2 + \tilde{\lambda}_2 - Ct^n| \leq \|\mathbf{v}\| + |\tilde{\lambda}_2 - Ct^n| = O(t^{n+1}).$$

This completes the lemma. \square

We adjust the control function u_{edge} along a set of measure zero in $[t_0, t_1]$ and assume without loss of generality that $u_{\text{edge}} \in \{-1/2, 1/2\}$.

If the conditions (8.1.8) hold, for each constant control $u_{\text{edge}} = \pm 1/2$, we can solve the state and costate ODEs explicitly for $x^\pm, y^\pm, \lambda_1^\pm, \lambda_2^\pm, \lambda_3^\pm$ as a function of $t \in [t_0, t_1]$. The solutions for x, y agree with the solutions obtained in Section 7.2. The costate ODEs can be solved without difficulty in Mathematica, but we do not record the (rather unruly) formulas here.

Remark 8.1.6. *We have an anomalous situation. In the proof of Theorem 8.1.4, we showed that $\lambda_{\text{cost}} \neq 0$ (that is, the trajectory is normal) when a point exists on the trajectory such that both $\lambda_2(t_2) = \lambda'_2(t_2) = 0$. At such a point, the trajectory lies on the wall $\lambda_2 = 0$ and is tangent to the wall.*

However, if we return to the full system of state and costate equations, still restricting the control function to $u_{\text{edge}}(t) \in [-1/2, 1/2]$, we show that an abnormal solution in fact exists! (This is similar to [17, Sec. 10], where the existence of an abnormal solution can depend on how state constraints are encoded.) Explicitly, there is an abnormal solution $\lambda_{\text{cost}} = 0$ such that the state equations are given by (g, X) , where g is given by (8.1.1), $X = \Phi(z)$, and $z = (x, y)$ given by ODE (8.1.3). The costate solutions are

$$\Lambda_R = \begin{pmatrix} x & y^2 - x^2 \\ 1 & -x \end{pmatrix}, \quad \Lambda_1 = \begin{pmatrix} -x & x^2 \\ -1 & x \end{pmatrix}.$$

It can be checked that Λ_R and Λ_1 satisfy the costate ODEs given in Section 6.5. It can be checked that the Hamiltonian is identically zero for these choices.

In particular, the Hamiltonian is independent of the control. Thus any measurable control function $u_{\text{edge}}(t) \in [-1/2, 1/2]$ maximizes the Hamiltonian, and we obtain a large family of abnormal trajectories. However, under the alternative encoding that was used in this section, these abnormal trajectories do not appear.

Remark 8.1.7. *A result about edges similar to this section is claimed in the preprint [16], but the proof there is shaky.*

8.2 Singular Locus and Singular Subarcs

We have stated earlier that the optimal control matrix Z_u^* is implicitly determined by the Hamiltonian maximization condition in equation (6.4.2).

Singular subarcs arise when this maximization condition fails to produce a unique candidate for the control matrix Z_u^* over an entire time interval. Throughout this section, we let J denote the infinitesimal generator of the rotation group, as usual.

Recall that we have partitioned the cotangent space $T^*\mathcal{O}_J$ according to subsets I of $\{1, 2, 3\}$, according to the set of maximizers in U_T of the Hamiltonian. The set $I = \{1, 2, 3\}$ corresponds to the part of the cotangent space on which the Hamiltonian is independent of the control $u \in U_T$.

Lemma 8.2.1. *For all $X \in \mathfrak{sl}_2(\mathbb{R})$ and all $\Lambda \in X^\perp$, if the control dependent term of the Hamiltonian $\mathcal{H}_2(\Lambda, X, Z_u)$ is independent of the control $u \in U_T$, then $\Lambda = 0$. If $\Lambda \neq 0$, then the set of controls maximizing the Hamiltonian is a vertex or edge of the control set U_T .*

Proof. The part of the Hamiltonian that is dependent on the control can be written

$$\langle \Lambda, Z_u / \langle X, Z_u \rangle \rangle.$$

We fix $X \in \mathfrak{sl}_2(\mathbb{R})$ and f be the vector field on $T_X \mathcal{O}_X$ defined by (4.5.1). The affine hull of the image of the vector field under U_T is the entire tangent space, by Lemma 6.1.2. The value of \mathcal{H}_2 must then be zero, and Λ must lie in the orthogonal complement $\{0\}$ of the entire tangent space. Thus, $\Lambda = 0$.

In contrapositive form, if $\Lambda \neq 0$, then the Hamiltonian is not constant as a function of the control. By Lemma 7.3.1, the set of maximizers is a vertex or edge. \square

Lemma 8.2.2. *The costate trajectory function Λ'_R is continuous at every time $t = t_0$ such that $\Lambda_R(t_0) = 0$. If $\Lambda_R(t_0) = \Lambda'_R(t_0) = 0$, for some $t = t_0$, then*

$$\lambda_{cost} \neq 0, \quad \Lambda_1(t_0) = \frac{3}{2} \lambda_{cost} J.$$

Proof. By inspection of the ODE, the right-hand side of the costate ODE for $\Lambda'_R(t_0)$ has a point of continuity when $\Lambda_R(t_0) = 0$. The maximum principle states that the Hamiltonian vanishes identically along the lifted extremal (See Section 6.2). Thus, we have

$$\mathcal{H}(\Lambda_1, \Lambda_R, X; Z_u) = \langle \Lambda_1 - \frac{3}{2} \lambda_{cost} J, X \rangle - \frac{\langle \Lambda_R, Z_u \rangle}{\langle X, Z_u \rangle} = \langle \Lambda_{1,cost}, X \rangle = 0 \quad \text{at } t = t_0,$$

where we set

$$\Lambda_{1,cost} = \Lambda_1 - 3\lambda_{cost}J/2. \quad (8.2.1)$$

Thus, $\Lambda_{1,cost}(t_0) \in X(t_0)^\perp$. The ODE for Λ_R gives

$$0 = \Lambda'_R(t_0) = -[\Lambda_{1,cost}, X(t_0)].$$

Together, these imply that $\Lambda_{1,cost} \in \mathbb{R}X \cap X^\perp = \{0\}$ at $t = t_0$. Thus, $\Lambda_{1,cost}(t_0) = 0$ and $\Lambda_1(t_0) = \frac{3}{2}\lambda_{cost}J$.

We must have $\lambda_{cost} \neq 0$ for otherwise we will have $\lambda_{cost} = 0$, $\Lambda_R(t_0) = 0$ and $\Lambda_1(t_0) = 0$, contradicting the non-vanishing of the costate variables in the maximum principle (see Section 6.2). \square

The following theorem describes the behavior when Λ_R vanishes on an interval.

Theorem 8.2.3. *If a lifted extremal has Λ_R vanishing identically on an interval (t_1, t_2) , then the control function is constant $u = (1/3, 1/3, 1/3)$ (the center of the control set U_T) for $t \in (t_1, t_2)$. Also, the optimal control matrix is $Z_u^*(t) = \frac{1}{3}J$ on this interval, and this determines an arc $g(t)\mathbf{s}_i^*$ of the circle as a singular subarc. Moreover, the trajectory is normal, and X, Λ_1 are constant:*

$$\lambda_{cost} \neq 0, \quad X = J, \quad \Lambda_1 = \frac{3}{2}\lambda_{cost}J, \quad g(t) = g_0 \exp(Jt).$$

Proof. Assume that along an extremal curve, for all $t \in [t_1, t_2]$ we have $\Lambda_R(t) \equiv 0$. On this interval we have $\Lambda_R(t) = \Lambda'_R(t) = 0$. By the lemma, $\lambda_{cost} \neq 0$ and $\Lambda_1(t) \equiv 3\lambda_{cost}J/2$. The costate equation for Λ_1 gives

$$0 = \Lambda'_1 = [\Lambda_1, X] = \frac{3}{2}\lambda_{cost}[J, X].$$

Thus, we have $[J, X] = 0$ and $X \in \mathbb{R}J \cap \mathcal{O}_J = \{J\}$. So $X \equiv J$ on $t \in (t_1, t_2)$.

Note that $\Lambda_R = 0$ means that the Hamiltonian (6.2.3) does not involve the control matrix Z_u^* and so the maximization fails to uniquely determine the control matrix in this interval. Thus, the lifted extremal in this interval is singular (according to Definition 6.2.1). The unique control function $u(t)$ which gives $0 = X' = [P, X] = [P, J]$ is $u(t) = (1/3, 1/3, 1/3)$ (almost everywhere) which is the centroid of the control set U_T .

Now, the curve $g(t) = \exp(Jt)$ satisfies $g' = gX = gJ$ and this is a rotation matrix in $\text{SL}_2(\mathbb{R})$ which gives rise to the circle in the packing plane as a centrally symmetric convex disk, assuming $g(0) = I_2$. \square

Thus, in the *singular locus* of the cotangent space, we must necessarily have

$$\begin{aligned} g(t) &= g_0 \exp(Jt), & X(t) &= J, & z(t) &= i, \\ \Lambda_1(t) &= \frac{3}{2} \lambda_{cost} J, & \Lambda_R(t) &= 0, \end{aligned}$$

where $g(0) = g_0$.

Definition 8.2.4 (Singular Locus). *The region of the extended state space $T^*(\mathrm{SL}_2(\mathbb{R}) \times \mathfrak{sl}_2(\mathbb{R}))$ given by*

$$\mathcal{S}_{sing} := \left\{ (g, \Lambda_1, X, \Lambda_R) = \left(g_0, \frac{3}{2} \lambda_{cost} J, J, 0 \right) \mid g_0 \in \mathrm{SL}_2(\mathbb{R}), \quad \lambda_{cost} \neq 0 \right\}$$

is called the singular locus. In the star domain of the upper half-plane, the singular locus lies over the point $z = i \in \mathfrak{h}^$. (That is, $\Phi(i) = J$.)*

Remark 8.2.5. Note that \mathcal{S}_{sing} gives the initial conditions corresponding to the circle in \mathfrak{K}_{ccs} (which has $g_0 = I_2 \in \mathrm{SL}_2(\mathbb{R})$ up to a transformation in $\mathrm{SL}_2(\mathbb{R})$).

We have seen in Theorem 8.1.4 that every Pontryagin extremal of the edge optimal control problem has a bang-bang control function with finitely many switches. The other possibility is a singular arc along which the Hamiltonian is independent of the control function. That is, the Hamiltonian-maximizing face of U_T is the entire two-simplex U_T . This is the situation considered in the following theorem.

Theorem 8.2.6. *Consider a Pontryagin extremal to the Reinhardt problem that contains a singular subarc along which the Hamiltonian is independent of the control. Then during that time interval, the extremal remains in the singular locus. Moreover, the unique solution to the system of state and costate equations on that interval is a multi-curve of circular arcs, up to affine transformation. Conversely, the lifted trajectory attached to a multi-curve of circular arcs is a Pontryagin extremal singular subarc.*

Proof. The proof is a summary of results already obtained.

If the maximum principle fails to determine a unique control over an open time interval, then the trajectory remains in the set

$$\bigcup_{|I| \geq 2} (T^* \mathcal{O}_J)_I \tag{8.2.2}$$

By the assumptions of the theorem, the Hamiltonian is independent of the control. Thus, a singular subarc must have the form of Lemma 8.2.1. That is, $\Lambda_R = 0$ over some time interval. By Theorem 8.2.3, the singular subarc is contained in the singular locus and gives an arc of a circle in \mathfrak{K}_{ccs} .

Conversely, the multi-curve of circular arcs is represented by $g = \exp(tJ)$, and by the ODE $g' = Xg$, where $X = J$, and $X' = 0$, and $g = g_0 \exp(Jt)$. As remarked in the proof of Lemma 8.2.3, $0 = X' = [P, X]$ implies that the control function is constant almost everywhere, taking value $(1/3, 1/3, 1/3)$ at the center of the control set U_T . Along the trajectory, the Hamiltonian is then independent of the control. By Lemma 8.2.1, we have $\Lambda_R = 0$. By Lemma 8.2.2, we have $\Lambda_1 = \frac{3}{2}\lambda_{cost}J$ and $\lambda_{cost} \neq 0$. These costate values lie in the singular locus. \square

Although the multi-curve of circular arcs is a Pontryagin extremal, we can invoke second-order conditions to show that it is not a global minimizer. By considering a second variation, Mahler proved that the circle is not a local minimizer of the Reinhardt problem [28].

Theorem 8.2.7. *The global minimizer of the Reinhardt problem does not contain any singular subarcs.*

Proof. We assume for a contradiction that the global minimizer contains a singular subarc. The previous theorem shows that the singular subarc comes from a multi-curve of circular arcs.

We use second order conditions to show that the circular arc is not a local minimizer on any time interval (t_1, t_2) so that the solution to the Reinhardt problem contains no circular arcs. We consider a deformation of a circular arc of the form

$$g_s(t) = \exp \left(s \begin{pmatrix} \psi_1(t) & \psi_2(t) \\ \psi_2(t) & -\psi_1(t) \end{pmatrix} \right) \exp(Jt) =: \Psi_s(t) \exp(Jt),$$

for sufficiently small $s > 0$ and compactly supported C^∞ functions ψ_1, ψ_2 to be determined on the interval $[t_1, t_2]$.

We point out that t is not a unit speed parameter so that $\det(X)$ need not equal 1. The cost is

$$-\frac{3}{2} \int_{t_1}^{t_2} \langle J, X \rangle dt = -\frac{3}{2} \int_{t_1}^{t_2} \langle J, g^{-1} dg \rangle,$$

where $g^{-1}dg$ is the Cartan-Maurer one-form on $\mathrm{SL}_2(\mathbb{R})$. This shows that the cost is independent of parameterization. If $g(t) = \Psi(t) \exp(Jt)$, where Ψ is an invertible C^∞ matrix of t , then the product rule gives

$$\langle J, g^{-1}dg \rangle = \langle J, J \rangle dt + \langle J, \Psi^{-1}d\Psi \rangle.$$

Computing the cost of g_s on $[t_1, t_2]$ by this formula, we find that

$$\mathrm{cost}(g_s) = \mathrm{cost}(g_0) - 3s^2 \int_{t_1}^{t_2} (\psi'_1(t)\psi_2(t) - \psi_1(t)\psi'_2(t)) dt + O(s^3).$$

This is a second order variation that is not detected by Pontryagin first order conditions. Choose nonnegative C^∞ compactly supported functions $\psi_1(t), \psi_2 \geq 0$ on (t_1, t_2) such that $\psi'_1(t) > 0$ and $\psi'_2(t) < 0$ on their common support to make the s^2 -contribution negative. Then for all sufficiently small $s > 0$, we have

$$\mathrm{cost}(g_s) < \mathrm{cost}(g_0) = \pi.$$

The curvatures of the curves $t \mapsto \sigma_i(t) = g_s(t)e_i^*$ are C^∞ functions of s and t . The curvature functions converge uniformly to the constant positive curvature of the circle as s tends to 0. We may pick $s > 0$ sufficiently small so that the curvatures of the curves are positive. The corresponding centrally symmetric convex disk in \mathfrak{K}_{ccs} shows that the circle is not a local minimizer of cost. \square

Remark 8.2.8. *To obtain rough intuition about the perturbation of the circle considered in the theorem, we consider piecewise linear continuous functions ψ_1 and ψ_2 that are periodic modulo $\pi/3$, where*

$$\psi_1(t) = \begin{cases} 0, & \text{if } t \in [0, \pi/9]; \\ t - \pi/9, & \text{if } t \in [\pi/9, 2\pi/9]; \\ -t + 3\pi/9, & \text{if } t \in [2\pi/9, 3\pi/9]. \end{cases}$$

$$\psi_2(t) = \begin{cases} t, & \text{if } t \in [0, \pi/9]; \\ -t + 2\pi/9, & \text{if } t \in [\pi/9, 2\pi/9]; \\ 0, & \text{if } t \in [2\pi/9, 3\pi/9]. \end{cases}$$

Then $\psi'_1\psi_2 - \psi_1\psi'_2 = \pi/9 > 0$ on $(\pi/9, 2\pi/9)$ and is zero on $(0, \pi/9)$ and $(2\pi/9, \pi/3)$. We plot the multi-curve $\sigma_j(t) = \exp(Js_0)\Psi_s(t)\exp(Jt)\mathbf{s}_j^$ for $t \in [0, \pi/3]$, $s = 0.12$, and $s_0 = -1/8$ (to rotate the entire figure) in Figure 8.2.1. The figure is approximately a smoothed octagon. The functions ψ_i are not C^∞ and s is so large that the simple closed curve is not convex. Nevertheless, this crude numerical example suggests that the deformation in the theorem can be used to smoothly interpolate between the circle and the smoothed octagon along an interpolation path that is strictly decreasing in area.*

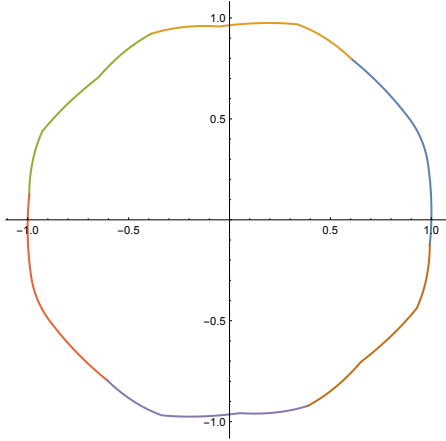


Figure 8.2.1: The deformation of Theorem 8.2.7 leads to a simple closed (multi) curve $\exp(Js_0)\Psi_s(t)\exp(Jt)\mathbf{s}_j^*$ that approximates the smoothed octagon.

8.3 Non-chattering away from the Singular Locus

Theorem 8.3.1. *Consider an extremal lifted trajectory on $[t_1, t_2]$ and $t_0 \in [t_1, t_2]$ such that the lifted trajectory does not meet the singular locus at time t_0 . Assume that the trajectory is also edge-extremal (8.1.1). Then there exists an edge $\{i, j\}$ and a neighborhood of t_0 in $[t_1, t_2]$ on which*

$$(X(t), \Lambda_R(t)) \in \bigcup_{I \subseteq \{i, j\}} (T^* \mathcal{O}_J)_I.$$

That is, near t_0 , the set of maximizers of the Hamiltonian is confined to a single edge of U_T .

Proof. We prove the theorem in contrapositive form. Assume that in every neighborhood of t_0 , the set of maximizers of the Hamiltonian is not confined to any edge of U_T . Reparameterizing by a time translation, we may assume that $t_0 = 0$. We will prove that the trajectory meets the singular locus at $t = 0$. We let $(X, \Lambda_1, \Lambda_R)$ be the controlled trajectory with optimal control function $u(t)$. By the continuity of the Hamiltonian, our assumption gives

$$(X(0), \Lambda_R(0)) \in (T^* \mathcal{O}_J)_{\{1, 2, 3\}}.$$

By Lemma 8.2.1, we have $\Lambda_R(0) = 0$.

We let $P(t) = Z_{u(t)}/\langle Z_{u(t)}, X(t) \rangle$ be the normalized control matrix. Set $\Lambda_{1,cost} = \Lambda_1 - 3\lambda_{cost}J/2$. It satisfies (by the costate equations 6.7.1)

$$\Lambda'_{1,cost} = [\Lambda_{1,cost}, X] + \frac{3}{2}\lambda_{cost}[J, X].$$

By the form of the right-hand-side, $\Lambda_{1,cost}$ is continuously differentiable. Define $Y(t) := -\int_0^t [\Lambda_{1,cost}, X] dt$, and set $\Lambda := \Lambda_R - Y$. Let

$$A(\Lambda, t) = [P(t), \Lambda] - \langle \Lambda, P(t) \rangle [P(t), X(t)],$$

viewed as a time-dependent linear function A on $\mathfrak{sl}_2(\mathbb{R})$, along the state trajectory given by $P = P(t)$ and $X = X(t)$. The costate ODE for Λ_R takes the form

$$\Lambda' = A(\Lambda, t) + A(Y, t).$$

We consider the initial value problem for Λ with initial conditions $\Lambda(0) = \Lambda_R(0) = Y(0) = 0$. Identifying $\mathfrak{sl}_2(\mathbb{R})$ with \mathbb{R}^3 , we use the Euclidean norm on the Lie algebra and use the natural matrix norm for A . By Cauchy-Schwarz, $\|\Lambda'\| \leq \|\Lambda'\|$. Then

$$\|\Lambda'\| \leq \|\Lambda'\| = \|A[\Lambda] + A[Y]\| \leq C_0 \|\Lambda\| + C_0 \|Y\|,$$

where $C_0 > 0$ is any time-independent bound on the matrix norms $\|A[\cdot, t]\|$ in a small neighborhood of $t = 0$. In integral form

$$\|\Lambda\| \leq C_0 \int_0^t \|Y\| dt + C_0 \int_0^t \|\Lambda\| dt. \quad (8.3.1)$$

We claim $\Lambda_{1,cost}(0) = 0$. Note that $\Lambda_{1,cost}(0) \in X(0)^\perp$ by the vanishing of the Hamiltonian $\langle \Lambda_{1,cost}, X \rangle - \langle \Lambda_R, P \rangle$ at $t = 0$. Thus, $\Lambda_{1,cost}(0) = 0$ if and only if $[\Lambda_{1,cost}(0), X(0)] = 0$. Suppose for a contradiction that $[\Lambda_{1,cost}(0), X(0)] \neq 0$. Then $\|Y\| = C_2 t + O(t^2)$, for some $C_2 \neq 0$, and the Gronwall inequality (Corollary A.1.3) applied to (8.3.1) gives

$$\|\Lambda_R - Y\| = \|\Lambda\| = O(t^2)$$

and

$$\Lambda_R = Y + O(t^2) = -[\Lambda_{1,cost}(0), X(0)]t + O(t^2).$$

The control dependent term of the Hamiltonian is

$$-\langle \Lambda_R, P \rangle = t \left\langle [\Lambda_{1,cost}(0), X(0)], \frac{Z_{u(t)}}{\langle X(0), Z_{u(t)} \rangle} \right\rangle + O(t^2).$$

By Lemma 8.2.1, for sufficiently small $t > 0$ (or for sufficiently small $t < 0$), there exists a vertex or edge of U_T , that maximizes this Hamiltonian. If the set of maximizers is an edge when t has one sign, then the maximizer is the complementary vertex of U_T when t has the other sign. If the set of maximizers is an edge (for a given sign of t), by the results of Theorem 8.1.4, the control function has finite bang-bang switching near $t = 0$. This is contrary to the assumption that the set of maximizers is not confined to any edge of U_T .

We claim that $\Lambda'_{1,cost}(0) = 0$. The proof is similar, and we give a brief sketch. By the form of the ODE for $\Lambda_{1,cost}$, we have $\Lambda'_{1,cost}(0) \in X(0)^\perp$. It is enough to show $[\Lambda'_{1,cost}(0), X(0)] = 0$. Suppose for a contradiction that $[\Lambda'_{1,cost}(0), X(0)] = 0$, but $[\Lambda'_{1,cost}(0), X(0)] \neq 0$. We again use estimates on the size of $\|Y\|$ and the Gronwall inequality (Corollary A.1.3) to show that Λ_R has an isolated zero at $t = 0$. Then a switching function has an isolated zero at $t = 0$, which again contradicts the hypothesis of the lemma.

$\Lambda_{1,cost}(0) = 0$ implies $\Lambda_1(0) = 3\lambda_{cost}J/2$. Also $\Lambda'_{1,cost}(0) = 0$ implies

$$0 = \Lambda'_1(0) = [\Lambda_1(0), X(0)] = (3/2)\lambda_{cost}[J, X(0)].$$

The non-vanishing of the costate vector at $t = 0$ implies that $\lambda_{cost} \neq 0$. $X(0) \in \mathbb{R}J \cap \mathcal{O}_J = \{J\}$, so $X(0) = J$. By definition, this is a point in the singular locus. \square

Theorem 8.3.2. *Consider a controlled extremal lifted trajectory that does not meet the singular locus \mathcal{S}_{sing} . Assume that the trajectory (g, X) is also edge-extremal. Then the control function is bang-bang with finitely many switches.*

Proof. According to the theorem, for every $t_0 \in [t_1, t_2]$, there exists a neighborhood of t_0 on which the control takes values in a single edge of U_T almost everywhere. By Theorem 8.1.4, the control is bang-bang with finite switching along the edge of the control simplex in a neighborhood of each t_0 . By the compactness of the interval $[t_1, t_2]$ the finite switching holds for the entire interval. \square

Remark 8.3.3. *In terms of Reinhardt's problem, the theorem implies that a trajectory (g, X) that is extremal and edge-extremal that does not meet the singular locus \mathcal{S}_{sing} defines a balanced disk $K(g, X) \in \mathfrak{K}_{bal}$ whose boundary is a smoothed polygon, consisting of finitely many straight edges and hyperbolic arcs.*

Lemma 8.3.4. *An extremal trajectory with constant control at a vertex of U_T does not meet the singular locus.*

(This lemma does not rule out the possibility of a chattering arc converging to the singular locus, as discussed in the next part of the book.)

Proof. We assume for a contradiction that the trajectory meets the singular locus at time $t = 0$ with constant control $u = \mathbf{e}_3 \in U_T$ (say). Consider the solutions to the state and costate ODEs with constant control at enumerated the vertex \mathbf{e}_3 of U_T and initial conditions at the singular locus. The solutions are analytic. At the singular locus, we have $\Lambda_{1,cost}(0) = \Lambda_R(0) = 0$ given by (8.2.1) and $X(0) = J$.

Let $P_i = Z_{\mathbf{e}_i}/\langle J, Z_{\mathbf{e}_i} \rangle$ be the normalized control matrix, evaluated at $t = 0$, $X(0)$, with the controls at the three vertices $\mathbf{e}_i \in U_T$. By using the costate ODEs, we also compute $\Lambda'_{1,cost}(0) = 0$. The following derivatives exist and have the following values.

$$\Lambda'_R(0) = \Lambda''_R(0) = 0, \quad \Lambda'''_R(0) = -6\lambda_{cost}[J, P_3].$$

The Lie bracket $[J, P_3]$ is orthogonal to J and P_3 . Also $P_1 + P_2 + P_3 \in \mathbb{R}J$. We have $\langle [J, P_3], P_1 \rangle = -\langle [J, P_3], P_2 \rangle \neq 0$. The leading term of the control term of the Hamiltonian evaluated at control $u = \mathbf{e}_i$ is

$$\begin{aligned} -\langle \Lambda_R(t), P_i \rangle &= -\frac{t^3}{3!} \langle \Lambda'''_R(0), P_i \rangle + O(t^4) \\ &\quad t^3 \langle [J, P_3], P_i \rangle + O(t^4). \end{aligned}$$

The leading term is zero when $i = 3$, but it is nonzero with opposite signs when $i = 1, 2$. Hence, the maximizer of the Hamiltonian is never \mathbf{e}_3 , when t is small. This is contrary to first-order conditions of extremality. \square

Part IV

Circular Control

Chapter 9

Circular Control Set

We are interested in a modification of the triangular control set to a circular disk. This will lead to a modified control problem that we view as a *toy control problem*. Insights from the toy problem will be applied in Part V to give a proof of Mahler's First conjecture. This part of the book is logically independent from the other parts, and it can be skipped without interrupting the flow of the text.

Definition 9.0.1 (Circular control sets).

- The circumscribed or disk control set is the set U_C which is the circumscribing disk of the two-simplex in \mathbb{R}^3 :

$$U_C := \left\{ (u_0, u_1, u_2) \mid 0 \leq u_i \leq 1, \sum_i u_i = 1, \sum_i u_i^2 \leq 1 \right\}.$$

- The inscribed control set is the set U_I which is the inscribed disk of the two-simplex in \mathbb{R}^3 :

$$U_I := \left\{ (u_0, u_1, u_2) \mid 0 \leq u_i \leq 1, \sum_i u_i = 1, \sum_i u_i^2 \leq \frac{1}{2} \right\}.$$

- Later (in Section 9.2), we will also be interested in control sets which interpolate between U_I and U_C . For $1/3 \leq r^2$ we define

$$U_r := \left\{ (u_0, u_1, u_2) \mid u_0 + u_1 + u_2 = 1, u_0^2 + u_1^2 + u_2^2 \leq r^2 \right\}.$$

We denote the boundary (relative to the affine hull) of these sets by ∂U_C , ∂U_I and ∂U_r respectively.

Remark 9.0.2. Controls (u_0, u_1, u_2) from $U_C \setminus U_T$ give rise to boundary curves σ_j of regions which fail to be convex. This is a consequence of the interpretation of the state-dependent curvatures $u_j \geq 0$ as a nonnegative curvature condition.

One motivation in considering these control sets is the following: we can observe that the triangular control set is invariant under $\mathbb{Z}/3\mathbb{Z}$ -rotations while the disk control set is invariant under rotations by the circle group S^1 . The latter is important for our investigations, as it will allow us to employ Noether's theorem to derive a *first integral* or a conserved quantity of the dynamics. A conserved quantity is useful because it facilitates a reduction in dimension of the original problem — if the group of symmetries is large enough, reduction by that group may even lead to a direct solution. Other motivations are enumerated in the introduction to the book.

Until now, we have been exclusively working with the simplex control set U_T . Now, we change our control set to be U_C , the circumscribing disk of U_T as described in Definition 9.0.1. This change is motivated by the following theorem.

Theorem 9.0.3. *Let \mathcal{H} be the Hamiltonian of the Reinhardt optimal control problem. Assuming that the control set is closed under rotations (i.e., if $A \in \text{SO}_2(\mathbb{R})$ is a rotation and Z_u is in the control set, then so is $\text{Ad}_A Z_u$), the Hamiltonian \mathcal{H} is invariant under the action of the subgroup $\text{SO}_2(\mathbb{R})$ of $\text{SL}_2(\mathbb{R})$.*

Proof. The Hamiltonian depends on the quantities X, Λ_1, Λ_R and the control matrix Z_u . Ignoring Z_u for the time being, if $A \in \text{SO}_2(\mathbb{R})$ is an arbitrary rotation, then let us see how these quantities transform. A acts on trajectories in \mathfrak{h} by linear fractional transformations and so, equivalently, we have $X \mapsto \text{Ad}_A X = AXA^{-1} =: \tilde{X}$ in the adjoint orbit picture. Now, Λ_1 transforms as $\Lambda_1 \mapsto A\Lambda_1 A^{-1} =: \tilde{\Lambda}_1$ since these transformed quantities satisfy the same ODE:

$$\tilde{\Lambda}'_1 = \text{Ad}_A \Lambda'_1 = \text{Ad}_A [\Lambda_1, X] = [\text{Ad}_A \Lambda_1, \text{Ad}_A X] = [\tilde{\Lambda}_1, \tilde{X}].$$

Similarly, we can also see that Λ_R transforms as $\Lambda_R \mapsto A\Lambda_R A^{-1}$. Now, the control set transforms as $Z_u \mapsto AZ_u A^{-1}$, which may, in general, fall outside the control set given by U_T . So, if we modify the control set so that it does not, a simple computation now using the expression for the control-dependent Hamiltonian in equation (6.4.1) shows that it is unchanged under these transformations by A . \square

Remark 9.0.4. Following the discussion at the end of Section 3.3, the control set U_T is only symmetric by discrete $\mathbb{Z}/3\mathbb{Z}$ -rotations and not under general $\text{SO}_2(\mathbb{R})$ rotations.

9.1 Conserved Quantity for the Circular Control Set

Recalling the discussion at the end of Section 3.3, we note that we enlarge the control set U_T to U_C to have continuous $\text{SO}_2(\mathbb{R})$ -symmetry in order to manufacture a conserved quantity for the dynamics. This is achieved by Noether's theorem.

The version of Noether's theorem which we use for optimal control is the one described by Sussmann [43]. Before recalling the statement, we begin with a few definitions. We let $\mathcal{Q} = (M, U, f, \phi)$ denote a general optimal control system satisfying the regularity conditions of Section 6.2. Also, we assume that the cost functional ϕ is independent of the control as in our case. In what follows, we will denote the vector field $f(u, q) \in T_q M$ for $u \in U$ by $f_u(q)$. The definitions below are all from Sussmann [43].

Definition 9.1.1 (Symmetry of a control system). *Let G be a Lie group with Lie algebra \mathfrak{g} and let $\mathcal{Q} = (M, U, f, \phi)$ be an optimal control system. A symmetry of this optimal control system is a diffeomorphism $\psi : V_1 \rightarrow V_2$ where $V_1, V_2 \subset M$ are open such that for every $u \in U$ there exist $u_1, u_2 \in U$ for which $d\psi(q)(f_u(q)) = f_{u_1}(\psi(q))$ and $d\psi(q)(f_{u_2}(q)) = f_{u_2}(\psi(q))$ for all $q \in V_1$.*

Definition 9.1.2 (Infinitesimal Group of Symmetries). *An infinitesimal group of symmetries of a control system \mathcal{Q} is a smooth action $\tau : \mathfrak{g} \rightarrow \Gamma^\infty(TM)$, which assigns to every Lie algebra element $X \in \mathfrak{g}$ a smooth vector field on M , such that every diffeomorphism $\exp(t\tau(X))$ is a symmetry of \mathcal{Q} .*

Definition 9.1.3 (Momentum Map). *To an infinitesimal group of symmetries $\tau : \mathfrak{g} \rightarrow \Gamma^\infty(TM)$ of an optimal control system \mathcal{Q} , we associate the momentum map $\mathbf{J}^\tau : T^*M \rightarrow \mathfrak{g}^*$ given by*

$$\mathbf{J}^\tau(q, p)(X) = \langle p, \tau(X)(q) \rangle_*,$$

where $X \in \mathfrak{g}$, $q \in M$, $p \in T_q^*M$ and $\tau(X)(q) \in T_q M$.

See Abraham and Marsden [1] for the general theory of momentum maps in symplectic geometry.

Theorem 9.1.4 (Noether-Sussmann Theorem). *Assume that $\mathcal{Q} = (M, U, f, \phi)$ is an optimal control system as above, let \mathfrak{g} be the Lie algebra of the Lie group G and let $\tau : \mathfrak{g} \rightarrow \Gamma^\infty(TM)$ be an infinitesimal group of symmetries of \mathcal{Q} . Let p be a lifted controlled trajectory in T^*M satisfying the Pontryagin Maximum Principle. Then the function $\mathbf{J}^\tau : T^*M \rightarrow \mathfrak{g}^*$ is constant along the trajectory p .*

Problem 9.1.5 (Circular Control Problem). *We start with problem 6.7.1 and enlarge the control set U_T to its circumscribing disk U_C . This control problem is called the circular control problem.*

Let us now apply the Noether-Sussmann theorem to the circular control problem. Define the angular momentum to be $\mathcal{A} := \langle J_{\mathfrak{su}}, \Lambda_1 + \Lambda_R \rangle$.

Theorem 9.1.6 (Angular Momentum). *We have that the angular momentum $\mathcal{A} = \langle J, \Lambda_1 + \Lambda_R \rangle$ is conserved along the optimal trajectory of the circular control problem.*

Proof. The proof analyzes the $\text{SO}_2(\mathbb{R})$ symmetry. Our optimal control system consists of data $(g, X, \Lambda_1, \Lambda_2) \in T^*(\text{TSL}_2(\mathbb{R}))$. Note that our Lie group here is $\text{SO}_2(\mathbb{R})$ and hence its Lie algebra is one-dimensional $\mathfrak{so}_2(\mathbb{R}) = J\mathbb{R}$, where J is the infinitesimal generator of rotations. This infinitesimal symmetry gives rise to rotations $\exp(J\theta) \in \text{SO}_2(\mathbb{R})$, which in turn give rise to the following action on our manifold:

$$\begin{aligned} \text{SO}_2(\mathbb{R}) \times T^*(\text{TSL}_2(\mathbb{R})) &\rightarrow T^*(\text{TSL}_2(\mathbb{R})) \\ (\exp(J\theta), (g, X, \Lambda_1, \Lambda_2)) &\mapsto (\exp(J\theta)g\exp(-J\theta), \text{Ad}_{\exp(J\theta)}X, \text{Ad}_{\exp(J\theta)}\Lambda_1, \text{Ad}_{\exp(J\theta)}\Lambda_2), \end{aligned}$$

where the action on g is by inner automorphisms and the rest are given by the adjoint action on each copy of $\mathfrak{sl}_2(\mathbb{R})$. (Note that throughout, we make the identification $\mathfrak{sl}_2(\mathbb{R})^* \cong \mathfrak{sl}_2(\mathbb{R})$ via the nondegenerate trace form.) These are *symmetries* by the proof of Theorem 9.0.3 and also since the rotation action on the control matrix Z_u is

$$Z_u \mapsto \text{Ad}_{\exp(J\theta)}Z_u \in U_C.$$

The momentum map is computed by the canonical pairing between the costate variables $(\Lambda_1, \Lambda_2) \in T_{(g,X)}^*(\text{TSL}_2(\mathbb{R}))$ and tangent vectors in $T_{(g,X)}(\text{TSL}_2(\mathbb{R}))$

giving the infinitesimal rotation action. The first component of this tangent vector is given by

$$\begin{aligned} \frac{d}{d\theta} \exp(J\theta)g \exp(-J\theta) \Big|_{\theta=0} &= \underbrace{Jg - gJ}_{\in T_g \mathrm{SL}_2(\mathbb{R})} \\ &= \underbrace{g}_{\in \mathrm{SL}_2(\mathbb{R})} \underbrace{(g^{-1}Jg - J)}_{\in \mathfrak{sl}_2(\mathbb{R})}. \end{aligned}$$

Thus, we can identify the first component with $g^{-1}Jg - J$ in the Lie algebra $\mathfrak{sl}_2(\mathbb{R})$. The second component is given by

$$\frac{d}{d\theta} \mathrm{Ad}_{\exp(J\theta)}X = \mathrm{ad}_J X = [J, X],$$

which is already in the Lie algebra $\mathfrak{sl}_2(\mathbb{R})$. So, putting all this together, we obtain the momentum map.

$$\begin{aligned} \mathbf{J}^\tau((g, \Lambda_1, X, \Lambda_2)) &= \langle (\Lambda_1, \Lambda_2), (\mathrm{Ad}_{g^{-1}}J - J, [J, X]) \rangle \\ &= \langle \Lambda_1, \mathrm{Ad}_{g^{-1}}J - J \rangle + \langle \Lambda_2, [J, X] \rangle \\ &= \langle \Lambda_1, \mathrm{Ad}_{g^{-1}}J \rangle - \langle \Lambda_1, J \rangle - \langle [\Lambda_2, X], J \rangle \\ &= \langle \Lambda_1, \mathrm{Ad}_{g^{-1}}J \rangle - \langle J, \Lambda_1 + \Lambda_R \rangle, \end{aligned}$$

where, as usual, $\langle \cdot, \cdot \rangle_*$ denotes the natural pairing between a vector space and its dual. Note however, from Corollary 6.5.3, that $\Lambda_1(t) = g^{-1}\Lambda_1(0)g(t)$ and so $\langle \Lambda_1, \mathrm{Ad}_{g^{-1}}J \rangle$ is a constant.

Thus, by the Noether-Sussmann theorem $\langle J, \Lambda_1 + \Lambda_R \rangle$ is a constant of motion along the optimal trajectory of the circular control problem. \square

Remark 9.1.7.

- Since it is the conserved quantity arising from a rotational symmetry, $\langle J, \Lambda_1 + \Lambda_R \rangle$ will be called the *angular momentum*.
- The spurious constant in the expression for the momentum map is a consequence of the action of $\mathrm{SO}_2(\mathbb{R})$ on $\mathrm{SL}_2(\mathbb{R})$ by inner automorphisms. This means that we could also modify the action to be $g \mapsto g \exp(-J\theta)$ to obtain a valid conserved quantity.
- We also obtain the same conserved quantity for a control set U_r which is a disk of any radius r whenever $r^2 > 1/3$. (See Definition 9.0.1.)

Conserved quantities are very useful since they introduce constraints and cut down the dimension of the problem. But an immediate application is that they give us a constraint on the optimal control matrix in terms of the state-costate variables, which is what we aim to derive. But before we do, we make a quick detour to understand the structure of the control sets when viewed in the Lie algebra $\mathfrak{su}(1, 1)$ of a unitary group.

9.2 Control Sets in the Special Unitary Group

The special unitary group $SU(1, 1)$ and its Lie algebra $\mathfrak{su}(1, 1)$ are introduced in Appendix A.4. From that appendix, we know that the Lie algebras $\mathfrak{su}(1, 1)$ and $\mathfrak{sl}_2(\mathbb{R})$ are isomorphic. This isomorphism is given by the Cayley transform.

$$\text{Cayley}(\mathfrak{sl}_2(\mathbb{R})) = \mathfrak{su}(1, 1).$$

Under the Cayley transform to $\mathfrak{su}(1, 1)$, the image of the control matrix Z_u , given in equation (3.3.2), is

$$\frac{1}{3} \begin{pmatrix} -i & 2(u_0 + \zeta u_1 + \zeta^2 u_2) \\ 2(u_0 + \zeta^2 u_1 + \zeta u_2) & i \end{pmatrix}, \quad (9.2.1)$$

where $\zeta = \exp(2\pi i/3)$ is a primitive cube root of unity.

Now, let ∂U_r denote the boundary of the disk control set U_r of radius r in \mathbb{R}^3 .

$$U_r := \{(u_0, u_1, u_2) \mid u_0 + u_1 + u_2 = 1, u_0^2 + u_1^2 + u_2^2 \leq r^2\}.$$

The following lemma gives a simplification of the control matrix.

Lemma 9.2.1. *The set ∂U_r and the circle*

$$\left\{ z \in \mathbb{C} \mid |z|^2 = \left(\frac{3r^2 - 1}{2} \right) \right\}$$

are in bijection by the map $(u_0, u_1, u_2) \mapsto u_0 + \zeta u_1 + \zeta^2 u_2$.

Proof. Consider the affine plane $\Pi = \{(u_0, u_1, u_2) \mid u_0 + u_1 + u_2 = 1\}$ and consider the map $L : \Pi \rightarrow \mathbb{C}$, defined by $L(u_0, u_1, u_2) := (u_0 + \zeta u_1 + \zeta^2 u_2)$. This map is the restriction of the linear map

$$(u_0, u_1, u_2) \mapsto \begin{pmatrix} 1 & 1 & 1 \\ 1 & \zeta & \zeta^2 \\ 1 & \zeta^2 & \zeta \end{pmatrix} \begin{pmatrix} u_0 \\ u_1 \\ u_2 \end{pmatrix} = \begin{pmatrix} 1 \\ z \\ \bar{z} \end{pmatrix},$$

which has non-zero determinant and so L is an isomorphism of affine planes. This isomorphism restricts to a bijection between the circles ∂U_r and

$$\{z \in \mathbb{C} \mid |z|^2 = \left(\frac{3r^2 - 1}{2}\right)\}$$

since

$$\begin{aligned} |(u_0 + \zeta u_1 + \zeta^2 u_2)|^2 &= \frac{3}{2}(u_0^2 + u_1^2 + u_2^2) - \frac{(u_0 + u_1 + u_2)^2}{2} \\ &= \frac{3r^2 - 1}{2}. \end{aligned}$$

□

The above lemma shows that if the control set is U_r , then we can take Z_u in general to be

$$\begin{aligned} Z_u &= \begin{pmatrix} -i\alpha & \beta z \\ \beta \bar{z} & i\alpha \end{pmatrix} \in \mathfrak{su}(1, 1), \quad \text{where} \\ |z| &= 1, \quad \text{and } \beta > 0, \end{aligned} \tag{9.2.2}$$

where $z \in \mathbb{C}$ and $\alpha, \beta \in \mathbb{R}$. Also, βz gives the polar coordinate decomposition of upper-right matrix entry of Z_u . With this notation, $\alpha = \frac{1}{3}$ and $\beta = \frac{2}{3}|u_0 + \zeta u_1 + \zeta^2 u_2|$. We obtain

$$\det(Z_u) = (\alpha^2 - \beta^2) = \frac{1 - 4\left(\frac{3r^2 - 1}{2}\right)}{9} = \frac{1 - 2r^2}{3}. \tag{9.2.3}$$

Later chapters will use the parameter ρ instead of radius r , where

$$\rho := \beta/\alpha, \quad \rho^2 = 6r^2 - 2.$$

Table 9.1 shows the square of the radii r^2 of the circumscribing disk, inscribed disk and center of the control simplex U_T and their corresponding radii when viewed as disks in the complex plane (following Lemma 9.2.1).

$\det(Z_u)$	Relation to U_T	r^2	Radius $(3r^2 - 1)/2$ in \mathbb{C}	(α, β)	$\rho = \beta/\alpha$
-1/3	Circumscribing disk U_C	1	1	(1/3, 2/3)	2
0	Inscribed disk U_I	1/2	1/4	(1/3, 1/3)	1
1/9	Center (1/3, 1/3, 1/3)	1/3	0	(1/3, 0)	0

Table 9.1: Various control sets and their radii.

9.3 Quadratic Equation for Optimal Control

Henceforth, we let Z^* denote the optimal control matrix for the costate equations 6.7.1 (with the control set U_r). It depends on a complex control variable z . We derive a constraint on Z^* from angular momentum conservation.

We begin with a few lemmas.

Lemma 9.3.1. *The set of maximizers of the Hamiltonian (considered as a function of the control) when the control set is the disk U_r is either the entire disk or just a point on ∂U_r .*

Proof. This is a direct corollary of Lemma 7.3.1. \square

Theorem 9.3.2. *Let Z^* be the optimal control matrix for the costate equations (6.7.1) (with the control set U_r). We then have*

$$\left\langle J_{\mathfrak{su}}, \text{ad}_{Z^*} \frac{\delta}{\delta Z^*} \frac{\langle \Lambda_R, Z^* \rangle}{\langle X, Z^* \rangle} \right\rangle = 0,$$

where $\frac{\delta}{\delta Z^*}$ is the functional derivative with respect to Z^* .¹

Proof. We give two proofs of this fact. For the first proof, we differentiate the angular momentum (in Theorem 9.1.6) with respect to time, to obtain

¹Note that the $J_{\mathfrak{su}}$ in this theorem is an element of $\mathfrak{su}(1, 1)$ and is given by Cayley transform of J .

$$J_{\mathfrak{su}} = \text{Cayley} \left(\begin{array}{cc} 0 & -1 \\ 1 & 0 \end{array} \right) = \left(\begin{array}{cc} -i & 0 \\ 0 & i \end{array} \right).$$

the following.

$$\begin{aligned}
0 = \langle J_{\mathfrak{su}}, \Lambda'_1 + \Lambda'_R \rangle &= \left\langle J_{\mathfrak{su}}, [\Lambda_1, X] + [P^*, \Lambda_R] + \left[-\Lambda_1 + \frac{3}{2} \lambda_{cost} J_{\mathfrak{su}}, X \right] - \langle P^*, \Lambda_R \rangle [P^*, X] \right\rangle \\
&= \langle J_{\mathfrak{su}}, [P^*, \Lambda_R] - \langle P^*, \Lambda_R \rangle [P^*, X] \rangle \tag{9.3.1} \\
&= \left\langle J_{\mathfrak{su}}, \text{ad}_{Z^*} \frac{\delta}{\delta Z^*} \frac{\langle \Lambda_R, Z^* \rangle}{\langle X, Z^* \rangle} \right\rangle \quad (\text{by Corollary 6.5.4}),
\end{aligned}$$

where $P^* = Z^* / \langle Z^*, X \rangle$.

For the second proof, note that from Lemma 9.3.1, the Hamiltonian is maximized at a point on ∂U_r . By the form of the control matrix Z^* , on the boundary of U_r we obtain two constraints.

$$\langle J_{\mathfrak{su}}, Z^* \rangle = \text{constant}, \quad \langle Z^*, Z^* \rangle = \text{constant}.$$

The Hamiltonian maximization of the maximum principle can be considered as a constrained maximization problem subject to the above two constraints. The functional derivatives of the above two constraints are $J_{\mathfrak{su}}$ and $2Z^*$ respectively. By Lagrange multipliers, we find the derivative $\delta\mathcal{H}/\delta Z^*$ should lie in the span of the derivatives $J_{\mathfrak{su}}, Z^*$ of the constraints. That is, $\text{ad}_{Z^*}(\frac{\delta\mathcal{H}}{\delta Z^*})$ is in the span of $\text{ad}_{Z^*} J_{\mathfrak{su}}$. Thus,

$$\left\langle \text{ad}_{Z^*} \frac{\delta\mathcal{H}}{\delta Z^*}, J_{\mathfrak{su}} \right\rangle = 0,$$

which gives us the required. \square

We also have the following result, which shows that the angular momentum and the Hamiltonian are in involution with respect to the Poisson bracket $\{\cdot, \cdot\}_{ex}$ on the extended state space $T^*TSU(1, 1)$.

Proposition 9.3.3. *The angular momentum \mathcal{A} Poisson commutes with the Hamiltonian on $T^*(TSU(1, 1))$, provided the control set is rotationally invariant.*

Proof. We use the Poisson bracket on the manifold $T^*(TSU(1, 1))$ derived in Section A.9, which we recall here. If F, G are two left-invariant smooth functions on $T^*TSU(1, 1)$, their extended space Poisson bracket is

$$\{F, G\}_{ex} := \left\langle \Lambda_1, \left[\frac{\delta F}{\delta \Lambda_1}, \frac{\delta G}{\delta \Lambda_1} \right] \right\rangle + \left\langle \frac{\delta F}{\delta X}, \frac{\delta G}{\delta \Lambda_2} \right\rangle - \left\langle \frac{\delta F}{\delta \Lambda_2}, \frac{\delta G}{\delta X} \right\rangle.$$

We compute using Theorem A.9.2 that

$$\begin{aligned}\{\mathcal{A}, \mathcal{H}\}_{ex} &= \langle \langle J_{\mathfrak{su}}, \Lambda_1 + \Lambda_R \rangle, \mathcal{H} \rangle_{ex} = \langle J_{\mathfrak{su}}, \{\Lambda_1 + \Lambda_R, \mathcal{H}\}_{ex} \rangle \\ &= \langle J_{\mathfrak{su}}, \Lambda'_1 + \Lambda'_R \rangle = 0,\end{aligned}$$

where Λ'_1 and Λ'_R are shorthand for the expressions on the right-hand side of the ODEs for Λ_1 and Λ_R . \square

Simplifying equation (9.3.1) above, we obtain a more symmetric expression for the optimal control matrix, which is homogeneous in Z^* .

$$\langle J_{\mathfrak{su}}, [Z^*, X] \rangle \langle Z^*, \Lambda_R \rangle = \langle J_{\mathfrak{su}}, [Z^*, \Lambda_R] \rangle \langle Z^*, X \rangle. \quad (9.3.2)$$

This is the same as saying

$$\begin{vmatrix} \langle [J_{\mathfrak{su}}, Z^*], X \rangle & \langle [J_{\mathfrak{su}}, Z^*], \Lambda_R \rangle \\ \langle Z^*, X \rangle & \langle Z^*, \Lambda_R \rangle \end{vmatrix} = 0. \quad (9.3.3)$$

Proposition 9.3.4. *The conservation of angular momentum gives the following constraint on the optimal control matrix.*

$$\langle Z^*, [\Lambda_R, X] \rangle = \frac{\langle Z^*, Z^* \rangle}{\langle Z^*, J_{\mathfrak{su}} \rangle} \langle J_{\mathfrak{su}}, [\Lambda_R, X] \rangle. \quad (9.3.4)$$

Proof. From (9.3.2) and Proposition A.6.2 specialized to $[J_{\mathfrak{su}}, Z^*]$, Z^* , X , and Λ_R , we obtain

$$0 = \langle [J_{\mathfrak{su}}, Z^*], \Lambda_R \rangle \langle Z^*, X \rangle - \langle Z^*, \Lambda_R \rangle \langle [J_{\mathfrak{su}}, Z^*], X \rangle = -\frac{\langle [[J_{\mathfrak{su}}, Z^*], Z^*], [\Lambda_R, X] \rangle}{2}. \quad (9.3.5)$$

For any $Z^*, J_{\mathfrak{su}} \in \mathfrak{sl}_2(\mathbb{C})$, we have that

$$[Z^*, [Z^*, J_{\mathfrak{su}}]] = (\text{ad}_{Z^*})^2 J_{\mathfrak{su}} = 2 \langle Z^*, Z^* \rangle J_{\mathfrak{su}} - 2 \langle Z^*, J_{\mathfrak{su}} \rangle Z^*.$$

If we substitute this equation back into (9.3.5), we obtain the result. \square

Definition 9.3.5 (Weighted Determinant). *For*

$$\Lambda = \begin{pmatrix} l_{11} & l_{12} \\ l_{21} & -l_{11} \end{pmatrix} \in \mathfrak{sl}_2(\mathbb{C})$$

and $\alpha, \beta \in \mathbb{R}$, define the weighted determinant

$$\det(\Lambda, \alpha, \beta) := -(\alpha^2 l_{11}^2 + \beta^2 l_{12} l_{21}).$$

If $\Lambda \in \mathfrak{su}(1, 1)$ and $\alpha^2, \beta^2 \in \mathbb{R}$, then $\det(\Lambda, \alpha, \beta) \in \mathbb{R}$. The ordinary determinant has weights $\alpha = \beta = 1$.

$$\det(\Lambda, 1, 1) = \det(\Lambda).$$

Proposition 9.3.6. *The optimal control (9.2.2) in the circular control case U_r is given by the root z of the quadratic equation (9.3.8).*

Proof. We know by Lemma 9.3.1 that the optimal control matrix Z^* takes values in the boundary of the disk. By equation (9.2.2), we can take

$$Z^* = \begin{pmatrix} -i\alpha & \beta z \\ \beta/z & i\alpha \end{pmatrix}, \quad (9.3.6)$$

where $|z| = 1$. With this notation, (9.3.4) becomes

$$\langle Z^*, [\Lambda_R, X] \rangle = \frac{(\alpha^2 - \beta^2)}{\alpha} \langle J_{\mathfrak{su}}, [\Lambda_R, X] \rangle, \quad (9.3.7)$$

where $\alpha, \beta \in \mathbb{R}$ and $\alpha > 0$.

Simplifying this, we obtain the following quadratic equation in z

$$\alpha[\Lambda_R, X]_{21}z^2 - 2i\beta[\Lambda_R, X]_{11}z + \alpha[\Lambda_R, X]_{12} = 0, \quad (9.3.8)$$

where the subscripts index matrix entries. We then solve for z to obtain two roots

$$z_{\pm} = i \left(\frac{\beta[\Lambda_R, X]_{11} \pm \sqrt{-\det([\Lambda_R, X], \alpha, \beta)}}{\alpha[\Lambda_R, X]_{21}} \right). \quad (9.3.9)$$

□

This determines the optimal control explicitly as a function of the state-costate variables. We see how modifying the control set to be more symmetrical has resulted in a conserved quantity which has in turn given us valuable information about the optimal control.

Chapter 10

Hyperboloid Coordinates

10.1 Coordinates

We begin with the following lemma.

Lemma 10.1.1. *The Cayley transform of*

$$\begin{pmatrix} a & b \\ c & -a \end{pmatrix} \in \mathfrak{sl}_2(\mathbb{R}) \quad \text{is} \quad \begin{pmatrix} it & z \\ \bar{z} & -it \end{pmatrix} \in \mathfrak{su}(1, 1), \quad (10.1.1)$$

where $z = (b + c)/2 + ia \in \mathbb{C}$ and $t = (b - c)/2 \in \mathbb{R}$.

Proof. This is an easy calculation. \square

The matrices in $\mathfrak{su}(1, 1)$ with a given determinant $d = \det(X)$ are in bijective correspondence with the points on a hyperboloid

$$\begin{pmatrix} it & z \\ \bar{z} & -it \end{pmatrix} \in \mathfrak{su}(1, 1) \leftrightarrow \{(t, z) \in \mathbb{R} \times \mathbb{C} \mid t^2 - |z|^2 = d\}.$$

This observation justifies our nomenclature of *hyperboloid coordinates*, for the Cayley transform of the \mathfrak{sl}_2 coordinate system. A matrix in $\mathfrak{su}(1, 1)$ is determined by its determinant and the complex number z , up to the ambiguity in the sign of t .

Notation.

- For a complex number z , and $\epsilon \in \{-1, 0, 1\}$, we set $\llbracket z \rrbracket_\epsilon := \sqrt{\epsilon + |z|^2}$, and $\llbracket z \rrbracket := \llbracket z \rrbracket_1 = \sqrt{1 + |z|^2}$.

- We write

$$\Re(z_1, z_2) := \Re(\bar{z}_1 z_2) \quad (\text{real part})$$

to denote the \mathbb{R} -bilinear form on \mathbb{C} , derived from the real part of a complex number.

We transform the ODE for $X, \Lambda_1, \Lambda_R \mathfrak{sl}_2(\mathbb{R})$ into ODEs given by hyperboloid coordinates. We now work consistently with the Cayley transformed version of X, Λ_R , and Λ_1 in $\mathfrak{su}(1,1)$. The ODEs from the costate equations 6.7.1 retain exactly the same form, except that J and Z^* must be replaced with their Cayley transforms $J_{\mathfrak{su}} = \text{diag}(-i, i)$ and $Z_{\mathfrak{su}(1,1)} \in \mathfrak{su}(1,1)$. Using these, our assumptions, and Lemma 10.1.1, we can write

$$X := \begin{pmatrix} -i[\![w]\!] & w \\ \bar{w} & i[\![w]\!] \end{pmatrix}, \quad \Lambda_1 := d_1 \begin{pmatrix} i[\![b]\!]_\epsilon & b \\ \bar{b} & -i[\![b]\!]_\epsilon \end{pmatrix}, \quad \Lambda_R := \begin{pmatrix} -i \frac{\Re(c,w)}{[\![w]\!]} & c \\ \bar{c} & i \frac{\Re(c,w)}{[\![w]\!]} \end{pmatrix}, \quad (10.1.2)$$

for variable complex numbers $w, b, c \in \mathbb{C}$, with $|b|^2 \geq -\epsilon$. The form of the expressions ensure that the constraints $\det(X) = 1$ and $\langle X, \Lambda_R \rangle = 0$ are satisfied. The parameters $\epsilon \in \{-1, 0, 1\}$ and $d_1 \in \Re$ are constants of motion, and $\det(\Lambda_1) = \epsilon d_1^2$. The sign of the upper-left matrix entry $-i[\![w]\!]$ of X is determined by the sign convention on the orbit \mathcal{O}_J , described in Lemma 4.1.1. Note that $(w, [\![w]\!])$ lies on the upper sheet of the hyperboloid $\{(w, t) \in \mathbb{C} \times \mathbb{R} \mid t^2 - |w|^2 = 1\}$, which justifies our nomenclature.

Remark 10.1.2. *The form of element Λ_1 is general enough to represent a general element of $\mathfrak{su}(1,1)$. We take $d_1 \in \mathbb{R}^\times$, except when $\Lambda_1 = 0$. If $\det(\Lambda_1) = 0$, then Λ_1 belongs to the nilpotent cone, which consists of three conjugacy classes: the vertex of the cone (the zero element) and the positive and negative cones (the two regular nilpotent classes). We can take $d_1 = \epsilon = b = 0$ (for the zero element) or $(d_1, \epsilon) = (\pm 1, 0)$ (for the regular nilpotent elements). In the case of the zero element, we omit the ODE for b . When Λ_1 is regular semisimple ($\det(\Lambda_1) \neq 0$), the scalar d_1 parameterizes nonzero elements within a given Cartan subalgebra. The hyperboloid has one or two sheets, depending on whether Λ_1 is split ($\det(\Lambda_1) < 0$), or elliptic $\det(\Lambda_1) > 0$. In the split case, the coordinate system breaks down around the neck $|b| = 1$ of the hyperboloid, and a better coordinate system is introduced in Remark 10.2.5.*

In the case of circular control, there are two real parameters α, β such that $\det(Z^*) = \alpha^2 - \beta^2$. See Table (9.1) and Equation (9.2.3). We assume

in this chapter that α, β are both positive, and we set $\rho = \beta/\alpha > 0$. In the case of circular control, we assume the star condition in the form $\langle X, Z^* \rangle < 0$. For a control matrix given by equation (9.3.6) (which is already in $\mathfrak{su}(1, 1)$ by the results of Section 9.2) and using Lemma 3.3.4, the star condition in these coordinates can be expressed as

$$\mu(w, z) := \|w\| - \rho \Re(w, z) = -\frac{\langle X, Z^* \rangle}{2\alpha} > 0.$$

We consider the system on a region slightly larger than the star domain defined by the condition $\mu(w, z^*) > 0$ (and $c \neq 0$), where z^* is the maximizing root of the quadratic equation for the control.

10.2 Hyperboloid ODE

The ODEs in Lie algebra coordinates for X, Λ_1 and Λ_R were derived in Sections 6.5 and 3.4. We now write them out in the hyperboloid coordinates we have defined above. This will enable us to better understand the dynamics near the singular locus.

Theorem 10.2.1 (ODE in Hyperboloid Coordinates). *In hyperboloid coordinates, the dynamics for X, Λ_1 and Λ_R take the form*

$$w' = i \frac{w - \rho \|w\| z^*}{\mu(w, z^*)}, \quad (10.2.1)$$

$$b' = 2i (\|b\|_\epsilon w + b \|w\|), \quad (10.2.2)$$

$$c' = \frac{i(1 - \rho^2) \Re(c \xi_0(w, c), z^*)}{2 \|w\| \mu(w, z^*)^2} z^* \\ - i ((2d_1 \|b\|_\epsilon + 3\lambda_{cost}) w + 2bd_1 \|w\|). \quad (10.2.3)$$

where z^* is the Hamiltonian maximizing root of the quadratic equation for the optimal control, and $\xi_0 = \xi_0(w, c) := 2 + |w|^2 - (w\bar{c}/|c|)^2$. Here w, b, c are complex valued functions, satisfying the restrictions of Section 10.1.

Proof. This is an elementary computation using the hyperboloid form of the state and costate equations as in equation (10.1.2) and substituting them into the state and costate ODE derived in Sections 3.4 and 6.5. \square

Similarly, we have expressions for the Hamiltonian and the angular momentum.

$$\mathcal{A} = 2d_1[\![b]\!]_\epsilon - 2\frac{\Re(w, c)}{[\![w]\!]} \quad (10.2.4)$$

$$\mathcal{H} = (2d_1 \Re(w, b) + (2d_1[\![b]\!]_\epsilon + 3\lambda_{cost})[\![w]\!]) - \frac{\Re(w - \rho[\![w]\!]z^*, c)}{\mu(w, z^*)[\![w]\!]} \quad (10.2.5)$$

Corollary 10.2.2. *The following additional ordinary differential equations hold.*

$$[\![w]\!]' = \frac{\Re(w', w)}{[\![w]\!]} = \rho \frac{\Re(iw, z^*)}{\mu(w, z^*)}, \quad (10.2.6)$$

$$[\![b]\!]'_\epsilon = \frac{\Re(b', b)}{[\![b]\!]_\epsilon} = 2\Re(iw, b), \quad (10.2.7)$$

$$\left(\frac{\Re(w, c)}{[\![w]\!]} \right)' = 2d_1 \Re(iw, b). \quad (10.2.8)$$

Moreover, the overall form of the ODEs is pseudo-linear.

$$\begin{pmatrix} w \\ b \\ c \end{pmatrix}' = iA \begin{pmatrix} w \\ b \\ c \\ z^* \end{pmatrix} \quad (10.2.9)$$

where A is a 3×4 matrix with real (rotationally invariant) entries.

$$A = \begin{pmatrix} 1/\mu^* & 0 & 0 & -\rho[\![w]\!]/\mu^* \\ 2[\![b]\!]_\epsilon & 2[\![w]\!] & 0 & 0 \\ -3\lambda_{cost} - 2d_1[\![b]\!]_\epsilon & -2d_1[\![w]\!] & 0 & \frac{(1 - \rho^2)\Re(c\xi_0(w, c), z^*)}{2[\![w]\!]\mu^{*2}} \end{pmatrix}, \quad (10.2.10)$$

where $\mu^* := \mu(w, z^*)$.

Proof. These equations are direct consequences of Theorem 10.2.1. \square

Remark 10.2.3. *The equations have a time-reversal symmetry. If (w, b, c, z^*) is a solution, then so is $(\tilde{w}, \tilde{b}, \tilde{c}, \tilde{z}^*)$, where*

$$\tilde{w}(t) = \bar{w}(-t), \quad \tilde{b}(t) = \bar{b}(-t), \quad \tilde{c}(t) = \bar{c}(-t), \quad \tilde{z}^*(t) = \bar{z}^*(-t).$$

Remark 10.2.4. *To double-check answers, we rederive the fact that the angular momentum and Hamiltonian are constant along trajectories. To show the constancy of \mathcal{A} , we show its derivative is zero. This is a direct consequence of (10.2.7) and (10.2.8). The direct verification of the constancy of \mathcal{H} is a tedious but direct calculation.*

Remark 10.2.5. *As mentioned in Remark 10.1.2, in the split case $\epsilon = -1$, the coordinate system for Λ_1 breaks down around the neck of the hyperboloid. It is helpful to replace b with better coordinates (r, θ) . In the split case, we write*

$$\Lambda_1 = d_1 \begin{pmatrix} ir & \exp(i\theta)\sqrt{r^2 + 1} \\ \exp(-i\theta)\sqrt{r^2 + 1} & -ir \end{pmatrix}, \quad r \in \mathbb{R}, \quad d_1 > 0.$$

and we replace the ODE for b with the system

$$\begin{aligned} r' &= 2\sqrt{1 + r^2} \Re(iw, \exp(i\theta)), \\ \theta' &= 2\llbracket w \rrbracket + \frac{2r \Re(w, \exp(i\theta))}{\sqrt{r^2 + 1}}. \end{aligned}$$

10.3 Optimal Control

Assume $c \neq 0$, and set

$$\tilde{w} := \bar{c}w/|c|, \quad \tilde{z} := \bar{c}z/|c|, \quad (10.3.1)$$

Note $\llbracket w \rrbracket = \llbracket \tilde{w} \rrbracket$ and $\mu(w, z^*) = \mu(\tilde{w}, \tilde{z}^*)$.

Lemma 10.3.1. *If $c \neq 0$, the optimal control is $z^* = c\tilde{z}^*/|c|$, where \tilde{z}^* is a root of the quadratic polynomial*

$$Q(\tilde{z}) := \xi_0 + \xi_1 \tilde{z} + \xi_2 \tilde{z}^2,$$

where

$$\begin{aligned} \xi_0 &= \xi_0(\tilde{w}) := 2 + |\tilde{w}|^2 - \tilde{w}^2 = 2 + |w|^2 - (w\bar{c}/|c|)^2 =: \xi_0(w, c), \\ \xi_1 &= \xi_1(\tilde{w}) := 2\rho(\tilde{w} - \bar{w})\llbracket \tilde{w} \rrbracket, \\ \xi_2 &= \xi_2(\tilde{w}) = -\bar{\xi}_0 = -(2 + |\tilde{w}|^2 - \tilde{w}^2). \end{aligned} \quad (10.3.2)$$

Proof. The lemma follows from the explicit description of the quadratic equation for the control in Proposition 9.3.6.

We can give a second proof as follows. The dependence of the Hamiltonian on \tilde{z} (that is, on the circular control set U_r), comes through the term

$$-\frac{\Re(w - \rho\llbracket w \rrbracket z, c)}{\mu(w, z)\llbracket w \rrbracket} = -\frac{|c|\Re(\tilde{w} - \rho\llbracket \tilde{w} \rrbracket \tilde{z}, 1)}{\mu(\tilde{w}, \tilde{z})\llbracket \tilde{w} \rrbracket} =: \mathcal{H}_0(\tilde{z}).$$

We compute

$$\frac{d\mathcal{H}_0(\tilde{z} \exp(i\theta))}{d\theta} \Big|_{\theta=0} = \frac{-iQ(\tilde{z})\rho|c|}{4\tilde{z}\mu^2\llbracket \tilde{w} \rrbracket},$$

where Q is the given quadratic polynomial. Thus, the derivative vanishes and the Hamiltonian is extremal when $Q(\tilde{z}^*) = 0$. \square

Thus, the root \tilde{z}^* is one of the two roots

$$\frac{(\xi_1 \pm \sqrt{\Delta})}{2\xi_0}, \quad \Delta := \xi_1^2 + 4|\xi_0|^2.$$

Let us now turn to selecting the Hamiltonian maximizing root.

Lemma 10.3.2. *On a punctured neighborhood of the singular locus, the root $\tilde{z}^* = \bar{c}z^*/|c|$ of the quadratic equation (10.3.2) giving the optimal control satisfies $\tilde{z}^* = 1 + O(|w|)$ and $z^* = c/|c| + O(|w|)$.*

Proof. Near the singular locus, the coefficients are $0 \neq \xi_0 = 2 + O(|w|^2)$ and $\xi_1 = O(|w|)$. Using this, we find the discriminant of the quadratic polynomial (10.3.2) is a positive real number and equals

$$\Delta = 4|\xi_0|^2 + \xi_1^2 = 16 + O(|w|^2).$$

Up to a positive scalar, the Hamiltonian (10.2.5) depends on the roots \tilde{z} of the quadratic through the term

$$\frac{\rho\llbracket w \rrbracket \Re(z, c) - \Re(w, c)}{|c|\mu(w, z)\llbracket w \rrbracket} = \frac{\rho\llbracket \tilde{w} \rrbracket \Re(\tilde{z}) - \Re(\tilde{w})}{\mu(\tilde{w}, \tilde{z})\llbracket \tilde{w} \rrbracket} = \frac{\pm\rho\sqrt{\Delta}}{4} + O(|\tilde{w}|). \quad (10.3.3)$$

The Hamiltonian is not constant in \tilde{z} , and $\Delta \neq 0$. The star domain defines a simply connected set given by the inequality

$$0 < \mu(|\tilde{w}|, 1) = \llbracket \tilde{w} \rrbracket - \rho|\tilde{w}|.$$

It follows that a coherent Hamiltonian-maximizing choice of the sign of $\pm\sqrt{\Delta}$ can be made throughout the star domain. The big-oh estimate (10.3.3) shows that the sign of the square root should be positive. So, the maximizing root z^* of the quadratic in (9.3.8) is

$$z^* = \frac{c}{|c|} \tilde{z}^* = \frac{c}{|c|} \frac{(\xi_1 + \sqrt{\Delta})}{2\bar{\xi}_0} = \frac{c}{|c|} + O(|w|), \quad (10.3.4)$$

which gives the required. \square

10.4 Application to Abnormal Solutions

In this section, we assume that $\rho = 1$ (inscribed circular control set), $\lambda_{cost} = 0$ (abnormal solution), and give a proof of the following theorem.

Theorem 10.4.1. *If $\rho = 1$ and $\lambda_{cost} = 0$, then there does not exist a periodic solution to the control system of ODEs such that Λ_R is nowhere zero.*

The first lemma gives a simple formula for the Hamiltonian and system of equations.

Lemma 10.4.2. *Assume $\rho = 1$, $\lambda_{cost} = 0$. Assume $\Lambda_R(t) \neq 0$, for all t . Then*

$$\begin{aligned} X' &= -\frac{[\Lambda_R, X]}{\sqrt{2\langle \Lambda_R, \Lambda_R \rangle}}, \\ \Lambda'_R &= [\Lambda_R - K, X], \\ \mathcal{H} &= \langle X, K \rangle + \sqrt{\frac{\langle \Lambda_R, \Lambda_R \rangle}{2}}, \end{aligned}$$

where

$$K := \begin{pmatrix} i\mathcal{A}/2 & K_{12} \\ \bar{K}_{12} & -i\mathcal{A}/2 \end{pmatrix},$$

is a constant.

Proof. $\Lambda_R \neq 0$ implies $c \neq 0$. Let \tilde{z}^* be the Hamiltonian maximizing root of the quadratic equation (10.3.2). We claim

$$\frac{w - \rho[\![w]\!]z^*}{\mu(w, z^*)} = -\frac{\xi_0 c}{|c|\eta}; \quad (10.4.1)$$

$$-\frac{\Re(w - \rho[\![w]\!]z^*, c)}{\mu(w, z^*)[\![w]\!]} = \frac{|c|\eta}{2[\![w]\!]}, \quad (10.4.2)$$

where $\xi_0 = 2 + |w|^2 - (w\bar{c}/|c|)^2$ is given by its usual formula, and where $\eta = \eta(\xi_0, \bar{\xi}_0) = \sqrt{\xi_0 + \bar{\xi}_0} > 0$ (noting that $\xi_0 + \bar{\xi}_0$ is a positive real number). We prove both identities at the same time. Let lhs and rhs be the left and right-hand sides of the first claimed identity (10.4.1). Combined as a single fraction, the numerator of $\text{lhs}^2 - \text{rhs}^2$ can be written as a polynomial in \tilde{z}^* with coefficients that are functions of \tilde{w}, c, \bar{c} . By a symbolic calculation in Mathematica, this polynomial is zero modulo the quadratic relation (10.3.2). Thus, $\text{lhs} = \pm \text{rhs}$. We then substitute $\pm \text{rhs}$ for lhs into the second claimed identity (10.4.2) and choose the sign that makes the entire expression positive (because this term is to be maximized in the Hamiltonian). With this choice of sign, both identities hold.

We have by direct calculation that

$$\frac{\langle \Lambda_R, \Lambda_R \rangle}{2} = \frac{|c|^2 \eta^2}{4[\![w]\!]^2} > 0, \quad \sqrt{\frac{\langle \Lambda_R, \Lambda_R \rangle}{2}} = \frac{|c|\eta}{2[\![w]\!]},$$

and the rightmost term is equal to the control-dependent term of the Hamiltonian (10.4.2). We compute

$$X' = r[\Lambda_R, X], \quad \text{where } w' = irc\xi_0/[\![w]\!]^2.$$

Comparing with the ODE (10.2.1) for w , the ODE for X follows.

The ODEs for w, b, c take the following form

$$w' = -i\xi_0 c / (|c|\eta), \quad (10.4.3)$$

$$d_1 b' = -c' = 2id_1([\![b]\!]_\epsilon w + b[\![w]\!]). \quad (10.4.4)$$

Hence, $K_{12} := bd_1 + c \in \mathbb{R}$ is a constant. Then using conservation of angular momentum, $K = \Lambda_1 + \Lambda_R$ equals the constant as stated in the lemma. The Hamiltonian (10.2.5) is

$$\mathcal{H} = 2d_1(\Re(w, b) + [\![b]\!]_\epsilon [\![w]\!]) + \frac{|c|\eta}{2[\![w]\!]} = \langle X, \Lambda_1 \rangle + \sqrt{\frac{\langle \Lambda_R, \Lambda_R \rangle}{2}}.$$

Expressing these formulas back in terms of X, Λ_R, K , we obtain the result. The ODE for Λ_R is obtained by the ODE for c in (10.2.3), by setting $\rho = 1$ and $\lambda_{cost} = 0$. \square

Remark 10.4.3. *If we assume the weaker condition $\rho = 1$ and $\Lambda_R \neq 0$ then a similar argument shows that the equations take a related form*

$$\begin{aligned} g' &= gX, & \Lambda'_1 &= [\Lambda_1, X], \\ X' &= -\frac{[\Lambda_R, X]}{\sqrt{2\langle \Lambda_R, \Lambda_R \rangle}}, & \Lambda'_R &= \left[-\Lambda_1 + \frac{3}{2}\lambda_{cost}J_{\mathfrak{su}}, X \right]. \end{aligned}$$

Lemma 10.4.4. *If K, X, Λ_R is a solution to the equations of Lemma 10.4.2, then so is $\text{Ad}_g K, \text{Ad}_g X, \text{Ad}_g \Lambda_R$ (where $g \in \text{SU}(1, 1)$) and they also satisfy the relations listed at the beginning of the section.*

Proof. This is simple to verify once we use the fact that the trace form is a non-degenerate invariant symmetric bilinear form and using properties of Lie brackets and bilinear forms. \square

Lemma 10.4.5. *Assume $\Lambda_R(t) \neq 0$, for all t . Assume $\rho = 1$, and $\lambda_{cost} = 0$. Then*

$$\langle \Lambda_R, \Lambda_R \rangle''' = 0.$$

Proof. Let $d_R := \langle \Lambda_R, \Lambda_R \rangle$. The ODE for Λ_R gives $d'_R = 2r$, where

$$r := \langle [\Lambda_R, X], K \rangle = (c\bar{w} - \bar{c}w)i\mathcal{A} + \frac{i}{\llbracket w \rrbracket}(\bar{K}_{12}\xi_0c - K_{12}\bar{\xi}_0\bar{c}).$$

Using the conserved quantities K_{12} and \mathcal{A} , the ODE (10.4.4) can be written

$$c' = \frac{i\xi_0c}{\llbracket w \rrbracket} - i(w\mathcal{A} + 2K_{12}\llbracket w \rrbracket). \quad (10.4.5)$$

We compute r' by using (10.4.5) and (10.4.3) in a tedious Mathematica calculation to obtain

$$\left(r' + 2\mathcal{H} \left(\frac{|c|\eta}{\llbracket w \rrbracket} - (2\Re(w, K_{12}) + \mathcal{A}\llbracket w \rrbracket) \right) \right)' = 0.$$

Since $\mathcal{H} = 0$ identically, we find that r' is constant, and $d'''_R = 0$ as claimed. (Adding the multiple of \mathcal{H} before taking the final derivative significantly simplifies the calculation.) \square

Proof of Theorem. Set

$$d_R = \langle \Lambda_R, \Lambda_R \rangle.$$

By the preceding lemma, d_R is a polynomial in t . If also periodic, d_R is constant. By the formulas derived in the previous proof, we have orthogonality:

$$d'_R = 2\langle [\Lambda_R, X], K \rangle = 0.$$

We write K as a linear combination of a basis of $\mathfrak{su}(1, 1)$:

$$K = r_1 X + r_2 \Lambda_R + r_3 [\Lambda_R, X].$$

Since K and $[\Lambda_R, X]$ are orthogonal, we have $r_3 = 0$. The vanishing Hamiltonian implies $r_1 = \sqrt{d_R/8}$. In particular, r_1 is constant. Then

$$\langle K, K \rangle = d_R(-1/4 + r_2^2),$$

and this implies that r_2 is constant. Then using the ODE for X and Λ_R , we obtain

$$0 = K' = r_1 X' + r_2 \Lambda'_R = (-1/4 + r_2(1 - r_2))[\Lambda_R, X].$$

This implies that $r_2 = 1/2$ and $\langle K, K \rangle = 0$. But $K \neq 0$. Thus, K is regular nilpotent. We also have that $\langle X, K \rangle$ is constant. This is the locus of a horocycle in hyperbolic space. Also X' , which is proportional to $[\Lambda_R, X]$, is never zero. Hence X is not periodic, moving along the horocycle for all time. \square

Remark 10.4.6. *We find that nonperiodic abnormal solutions exist. Following the proof of the lemma, we impose the condition $\langle \Lambda_R, \Lambda_R \rangle = 8$ and set $K = X + \Lambda_R/2$. Then K is a nilpotent constant, and the ODE for X becomes $X' = -[K, X]/2$, which is Lax's equation with constant $-K/2$, which is easily solved.*

Chapter 11

The Fuller System

In this chapter, we restrict to normal solutions, and take $\lambda_{cost} = -1$. The singular locus, as defined in Section 8.2 is the region of the cotangent space $T^*(T\mathrm{SL}_2(\mathbb{R}))$ given by

$$\mathcal{S}_{sing} = \left\{ \left(g_0, -\frac{3}{2}J, J, 0 \right) \mid g_0 \in \mathrm{SL}_2(\mathbb{R}) \right\} \subset \mathrm{SL}_2(\mathbb{R}) \times \mathfrak{sl}_2(\mathbb{R}) \times \mathfrak{sl}_2(\mathbb{R}) \times \mathfrak{sl}_2(\mathbb{R}).$$

Recall that Pontryagin extremals which avoid the singular locus that are also edge-extremal are given by bang-bang controls with finitely many switches. (See Theorem 8.3.2.) The global optimal trajectory of the Reinhardt control problem with the control set U_T cannot stay within the singular locus for any positive interval of time. (See Theorem 8.2.7.)

By Lemma 8.3.4, if we are considering the control set U_T , for a Pontryagin extremal to approach the singular locus, the control must switch infinitely many times around the boundary of U_T in a finite interval of time. This is the *chattering* phenomenon (see Fuller [11] and Zelikin and Borisov [50]).

If we use a control set U_r which has a smooth boundary, we would expect the optimal control to perform infinitely many rotations along the boundary ∂U_r to approach the singular locus in finite time. A system with exactly this behaviour is described in Manita and Ronzhina and the associated trajectory is spiral-like [30]. The results of this section are motivated by that paper.

These results warrant a study of the behavior of the system near the singular locus. To this end, we introduce convenient coordinates and re-express the state, costate and optimal control equations in these coordinates. Throughout this section, unless otherwise specified, we work with the circular

control sets U_r and we assume that the control matrix parameter α is positive. (See Section 9.2).

We will find that the system of equations we obtain is a special case of the Fuller system, which we define in the following way.

Definition 11.0.1 (Length- n Fuller system). *Let $\mathbb{F} = \mathbb{R}$ or $\mathbb{F} = \mathbb{C}$. Let $z_i : (0, \epsilon) \rightarrow \mathbb{F}^m$ be functions, where z_n is nonzero on $(0, \epsilon)$, and let A be a nonsingular $m \times m$ matrix with coefficients in \mathbb{F} . Let $\|\cdot\|$ be the Euclidean norm on \mathbb{F}^m . The Fuller system of length n , (real or complex) dimension m , and multiplier A is the system of ODEs given by*

$$z'_n = z_{n-1}, \quad z'_{n-1} = z_{n-2}, \quad \dots \quad z'_2 = z_1, \quad z'_1 = \frac{Az_n}{\|z_n\|}. \quad (11.0.1)$$

Remark 11.0.2. By identifying \mathbb{C} with \mathbb{R}^2 , a Fuller system of complex dimension m can be written as a Fuller system of real dimension $2m$. We are particularly interested in the Fuller system of complex dimension 1. In that case $A = \gamma \in \mathbb{C}^\times$, a nonzero complex scalar. By scaling each $z_j \mapsto z_j/\gamma$, the constant γ in equation (11.0.1) scales by $\gamma \mapsto \gamma/|\gamma|$. Thus, there is no loss of generality in assuming that $|\gamma| = 1$.

11.1 Trajectories near the Singular Locus

An advantage of switching to hyperboloid coordinates is that at the singular locus, we have $w = b = c = 0$.

Assumptions. *In general, the determinant d of Λ_1 may be positive, negative or zero. The determinant is constant along trajectories. Different coordinate systems (other than the one presented below) need to be used when $d = 0$ or $d < 0$. Here, we make the assumption $d > 0$, because this is the case for the singular locus, and set $d_1 = \sqrt{d} > 0$. We also assume that the sign of $\langle J, \Lambda_1 \rangle$ is positive, because that is the sign at the singular locus: $\langle J, 3J\lambda_{\text{cost}}/2 \rangle = 3 > 0$. The sign $d_1 > 0$ in Λ_1 is chosen (according to our assumptions) to make $\langle J_{\text{su}}, \Lambda_1 \rangle > 0$. We also have $\epsilon = 1$ and $\llbracket b \rrbracket_\epsilon = \llbracket b \rrbracket$, based on the value of ϵ at the singular locus.*

Assumptions. *At the singular locus*

$$\mathcal{H} = 0, \quad \mathcal{A} = 3, \quad d_1 = 3/2, \quad \epsilon = 1, \quad \lambda_{\text{cost}} = -1. \quad (11.1.1)$$

These values are constant along extremal trajectories. We assume these values of the constants throughout this section. We consider an extremal trajectory with the property that $c(t_0) \neq 0$ but as we follow the trajectory back in time there is a most recent time $t_1 < t_0$ when $c(t_1) = 0$. We assume at time t_1 , the trajectory meets the singular locus: $w(t_1) = b(t_1) = c(t_1) = 0$. Reparameterizing by a time shift, we assume $t_1 = 0$ and find $t_0 > 0$ such that

$$w(0) = b(0) = c(0) = 0, \quad \text{and } c(t) \neq 0, \text{ for } t \in (0, t_0). \quad (11.1.2)$$

Definition 11.1.1. We write

$$f_1 = f_2 + O(f_3) \quad (11.1.3)$$

to mean that for some $t_1 > 0$, and some $C > 0$, we have $|f_1(t) - f_2(t)| \leq C|f_3(t)|$ for all $t \in (0, t_1)$. By a *punctured neighborhood* of the singular locus, we mean an interval $(0, t_1)$ on which c is defined and nonzero. (The definition of Landau's O here departs slightly from the definition before Lemma 8.1.5, because the definition here is one-sided and uses absolute values.)

The aim of this section is to analyze the asymptotic behavior of solutions as t tends to zero. With minor modifications, the same analysis will apply to trajectories approaching the singular locus from the left on $(-t_1, 0)$.

Theorem 11.1.2. *In the context of the assumptions of this section, let w, b, c be a solution to the ODE of Theorem 10.2.1 on $(0, t_1)$, with $c(t) \neq 0$ for all $t \in (0, t_1)$. Assume the solution extends continuously to $w(0) = b(0) = c(0) = 0$ at time $t = 0$. The ODEs and solutions w, b, c satisfy the following estimates.*

$$\begin{aligned} w' &= -i\rho \frac{c}{|c|} + O(|w|), \\ b' &= 2iw + O(|b|), \\ c' &= -3ib + O(|c| + |bw^2| + |b|^2|w|). \end{aligned}$$

$$|w| = O(t), \quad |b| = O(t^2), \quad |c| = O(t^3), \quad |c| + |bw^2| + |b|^2|w| = O(t^3).$$

Remark 11.1.3. *The proof uses the assumptions $d_1 = 3/2$ and $\lambda_{\text{cost}} = -1$, but not the assumptions $\mathcal{H} = 0$ and $\mathcal{A} = 3$. If we do not assume the circular control condition of Lemma 10.3.2, but only that $|z^*| \leq 1$, then the ODE for w takes the form*

$$w' = -i\rho z^* + O(|w|).$$

Proof. We start with some easy approximations of the sizes of terms in the ODEs. The terms $\llbracket w \rrbracket$ and $\mu(w, z^*)$ in the system of ODEs tend to 1 as $t \rightarrow 0$. The right-hand side of the ODEs are bounded near $t = 0$ and the initial conditions are $w(0) = b(0) = c(0) = 0$. Thus, $|w'| \leq |w'| \leq C$, so that $|w| = O(t)$. Similarly,

$$|b| = O(t), \quad |c| = O(t).$$

Feeding these bounds back into the ODE (10.2.2) for b , we obtain $|b'| \leq |b'| = O(t)$. Thus, $|b| = O(t^2)$. Now

$$\llbracket w \rrbracket = 1 + O(|w|^2), \quad \llbracket b \rrbracket = 1 + O(|b|^2), \quad \mu(w, z^*) = 1 + O(|w|).$$

We return to the ODE (10.2.1) for w and use Lemma 10.3.2 to write it

$$w' = -i\rho\llbracket w \rrbracket z^*/\mu + iw/\mu = -i\rho c/|c| + O(|w|).$$

We return to the ODE (10.2.2) for b and write it

$$b' = 2i\llbracket b \rrbracket w + 2ib\llbracket w \rrbracket = 2iw + O(|b|).$$

The ODE (10.2.3) for c takes the form $c' = A(c) + f$, where

$$A(c) = \frac{i(1 - \rho^2)\Re(c\xi_0(w, c), z^*)}{2\llbracket w \rrbracket \mu(w, z^*)^2} z^* = O(|c|)$$

is a bounded operator, which is linear in the real and imaginary parts of c through the subterm $c\xi_0(w, c) = 2c + |w|^2c - \bar{c}w^2$. The inhomogeneous term f is

$$\begin{aligned} -i(2bd_1\llbracket w \rrbracket + (2d_1\llbracket b \rrbracket_\epsilon + 3\lambda_{cost})w) \\ = -3ib\llbracket w \rrbracket - 3i(\llbracket b \rrbracket_\epsilon - 1)w \\ = -3ib + O(|b||w|^2 + |b|^2|w|). \end{aligned}$$

So the ODE for c takes the form

$$c' = -3ib + O(|bw^2| + |b|^2|w| + |c|).$$

We then have $|c'| \leq |c'| \leq C_0|c| + O(t^2)$, for some $C_0 > 0$. So $|c| = O(t^3)$. This completes the proof. \square

11.2 Hamiltonian Dynamics of the Truncated System

Following Theorem 11.1.2, we create a *truncated system* of ODEs given by

$$c'_F = -3ib_F \quad (11.2.1)$$

$$b'_F = 2iw_F \quad (11.2.2)$$

$$w'_F = -i\rho \frac{c_F}{|c_F|}, \quad (11.2.3)$$

where the big-oh terms are discarded. This new system governs the dynamics of the Reinhardt system very close to the singular locus. We introduce new coordinates

$$z_3 := c_F/(6\rho), \quad z_2 := c'_F/(6\rho) = -ib_F/(2\rho), \quad z_1 := c''_F/(6\rho) = w_F/\rho \quad (11.2.4)$$

so that the truncated system in equations (11.2.1), (11.2.2), (11.2.3) becomes

$$z'_3 = z_2, \quad z'_2 = z_1, \quad z'_1 = -i \frac{z_3}{|z_3|}. \quad (11.2.5)$$

This is the Fuller system of length 3, complex dimension 1, and multiplier $-i$. We also write $z_0 = -iz_3/|z_3|$, so that $z'_1 = z_0$. In this section, we study this Fuller system.

The truncated Hamiltonian and angular momentum are defined as

$$\begin{aligned} \mathcal{H}_F &:= \frac{i}{2} (z_2 \bar{z}_1 - \bar{z}_2 z_1) + \sqrt{z_3 \bar{z}_3} \\ \mathcal{A}_F &:= z_2 \bar{z}_2 - (z_1 \bar{z}_3 + \bar{z}_1 z_3). \end{aligned} \quad (11.2.6)$$

Remark 11.2.1. *These definitions come from the leading term of the Hamiltonian and angular momentum for the Reinhardt system. Writing the Reinhardt quantities \mathcal{H} and \mathcal{A} as functions of w, b, c and $z^* = c/|c| + O(t)$ and their conjugates, we formally expand using (11.2.4).*

$$\begin{aligned} \mathcal{H}(tw_F, t\bar{w}_F, t^2b_F, t^2\bar{b}_F, t^3c_F, t^3\bar{c}_F, \dots) &= 6\rho^2 t^3 \mathcal{H}_F + O(t^4) \\ \mathcal{A}(tw_F, t\bar{w}_F, t^2b_F, \dots) &= 3 + 6\rho^2 t^4 \mathcal{A}_F + O(t^5), \end{aligned}$$

Also, if a Hamiltonian for the Fuller system depends on a control through a term $\Re(z_3, u)$, where the control u satisfies $|u| \leq 1$, then the maximized

Hamiltonian is achieved when $u = z_3/|z_3|$, and the term in the Hamiltonian becomes $\Re(z_3, u) = \sqrt{z_3 \bar{z}_3}$, as we find in the formula for \mathcal{H}_F . Thus, \mathcal{H}_F is to be viewed as the maximized Hamiltonian.

Theorem 11.2.2 (Fuller Hamiltonian System). *The Fuller system (11.2.5) is Hamiltonian with respect to a non-standard Poisson bracket (11.2.7). The angular momentum is in involution with the Hamiltonian with respect to this bracket (11.2.9). The Poisson bracket satisfies the Jacobi identity.*

Proof. We regard z_1 , z_2 , and z_3 as coordinate functions $\mathbb{C}^3 \rightarrow \mathbb{C}$ and let \bar{z}_j denote the conjugates of these coordinate functions. For smooth functions $F, G : \mathbb{C}^3 \rightarrow \mathbb{C}$, expressed as functions of z_j and \bar{z}_j , we define their non-standard Poisson bracket as

$$\{F, G\}_F := \sum_{j=1}^3 (-1)^j 2i \left(\frac{\partial F}{\partial z_j} \frac{\partial G}{\partial \bar{z}_{4-j}} - \frac{\partial F}{\partial \bar{z}_{4-j}} \frac{\partial G}{\partial z_j} \right) \quad (11.2.7)$$

$$= \frac{2}{i} \left(\frac{\partial F}{\partial z_1} \frac{\partial G}{\partial \bar{z}_3} - \frac{\partial F}{\partial \bar{z}_3} \frac{\partial G}{\partial z_1} \right) + \frac{2}{i} \left(- \frac{\partial F}{\partial z_2} \frac{\partial G}{\partial \bar{z}_2} + \frac{\partial F}{\partial \bar{z}_2} \frac{\partial G}{\partial z_2} \right) + \frac{2}{i} \left(\frac{\partial F}{\partial z_3} \frac{\partial G}{\partial \bar{z}_1} - \frac{\partial F}{\partial \bar{z}_1} \frac{\partial G}{\partial z_3} \right). \quad (11.2.8)$$

We can now verify directly that the Fuller equations (11.2.5) become

$$\begin{aligned} z'_1 &= \{z_1, \mathcal{H}_F\}_F, \\ z'_2 &= \{z_2, \mathcal{H}_F\}_F, \\ z'_3 &= \{z_3, \mathcal{H}_F\}_F, \end{aligned}$$

which are Hamilton's equations for this Poisson bracket. We can also verify that

$$\{\mathcal{H}_F, \mathcal{A}_F\}_F = 0 \quad (11.2.9)$$

and that the Jacobi identity is satisfied. \square

Definition 11.2.3 (virial action). *Define the virial group to be the two-dimensional scaling group $\mathcal{G} = \text{SO}_2(\mathbb{R}) \times \mathbb{R}_{>0}$. The virial group acts on the Fuller system (11.2.5) by the rule*

$$(\exp(i\theta), r) \cdot (z_1(t), z_2(t), z_3(t)) := (\exp(i\theta) r z_1(t/r), \exp(i\theta) r^2 z_2(t/r), \exp(i\theta) r^3 z_3(t/r)). \quad (11.2.10)$$

The name *virial group* comes from a similar group that goes by this name, which acts on the Kepler dynamical system [8].

If $z = (z_1, z_2, z_3)$ is a solution, then $(\exp(i\theta), r) \cdot z$ is also a solution. We also have an involution given by time reversal

$$\tau \cdot (z_1(t), z_2(t), z_3(t)) := (\bar{z}_1(-t), -\bar{z}_2(-t), \bar{z}_3(-t))$$

that carries solutions to solutions.

It is noteworthy that the rotation group $\mathrm{SO}_2(\mathbb{R})$ is a symmetry of the system and as a result of the classical Noether theorem, we recover \mathcal{A}_F as a conserved quantity. The truncated angular momentum and the Hamiltonian are *exactly conserved* for the truncated system. Both are identically zero along trajectories that approach the singular locus. The next proposition shows that the Poisson bracket in (11.2.7) arises via a symplectic structure on \mathbb{C}^3 .

Proposition 11.2.4. *Let F, G be smooth, real-valued functions on \mathbb{C}^3 . Consider the following symplectic form on \mathbb{C}^3 :*

$$\omega_F := \sum_{j=1}^3 \frac{(-1)^j}{2i} dz_j \wedge d\bar{z}_{4-j}, \quad (11.2.11)$$

Let \vec{F} and \vec{G} denote the Hamiltonian vector fields of smooth functions F, G with respect to this symplectic form. Then we have

$$\{F, G\}_F = \omega_F(\vec{F}, \vec{G}).$$

Proof. We claim that

$$\vec{F} = \sum_{j=1}^3 (-1)^j 2i \left(\frac{\partial F}{\partial \bar{z}_{4-j}} \frac{\partial}{\partial z_j} - \frac{\partial F}{\partial z_{4-j}} \frac{\partial}{\partial \bar{z}_j} \right). \quad (11.2.12)$$

To see this, we check that if \vec{F}_{rhs} is the right-hand side of (11.2.12), then the defining conditions of \vec{F} all hold

$$\begin{aligned} \omega_F(\vec{F}_{rhs}, \partial/\partial z_k) &= \langle dF, \partial/\partial z_k \rangle_* = \partial F / \partial z_k \\ \omega_F(\vec{F}_{rhs}, \partial/\partial \bar{z}_k) &= \langle dF, \partial/\partial \bar{z}_k \rangle_* = \partial F / \partial \bar{z}_k, \quad k = 1, 2, 3. \end{aligned}$$

We leave this as a routine exercise for the reader. Similarly,

$$\vec{G} = \sum_j (-1)^j 2i \left(\frac{\partial G}{\partial \bar{z}_{4-j}} \frac{\partial}{\partial z_j} - \frac{\partial G}{\partial z_{4-j}} \frac{\partial}{\partial \bar{z}_j} \right).$$

From these explicit formulas for \vec{F} and \vec{G} , we find that the Poisson bracket of two functions F and G is

$$\{F, G\}_F = \left\langle dF, \vec{G} \right\rangle_* = \omega_F(\vec{F}, \vec{G}) = \sum_j (-1)^j 2i \left(\frac{\partial F}{\partial z_j} \frac{\partial G}{\partial \bar{z}_{4-j}} - \frac{\partial F}{\partial \bar{z}_j} \frac{\partial G}{\partial z_{4-j}} \right).$$

and thus, we obtain the required. \square

We can also generalize to the length n Fuller system of complex dimension 1 and multiplier $\gamma = i^n$.

$$z'_n = z_{n-1}, \quad z'_{n-1} = z_{n-2}, \dots, \quad z'_1 = \gamma z_n / |z_n| = z_0, \quad \gamma = i^n. \quad (11.2.13)$$

Definition 11.2.5 (Fuller symplectic form). *On \mathbb{C}^n , we have the following symplectic form.*

$$\omega_n := \bar{\gamma} \sum_{j=1}^n (-1)^{j-1} dz_j \wedge d\bar{z}_{n-j+1}.$$

Theorem 11.2.6. *The length n Fuller system (11.2.13) is the Hamiltonian vector field (with respect to the Fuller symplectic form) of the Hamiltonian.*

$$\mathcal{H}_n := \sum_{j=0}^n (-1)^j \Re(z_j, i^n z_{n-j}).$$

The angular momentum

$$\mathcal{A}_n := \sum_{j=1}^n (-1)^j \Re(i^{n+1} z_j, z_{n-j+1})$$

is conserved along this system.

Proof. If G is a smooth function, the above proof generalizes in a straightforward way to give the following expression for the Hamiltonian vector field of G :

$$\vec{G} = \frac{1}{\bar{\gamma}} \sum_{j=1}^n (-1)^{j-1} \left(\frac{\partial G}{\partial \bar{z}_{n-j+1}} \frac{\partial}{\partial z_j} - \frac{\partial G}{\partial z_j} \frac{\partial}{\partial \bar{z}_{n-j+1}} \right).$$

Using this expression, we can compute the Hamiltonian vector field of \mathcal{H}_n and we recover exactly the system (11.0.1), showing that

$$z_{j-1} = \{z_j, \mathcal{H}_n\}, \quad j = 1, \dots, n.$$

Differentiating \mathcal{H}_n and \mathcal{A}_n along the length- n Fuller system shows that they are conserved. \square

11.3 Log-Spiral Solutions

The system (11.2.5) admits the following outward-moving logarithmic spiral solution, for $t > 0$.

$$\begin{aligned} z_3^*(t) &= \frac{1}{10} t^{3-i} & (11.3.1) \\ z_2^*(t) &= \frac{(3-i)}{10} t^{2-i} \\ z_1^*(t) &= \frac{(2-i)(3-i)}{10} t^{1-i} \\ z_0^*(t) &= -it^{-i} \\ u^*(t) &= \rho t^{-i}. \end{aligned}$$

Here $i = \sqrt{-1}$ in the formulas.¹ Other log-spiral solutions are obtained by the action of the viral group \mathcal{G} . Note that the log-spiral is self-similar by a one-dimensional subgroup of \mathcal{G} :

$$(r^{-i}, r) \cdot z^* = z^*.$$

We can also verify that $\mathcal{H}_F(z_3^*, z_2^*, z_1^*) = \mathcal{A}_F(z_3^*, z_2^*, z_1^*) = 0$.

¹The well-known Euler-Manchin identity $(3-i)(2-i)(1-i) = -10i$ is used to verify the solution. In a different context, Manchin-like formulas are used to compute digits of π .

Time-reversal τ transforms the outward log-spiral into an inward log-spiral. The inward spiral is defined for $t < t_1$.

$$\begin{aligned} z_3^\tau(t) &= \bar{z}_3^*(t_1 - t) = \frac{1}{10}(t_1 - t)^{3+i}, \\ z_2^\tau(t) &= -\bar{z}_2^*(t_1 - t) = -\frac{(3+i)}{10}(t_1 - t)^{2+i}, \\ z_1^\tau(t) &= \bar{z}_1^*(t_1 - t) = \frac{(3+i)(2+i)}{10}(t_1 - t)^{1+i}, \\ z_0^\tau(t) &= -\bar{z}_0^*(t_1 - t) = -i(t_1 - t)^i. \end{aligned}$$

Here t_1 is arrival time at the singular locus. The trajectory can be verified by differentiating. During approach to the singular locus, the optimal control for the inward log-spiral performs an infinite number of rotations along the circle ∂U_r in finite time.

11.4 Literature on Fuller Systems

Fuller systems (over \mathbb{R}) were first described in Fuller [11] and arises as the Pontryagin system of what is now called the classical Fuller optimal control problem. This problem can be described as

$$x' = y, \quad y' = u, \quad \int_0^\infty x^2 dt \rightarrow \min,$$

with initial conditions $x(0) = x_0$, $y(0) = y_0$ and $u \in [-1, 1]$ is a control variable taking values in an interval. The optimal trajectory for this problem consists of an arc whose control switches infinitely many times at the extremes of the control set in a finite amount of time.

Generalizations of the Fuller phenomenon are studied in the book of Zelikin and Borisov [50]. Problem 5.1 is Chapter 5 of this book is exactly the length n Fuller system in equation (11.0.1) specialized to \mathbb{R} . This system is called the *multi-dimensional Fuller problem* with 1-dimensional control.

Our system in equation (11.0.1) is a mild generalization of that system. Problem 7.2 of Zelikin and Borisov studies a Fuller problem with multidimensional control. In particular, equation (7.11) on page 230 of their book is exactly our system (11.0.1) for $n = 4$. Just as we did, Zelikin and Borisov construct log-spiral solutions to the Fuller problem for 2-dimensional control

but leave the exploration of other solutions as a research problem in Chapter 7.

The Fuller systems considered in the literature have even length. Our system, because of left-invariance, has odd chain length. The same remark also applies in our derivation of the extended state space Poisson bracket (see Section A.9). Also, in our case, the extra dimension for the control and the circular symmetry of the control set gives us an additional symmetry and thus another conservation law.

At first, Fuller's problem was viewed as an oddity [11], but was later shown to be *ubiquitous* in a very precise sense in a paper of Kupka [24]: so long as the extended state space of our optimal problem is of sufficiently high dimension, one can find a Fuller trajectory as an extremal.

Recently, Zelikin, Lokutsievskii and Hildebrand [51] show that for a linear-quadratic optimal problem with control variables in a two-dimensional simplex, the extremals perform infinite switchings in finite time, and their switches are chaotic in nature. Further, they prove that this behavior is generic for piecewise smooth Hamiltonian systems near the junction where three hyper-surfaces meet in a codimension 2 manifold. The main innovation in Zelikin, Lokutsievskii and Hildebrand [51] is the so-called *descending system of Poisson brackets*, which is a clever change of coordinates of the generic system near the singularity made so that the results of the model problem are applicable. This method is illustrated in the very recent paper of Manita, Ronzhina and Lokutsievskii [41].

A Fuller system with chattering, which is similar to ours in some respects, has been analyzed by Zelikin, Lokutsievskii, and Hildebrand [51]. They have found that on a set of full Lebesgue measure, the dynamics of their system is particularly simple (page 24, sec 2.8). However, on a set of measure zero, their dynamical system exhibits complex behavior: chaotic trajectories and a “Cantor-like structure as in Smale's Horseshoe.” However, in our Fuller system, we prove that no such complexities appear. It remains to be seen whether Zelikin-type results can be derived for the Reinhardt problem.

Chapter 12

Global Dynamics of Fuller System

In this chapter, we make a thorough analysis of the global dynamics of the Fuller system (with circular control). Define

$$M := \{z = (z_1, z_2, z_3) \in (\mathbb{C}^\times)^3 \mid \mathcal{H}_F(z) = \mathcal{A}_F(z) = 0\},$$

where \mathcal{H}_F and \mathcal{A}_F are the truncated Hamiltonian and angular momentum, defined in (11.2.6). Since \mathcal{A}_F and Hamiltonian \mathcal{H}_F are constant along trajectories, the Fuller system (11.2.5) can be restricted to M .

Lemma 12.0.1. *M is a real analytic manifold of real dimension four in \mathbb{C}^3 .*

Proof. At every point of M , the gradients of \mathcal{A}_F and \mathcal{H}_F are linearly independent. \square

12.1 A Fiber Bundle

Define

$$\Omega := \{(x_2, x_3) \in \mathbb{R}^2 \mid x_2 > 0, x_3 > 0, x_3 \leq x_2, \frac{1}{2}x_2^2 \leq x_3\} \subset [0, 2] \times [0, 2].$$

Let Ω^0 be the interior of Ω , obtained by making the inequalities strict. Define $\pi : M \rightarrow \mathbb{R}^2$ by

$$\pi(z) = \pi(z_1, z_2, z_3) := \left(\frac{|z_2|}{|z_1|^2}, \frac{|z_3|}{|z_1|^3} \right) = (x_2, x_3).$$

Lemma 12.1.1. *The image $\pi(M)$ lies in Ω .*

Proof. The equality $\mathcal{A}_F = 0$, after applying the Cauchy-Schwarz inequality to the term $\Re(z_1, z_3)$ appearing in \mathcal{A}_F , gives that $\pi(z)$ satisfies $x_2^2/2 \leq x_3$. The equality $\mathcal{H}_F = 0$, after applying the Cauchy-Schwarz inequality to the term $\Re(z_1, z_2i)$ appearing in \mathcal{H}_F , gives that $\pi(z)$ satisfies $x_3 \leq x_2$. By definition, on M we have $z_j \neq 0$. Thus, the image of π is contained in Ω . \square

Recall that the virial group acts as symmetries of the Fuller system. The virial group \mathcal{G} restricts to an action on M because of the homogeneities.

$$\begin{aligned}\mathcal{H}_F(tz_1, t^2z_2, t^3z_3) &= t^3\mathcal{H}_F(z_1, z_2, z_3) \\ \mathcal{A}_F(tz_1, t^2z_2, t^3z_3) &= t^4\mathcal{H}_F(z_1, z_2, z_3),\end{aligned}$$

for $t > 0$. The morphism $\pi : M \rightarrow \Omega$ is equivariant with respect to the trivial action of the virial group on Ω , and each fiber of π is a union of orbits of the group action.

Lemma 12.1.2. *The fiber of π over $(x_2, x_3) \in \Omega$ is given by*

$$\begin{aligned}z_1 &\in \mathbb{C}^\times, \\ z_2 &= x_2 z_1 |z_1| (\epsilon_2 \cos_2 + i \sin_2), \\ z_3 &= x_3 z_1 |z_1|^2 (\cos_3 + i \epsilon_3 \sin_3),\end{aligned}$$

where

$$\begin{aligned}\sin_2 &:= x_3/x_2, & \cos_2 &:= \sqrt{1 - \sin_2^2} = \sqrt{1 - (x_3/x_2)^2}, \\ \cos_3 &:= x_2^2/(2x_3), & \sin_3 &:= \sqrt{1 - \cos_3^2} = \sqrt{1 - x_2^4/(4x_3^2)},\end{aligned}\tag{12.1.1}$$

and $\epsilon_2, \epsilon_3 \in \{\pm 1\}$.

Remark 12.1.3. *The fiber satisfies identities:*

$$\begin{aligned}\frac{z_2}{|z_2|} &= \frac{z_1}{|z_1|} (\epsilon_2 \cos_2 + i \sin_2), \\ \frac{z_3}{|z_3|} &= \frac{z_1}{|z_1|} (\cos_3 + i \epsilon_3 \sin_3).\end{aligned}$$

Proof. We analyze the fibers of $\pi : M \rightarrow \Omega$. Note that $x_2, x_3 > 0$, and $\sin_2, \cos_3 \in [0, 1]$, so that the formulas are well-defined. Let $(x_2, x_3) \in \Omega$. Using the virial action on fibers, if the fiber over (x_2, x_3) is nonempty, then it contains a point with $z_1 = 1$, which we now assume without loss of generality. Then $|z_2| = x_2 \geq 0$ and $|z_3| = x_3 > 0$. Thus, there exist $\cos_2, \sin_2, \cos_3, \sin_3 \in \mathbb{R}$, and signs ϵ_2, ϵ_3 such that

$$\begin{aligned} z_2 &= x_2(\epsilon_2 \cos_2 + i \sin_2), & z_3 &= x_3(\cos_3 + i \epsilon_3 \sin_3), \quad \text{where} \\ 1 &= \cos_2^2 + \sin_2^2 = \cos_3^2 + \sin_3^2, & \cos_2 &\geq 0, \sin_3 \geq 0. \quad \epsilon_2, \epsilon_3 \in \{\pm 1\}. \end{aligned}$$

The condition $\mathcal{A}_F = 0$ gives an additional constraint $\cos_3 = x_2^2/(2x_3) > 0$, and the condition $\mathcal{H}_F = 0$ gives the constraint $\sin_2 = x_3/x_2 > 0$. Thus, every point in the preimage of (x_2, x_3) has the form asserted in the lemma.

Conversely, every (z_1, z_2, z_3) of the given form belongs to M and maps to (x_2, x_3) in Ω . In particular, the image of π is Ω . \square

We let $\Omega_{\epsilon_2, \epsilon_3} := \Omega \times \{\epsilon_2\} \times \{\epsilon_3\}$, where $\epsilon_2, \epsilon_3 \in \{\pm 1\}$, be four copies of Ω . Let $\partial\Omega_{\epsilon_2, \epsilon_3}^+$ (or $\partial_{\epsilon_2, \epsilon_3}^+$, for short) be the upper boundary curve of $\Omega_{\epsilon_2, \epsilon_3}$ defined by $x_3 \leq x_2$. Let $\partial\Omega_{\epsilon_2, \epsilon_3}^-$ (or $\partial_{\epsilon_2, \epsilon_3}^-$, for short) be the lower boundary curve of $\Omega_{\epsilon_2, \epsilon_3}$ defined by $x_2^2/2 \leq x_3$.

We glue these four copies of Ω together along boundaries to form a topological plane \mathbb{R}_Ω^2 as follows. Along the boundary edge $x_2 = x_3$, we identify $\Omega_{+,+}$ with $\Omega_{-,-}$ (for $\epsilon_3 = \pm 1$), and along the boundary edge $x_3 = x_2^2/2$, we identify $\Omega_{+,+}$ with $\Omega_{-,-}$ (for $\epsilon_2 = \pm 1$). All four copies of the corner $(2, 2) \in \Omega_{\pm, \pm}$ are identified by this process. The corner $(0, 0)$ is excluded from Ω and from $\Omega_{\pm, \pm}$ by definition.

$$\mathbb{R}_\Omega^2 = \left(\bigcup_{\epsilon_2, \epsilon_3} \Omega_{\epsilon_2, \epsilon_3} \right) / \{ \partial_{-+}^+ = \partial_{++}^+, \partial_{--}^+ = \partial_{+-}^+, \partial_{--}^- = \partial_{-+}^-, \partial_{+-}^- = \partial_{++}^-\}.$$

Visually, it helps to imagine \mathbb{R}_Ω^2 as follows. We take a conformal transformation of $\Omega_{\epsilon_2, \epsilon_3}^0$ onto the open (ϵ_2, ϵ_3) quadrant, which sends the point $(0, 0)$ to ∞ , the point $(2, 2)$ to $(0, 0)$, and the boundary $\partial_{\epsilon_2, \epsilon_3}^+$ with equation $x_2 = x_3$ to the vertical axis, and the boundary $\partial_{\epsilon_2, \epsilon_3}^-$ with equation $x_3 = x_2^2/2$ to the horizontal axis. See Figure 12.1.1.

Lemma 12.1.2 shows that there is a multiplicity of signs ϵ_2, ϵ_3 along each fiber. This suggests that we should extend $\pi : M \rightarrow \Omega$ to a map $\pi : M \rightarrow \mathbb{R}_\Omega^2$

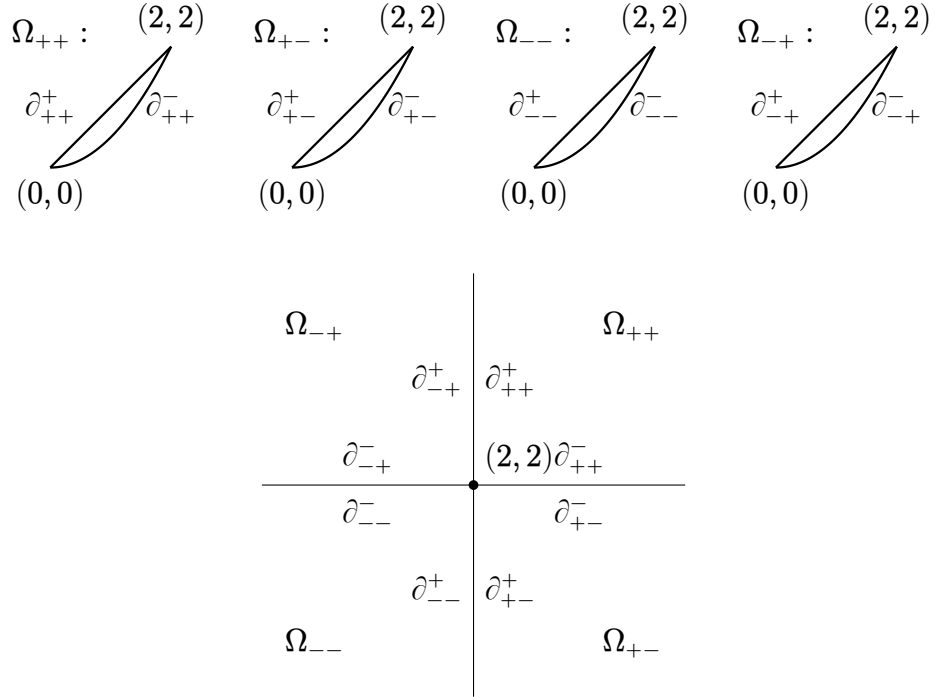


Figure 12.1.1: The four regions $\Omega_{\pm\pm}$ map conformally to the four quadrants in the plane. Identifying boundary edges, they form a topological plane \mathbb{R}_Ω^2 .

(overloading the notation π) as follows. Set

$$\begin{aligned}\epsilon_2 &= \text{sign}(\Re(z_2\bar{z}_1)) \in \{\pm 1\} \\ \epsilon_3 &= \text{sign}(\Im(z_3\bar{z}_1)) \in \{\pm 1\},\end{aligned}\tag{12.1.2}$$

and extend the definition of π so that

$$\pi(z_1, z_2, z_3) = \left(\frac{|z_2|}{|z_1|^2}, \frac{|z_3|}{|z_1|^3}, \epsilon_2, \epsilon_3 \right) \in \Omega_{\epsilon_2, \epsilon_3}.\tag{12.1.3}$$

Along the boundary edges of $\Omega_{\epsilon_2, \epsilon_3}$ that have been identified, there are ambiguities, but the definition of π has been crafted in such a way that $\pi : M \rightarrow \mathbb{R}_\Omega^2$ is well-defined. For example, the sign ϵ_2 cannot be determined from the given formula when $\cos_2 = 0$, but this occurs precisely along the edge $x_2 = x_3$, where Ω_{+, ϵ_3} is glued to Ω_{-, ϵ_3} .

Theorem 12.1.4. $\pi : M \rightarrow \mathbb{R}_\Omega^2$ is a trivial principal topological bundle of the virial group.

Proof. By the preceding constructions, each fiber $\pi^{-1}(x_2, x_3, \epsilon_2, \epsilon_3)$ is a single orbit of the virial group, given by the formula of Lemma 12.1.2. Note that the virial group acts simply transitively on $z_1 \in \mathbb{C}^\times$, which serves as a coordinate along each fiber.

We give a global trivialization of the bundle $M \simeq \mathbb{R}_\Omega^2 \times \mathcal{G}$, by constructing a global section:

$$\begin{aligned}\psi(x_2, x_3, \epsilon_2, \epsilon_3) &= (z_1, z_2, z_3), \text{ where} \\ z_1 &= 1, \quad z_2 = x_2(\epsilon_2 \cos_2 + i \sin_2), \quad z_3 = x_3(\cos_3 + i \epsilon_3 \sin_3)\end{aligned}$$

and $\sin_2, \cos_2, \sin_3, \cos_3$ are given as above.

This section is continuous. In fact, the jumps in signs ϵ_2, ϵ_3 occur exactly where $\cos_2 = 0$ or $\sin_3 = 0$, and this occurs along the identifications of the boundary curves of \mathbb{R}_Ω^2 . The section gives the global trivialization of the bundle. \square

12.2 A Vector Field on the Base Space

We define a vector field (v_2, v_3) on $\Omega_{\epsilon_2, \epsilon_3}$ taking value

$$\begin{aligned}v_2 &= \epsilon_2 \cos_2 - 2x_2 \epsilon_3 \sin_3, \\ v_3 &= x_2(\epsilon_2 \cos_2 \cos_3 + \epsilon_3 \sin_2 \sin_3) - 3x_3 \epsilon_3 \sin_3\end{aligned}\tag{12.2.1}$$

at $(x_2, x_3, \epsilon_2, \epsilon_3)$, where $\cos_2, \sin_2, \cos_3, \sin_3$ are the functions given earlier (12.1.1). We remark that this gives a well-defined vector field on \mathbb{R}_Ω^2 , because the definitions agree, wherever there might be an ambiguity along boundary curves that are identified to form \mathbb{R}_Ω^2 .

Lemma 12.2.1. *Consider the vector field f on M given by the Fuller system. Then (v_2, v_3) is the scaled image of f in the tangent space of \mathbb{R}_Ω^2 . That is, $|z_1|T\pi(f) = (v_2, v_3) \in T\mathbb{R}_\Omega^2$, which is independent of the point on the fiber over $(x_2, x_3, \epsilon_2, \epsilon_3)$.*

The rescaling factor $|z_1|$ only affects the integral curves of the vector field by a time reparameterization.

Proof. Let $z = (z_1, z_2, z_3)$ follow a trajectory of the Fuller system in M let

$\pi(z) = (x_2, x_3, \epsilon_2, \epsilon_3)$ be the image trajectory. We compute for $j = 2, 3$:

$$\begin{aligned} |z_1| \frac{d}{dt} (|z_j|/|z_1|^j) &= |z_1| \Re(z_{j-1}, \frac{z_j}{|z_j|}) |z_1|^{-j} - |z_1| j |z_j| |z_1|^{-j-1} \Re(z_0, \frac{z_1}{|z_1|}) \\ &= x_{j-1} r_j - j x_j r_1, \quad \text{where} \\ r_j &= \Re \left(\frac{z_{j-1}}{|z_{j-1}|}, \frac{z_j}{|z_j|} \right). \end{aligned}$$

The functions r_j are invariant under the virial group and descend to \mathbb{R}_Ω^2 . It is enough to show that $(v_2, v_3) = (x_1 r_2 - 2x_2 r_1, x_2 r_3 - 3x_3 r_1)$. This is a routine calculation. \square

12.3 Equilibrium Points

In this section, we investigate the qualitative behavior of the vector field (v_2, v_3) . The vector field (v_2, v_3) is *odd*: the values of the vector field at $(x_2, x_3, \epsilon_2, \epsilon_3)$ and at $(x_2, x_3, -\epsilon_2, -\epsilon_3)$ have opposite signs. This means that trajectories are the same, except reversed in time at points with opposite signs. Earlier, we introduced a time-reversal operation τ on trajectories on M . The image under π of a time reversed trajectory in M is the sign reversed $\epsilon_j \mapsto -\epsilon_j$ trajectory in \mathbb{R}_Ω^2 .

Next we analyze the zeros of the vector field.

Lemma 12.3.1. *The vector field (v_2, v_3) is zero if and only if $(x_2, x_3, \epsilon_2, \epsilon_3)$ is one of the following three points:*

$$(x_2, x_3) = (2, 2) \text{ (all choices of signs give the same point),}$$

$$(x_2^*, x_3^*) := (2/\sqrt{10}, \sqrt{2}/5) \text{ where } \epsilon_2 = \epsilon_3 \in \{\pm 1\} \text{ (one point for each sign choice).}$$

Moreover, the image under π of the outward log-spiral $z^* = (z_1^*, z_2^*, z_3^*)$ constructed in (11.3.1) is the single point $q_+^* := (x_2^*, x_3^*, +, +) \in \Omega_{++}$, while the image of the inward log-spiral is the single point $q_-^* := (x_2^*, x_3^*, -, -) \in \Omega_{--}$.

Proof. It is clear that these three points give zeros of the vector field, by direct substitution into the formulas for (v_2, v_3) . By the observation that the vector field is odd, we can assume that $\epsilon_2 = +1$. Then we consider the different regions $\Omega_{+1, \epsilon_3}^0$ and its boundary, solving the equations $v_2 = v_3 = 0$ for x_2 and x_3 .

We illustrate the case Ω_{++}^0 , leaving the other cases as exercises. From the formulas for v_2, v_3 , we find that a zero in Ω_{++}^0 satisfies the equations

$$\cos_2 = 2x_2 \sin_3, \quad \cos_2 \cos_3 = 2 \sin_2 \sin_3,$$

which has $(x_2^*, x_3^*) = (2/\sqrt{10}, \sqrt{2}/5)$ as the unique solution.

Each spiral trajectory is contained in a single orbit of the virial group and must map to a single point in \mathbb{R}_Ω^2 . Explicit formulas have been given for the log spirals and for the map π , and it is an easy calculation to determine which spiral is mapped to which zero of the vector field. \square

Next we analyze stability at the equilibrium points. Because of a square root, the vector field (v_2, v_3) is not differentiable at $(x_2, x_3) = (2, 2)$ and we cannot compute a Jacobian. However, we can compute eigenvalues of the Jacobian for the other two equilibrium points.

Lemma 12.3.2. *Let Jac be the 2×2 Jacobian matrix with entries $\partial v_j / \partial x_k$, where $j, k \in \{2, 3\}$. The eigenvalues of Jac are $-\sqrt{2} \pm i\sqrt{3}$ at q_+^* . In particular, the eigenvalues have negative real part, and q_+^* is a stable equilibrium point.*

By symmetry, the equilibrium point q_-^* is unstable.

Proof. This is an elementary calculation. \square

12.4 Global Behavior

Remark 12.4.1. *We warn the reader that the square roots appearing in the definition of \cos_i, \sin_i cause the vector field (v_2, v_3) to be non-Lipschitz along the boundary curves of $\Omega_{\epsilon_2, \epsilon_3}$. Thus, trajectories are not uniquely determined by the vector field (v_2, v_3) . This is not an idle warning. The trajectories truly fail to be unique. Along these boundary curves where uniqueness breaks down, we make reference to the trajectory upstairs in M (where trajectories are uniquely determined) to determine which path the trajectory downstairs should follow. Nevertheless, on each interior part $\Omega_{\epsilon_2, \epsilon_3}^0$, the trajectories are uniquely determined by the vector field.*

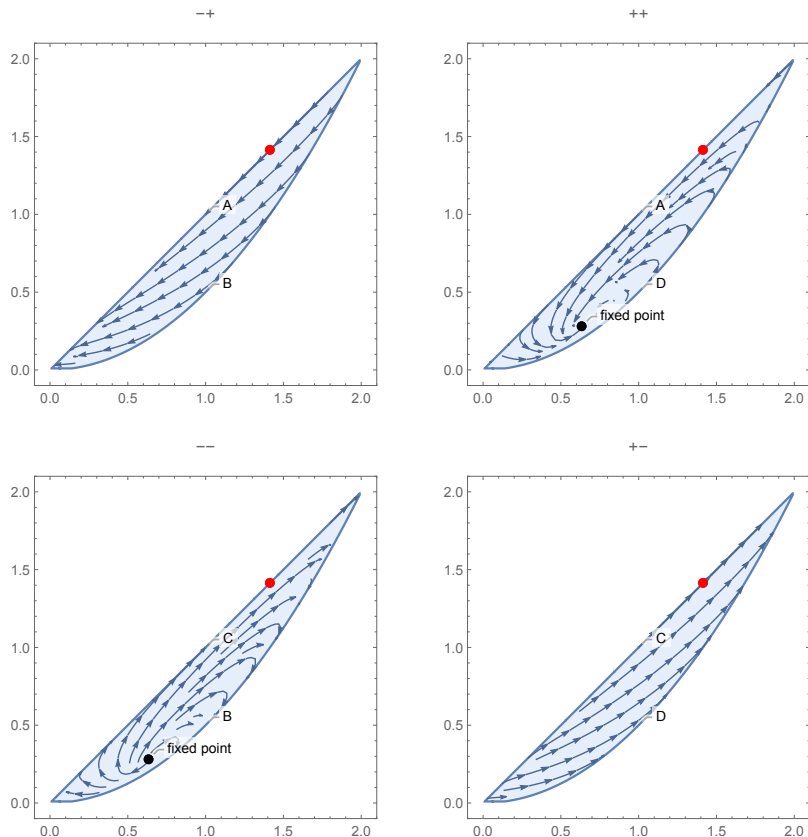


Figure 12.4.1: The dynamical system on \mathbb{R}_Ω^2 . The unstable $q_-^* \in \Omega_{--}$ and stable fixed points $q_+^* \in \Omega_{++}$ are shown. In the four frames, the two edges marked A are to be identified, as are the two edges marked B , the two marked C , and the two marked D . In this way, the four frames belong to a single dynamical system in the topological plane \mathbb{R}_Ω^2 . The four red points have coordinates $(\sqrt{2}, \sqrt{2})$. The direction of the flow across the upper boundary is reversed at $(\sqrt{2}, \sqrt{2})$.

Figure 12.4.1 depicts the dynamical system in the plane \mathbb{R}_Ω^2 and two fixed points. A third fixed point $(2, 2) \in \mathbb{R}_\Omega^2$ lies at the upper corner of the figures. The main result of this chapter is the following theorem. From Figure 12.4.1, we observe that the theorem is geometrically plausible.

Theorem 12.4.2. *Let $z(t)$ be any Fuller trajectory in M . Assume that $\pi(z(t)) \notin \{q_\pm^*\}$. Then*

- *The trajectory $z(t)$ is defined for all $t \in \mathbb{R}$.*
- *The trajectory $\pi(z(t))$ remains bounded away from $(0, 0) \in \mathbb{R}_\Omega^2$.*
- *If $U \subseteq \mathbb{R}_\Omega^2$ is any neighborhood of q_+^* , the trajectory $\pi(z(t))$ eventually enters and remains in U .*
- *If $U \subseteq \mathbb{R}_\Omega^2$ is any neighborhood of q_-^* , the trajectory $\pi(z(t))$ was in U for all sufficiently negative times.*

The proof appears at the end of the chapter in Section 12.6, after a series of lemmas. The first of these lemmas describes the movement of trajectories in \mathbb{R}_Ω^2 across the boundaries of the regions $\Omega_{\epsilon_2 \epsilon_3}$.

Lemma 12.4.3. *Along each boundary curve between regions $\Omega_{\epsilon_2 \epsilon_3}$ the vector field points along the tangent to the curve. At the boundary curve $x_3 = x_2^2/2$ (excluding endpoints $(0, 0)$ and $(2, 2)$), the images $\pi(z(t))$ of Fuller trajectories pass from Ω_{ϵ_2-} into Ω_{ϵ_2+} , for $\epsilon_2 = \pm 1$. At the boundary curve $x_3 = x_2$ (excluding endpoints $(0, 0)$ and $(2, 2)$), the images of Fuller trajectories pass from $\Omega_{-\epsilon_3}$ into $\Omega_{+\epsilon_3}$ if $x_2 = x_3 < \sqrt{2}$; and they pass in the other direction from $\Omega_{+\epsilon_3}$ into $\Omega_{-\epsilon_3}$ if $x_2 = x_3 > \sqrt{2}$, for $\epsilon_3 = \pm 1$.*

Proof. Along the boundary $x_2 = x_3$ the vector field has the form $v_2 = v_3$, so that the vector field is tangent to the boundary. Similarly, the vector field along the boundary $x_3 = x_2^2/2$ is also tangent to the boundary. However, because of non-uniqueness of trajectories, the flow does *not* move along the boundaries!

We obtain a better approximation to the flow near a boundary of $\Omega_{\epsilon_2 \epsilon_3}$ by taking the section $p = \psi(x_2, x_3, \epsilon_2, \epsilon_3) \in M$, then expanding the Fuller trajectory $z(t)$ with initial condition p at $t = 0$ in a Taylor approximation f , then taking $\pi(z(t))$.

Following this procedure at the boundary point $(x_2, x_3, \epsilon_2, \epsilon_3) = (s, s^2/2, \epsilon_2, \epsilon_3)$, for $s \in (0, 2)$, with normal $\mathbf{u} = (s, -1)$, we find that the trajectory moves from Ω_{ϵ_2-} to Ω_{ϵ_2+} .

$$\mathbf{u} \cdot \pi(z(t)) = -\frac{(4 + 7s^2)}{8}t^2 + O(t^3) \quad \epsilon_2 = \epsilon_2, \quad \epsilon_3 = \text{sign}(t).$$

Following this procedure at the boundary point $(x_2, x_3, \epsilon_2, \epsilon_3) = (s, s, \epsilon_2, \epsilon_3)$, for $s \in (0, 2)$, with normal $\mathbf{u} = (-1, 1)$, we find that the trajectory moves from $\Omega_{-\epsilon_3}$ to $\Omega_{+\epsilon_3}$ if $s < \sqrt{2}$, and the direction between regions reverses when $s > \sqrt{2}$.

$$\mathbf{u} \cdot \pi(z(t)) = -\frac{(s^2 - 2)^2}{8u}t^2 + O(t^3), \quad \epsilon_2 = \text{sign}(t(2 - s^2)), \quad \epsilon_3 = \epsilon_3.$$

□

The next lemma analyzes behavior near $(x_2, x_3) = (0, 0)$.

Lemma 12.4.4. *Let z be a Fuller trajectory in M , defined on some open time interval. The trajectory z extends to a trajectory in M for all $t \in \mathbb{R}$. Moreover, the image $t \mapsto \pi(z(t))$ is bounded away from $(x_2, x_3) = (0, 0)$.*

Proof. The vector field (v_2, v_3) is bounded. The base space \mathbb{R}_Ω^2 fails to be compact because of the omission of the corner point $(0, 0)$ from Ω . The image $\pi(z(t))$ of a Fuller trajectory on an open time interval can be extended in \mathbb{R}_Ω^2 to all time, then lifted to M to extend $z(t)$, provided the trajectory downstairs remains bounded away from $(0, 0)$. Thus, the lemma will follow if we prove that trajectories downstairs are bounded away from $(0, 0)$, the common endpoint of all boundary curves.

We use polar coordinates $(x_2, x_3) = (r \cos(\theta), r \sin(\theta))$. We may assume that (x_2, x_3) is not on a boundary edge of $\Omega_{\epsilon_2, \epsilon_3}$, because earlier analysis shows that Fuller trajectories cross the boundary edges at isolated times. We analyze several subcases according to small neighborhoods of $(0, 0)$ in the following separate pieces. We use a hodgepodge of arguments.

On Ω_{+-} ,

$$v_3 = 2x_3 + O(r^2),$$

so that $x_3(t)$ is increasing, moving away from $(0, 0)$.

On Ω_{++}^0 , we consider two subcases. In the first subcase, if $x_3 \leq x_2/2$ in a small neighborhood of $(0, 0)$, then θ is decreasing and

$$r' = \cos \theta \sqrt{1 - \tan^2 \theta} + O(r),$$

so that r' is positive and bounded away from 0, so that the trajectory moves away from $(0, 0)$. In the other subcase, if $x_3 \geq x_2/2$ in a sufficiently small neighborhood of $(0, 0)$, then the sign of the planar curvature of $(x_2(t), x_3(t))$ is positive and the tangent to the curve separates the trajectory from $(0, 0)$.

Next, consider Ω_{--}^0 . In the subcase near $(0, 0)$ where $x_3 \geq x_2/10$, the curvature argument from Ω_{++} also applies here. In the subcase near $(0, 0)$ where $x_3 \leq x_2/10$, then $v_2 < 0$ and $v_3 > 0$. Along a trajectory, x_3 is a function of x_2 , and we have

$$\frac{dx_3}{dx_2} = \frac{v_3}{v_2} \leq \sqrt{2x_3}. \quad (12.4.1)$$

Integrating this differential inequality, we obtain

$$\sqrt{2x_3(t)} \geq x_2(t) + c,$$

where $c = \sqrt{2x_3(0)} - x_2(0)$ is positive on the interior of Ω_{--} . This inequality bounds the trajectory away from $(0, 0)$.

Finally, consider Ω_{-+}^0 . We have $v_2, v_3 < 0$. In this case, inequality (12.4.1) holds, and we proceed as in the previous case. \square

12.5 A Special Trajectory

Modulo the action of the virial group, there is a unique Fuller trajectory whose image in \mathbb{R}_Ω^2 passes through equilibrium point $q_{2,2} := (x_2, x_3, \epsilon_2, \epsilon_3) = (2, 2, -1, 1)$. Using the section ψ of the bundle, the Fuller trajectory is determined by the initial condition $(z_1(0), z_2(0), z_3(0)) = (1, 2i, 2) = \psi(q_{2,2})$ at $t = 0$. We call this particular trajectory z_{spec} the *special* Fuller trajectory. Figure 12.5.1 shows the image (in red) of the special Fuller trajectory in Ω_{-+} and its subsequent trajectory in Ω_{++} . The signs (ϵ_2, ϵ_3) are discarded, so that the figure shows Ω_{-+} superimposed on Ω_{++} . At the point where $\pi(z(t))$ meets the edge $x_2 = x_3$, with $x_2 < 2$, the curve crosses from Ω_{-+} to Ω_{++} . Figure 12.5.2 shows that the crossing occurs at the positive zero of $\pi(z(t)) \cdot (1, -1)$ near $t = 0.9$. When t is large, the special trajectory approaches the stable equilibrium point $q_+^* \in \Omega_{++}$.

At $(x_2(0), x_3(0)) = (2, 2)$, the image trajectory $(x_2(t), x_3(t))$ moves from Ω_{+-} to Ω_{-+} (so that $(2, 2)$ is not a true fixed point, when higher order information from the Fuller trajectory in M is retained).

$$x_2(t) = 2 - \frac{17}{4}t^2 + O(t^3), \quad x_3(t) = 2 - \frac{9}{2}t^2 + O(t^3), \quad \epsilon_2 = -\text{sign}(t), \quad \epsilon_3 = \text{sign}(t).$$

The special trajectory invariant under time reversal τ . Its trajectory for negative times is obtained by symmetry.

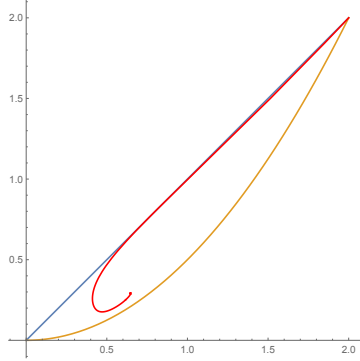


Figure 12.5.1: This figure shows the image (in red) in Ω of the special Fuller trajectory through $z = (1, 2i, 2)$. (All four regions $\Omega_{\pm\pm}$ are superimposed in this figure.) The red curve meets the boundary $x_2 = x_3$ of Ω_{++} at two points: at $(2, 2)$ at time zero and at a second point at about time $t = 0.9$. For large values of t , the curve approaches the stable equilibrium point q_+^* in Ω_{++} .

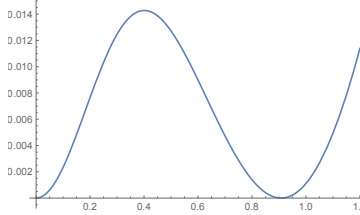


Figure 12.5.2: This figure shows $\mathbf{u} \cdot \pi(z(t))$, where $\mathbf{u} = (1, -1)$. The graph gives the deviation of $\pi(z(t))$ from the boundary curve $x_2 = x_3$. Here $z(t)$ is the special Fuller trajectory with initial condition $z = (1, 2i, 2)$ at $t = 0$. The signs (ϵ_2, ϵ_3) are ignored, but $\pi(z(t)) \in \Omega_{-+}$ for t less than the positive zero near $t = 0.9$, then $\pi(z(t))$ passes into Ω_{++} .

Let $t_c \approx 0.9$ be the time at which $q_c := \pi(z_{spec}(t_c)) \in \{x_2 = x_3\}$. Let Ω_{spec+} be the narrow region in Ω_{-+} bounded by $\pi(z_{spec}(t))$, for $t \in [0, t_c]$, and by the linear segment $[q_c, (2, 2)]$ from q_c to $(2, 2)$ along the edge $x_2 = x_3$. By our analysis of boundary behavior, trajectories in Ω_{spec+} , must enter through Ω_{++} along the segment $[(\sqrt{2}, \sqrt{2}), (2, 2)]$ and exit back into Ω_{++} along the segment $[q_c, (\sqrt{2}, \sqrt{2})]$. The component v_3 of the vector field is negative on

Ω_{spec+} , so that the trajectories always progress southward monotonically from entrance to exit.

12.6 Proof

Proof. We sketch a proof of Theorem 12.4.2, relying on a few numerical calculations as needed. The first two claims of the theorem follow from Lemma 12.4.4.

Consider trajectories in $\Omega_{-+} \setminus \Omega_{spec+}$. The component v_3 of the vector field is negative on Ω_{-+} . Trajectories must enter from Ω_{--} along the lower boundary $x_3 = x_2^2/2$ and have a soutward drift until exiting along the edge $x_2 = x_3$ into Ω_{++} along the open segment between $(0, 0)$ and q_c .

Let $\Omega_{spec-} \subset \Omega_{-+}$ be the region obtained from Ω_{spec+} by reversing signs $\epsilon_2 \mapsto -\epsilon_2$ and $\epsilon_3 \mapsto -\epsilon_3$. Then the flow on $\Omega_{-+} \setminus \Omega_{spec-}$ is obtained by reversing the flow on $\Omega_{-+} \setminus \Omega_{spec+}$: the trajectories move northward, entering from Ω_{--} and exiting into Ω_{++} along the lower boundary $x_3 = x_2^2/2$.

Similarly, the behavior on $\Omega_{spec-} \cup \Omega_{--}$ will be the time reversal of $\Omega_{spec+} \cup \Omega_{++}$, which we describe next.

Finally, we describe the flow on $\Omega_{spec+} \cup \Omega_{++}$. The flow on Ω_{spec+} is described in the previous section. Consider Ω_{++} . The point q_+^* is a stable equilibrium point. By a constructive procedure using the Lyapunov equation, there exists an explicit Lyapunov function on a small disk

$$D_r = \{x = (x_2, x_3) \mid \|x - q_+^*\| = r\}.$$

around q_+^* [37]. Let t_1 be the time at which $\pi(z_{spec}(t))$ enters the disk D_r . We consider the curve γ from q_c to q_+^* to given by the arc $\pi(z_{spec}(t))$ for $t \in [t_c, t_1]$ followed by the linear segment from $\pi(z_{spec}(t_1))$ to q_+^* .

We compute $\det((x_2, x_3) - q_+^*, (v_2, v_3)) \geq 0$ on Ω_{++} with equality if and only if (x_2, x_3) is one of the three points $(0, 0)$, $(2, 2)$, or q_+^* . This means that the trajectories always wind monotonically around the fixed point q_+^* . In particular, as it winds, every trajectory must meet the curve γ . By the uniqueness of trajectories, a trajectory meeting the special trajectory $\pi(z_{spec}(t))$ must equal the special trajectory. Every other trajectory must meet γ inside D_r . Thus, every trajectory (excluding the fixed point at q_+^*) must enter the Lyapunov disk D_r , and from there be attracted q_+^* .

The point q_-^* is related to q_+ by time reversal, so the final claim of Theorem 12.4.2 follows from what we have already proved about q_+^* . \square

Part V

A Proof of Mahler's First Conjecture

Chapter 13

Fuller System for Triangular Control

13.1 Introduction

The Reinhardt conjecture of 1934 asserts that among centrally symmetric convex disks, the smoothed octagon has the least greatest packing density. The smoothed octagon is a modification of the regular octagon obtained by rounding its corners with hyperbolic arcs. In 1947, Kurt Mahler conjectured a weak form of the Reinhardt conjecture, when he wrote

It seems highly probable from the convexity condition, that the boundary of an extreme convex domain consists of line segments and arcs of hyperbolae. So far, however, I have not succeeded in proving this assertion. —Mahler 1947.

We refer to this assertion as *Mahler's First conjecture*. The next year, Mahler rediscovered Reinhardt's conjecture from 1934, which we call Mahler's Second conjecture.

In this part of the book, we give a proof of Mahler's First conjecture. The basic outline of the proof is as follows. We make a detailed study of the Fuller system. By restriction of the dynamical system to switching times, the Fuller system becomes a discrete dynamical system with dynamics given by a Poincaré first recurrence map. We blow up the space at the singular locus. Doing so introduces an exceptional divisor, which becomes the focus of attention. We find that the discrete Fuller-Poincaré map has exactly two fixed

points on the exceptional divisor. One is stable and the other is unstable. The fixed points are exchanged by a time-reversing symmetry. (These fixed points can be interpreted as inward and outward self-similar spirals of the Fuller system.) We analyze the global dynamics of the Fuller system on the exceptional divisor and show that the basin of attraction of the stable fixed point is the entire exceptional divisor (excluding the other fixed point).

Returning to the Reinhardt dynamical system, we consider its discrete Poincaré map. We study the stable and unstable manifolds at the two fixed points (which are also fixed points of the Reinhardt dynamics). We show that any trajectory of the discrete Reinhardt dynamical system that has a cluster point on the exceptional divisor, must approach the exceptional divisor along the stable manifolds of the fixed points. However, we show that the stable and unstable manifolds at the fixed points do not contain any periodic trajectories, as required by the solution to the Reinhardt problem. We conclude that the solution of the Reinhardt problem is given by a trajectory that does not meet the singular locus. From this, it follows that the solution is bang-bang with finitely many switches. It then follows that the solution to the Reinhardt problem is a smoothed polygon.

13.2 Fuller system for Triangular Control

We define the Fuller system for triangular control to be the following controlled system of ordinary differential equations, taking values in \mathbb{C} .

$$z'_3 = z_2, \quad z'_2 = z_1, \quad z'_1 = -iu, \quad u(t) \in \{1, \zeta, \zeta^2\} =: V_T, \quad (13.2.1)$$

where $\zeta = \exp(2\pi i/3)$ is a primitive cube root of unity. The control function u is a measurable function of a real variable, taking values in V_T . We set $z_0 := -iu$ so that $z'_1 = z_0$. When $u \in \mathbb{C}$ is constant, we can solve the Fuller system ODEs, to obtain

$$\begin{aligned} z_0 &= -iu, \\ z_1(t) &= -itu + z_1^0, \\ z_2(t) &= -it^2u/2! + z_1^0t + z_2^0, \\ z_3(t) &= -it^3u/3! + z_1^0t^2/2! + z_2^0t + z_3^0, \end{aligned} \quad (13.2.2)$$

with initial conditions (z_1^0, z_2^0, z_3^0) at $t = 0$.

13.2.1 Hamiltonian

The Hamiltonian for the Fuller system is

$$\mathcal{H}_F(z, u) = \Re(z_1, z_2 i) + \Re(u, z_3), \quad z = (z_1, z_2, z_3) \quad (13.2.3)$$

$$= \frac{1}{2} \sum_{j=0}^3 (-1)^j \Re(z_{3-j}, iz_j). \quad (13.2.4)$$

We seek solutions on an interval $[t_1, t_2]$ for which the control function u maximizes the Hamiltonian.

$$\mathcal{H}_F(z(t), u(t)) \geq \mathcal{H}_F(z(t), \zeta^k), \quad \zeta^k \in \{1, \zeta, \zeta^2\}, \quad (13.2.5)$$

and such that

$$\mathcal{H}_F(z(t), u(t)) = 0, \quad \forall t \in [t_1, t_2]. \quad (13.2.6)$$

We define the maximized Hamiltonian to be

$$\mathcal{H}_F^+(z) := \max_{u \in V_T} \mathcal{H}_F(z, u).$$

It is easy to check that \mathcal{H}_F is constant along every segment with constant control. Also, if u is chosen according to the maximum principle, then \mathcal{H}_F is constant along trajectories.

13.2.2 Switching Function

We say that $u \in V_T$ is the *first control*, if it is the optimal control starting at switching time $t = 0$ until the first positive switching time $t_{sw} > 0$, for a given initial condition $z^0 \in \mathbb{C}^3 \setminus \mathbf{0}$. (It will become clear from the proof of Lemma 13.2.6 that $t = 0$ is an isolated zero of the relevant switching function, and that the notion of first control is well-defined.)

Let $z^0 = (z_1^0, z_2^0, z_3^0) \in \mathbb{C}^3$. We write the initial conditions in polar coordinates: $z_j^0 = r_j e^{i\theta_j}$. Let $z_3(t, u, z^0)$ be the solution (13.2.2) to the Fuller system with first control $u = \zeta^k$ and initial condition z^0 . Set $r_0 = 1$, $\theta_0 = (2\pi k/3) - \pi/2$, and $z_0^0 = -iu = r_0 e^{i\theta_0}$. The switching function from control ζ^i to ζ^j is

$$\chi_{u_i - u_j}^{u_k}(t) = \chi_{ij}^k(t) = \chi_{ij}^{u_k}(t) := \frac{1}{\sqrt{3}} \Re(u_i - u_j, z_3(t, u_k, z^0)).$$

When $k = i$, we drop the superscript and write χ_{ij} for χ_{ij}^i . We assume $i \neq j \pmod{3}$ so that $|u_i - u_j| = \sqrt{3}$, and write

$$u_i - u_j = \sqrt{3}e^{i\theta_{ij}}, \quad i, j \in \mathbb{Z}, \quad (\text{and } i = \sqrt{-1}).$$

Then $\chi_{ij}^u(t) = \Re(e^{i\theta_{ij}}, z_3(t, u, z^0))$. We have

$$\begin{aligned} \theta_{i,i+1} &= -\pi/6 + 2\pi i/3 \\ \theta_{i+1,i} &= 5\pi/6 + 2\pi i/3, \quad \theta_{i,i-1} = \pi/6 + 2\pi i/3, \quad i \in \mathbb{Z}. \end{aligned}$$

The switching function simplifies to the form

$$\chi_{ij}^k(t) = \sum_{m=0}^3 \frac{t^m}{m!} r_{3-m} \cos(\theta_{3-m} - \theta_{ij}).$$

13.2.3 Symmetry

We consider the symmetries of the system. We start with positive scaling.

Lemma 13.2.1. *If (z_1, z_2, z_3, u) is a solution to the Fuller system on $[t_1, t_2]$ satisfying (13.2.5) and (13.2.6), then $(\tilde{z}_1, \tilde{z}_2, \tilde{z}_3, \tilde{u})$ is a solution on $[t_1r, t_2r]$ satisfying the same constraints, where $\tilde{z}_j(t) = r^j z_j(t/r)$, $\tilde{u}(t) = u(t/r)$, and where r is real and positive.*

Proof. This holds by direct substitution into the Fuller system and into the Hamiltonian. \square

There is a discrete rotational symmetry.

Lemma 13.2.2. *If (z_1, z_2, z_3, u) is a solution to the Fuller system satisfying (13.2.5) and (13.2.6) with initial value $z^0 = (z_1^0, z_2^0, z_3^0)$, then $(\zeta z_1, \zeta z_2, \zeta z_3, \zeta u)$ is also a solution with initial value ζz^0 satisfying the same constraints.*

Proof. Again, this holds by direct substitution. \square

We call the group \mathcal{G} generated by discrete rotational symmetry and rescalings the *virial group*. (This virial group is analogous to but not identical to the virial group that was introduced earlier for circular control.) We say that z and \tilde{z} are *equivalent* and write $z \equiv \tilde{z}$ if one can be carried to the other by the virial group, that is, by a combination of scaling and discrete rotations, as described by Lemmas 13.2.1 and 13.2.2.

There is also a time-reversal symmetry. Let $\bar{\cdot}$ denote complex conjugation. If $(z_1, z_2, z_3) \in \mathbb{C}^3$, set $\tau(z_1, z_2, z_3) = (\bar{z}_1, -\bar{z}_2, \bar{z}_3)$.

Lemma 13.2.3. *If (z_1, z_2, z_3, u) is a solution to the Fuller system on $[t_1, t_2]$ satisfying (13.2.5) and (13.2.6), then $(\bar{z}_1(-t), -\bar{z}_2(-t), \bar{z}_3(-t), \bar{u}(-t))$ is a solution on $[-t_2, -t_1]$ satisfying the same constraints and with terminal value $\tau(z^0)$.*

Proof. Direct substitution. □

The following simple lemma will allow us to draw powerful conclusions about the discontinuities of Fuller system dynamics. It relates the multiplicities of roots of one switching function to the multiplicities of roots of another switching function at time $t = 0$.

Lemma 13.2.4. *Let $t_0 \in \mathbb{R}$, $z^0 \in \mathbb{C}^3$, and $u \in \mathbb{C}$. Let $z^* = z(t_0, z^0, u)$ be the value of the Fuller ODE at time t_0 , with initial condition z^0 at time $t = 0$, using constant control u for all t . For any $v_1 - v_2 \in \mathbb{C}$, the switching function satisfies*

$$\chi_{v_1-v_2}^u(t_0 - t, z^0) = \chi_{\bar{v}_1-\bar{v}_2}^{\bar{u}}(t, \tau(z^*)).$$

Proof. Direct substitution. □

We also have invariance with respect to multiplication by ζ .

$$\chi_{\zeta(v_1-v_2)}^{\zeta u}(t, \zeta z^0) = \chi_{v_1-v_2}^u(t, z^0). \quad (13.2.7)$$

We say that $u \in V_T$ is the *most recent control*, if it is the optimal control for small negative time $t < 0$ until switching time $t = 0$, for a given initial condition $z^0 \in \mathbb{C}^3 \setminus \mathbf{0}$.

For each $z^0 = (z_1^0, z_2^0, z_3^0) \in \mathbb{C}^3$, and $u \in V_T$, let $z(t, z^0, u)$ be the solution to the Fuller ODE with initial condition (z_1^0, z_2^0, z_3^0) and control u .

Lemma 13.2.5. *We have for each $t \in \mathbb{R}$,*

$$\tau(z(-t, z^0, u)) = z(t, \tau(z^0), \bar{u}).$$

Also, the most recent control of z^0 is u , if \bar{u} is the first control of $\tau(z^0)$. Moreover, the most recent switching time for initial condition z^0 is $-t_{sw}$, where t_{sw} is the first positive switching time for $\tau(z^0)$.

Proof. The lemma follows from the time-reversal symmetry (Lemma 13.2.3). □

13.2.4 Walls

We consider the Hamiltonian maximization condition (13.2.5) in more detail. The part of the Hamiltonian depending on the control u is $\Re(z_3, u)$. At a switching time, up to equivalence by a discrete rotation, the maximization principle takes the form

$$\Re(z_3, \zeta) = \Re(z_3, \zeta^2) \geq \Re(z_3, 1).$$

This defines the switching between controls ζ and ζ^2 . The set of solutions in z_3 is $\mathbb{R}_{\leq 0}$. We call this set a *wall*. Now allowing discrete rotations, we define the set of walls

$$\mathcal{W} := \mathbb{R}_{\leq 0} \cup \mathbb{R}_{\leq 0}\zeta \cup \mathbb{R}_{\leq 0}\zeta^2 =: \mathcal{W}_0 \cup \mathcal{W}_1 \cup \mathcal{W}_2.$$

Switching of controls can only occur when $z_3 \in \mathcal{W}$.

13.2.5 Switching Times

Define the following function

$$\begin{aligned} \mathbf{v} : (\mathbb{C}^3 \setminus \mathbf{0}) \times V_T &\rightarrow \mathbb{R}^3 \\ \mathbf{v}(z^0, u) &= (\Re(z_3^0, u), \Re(z_2^0, u), \Re(z_1^0, u)). \end{aligned}$$

(Note the backwards indexing.) We call $\mathbf{v}(z^0, u)$ the *control vector* of u .

We define the lexicographic order on vectors $\mathbf{v} = (\mathbf{v}_1, \dots)$ by

$$\begin{aligned} \mathbf{0} < \mathbf{v} &\iff 0 = \mathbf{v}_1 = \mathbf{v}_2 = \dots = \mathbf{v}_k, \quad 0 < \mathbf{v}_{k+1} \\ \mathbf{u} < \mathbf{v} &\iff \mathbf{0} < \mathbf{v} - \mathbf{u} \end{aligned}$$

Lemma 13.2.6. *Suppose $z^0 = (z_1^0, z_2^0, z_3^0) \in \mathbb{C}^3 \setminus \mathbf{0}$. Let $V_{T,\max} \subset V_T = \{1, \zeta, \zeta^2\}$ be the set of controls that have the maximum lexicographical value among $\{\mathbf{v}(z^0, 1), \mathbf{v}(z^0, \zeta), \mathbf{v}(z^0, \zeta^2)\}$. (That is, let $V_{T,\max} = \arg \max_{u \in V_T} \mathbf{v}(z^0, u) \subseteq V_T$.) Then*

- If $V_{T,\max} = \{u\}$, then u is the first control.
- If $V_{T,\max} = \{\zeta^i, \zeta^{i+1}\}$ has two elements, then the first control is ζ^i .
- $V_{T,\max} \neq V_T$.

Proof. If two vectors have the same lexicographical order then the two vectors are equal. If $V_{T,\max} = V_T$, then all three control vectors are equal. This implies that $z^0 = \mathbf{0}$, which is contrary to hypothesis. Thus, $V_{T,\max}$ is a proper subset of V_T .

The first control is determined by the maximum principle for t small and nonnegative. By the maximum principle at $t = 0$ and the form of the Hamiltonian, the first control must be among the controls $u \in V_T$ that maximize $\Re(z_3^0, u)$. If there is more than one maximizer, then we break the tie by passing to the first-order term in the control function $z_3(t) = z_3^0 + z_2^0 t + \dots$. That means we consider terms $\Re(z_2^0, u)$. If again, there is a tie, we consider terms $\Re(z_1^0, u)$. In this way, the first control must maximizes the lexicographical order.

Finally, if $V_{T,\max}$ contains two controls, we break the tie by considering the highest order term $-iut^3/3!$ of $z_3(t)$, where now u is itself the first control. By rotational symmetry, assume without loss of generality that $V_{T,\max} = \{1, \zeta\}$. Assume for a contradiction that the first control is $u = \zeta$. By the maximum principle we obtain the following contradiction for t small and positive,

$$-\frac{t^3}{4\sqrt{3}} = \Re(-i\zeta t^3/3!, \zeta - 1) \geq 0.$$

This contradiction implies that $u = 1$. \square

Corollary 13.2.7. *Let $(z_1, z_2, z_3) \in \mathbb{C}^3 \setminus \mathbf{0}$ satisfy $|z_i| \leq r^i$, for $i = 1, 2, 3$. Let u be the first control. Then the switching function from u to u/ζ has a positive root that is less than $10r$. In particular, the first switching time t_{sw} is less than $10r$.*

Proof. Permuting by V_T , we may assume without loss of generality that the first control mode is $u = \zeta$.

We claim that $\mathbf{v}(z, \zeta)$ is greater than $\mathbf{v}(z, 1)$ in the lexicographic order. By the choice of first control mode, $\mathbf{v}(z, \zeta)$ is at least as great as $\mathbf{v}(z, 1)$. Assume for a contradiction, that the two vectors are equal. By the lemma $V_{T,\max} = \{\zeta, 1\}$. Again, by the lemma, this implies that the first control is $u = 1$, which is contrary to hypothesis.

The switching function from $u = \zeta$ to $u/\zeta = 1$ is

$$\sqrt{3}\chi(t) = \Re(\zeta - 1, z_3(t)) = -\frac{t^3}{4\sqrt{3}} + \sum_{k=0}^2 \Re(\zeta - 1, z_{3-k}) \frac{t^k}{k!}.$$

The highest order term has negative coefficient, and by our claim about control vectors, the lowest order nonzero coefficient of the polynomial is positive. Hence a positive root exists. If $t \geq 10r$, then the bound

$$t^{-3} \sum_{k=0}^2 |\Re(\zeta - 1, z_{3-k})| t^k / k! \leq \sum \sqrt{3} |z_{3-k}| t^{k-3} / k! < \sqrt{3} \sum 10^{k-3} / k! < 1/(4\sqrt{3})$$

on the lower order terms of $\chi(t)$ implies that $\chi(t) < 0$. This completes the proof. \square

The switching function has a simple but remarkable symmetry.

Lemma 13.2.8. *Fix $z^0 \in \mathbb{C}^3 \setminus \{\mathbf{0}\}$, with $z_3^0 \in \mathbb{R}_{\leq 0}$, the wall between control modes ζ and ζ^2 . Then the switching functions with initial conditions z^0 at $t = 0$ satisfy*

$$\chi_{\zeta, \zeta^2}(t) + \chi_{\zeta^2, \zeta}(t) = 0,$$

for all t .

Proof. This is an easy computation. \square

As a corollary, as we switch back and forth between control modes ζ and ζ^2 , the consecutive switching times are given by the consecutive spacings between roots of a single cubic polynomial. Upon reaching the largest root of the cubic, the control mode is forced to switch to $u = 1$.

13.3 Singular Locus

We define the *singular locus* to be the origin in \mathbb{C}^3 . The next lemma shows that we cannot reach the singular locus, with a bang-bang solution with finitely many switches.

Lemma 13.3.1. *Let $z^0 \in \mathbb{C}^3 \setminus \mathbf{0}$ with $z_3^0 \in \mathcal{W}$ and let z be the trajectory for $t \geq 0$ with initial condition $z(0) = z^0$ at $t = 0$ with constant control given by the maximum principle. Then $z(t) \neq \mathbf{0}$, for all t .*

Proof. Up to equivalence, we can assume that the constant control is $u = 1$. Assume for a contradiction that $z(t_0) = \mathbf{0}$. Solving the system of linear equations (13.2.2) with control $u = 1$, we obtain

$$z_j^0 = (-1)^{j+1} i t_0^j / j!, \quad j = 1, 2, 3.$$

By assumption $z^0 \neq \mathbf{0}$, so that $t_0 \neq 0$. Then $z_3^0 = it_0^3/6 \notin \mathcal{W}$, which is contrary to assumption. Thus, $z(t) \neq 0$, for all t . \square

Let $U_T \subset \mathbb{C}$ be the convex hull of V_T . The Fuller system has a singular arc given by $z_1(t) = z_2(t) = z_3(t) = 0$ and $u(t) = 0$ (the center of U_T) for all t . This is an obvious solution to the Fuller ODE. We show the nonexistence of singular arcs, other than this one. The nonexistence of singular arcs was proved previously for the Reinhardt system. It comes as no surprise that it holds for the Fuller system.

Lemma 13.3.2. *Let (z_1, z_2, z_3, u) , $z_j : [t_1, t_2] \rightarrow \mathbb{C}^3$ absolutely continuous, $u : [t_1, t_2] \rightarrow U_T$ measurable, be a controlled Fuller trajectory satisfying the maximum principle for the Hamiltonian \mathcal{H}_F . Suppose that the trajectory is singular in the sense that for all $t \in [t_1, t_2]$, the set of controls maximizing the Hamiltonian is a face (and not a vertex). Then (z_1, z_2, z_3) is identically zero, and the control function is zero almost everywhere.*

Proof. We may assume $t_1 = 0$. Let $u : [0, t_2] \rightarrow U_T$ be a measurable control function. Let u_3 be a solution to the initial value problem $u_3''' = u$, $u(0) = u'(0) = u''(0) = 0$. (More precisely, we assume that u_3'' is absolutely continuous and its derivative is u almost everywhere.) A solution to the initial value problem is

$$u_3(t) = \frac{1}{2} \int_0^t u(s)(t-s)^2 ds. \quad (13.3.1)$$

This representation of a solution leads to an estimate

$$|u_3| \leq \frac{1}{2} \int_0^t s^2 ds = O(t^3).$$

Then

$$z_3(t) = -iu_3 + z_1^0 t^2/2! + z_2^0 t + z_3^0. \quad (13.3.2)$$

We consider two cases. In the first case, suppose that over the interval $[0, t_2]$, the Hamiltonian is independent of the control in U_T , so that the set of maximizers is all of U_T . Since U_T spans \mathbb{C} , by the form of the Hamiltonian, this implies that $z_3(t) = 0$ on $[0, t_2]$. By the form of the solution z_3 and the $O(t^3)$ estimate on u_3 , we have $z_1^0 = z_2^0 = z_3^0 = 0$. Then $z_3 = -iu_3 = 0$, identically. Then also $u(t) = u_3''(t) = 0$, almost everywhere. This is the singular arc described above.

In the second case, assume for a contradiction that over the interval $[0, t_2]$, the Hamiltonian is independent of the control function $u(t)$ taking values in the edge $[\zeta, \zeta^2] \subset U_T$ (say). If $u(t) \in [\zeta, \zeta^2]$, then $\Re(u(t)) = -1/2$ and $\Re(u_3(t)) = -t^3/12$. The independence of the Hamiltonian and (13.3.2) imply

$$0 = \Re(z_3(t), \zeta - \zeta^2) = \frac{\sqrt{3}}{2} \frac{t^3}{3!} + (\text{quadratic in } t)$$

for all t . This is absurd. \square

13.4 Blowing up Fuller

We describe a (weighted) blowing up process at the singular locus. Set

$$\phi(z) = \phi(z_1, z_2, z_3) := \left(\sum_{j=1}^3 |z_j|^{6/j} \right)^{1/6}, \quad z = (z_1, z_2, z_3) \in \mathbb{C}^3.$$

Then

$$\phi(rz_1, r^2z_2, r^3z_3) = r\phi(z_1, z_2, z_3), \quad r > 0.$$

Set $\Xi := \{\xi \in \mathbb{C}^3 \mid \phi(\xi) = 1\}$. We have a diffeomorphism

$$\begin{aligned} \mathbb{C}^3 \setminus \mathbf{0} &\leftrightarrow (\mathbb{R}_{>0} \times \Xi), \\ (z_1, z_2, z_3) &\mapsto (r, (\xi_1, \xi_2, \xi_3)) = (r, (z_1/r, z_2/r^2, z_3/r^3)), \quad r = \phi(z), \\ (z_1, z_2, z_3) &= (r\xi_1, r^2\xi_2, r^3\xi_3) \leftrightarrow (r, (\xi_1, \xi_2, \xi_3)). \end{aligned}$$

We will often move between the two sides of this diffeomorphism without warning, considering the right-hand side as weighted spherical coordinates for the left-hand side. Let $\pi_{rad} : \mathbb{R}_{>0} \times \Xi \rightarrow \mathbb{R}_{>0}$ and $\pi_{ang} : \mathbb{R}_{>0} \times \Xi \rightarrow \mathbb{C}^3$ be the first (radial) and second (angular) projections. We refer to $\pi_{rad}(q)$ as the radial component of q and $\pi_{ang}(q)$ as the angular component, by analogy with spherical coordinates. We refer to the left-hand side as the Cartesian coordinates.

From a slightly different perspective, $\mathbb{R}_{\geq 0} \times \Xi \rightarrow \mathbb{C}^3$ can be viewed as an *oriented weighted real blowup* of \mathbb{C}^3 at the origin (the singular locus), where Ξ is a *weighted space*, $\{0\} \times \Xi$ is the exceptional divisor over the origin $\mathbf{0} \in \mathbb{C}^3$, and each $\mathbb{R}_{\geq 0} \times \{\xi\}$ is a real positive ray through the origin.

The diffeomorphism is equivariant with respect to the virial group, where rescalings act by multiplication on the radial component and the cyclic group V_T acts by scalar multiplication on the angular component of $\mathbb{R}_{>0} \times \Xi$.

Set

$$\Xi_{\mathcal{W}} = \{(\xi_1, \xi_2, \xi_3) \in \Xi \mid \xi_3 \in \mathcal{W}\}.$$

We view it as the Poincaré section for the Fuller system. Let $\Xi_{\mathcal{W}}/V_T$ be the quotient of $\Xi_{\mathcal{W}}$ by the cyclic group action of V_T on $\Xi_{\mathcal{W}}$, acting diagonally. Under the group action, the three walls of \mathcal{W} are identified with one another.

13.5 Dynamical System and Equilibrium Points

We define a discrete-time autonomous dynamical system $F : (\mathbb{R}_{>0} \times \Xi)_{\mathcal{W}} \rightarrow (\mathbb{R}_{>0} \times \Xi)_{\mathcal{W}}$ as follows. Let $q \in (\mathbb{R}_{>0} \times \Xi)_{\mathcal{W}_i}$. The point q has Cartesian coordinates $z^0 \in \mathbb{C}^3 \setminus \mathbf{0}$ with z_3^0 lying in the i th wall. Let $z(t)$ be the solution to the Fuller differential equations with initial condition $z(0) = z^0$ at time $t = 0$ and control defined by the maximum principle. Let $t_{sw} > 0$ be the first positive switching time. Then let $F(q) \in (\mathbb{R}_{>0} \times \Xi)_{\mathcal{W}}$ equal $z(t_{sw})$, rewritten in spherical coordinates $\mathbb{R}_{>0} \times \Xi$. By the equivariance of the construction with respect to cyclic rotations V_T , we find that F descends to a well-defined map (denoted by the same symbol):

$$F : (\mathbb{R}_{>0} \times \Xi)_{\mathcal{W}}/V_T \rightarrow (\mathbb{R}_{>0} \times \Xi)_{\mathcal{W}}/V_T.$$

We can go further by considering scaling symmetries of the Fuller system. By the scaling symmetries, it is clear that if the angular components $\pi_{ang}(q_1) = \pi_{ang}(q_2)$ are equal, then the angular components $\pi_{ang}F(q_1) = \pi_{ang}F(q_2)$ of the images are equal. Thus, F gives a well defined discrete-time autonomous dynamical system

$$F_{ang} : \Xi_{\mathcal{W}} \rightarrow \Xi_{\mathcal{W}}, \quad \text{and by equivariance} \quad F_{ang} : \Xi_{\mathcal{W}}/V_T \rightarrow \Xi_{\mathcal{W}}/V_T.$$

By *Poincaré map*, we will always mean a map that discretizes a bang-bang dynamical system, by passing from one switching time to the next. In this sense, we think of $\Xi_{\mathcal{W}}$ as the Poincaré section and F_{ang} as the Poincaré map of the Fuller dynamical system on the angular component (with the understanding that the virial group symmetries have been built into F_{ang}).

Remark 13.5.1. *The notation F will be used in this chapter for various versions of the Poincaré map in a context-dependent way. The symbol F can denote either the Poincaré map for the Fuller system or the Poincaré map for the Reinhardt system, depending on the context. For the Fuller system, various domains are possible:*

$$\mathbb{C}^3 \setminus \{\mathbf{0}\}, \quad \Xi_{\mathcal{W}}, \quad \Xi_{\mathcal{W},0}, \quad \Xi_{\mathcal{W}}/V_T, \quad \Xi_{\mathcal{W},0}/V_T,$$

or various coordinate charts of these domains.

We analyze the equilibrium points of the dynamical system F_{ang} .

Lemma 13.5.2. *The dynamical system F_{ang} has exactly two fixed points in $\Xi_{\mathcal{W}}/V_T$ at which the Hamiltonian vanishes. They are the switching points q_{out}, q_{in} of outward and inward triangular spirals. They are related by time-reversing symmetry: $\tau(q_{out}) = q_{in}$. After virial rescaling to make the real part of the first coordinate equal to -1 , the fixed point q_{out} takes the form*

$$q_{out} \equiv \left(-1 + i \frac{-1+r}{\sqrt{3}(1+r)}, -\frac{-1+r^3}{\sqrt{3}(1+r^3)} + i \frac{1-3r-2r^2-3r^3+r^4}{3(1+r+r^3+r^4)}, \frac{-2(1+r-4r^3-7r^4-9r^5-7r^6-4r^7+r^9+r^{10})}{9(1+r)^2(1-r+r^2)(1+r^3+r^6)} \right) \bmod \mathcal{G}, \quad (13.5.1)$$

where $r = r_{scale} \approx 6.27$ is the unique real root greater than 1 of the palindromic polynomial

$$1 - 5r - 7r^2 - 5r^3 - 7r^4 - 5r^5 + r^6.$$

The first switching time of the initial conditions on the right-hand side of (13.5.1) is

$$t_{sw} = \frac{2(1+r+r^2)}{\sqrt{3}(r+1)} \approx 7.4$$

Proof. Let q be a lift to $\Xi_{\mathcal{W}}$ of a fixed point in $\Xi_{\mathcal{W}}/V_T$. Let $u \in V_T$ be the control, starting at $t = 0$ until the first positive switching time t_{sw} . Let $z^0 \in \mathbb{C}^3 \setminus \mathbf{0}$ be the Cartesian coordinates of $(1, q) \in \mathbb{R}_{>0} \times \Xi_{\mathcal{W}}$. The fixed-point conditions are

$$z_j(t_{sw}) = r^j \zeta_1 z_j^0, \quad (\text{modulo } \mathcal{G}), \quad (13.5.2)$$

for some $r > 0$ and some $\zeta_1 \in V_T$, where $z_j(t_{sw})$ is given by (13.2.2). Solving the linear equations (13.2.2) for z_3^0 , we find

$$z_3^0 = -i \frac{t_{sw}^3 u (1 + 2r\zeta_1 + 2r^2\zeta_1 + r^3\zeta_1^2)}{6(-1 + r\zeta_1)(-1 + r^2\zeta_1)(-1 + r^3\zeta_1)}.$$

It follows that $z_3^0 \neq 0$ (because $r > 0$, $t_{sw} > 0$ and $\zeta_1 \in V_T$). From the control u , at times $t = 0, t_{sw}$ we must have by the maximum principle

$$\begin{aligned} \Re(z_3^0, u) &\geq \Re(\zeta_2 z_3^0), \quad \forall \zeta_2 \in V_T \\ r^3 \Re(z_3^0 \zeta_1, u) &= \Re(z_3(t_{sw}), u) \geq \Re(\zeta_2 z_3(t_{sw})), \quad \forall \zeta_2 \in V_T \\ \Re(z_3^0 \bar{u}) &= \Re(z_3^0 \zeta_1 \bar{u}) \geq \Re(z_3^0 \zeta_1^2), \\ z_3^0 \bar{u} \zeta_1^2 &\in \mathbb{R}_{\leq 0}. \end{aligned}$$

This final condition implies that the scaling factor in the virial group is

$$(r, \zeta_1) \in \{(1, \zeta), (r_{scale}, \zeta^2), (1/r_{scale}, \zeta^2)\} \subset \mathbb{R}_{>0} \times V_T,$$

where the scaling factor $r_{scale} \approx 6.27$ and $1/r_{scale}$ are the only two real roots of the palindromic polynomial given in the lemma, and $\zeta = \exp(2\pi i/3)$. If $r = 1$, then $\mathcal{H}_F(z^0, u) = 1/(4\sqrt{3}) \neq 0$, and the solution is rejected. The two other solutions are the outward triangular spiral with parameters $(r, \zeta_1) = (r_{scale}, \zeta^2)$ and the inward triangular spiral with parameters $(1/r_{scale}, \zeta^2)$. The coordinates in the statement of the lemma have been rotated by V_T , choosing the first control $u = \zeta_1^2$, to make the third coordinate real and negative. \square

Remark 13.5.3. *The fixed point q_{out} of F_{ang} is an outward triangular spiral for F in a precise sense. By (13.5.2), the iterates of F satisfy*

$$F^k(q_{out}) = (r_{scale}, \zeta^2)^k \cdot q_{out},$$

where \cdot is the virial action. These are discrete points on a logarithmic spiral. The points move outward because $r_{scale} > 1$. Similarly, $F^k(q_{in})$ are points on an inward moving logarithmic spiral.

Remark 13.5.4. *The fixed point q_{fix} corresponding to $(r, \zeta_1) = (1, \zeta) \in \mathcal{G}$ in the proof has the form*

$$q_{fix} = (1, -i/2, -1/2) \mod \mathcal{G}.$$

This fixed point has a nice interpretation. In Section 7.5, we constructed a one-dimensional family of Pontryagin extremals of the Reinhardt control problem, indexed by a parameter $y_0 \in (1/\sqrt{3}, 1)$. This family includes the smoothed octagon and the smoothed $6k + 2$ -gons. Setting $y_0 = 1 - r$, we may express this one-parameter family of extremals in coordinates $(z_1(r), z_2(r), z_3(r))$, following a procedure described below in Section 14.2. Letting r tend to zero, we have asymptotics

$$(z_1(r), z_2(r), z_3(r)) = q_{fix} + \text{higher order terms} \pmod{\mathcal{G}}.$$

Thus, in a precise sense, q_{fix} is the fixed point in the Fuller system coming from the family of extremals in Reinhardt system that includes the smoothed octagon. It is particularly noteworthy that the Fuller-system Hamiltonian is not zero at q_{fix} , although it is constructed as a limit of points in the Reinhardt-system Hamiltonian zero set.

By the constancy of the Hamiltonian, the map F restricts to the zero set of the Hamiltonian.

Lemma 13.5.5. *Restrict F_{ang} to the subset $\Xi_{\mathcal{W},0}/V_T$ of $\Xi_{\mathcal{W}}/V_T$ on which the Hamiltonian vanishes. On that subset, the fixed point $q_{out} \in \Xi_{\mathcal{W},0}/V_T$ is an asymptotically stable equilibrium, and the fixed point q_{in} is unstable.*

Proof. The second assertion follows from the first, because q_{in} is obtained by time reversal from q_{out} . It suffices to show that q_{out} is asymptotically stable. This is a routine stability calculation. An open neighborhood of q_{out} in $\Xi_{\mathcal{W},0}/V_T$ is diffeomorphic to an open subset of \mathbb{R}^3 . An explicit calculation of the eigenvalues of the Jacobian matrix in terms of local coordinates centered at q_{out} gives the result. Numerically, the three eigenvalues have absolute value less than 0.1. The calculations were made in Mathematica. \square

Chapter 14

Stable and Unstable Manifolds at Fixed Points

In this chapter, we return to the Reinhardt dynamical system. More specifically, we return to the blowup of the Reinhardt system and consider the Fuller system as the restriction of the Reinhardt system to the exceptional divisor of the blowup. We describe the stable and unstable manifolds at the fixed points q_{in} and q_{out} , now viewed as fixed points in the blowup of the Reinhardt system.

We use the parameter values $d_1 = 3/2$, $\epsilon = 1$, $\rho = 2$, $\lambda_{cost} = -1$. Any trajectory that meets the singular locus must have these parameter values. Figure 14.0.1 gives a schematic representation of the Poincaré map for Reinhardt system trajectories meeting the singular locus. This chapter and the next one will prove theorems about the qualitative features of this picture. In particular, the trajectories approach the singular locus toward the fixed point q_{in} along a stable curve $W^s(q_{in})$. The flow along the exceptional divisor is governed by the Fuller system, and every point except q_{in} lies in the basin of attraction of q_{out} . The unstable manifold $W^u(q_{in})$ flows into the fixed point q_{out} . The trajectories exit the exceptional divisor along an unstable curve $W^u(q_{out})$ at q_{out} that meets the boundary of the star domain.

14.1 Lie Algebra Coordinates

In much of this book, we have worked with hyperboloid coordinates in both Cartesian z and spherical (r, ξ) coordinate form. We now return to Lie

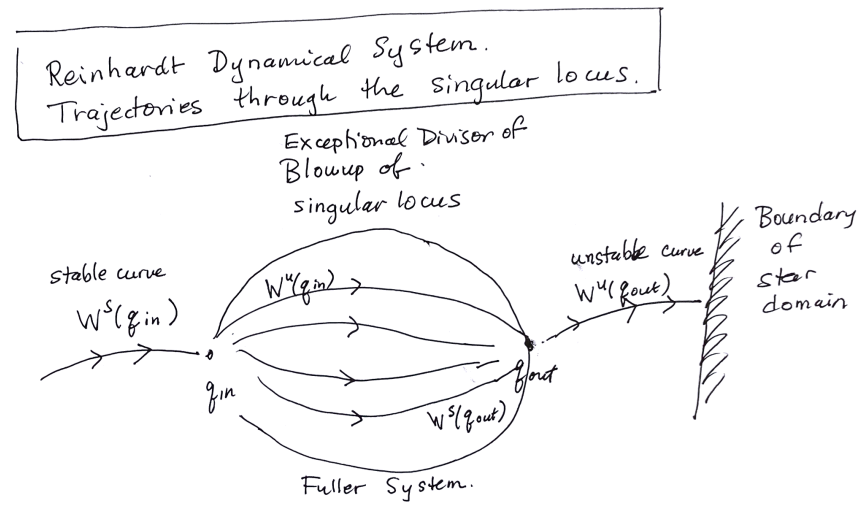


Figure 14.0.1: Schematic representation of the Poincaré map of the Reinhardt system along trajectories that meet the singular locus. The picture is four-dimensional and the exceptional divisor is three dimensional. The picture has a time-reversing symmetry that reverses the direction of arrows.

algebra $\mathfrak{sl}_2(\mathbb{R})$ coordinates. Moving forward, we will use the explicit solutions to the ODEs with constant control, expressed in Lie algebra coordinates. For computer calculations, \mathfrak{sl}_2 coordinates have the slight advantage of avoiding complex numbers.

In the interest of developing asymptotic formulas near the singular locus, for any $X, \Lambda_1, \Lambda_R \in \mathfrak{sl}_2$ subject to the usual conditions $\det(X) = 1$, $\det(\Lambda_1) = d_1^2 = 9/4$, we write¹

$$X = J + r\tilde{X}, \quad \Lambda_1 = (-3/2)J + r^2\tilde{\Lambda}_1, \quad \Lambda_R = r^3\tilde{\Lambda}_R, \quad (14.1.1)$$

for some \tilde{X} , $\tilde{\Lambda}_1$, and $\tilde{\Lambda}_R \in \mathfrak{sl}_2$, where $r > 0$ is a real parameter. Let \tilde{X} , $\tilde{\Lambda}_1$ and $\tilde{\Lambda}_R$ have matrix entries \tilde{x}_{ij} , $\tilde{\ell}_{ij}$ and $\tilde{\ell}_{Rij}$, respectively.

$$\tilde{X} = \begin{pmatrix} \tilde{x}_{11} & \tilde{x}_{12} \\ \tilde{x}_{21} & \tilde{x}_{22} \end{pmatrix} \quad \tilde{\Lambda}_1 = \begin{pmatrix} \tilde{\ell}_{11} & \tilde{\ell}_{12} \\ \tilde{\ell}_{21} & \tilde{\ell}_{22} \end{pmatrix} \quad \tilde{\Lambda}_R = \begin{pmatrix} \tilde{\ell}_{R11} & \tilde{\ell}_{R12} \\ \tilde{\ell}_{R21} & \tilde{\ell}_{R22} \end{pmatrix}.$$

We are particularly interested in points where r is small and positive, and where $\tilde{x}_{11} > 0$. We make the representation (14.1.1) unique by scaling by $r > 0$ so that $\tilde{x}_{11} = 1$.

In Lie algebra coordinates, the rotational group action by the cyclic group of order three is the action by powers of Ad_R . The walls are determined by the vanishing of the switching functions. Up to rotational symmetry, we can assume that the trajectory starts at the wall $\chi_{23} = 0$ between control matrices Z_{010} and Z_{001} .

To introduce a coordinate system, we restrict the domain by the conditions

$$0 < r, \quad \tilde{x}_{11} = 1, \quad \tilde{\ell}_{21}r^2 < 3/2. \quad (14.1.2)$$

Suppose $\Phi(z) = J + r\tilde{X}$, $z = x + iy \in \mathfrak{h}^*$, with $x > 0$. We have $\tilde{x}_{21} \leq \sqrt{3} - 1/r$ if and only if $x \geq 1/\sqrt{3}$, which lies outside the star domain $\mathfrak{h}^* \subset \mathfrak{h}$. Therefore we assume $\tilde{x}_{21} > \tilde{x}_{21}^*(r) := \sqrt{3} - 1/r$. Set

$$H^* := \{(r, \tilde{x}) \in \mathbb{R}^4 \mid \tilde{x}_{21} > \tilde{x}_{21}^*(r), \quad \tilde{\ell}_{21}r^2 < 3/2\}.$$

where we write $\tilde{x} := (\tilde{x}_{21}, \tilde{\ell}_{11}, \tilde{\ell}_{21}) \in \mathbb{R}^3$.

If $r > 0$ and $\tilde{x}_{21} > \tilde{x}_{21}^*$, then

$$1 + r\tilde{x}_{21} \geq 1 + r\tilde{x}_{21}^* = \sqrt{3}r > 0.$$

¹Here, $\tilde{\Lambda}_R$ is unrelated to an earlier term with the same name.

Hence, we may invert $1 + r\tilde{x}_{21}$. Then X is determined uniquely by r and \tilde{x}_{21} . Specifically,

$$\tilde{X} = \begin{pmatrix} r & \frac{-(1+r^2)}{1+r\tilde{x}_{21}} \\ 1+r\tilde{x}_{21} & -r \end{pmatrix}.$$

The element Λ_1 is uniquely determined by r , \tilde{l}_{11} and \tilde{l}_{21} when $\tilde{l}_{21}r^2 < 3/2$ via the relations $\det(\Lambda_1) = 9/4$, $\text{trace}(\Lambda_1) = 0$. Furthermore, $\Lambda_R \in \mathfrak{sl}_2$ is uniquely determined as a function of $(r, \tilde{x}) \in H^*$ with $r > 0$ by the three linear equations

$$\langle X, \Lambda_R \rangle = \mathcal{H}(Z_{010}, X, \Lambda_1, \Lambda_R) = \chi_{23}(X, \Lambda_R) = 0, \quad (14.1.3)$$

(which is always a full rank system of linear equations for Λ_R). The diagonal entries of Λ_R have order $O(r^4)$ and the off-diagonal entries have order $O(r^3)$. The entries of Λ_R are polynomials in r , \tilde{x}_{ij} , \tilde{l}_{ij} , $(1+r\tilde{x}_{21})^{-1}$, and $(3/2-\tilde{l}_{21}r^2)^{-1}$. In summary, $(r, \tilde{x}) \in H^*$ with $r > 0$ is a local coordinate for $(X, \Lambda_1, \Lambda_R)$.

14.2 Asymptotics

Let

$$\tilde{x} = (\tilde{x}_{21}, \tilde{l}_{11}, \tilde{l}_{21}) \in \mathbb{R}^3, \quad \tilde{x}_{11} = 1.$$

We construct a uniquely determined element $\xi(\tilde{x}) \in \Xi_{\mathcal{W},0}$ as follows. For each $r > 0$ sufficiently small, we have $1+r\tilde{x}_{21} \neq 0$, $\tilde{l}_{21}r^2 < 3/2$, and these conditions allow us to form a triple $(X(r, \tilde{x}), \Lambda_1(r, \tilde{x}), \Lambda_R(r, \tilde{x}))$, as just described. By the Cayley transform to $\text{SU}(1, 1)$, expressed in terms of hyperboloid coordinates, the triple determines $(w_r, b_r, c_r) \in \mathbb{C}^3$. We set

$$\hat{z}_1(r, \tilde{x}) = w_r/\rho, \quad \hat{z}_2(r, \tilde{x}) = -ib_r/(2\rho), \quad \hat{z}_3(r, \tilde{x}) = c_r/(6\rho), \quad \rho = 2,$$

according to the truncation rules of Equation (11.2.4). We use Landau O to describe asymptotic behavior as r tends to 0. A calculation gives

$$\begin{aligned} \hat{z}_1(r, \tilde{x}) &= \frac{r}{2}(\tilde{x}_{21} + i\tilde{x}_{11}) + O(r^2), \\ \hat{z}_2(r, \tilde{x}) &= \frac{r^2}{3!}(\tilde{l}_{11} - i\tilde{l}_{21}) + O(r^3), \\ \hat{z}_3(r, \tilde{x}) &= \frac{r^3}{4!}(\tilde{l}_{R12} + \tilde{l}_{R21}) + O(r^4). \end{aligned}$$

Then we define $\xi(\tilde{x}) \in \Xi_{\mathcal{W},0}$ to be the angular component of

$$z(\tilde{x}) := \lim_{r \rightarrow 0} (\hat{z}_1(r, \tilde{x})/r, \hat{z}_2(r, \tilde{x})/r^2, \hat{z}_3(r, \tilde{x})/r^3).$$

(This limit exists and is nonzero.) By developing in a series, we have an asymptotic relation between the Hamiltonians in the Reinhardt and Fuller systems.

$$\mathcal{H}(Z_u, X(r, \tilde{x}), \Lambda_1(r, \tilde{x}), \Lambda_R(r, \tilde{x})) = 24r^3 \mathcal{H}_F(\tilde{u}, z(\tilde{x})) + O(r^4),$$

where controls $u \in \{\mathbf{e}_j\}$ for Reinhardt and $\tilde{u} \in V_T$ for Fuller correspond by $\mathbf{e}_j \mapsto \zeta^{j-1}$, for $j = 1, 2, 3$. The equations (14.1.3) imply

$$\mathcal{H}_F(z(\tilde{x}), \zeta) = \mathcal{H}_F(z(\tilde{x}), \zeta^2) = 0.$$

We are particularly interested in the controls Z_{010} (and $\zeta \in V_T$), because they are the controls at the fixed point q_{out} , when represented according to our conventions.

Remark 14.2.1. *For example, if we take*

$$\tilde{x}_{out} := (\tilde{x}_{21out}, \tilde{\ell}_{11out}, \tilde{\ell}_{21out}) = \left(\frac{x_1}{y_1}, \frac{3x_2}{2y_1^2}, \frac{-3y_2}{2y_1^2} \right) \approx (-2.39, -4.90, -1.12),$$

where $z_{out,i} = x_i + iy_i$, then $\xi(\tilde{x}_{out})$ is equal to the outward fixed point q_{out} of the Fuller system modulo the virial group.

We can write the Reinhardt-Poincaré map F in local coordinates $(r, \tilde{x}) \mapsto F(r, \tilde{x})$. We expect asymptotic expansions in r of the Reinhardt system whose leading term is given by the Fuller system. By Lemma 13.2.1, when taking asymptotics, we should work with a rescaled time

$$s := t/r.$$

Remark 14.2.2. *A general strategy is given by Manita and Ronzhina in their inverted pendulum paper. We produce essentially equivalent results by working with our explicit solutions to the constant control ODEs and computing asymptotics using Mathematica. Their paper has also inspired our discussion of blowup.*

The next lemma shows that the leading term in the constant control solution for $(X, \Lambda_1, \Lambda_R)$ is given by the Fuller system. By cyclic symmetry, we may confine ourselves without loss of generality to the constant control matrix Z_{010} . For a given \tilde{x} , the first control of $(X(r, \tilde{x}), \Lambda_1(r, \tilde{x}), \Lambda_R(r, \tilde{x}))$ is $u = \mathbf{e}_2$ for all sufficiently small $r > 0$, provided we assume

$$\tilde{\ell}_{11} + \tilde{\ell}_{21}\tilde{x}_{21} < 0, \quad \text{and} \quad \tilde{\ell}_{21} < 0.$$

Lemma 14.2.3. *Let $(X, \Lambda_1, \Lambda_R)$ be solutions (expressed in local coordinates as $(r(s), \tilde{x}(s))$ in rescaled time $s = t/r_0$) to the Reinhardt ODE with constant control Z_{010} and initial condition (r_0, \tilde{x}^0) (in local coordinates). Let $z = z(s) = (z_1(s), z_2(s), z_3(s))$ be solutions to the Fuller ODE with constant control $u = \zeta \in V_T$ and initial condition $z(\tilde{x}^0)$. Then for each s such that $r(s) < 1$, we have*

$$\begin{aligned}\hat{z}_1(r(s), \tilde{x}(s)) &= z_1(s)r_0 + O(r_0^2) \\ \hat{z}_2(r(s), \tilde{x}(s)) &= z_2(s)r_0^2 + O(r_0^3) \\ \hat{z}_3(r(s), \tilde{x}(s)) &= z_3(s)r_0^3 + O(r_0^4).\end{aligned}$$

That is, the leading term of the solutions of the Reinhardt and Fuller systems are in agreement.

Proof. We go from the SL_2 picture to $SU(1, 1)$ by means of the Cayley transform, then switch to hyperboloid coordinates. Use the explicit solutions on both sides and expand as a series in the parameter r_0 . \square

Lemma 14.2.4. *With the same setup and matching initial conditions as in the previous lemma, we have switching function asymptotics*

$$\chi_{21}(X(sr_0), \Lambda_1(sr_0), \Lambda_R(sr_0)) = 24r_0^3 \Re(\zeta - 1, z_3(s)) + O(r_0^4) \quad (14.2.1)$$

Note that the term on the right is the switching function of the Fuller system for the control mode transition $\zeta \rightarrow 1$. Similar formulas hold for the other switching functions.

Proof. Expand both sides in an explicit series. \square

14.3 Analytic Extension of the Reinhardt system

The following is the key lemma. It shows that we have succeeded in transforming the behavior near the singular locus into something quite pleasant.

Lemma 14.3.1. *Let $\tilde{x}_{out} \in \mathbb{R}^3$ be the parameter associated with the outward fixed point of the Fuller system. The Reinhardt-Poincaré map F (initially defined for $r > 0$) extends to an analytic diffeomorphism in a neighborhood of the fixed point $(0, \tilde{x}_{out}) \in \mathbb{R}^4$ (including non-positive values of r), such that F coincides with the Fuller-Poincaré map at $r = 0$.*

Remark 14.3.2. *Similar analytic extensions across $r = 0$ can be carried out under more general conditions in a neighborhood of other points \tilde{x} . However, we must be cautious when the least positive root of the cubic of the Fuller system (14.2.1) is not simple, when $s = 0$ is a root of the cubic, or when the resultant of two Fuller switching functions is zero.*

Proof. We begin by establishing analyticity of F on some neighborhood of the fixed point, expressed in the coordinates (r_0, \tilde{x}_0) . (We add subscript 0 to suggest that these are initial conditions of the Reinhardt ODEs.) We can take these coordinates with values in either \mathbb{R} or \mathbb{C} . Lie algebra coordinates $(X_0, \Lambda_{10}, \Lambda_{R0})$ are rational functions with nonzero denominators (and hence analytic) in the variables (r_0, \tilde{x}_0) and $(1 + r_0 \tilde{x}_{21})^{-1}$. (The denominators are nonzero in a neighborhood of the fixed point.) The constant control Z_{010} solutions $(X(t), \Lambda_1(t), \Lambda_R(t))$ to the Reinhardt ODEs are given by matrix exponentials and are hence analytic in time t and initial conditions $(X_0, \Lambda_{10}, \Lambda_{R0})$. We make a substitution $t = sr_0$ to give reparameterized time.

By Lemma 14.2.4, by division of power series, the function

$$\chi_{21}(X(sr_0), \Lambda_1(sr_0), \Lambda_R(sr_0))/r_0^3$$

extends to an analytic function $\tilde{\chi}_{21}(s, r_0, \tilde{x}_0)$ in a neighborhood of $r_0 = 0$.

Restricting at first to real coordinates and $r_0 \geq 0$, the switching time in rescaled coordinates is defined by the least positive zero $s_{sw} = s_{sw}(r_0, \tilde{x}_0)$ of $\tilde{\chi}_{21}(s, r_0, \tilde{x}_0) = 0$. At the fixed point $(r_0, \tilde{x}_0) = (0, \tilde{x}_{out})$, the least positive zero $s_{sw,out} \approx 8.84 > 0$ is a simple zero, and $s = 0$ is not a zero. If we remove the condition $r_0 \geq 0$, then by the analytic implicit function theorem, we have a

unique analytic extension of the switching time $s_{sw}(r_0, \tilde{x}_0)$ to a neighborhood of the fixed point such that

$$\tilde{\chi}_{21}(s_{sw}(r_0, \tilde{x}_0), r_0, \tilde{x}_0) = 0, \quad s_{sw}(0, x_{out}) = s_{sw,out}.$$

Evaluating the solutions to the ODEs at the unscaled switching time $t_{sw} = r_0 s_{sw}$, and rotating by cyclic virial symmetries $(\text{ad}_{R^{-1}})$, we obtain analytic functions of (r_0, \tilde{x}_0) :

$$Y_{sw}(r_0, \tilde{x}_0) := \text{ad}_{R^{-1}}(Y(r_0 s_{sw}(r_0, \tilde{x}_0), r_0, \tilde{x}_0)), \quad \text{where } Y = X, \Lambda_1, \Lambda_R.$$

We write $X = X(t, r_0, \tilde{x}_0)$, etc. to make the dependence on initial conditions (r_0, \tilde{x}_0) explicit. The rotation is chosen to make the fixed point property hold exactly, and not just up to rotation. These functions give the value of the Reinhardt-Poincaré map.

Finally, we show that we can analytically convert the Lie algebra coordinates $(X, \Lambda_1, \Lambda_R)$ back to the coordinate system (r, \tilde{x}) . The matrix coefficients of

$$X(r_0 s_{sw}, r_0, \tilde{x}_0) - J, \quad \text{and } \Lambda_1(r_0 s_{sw}, r_0, \tilde{x}_0) + (3/2)J$$

are divisible by r_0 , and r_0^2 , respectively (regardless of the precise form of s_{sw}). The same is true of $X_{sw} - J$ and $\Lambda_{1sw} + (3/2)J$. Because of our convention $\tilde{x}_{11} = 1$, we must take the reciprocal of the $(1, 1)$ matrix coefficient of $(X_{sw} - J)/r_0$. The value of this matrix coefficient at $(0, \tilde{x}_{out})$ is

$$r_{scale} \approx 6.27 \neq 0.$$

This is the scaling factor, obtained as a root of the palindromic polynomial considered above. Since this $(1, 1)$ matrix coefficient is an analytic function that is nonzero in a neighborhood of the fixed point, its reciprocal is an analytic function. This completes the proof of analytic continuation to a neighborhood of the fixed point.

The asymptotic formulas given above show that the restriction of (the analytic continuation of) F to $r = 0$ is precisely the Fuller system.

Next, we show that the Reinhardt-Poincaré map is a diffeomorphism. In similar way to what we have done, we can show analyticity and analytic continuation of the Reinhardt-Poincaré map F^{-1} that moves backwards in time. When the parameter r_0 is positive and in a sufficiently small neighborhood of the fixed point, we have that F and F^{-1} are inverse functions. By analytic continuation, they are inverse functions in a neighborhood of the fixed point. Hence, F is a diffeomorphism. \square

We refer to the hypersurface $r = 0$ as the exceptional divisor. We refer to Irwin for background material about local unstable and stable manifolds near a hyperbolic fixed point of a diffeomorphism [18]. A brief summary appears in Appendix A.3. We write F for the analytic diffeomorphism that we have constructed, which extends the Reinhardt-Poincaré map.

Theorem 14.3.3. *The fixed point $(0, \tilde{x}_{out})$ of the diffeomorphism F is hyperbolic. The local unstable manifold is a C^∞ curve. In a neighborhood of the fixed point, the local stable manifold coincides with the three-dimensional exceptional divisor $r = 0$.*

Remark 14.3.4. *By time reversal, the Reinhardt-Poincaré map F has a hyperbolic fixed point at $(0, x_{in}) \in \mathbb{R}^4$, its local stable manifold is one-dimensional, and its local unstable manifold is the three-dimensional exceptional divisor.*

Proof. Near the fixed point, the analytic continuation F of the Reinhardt-Poincaré map agrees with the Fuller-Poincaré map, when $r = 0$, when we use coordinates $\tilde{x} \in \mathbb{R}^3$ for points on the exceptional divisor $\xi(\tilde{x}) \in \Xi_{W,0}$ as above. The exceptional divisor $r = 0$ is a three-dimensional invariant subset of the diffeomorphism. We have seen that the linearization of the Fuller-Poincaré map F near the fixed point is a contraction on the three dimensional exceptional divisor. Moving away from the exceptional divisor in the radial direction, the Reinhardt-Poincaré map has scaling factor $r_{scale} > 1$. The Fuller-Poincaré map is therefore hyperbolic, with three eigenvalues $|\lambda| < 1$ and one eigenvalue $|\lambda| > 1$. By general theory, the unstable curve is C^∞ , because the diffeomorphism is C^∞ . \square

14.4 A Computation of the Unstable Manifold

We extend the local unstable manifold to the global unstable manifold. The previous theorem shows the existence of a C^∞ curve (the global unstable manifold around the fixed point $(0, x_{out})$):

$$t \mapsto (r(t), \tilde{x}(t)) \in \mathbb{R}^4, \quad (r(0), \tilde{x}(0)) = (0, x_{out}), \quad t \geq 0,$$

for some local parameter t . In fact, we use $t = r$ (the first coordinate of the system (14.1.1)) as the local parameter. Figure 14.4.1 shows a numerical

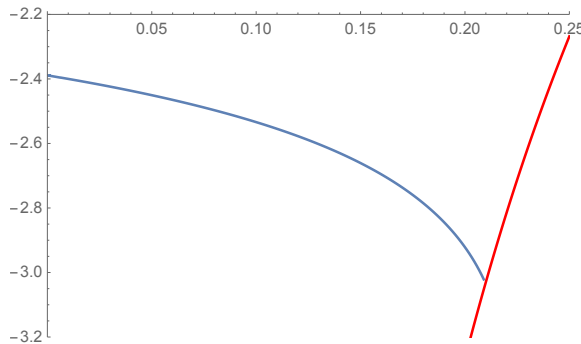


Figure 14.4.1: The unstable curve $r \mapsto (r, \tilde{x}_{21}(r))$ (in blue) starts at the outward fixed point $\tilde{x}_{21out} \approx -2.39$ and continues to the boundary $\tilde{x}_{21}^*(r) = \sqrt{3} - 1/r$ of the star domain (in red). The curve has been approximated in Mathematica, using the *ListLinePlot* command to create a piecewise linear curve joining 434 data points.

computation of the unstable curve. Although we have not done so because it did not seem especially worthwhile, these calculations might be repeated using more rigorous numerical methods such as interval arithmetic. The numerical situation is favorable: because of contraction in the stable directions, any numerical errors in computing the *unstable* curve will tend to be self-effacing (in the same way that under mild assumptions, Von Mises iteration of matrix powers converge to the dominant eigenvalue). Another numerical advantage is that three contractive eigenvalues are small (less than 0.1 according to the proof of Lemma 13.5.5).

As we move away from the fixed point, computations use the unscaled switching time $t_{sw} = t_{sw}(r, \tilde{x}(r))$ rather than the scaled switching time. We check that the other switching functions χ_{ij} remain positive, so that the switching sequence is always cyclical $3 \mapsto 2 \mapsto 1 \mapsto 3 \mapsto \dots$. The unstable curve reaches the boundary of the star domain near $(r, \tilde{x}_{21}) \approx (0.21, -3.03)$. Once r is at least about 0.065, a Reinhardt trajectory starting on the unstable curve reaches the boundary of the star domain before the next switching time, and the forward step of the Reinhardt-Poincaré map is no longer defined.

Theorem 14.4.1. *A trajectory of the Reinhardt system that emanates from the fixed point $(r, \tilde{x}) = (0, x_{out})$ on the exceptional divisor does not return to the exceptional divisor. A trajectory of the Reinhardt system that tends to the fixed point $(r, \tilde{x}) = (0, x_{in})$ on the exceptional divisor did not emanate at an*

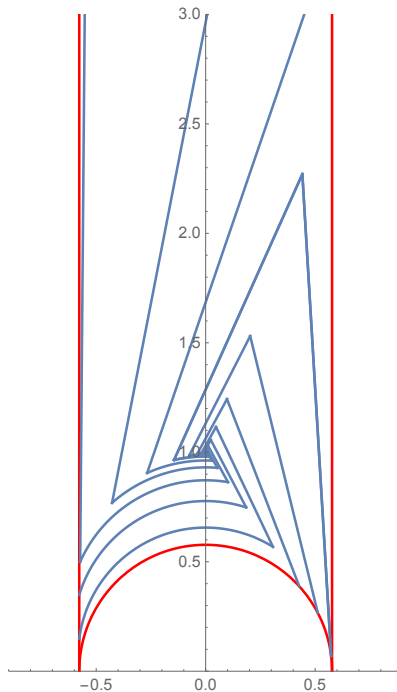


Figure 14.4.2: Outward triangular spirals of the Reinhardt system that start at the singular locus. The figure shows the image of trajectories $z(t) \in \mathfrak{h}^*$ in the upper half plane.

earlier time from the exceptional divisor.

Proof. All switches must be on the unstable curve, which meets that exceptional divisor at a single point $(0, x_{out})$. Any trajectory that returns to the singular locus must chatter (that is, must use infinitely many switches to arrive). This would require the unstable curve to contain a sequence of *forward* iterates of points tending to the exceptional divisor. This does not happen, because the unstable curve hits the boundary of the star domain.

The second statement follows from the first by time reversal. \square

Figure 14.4.2 shows the resulting outward spiral trajectories $z(t) \in \mathfrak{h}^*$ (where $\Phi(z(t)) = X(t)$). Trajectories chatter as they exit from the singular locus, and move in a triangular spiral until they hit the boundary of the star domain in finite time. The switching points are clearly visible as corners of the triangular spirals. The unstable curves, which are related by rotations, are obtained by joining these switching points by smooth curves.

Chapter 15

Geometry of the Fuller-Poincaré Map

Throughout this section, dropping the subscript on F_{ang} , we let F denote the Poincaré map for the Fuller system on the Poincaré section $\Xi_{\mathcal{W},0}/V_T$ or on the domain given by the cells covering $\Xi_{\mathcal{W},0}/V_T$, as described below.

15.1 Three-Cells

Let $z = (z_1, z_2, z_3) \in \mathbb{C}^3$. Write $z_j = r_j e^{i\theta_j} = x_j + iy_j$, for $j = 1, 2, 3$. Assume that $z_3 \in \mathcal{W}$, a wall. By passing to a V_T -equivalent point, we may assume that $z_3 = \Re(z_3) = x_3 \leq 0$.

Assume that the Hamiltonian vanishes at $z = (z_1, z_2, z_3)$ for some control $u \in V_T$. The vanishing Hamiltonian condition implies

$$x_3 = 2r_1r_2 \sin(\theta_1 - \theta_2) = -2r_1r_2 \sin \psi, \quad (15.1.1)$$

where $\psi := \theta_2 - \theta_1$. If $x_3 < 0$, this implies $r_1r_2 \neq 0$ and $\psi \in (0, \pi)$ (modulo integer multiples of 2π).

Lemma 15.1.1. *For each $z = (z_1, z_2, z_3) \neq \mathbf{0}$ satisfying (15.1.1), there is a unique rescaling by a positive scalar in the virial group so that $r_1 + r_2 = 1$ (and $r_1, r_2 \geq 0$).*

Proof. If $r_1 = r_2 = 0$, then $z = \mathbf{0}$ by (15.1.1), which is contrary to assumption. Hence, we may assume $r_1 + r_2 > 0$. Solve the following quadratic equation

for its unique positive root $s > 0$,

$$r_1/s + r_2/s^2 = 1.$$

Then scale $r_i \mapsto r_i/s^i$. □

Thus, we may write $r_1 = 1 - r_2$, with $r_2 \in [0, 1]$.

The time reversal symmetry τ , when expressed in terms of coordinates (r_2, ψ, θ_2) takes the form

$$\tau(r_2, \psi, \theta_2) = (r_2, \pi - \psi, \pm\pi - \theta_2).$$

If $\theta_2 \in [-\pi, \pi]$, then the sign $\pm\pi$ in the third coordinate $\pm\pi - \theta_2$ is chosen to give a value again in $[-\pi, \pi]$.

We now enumerate the cells partitioning the domain $\Xi_{W,0}/V_T$ starting with the two three-dimensional cells. We use notation $\mathbf{C}_k(u, m_A, m_B)$ for cells. The subscript k denotes the dimension of the cell; u is the first control; m_A (resp. m_B) is the multiplicity of $t = 0$ in the switching polynomial $\chi_A = \chi_{u-1}^u$ (resp. $\chi_B = \chi_{u-\bar{u}}^u$). Let $\chi_{A,m_A} := \chi_A/t^{m_A}$ and $\chi_{B,m_B} := \chi_B/t^{m_B}$. Let $\Delta_{A,m_A}, \Delta_{B,m_B}$ be the discriminants of χ_{A,m_A} and χ_{B,m_B} . We sometimes also affix a superscript \mathbf{C}_k^A or \mathbf{C}_k^B to indicate whether the active switching function is χ_{A,m_A} or χ_{B,m_B} .

Definition 15.1.2. *The cell $\mathbf{C}_3(\zeta)^0 = \mathbf{C}_3(u, m_A, m_B)^0 = \mathbf{C}_3(\zeta, 0, 1)^0$ is defined by conditions $x_3 \neq 0$ and $y_2 > 0$. The cell $\mathbf{C}_3(\zeta^2)^0 = \mathbf{C}_3(u, m_A, m_B)^0 = \mathbf{C}_3(\zeta^2, 0, 1)^0$ is defined by conditions $x_3 \neq 0$ and $y_2 < 0$. We call $\mathbf{C}_3(u)^0$ the big open cells.*

(We will construct compactifications $\mathbf{C}_3(u, 0, 1)$ of the open cells below.) $\mathbf{C}_3(\zeta)^0$ is a three-dimensional open rectangle in \mathbb{R}^3 with coordinates $r_2 \in (0, 1)$, $\psi \in (0, \pi)$, and $\theta_2 \in (0, \pi)$. The first control is ζ . Also, $\mathbf{C}_3(\zeta^2)^0$ is a three-dimensional open rectangle in \mathbb{R}^3 with coordinates $r_2 \in (0, 1)$, $\psi \in (0, \pi)$, and $\theta_2 \in (-\pi, 0)$. The first control is ζ^2 . The complement of $\mathbf{C}_3(\zeta)^0 \cup \mathbf{C}_3(\zeta^2)^0$ is a union of strata of dimension at most two. Thus, these two three-dimensional cells cover most of the domain. We also refer to $\mathbf{C}_3(\zeta)^0$ and $\mathbf{C}_3(\zeta^2)^0$ as the *first and second big cells*, respectively. The involution τ is given by $\tau(r_2, \psi, \theta_2) = (r_2, \pi - \psi, \pi - \theta_2)$ on the first big cell and by $\tau(r_2, \psi, \theta_2) = (r_2, \pi - \psi, -\pi - \theta_2)$ on the second big cell.

Note that $\chi_{A,0}(0) \neq 0$ and $\chi_{B,1}(0) \neq 0$ on the big open cells, and the roots are nonzero. As above, let $\Delta_{A,0}$ and $\Delta_{B,1}$ be their discriminants, and

let res_{AB} be the resultant of $\chi_{A,0}$ and $\chi_{B,1}$. The first switching time t_{sw} is a discontinuous function on the cell. The discontinuities can only appear along the loci $\Delta_{A,0} = 0$, $\Delta_{B,1} = 0$ and $\text{res}_{AB} = 0$. However, the loci do not always force a discontinuity in t_{sw} . For example, $\text{res}_{AB} = 0$ does not give a discontinuity when it represents the equality of negative roots of $\chi_{A,0}$ and $\chi_{B,1}$.

We study the boundaries of the first and second big cells, with the aim of extending the dynamical system continuously to the boundaries (with noted exceptions).

We identify points along the face $r_2 = 0$, if they have the same image under the mapping $f : [0, \pi] \times [0, \pi]$, $f(\psi, \theta_2) = \theta_2 - \psi = \theta_1 \in [-\pi, \pi]$ on the first cell, and the mapping $f : [-\pi, 0] \times [0, \pi]$, $f(\psi, \theta_2) = \theta_2 - \psi = \theta_1 \in [0, 2\pi]$ on the second cell. (When $r_2 = 0$, the coordinate $z_2 = r_2 e^{i\theta_2}$ does not depend on θ_2 .) On each cell separately, we identify points along the face $r_2 = 1$, if they have the same image under the projection $f(\psi, \theta_2) = \theta_2$, for similar reasons: the coordinates $z_1 = r_1 e^{i\theta_1}$ does not depend on θ_1 . We do *not* identify points $\theta_2 = 0$ on the bottom face of the first big cell with points $\theta_2 = 0$ on the top face of the second big cell, because they have different first controls u and behave differently in the Fuller dynamical system. For the same reason, we do *not* identify points $\theta_2 = \pi$ on the top face of the first big cell with points $\theta_2 = -\pi$ on the bottom face of the second big cell.

Figure 15.1.1 shows shaded in red those points p_0 on the boundary of the two cells where the first switching time satisfies $\lim_{p \rightarrow p_0} t_{sw}(p) = 0$, where the limit is taken over interior points of the cells. Although the switching time is zero, the dynamical system is best treated as nontrivial (by refraining from identifying V_T -equivalent points on the boundary of the cells).

By taking points in the big open cells near the boundary, we can determine that the Fuller-Poincaré map acts in the following way on the (red-shaded regions of the) boundary (by continuous extension of the map on the interior of the cells). The bottom face $\theta_2 = 0^+$ of the first big cell maps to the top face $\theta_2 = 0^-$ of the second big cell (by the identity map $(r_2, \psi) \mapsto (r_2, \psi)$). The bottom face $\theta_2 = (-\pi)^+$ of the second big cell maps to the top face $\theta_2 = \pi^-$ of the first big cell by the map $(r_2, \psi, \theta_2) \mapsto (r_2, \psi, 2\pi + \theta_2)$. The boundary region $\psi \in \{0, \pi\}$, $\theta_2 \in [0, \pi/3]$ on the first big cell is shifted to V_T -equivalent points $(\psi, \theta_2) \mapsto (\psi, \theta_2 + 2\pi/3)$ on the same faces. Also, the boundary region $\psi \in \{0, \pi\}$, $\theta_2 \in [-\pi/3, 0]$ on the first big cell is shifted to V_T -equivalent points $(\psi, \theta_2) \mapsto (\psi, \theta_2 - 2\pi/3)$ on the same faces. Finally, the right and left faces $r_2 = 0$ and $r_2 = 1$ of the cells have been collapsed to edges along the front

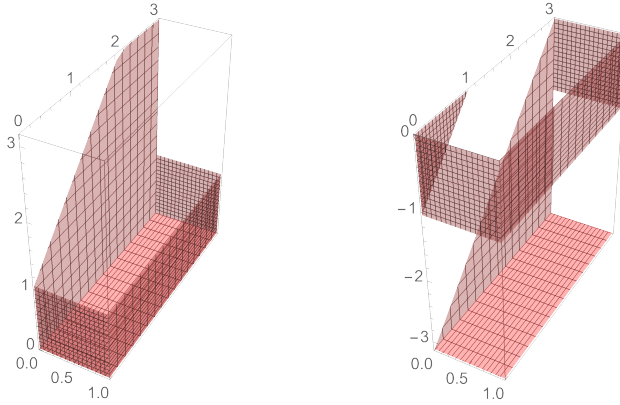


Figure 15.1.1: Shaded regions are points on the boundary of the first and second big cells where the first switching time t_{sw} has limiting value 0. Smaller cells $y_2 = 0$ will be attached to the top faces of both 3-cells to cap the top faces, and further smaller cells $z_3 = 0$ will be attached to the unshaded regions of the front and back faces to fill the unshaded regions of the faces.

and back faces $\psi \in \{0, \pi\}$, and their behavior is dictated by the behavior on the other faces. (As stated above, all these boundary behaviors are obtained by studying the behavior of the dynamical system on the interior of the cells and taking limits to the boundary.)

15.2 Smaller cells

In this section, we partition the complement of the union $\mathbf{C}_3(\zeta^{\pm 1})^0$ into cells of lower dimension. We find that the cells of lower dimension can be attached to the faces of the first and second big cells in a way that preserves continuity. We continue to use polar coordinates $z_j = r_j e^{i\theta_j} = x_j + iy_j$. We may assume $r_2 = 1 - r_1 \in [0, 1]$ and $x_3 = -2r_1r_2 \sin \psi$, $\psi = \theta_2 - \theta_1 \in [0, \pi]$

by (15.1.1).

We begin with the cases such that $x_3 \neq 0$. To be in the complement of the big open cells, we must have $\sin \theta_2 = 0$ and $y_2 = 0$. The two-dimensional cells of this form have parameters $u \in \{\zeta^{\pm 1}\}$, $(m_A, m_B) = (0, 2)$. That is, χ_B has a double root at $t = 0$. We denote these cells $\mathbf{C}_2(u, m_A, m_B)$, according to the their parameters.

The cell $\mathbf{C}_2(u, m_A, m_B) = \mathbf{C}_2(\zeta, 0, 2)$ is defined by $x_3 \neq 0$ and $\theta_2 = \pi$. Coordinates are $r_2 \in (0, 1)$, $\psi \in (0, \pi)$. The first control is ζ . The switching function $\chi_{B,2}$ never has a positive root. Thus, the switching function is always $\chi_{A,0}$. By Descartes's rule of signs, $\chi_{A,0}$ always has a unique positive root. The first switching time is then a continuous function on the cell. If we identify this cell with the top face $\theta_2 = \pi$ of the first three-cell $\mathbf{C}_3(\zeta)^0$, then the dynamical system extends continuously from the interior of the first big cell to its top face.

The cell $\mathbf{C}_2(u, m_A, m_B) = \mathbf{C}_2(\zeta^2, 0, 2)$ is defined by $x_3 \neq 0$, and $\theta_2 = 0$. Coordinates are $r_2 \in (0, 1)$, $\psi \in (0, \pi)$. The first control is ζ^2 . If we identify this 2-cell with the top face $\theta_2 = 0$ of the second three-cell $\mathbf{C}_3(\zeta^2)^0$, then the dynamical system extends continuously from the interior of the second big cell to its top face (with exceptional discontinuities, where the dynamical system is already discontinuous on $\mathbf{C}_2(\zeta^2, 0, 2)$, as noted below).

Note that we cannot have parameter values $(m_A, m_B) = (0, 3)$. In fact, if $m_B = 3$, the $y_1 = y_2 = 0$. This implies that $r_1 = 0$, $r_2 = 0$ or $\theta_1, \theta_2 \in \pi\mathbb{Z}$. Then $x_3 = -2r_1r_2 \sin \psi = 0$ by (15.1.1), and $m_A > 0$.

In the remaining region, $z_3 = 0$ (and $m_A > 0$). By (15.1.1), we have $r_2 \in \{0, 1\}$, or $\sin \psi = 0$. Each angle θ_2 is V_T -equivalent to a unique angle $\theta_2 \in (\pi/3, \pi]$. We define a *closed* 2-cell $\mathbf{C}_2(\zeta) = \mathbf{C}_2(\zeta, 1, 1)$ with first control $u = \zeta$ as follows. The coordinates are $\tilde{r}_1 \in [-1, 1]$ and $\theta_2 \in [\pi/3, \pi]$. If we define the first switching time t_{sw} over the entire closed 2-cell by continuous extension of the first switching time on the interior of the closed 2-cell, then Figure 15.1.1 shows the parts of the boundary where the continuous extension gives $t_{sw} = 0$. Setting $r_1 = \tilde{r}_1 e^{i\psi}$, and $r_2 = 1 - r_1$, with $\psi \in \{0, \pi\}$ and $r_1 \in (0, 1)$, we recover the coordinates (r_2, ψ, θ_2) . (Exceptionally, on the segment $\tilde{r}_1 = 0$, $r_2 = 1$, we disregard ψ and only use θ_2 .) If we attach each point (r_2, ψ, θ_2) of this cell to the point on the front and back boundary faces $\psi \in \{0, \pi\}$ of the first 3-cell with the same coordinates (r_2, ψ, θ_2) , then the dynamical system on the interior of the 3-cell extends continuously to the front and back faces, in agreement with the dynamics on the 2-cell $\mathbf{C}_2(\zeta)$. Note that the segment $\tilde{r}_1 = 0$ maps to the right face of the 3-cell, which has

been collapse to a segment, and with this collapsed right face, the map from the 2-cell to the front and back faces of the 3-cell is continuous.

In a similar way, by V_T -equivalence, the angle θ_2 can be brought into the interval $\theta_2 \in (-\pi, -\pi/3]$ by the V_T -action. In this case, the first control is $u = \zeta^2$ and a closed cell $\mathbf{C}_2(\zeta^2, 1, 1)$ can be attached in a similar way to the front and back faces of the second 3-cell $\mathbf{C}_3(\zeta^2)^0$ in a way that agrees with the dynamics.

Remark 15.2.1. *A symmetry of V_T carries the closed cell $\mathbf{C}_2(\zeta, 1, 1)$ to $\mathbf{C}_2(\zeta^2, 1, 1)$, but we refrain from identifying these two closed cells with each other. Instead, we consider the two closed big cells as disjoint from each other. We will see that $F^{-1}(\mathbf{C}_2(\zeta))$ and $F^{-1}(\mathbf{C}_2(\zeta^2))$ are the two sides of a hypersurface ∂_{res} in the first big cell, along which the Fuller-Poincaré map is discontinuous. Because of this discontinuity, it is best to keep the two two-cells separate.*

We summarize our results in the following lemma.

Proposition 15.2.2. *Every point in the domain of $\Xi_{W,0}/V_T$ is equivalent to a point in the union of the closures $\mathbf{C}_3(\zeta^{\pm 1})$ of the first and second big cells (with identifications on the boundaries of each cell as given above). The first control u is ζ on the first big cell and ζ^2 on the second big cell. The dynamics on the faces of the cells is given as the continuous extension from the dynamics on the interior of the cells. Every point on every face of the cells that is not identified with a point in the domain $\Xi_{W,0}/V_T$ is a point with vanishing (limiting) first switching time $t_{sw} = 0$.*

Proof. See the discussion leading up to the statement of the proposition. \square

15.3 Involution

Let F be the Fuller-Poincaré map, and let τ be the time reversing symmetry. Both have domain given by the union of two closed 3-cells. Since $F^{-1} = \tau \circ F \circ \tau$ and $\tau = \tau^{-1}$, it follows that $\iota_{\tau F} := \tau \circ F$ is an involution: $\iota_{\tau F} = \iota_{\tau F}^{-1}$. In this section, we use properties of this involution to describe discontinuities of the Fuller-Poincaré map.

We say that two subset $\mathbf{D}, \tilde{\mathbf{D}}$ of the domain are *in involution* if $\iota_{\tau F}(\mathbf{D}) = \tilde{\mathbf{D}}$ (and $\iota_{\tau F}(\tilde{\mathbf{D}}) = \mathbf{D}$). Let $\mathbf{C}_2(\zeta, 1, 1)$ be the closed 2-cell defined above, viewed as a subset of the front and back faces of the first big cell. Define the resultant

locus as $\partial_{res} = \iota_{\tau F}(\mathbf{C}_2(\zeta))$. By Lemma 13.2.4, the resultant of the switching functions χ_{A0} and χ_{B1} is zero along ∂_{res} . By construction ∂_{res} and $\mathbf{C}_2(\zeta, 1, 1)$ are in involution. Define $\partial_A = \iota_{\tau F}(\mathbf{C}_2(\zeta, 0, 2))$, where $\mathbf{C}_2(\zeta, 0, 2)$ is viewed as the top face $\theta_2 = \pi$ of the first big cell. By Lemma 13.2.4, the discriminant of the switching function χ_{A0} is zero along ∂_A and F is discontinuous along ∂_A . By construction ∂_A and $\mathbf{C}_2(\zeta)$ are in involution. The locus $\partial_{res} \cup \partial_A$ lies in the first big cell and geometrically partitions the first big cell into two parts. (Here, by a *geometric partition* of a set, we mean a collection of *regular closed subsets* covering the set whose interiors are disjoint. A closed set is *regular*, if it is the closure of its interior.)

Let \mathbf{D}_1 be the part of the geometric partition containing the face $\mathbf{C}_2(\zeta, 0, 2)$ (that is, the face $\theta_2 = \pi$). There are no further discontinuities in \mathbf{D}_1 ; that is, F on the interior of \mathbf{D}_1 extends continuously to a function F_1 with domain \mathbf{D}_1 , with first control $u = \zeta$ and switching function χ_{A0} . The domain \mathbf{D}_1 is in self involution. The two fixed points $q_{in}, q_{out} \in \mathbf{D}_1$ are in involution. See Figure 15.3.1.

We geometrically partition the 2-cell $\mathbf{C}_2(\zeta^2, 0, 2)$ according to the active switching function (Figure 15.3.2). On one part \mathbf{C}_2^A , we have $\Delta_{A,0} \geq 0$. By Descartes's rule of signs, $\chi_{A,0}$ has two positive roots (counted with algebraic multiplicity). The first switching time is a root of $\chi_{A,0}$ and is continuous on \mathbf{C}_2^A . On the interior of the part \mathbf{C}_2^B , we have $\Delta_{A,0} < 0$. In this case, $\chi_{A,0}$ has no positive root, and the first switching time is the unique root of the linear polynomial $\chi_{B,2}$. The map F is discontinuous along the discriminant locus $\Delta_{A,0} = 0$. However, the first switching time and the Fuller-Poincaré map F extend continuously to give F_A with domain \mathbf{C}_2^A and F_B with domain \mathbf{C}_2^B .

Set $\partial_{A,\zeta^2} := \iota_{\tau F}(\mathbf{C}_2^A)$. It is a subset of the second big cell, and it geometrically partitions the big cell into two parts. The discriminant $\Delta_{A,0}$ vanishes along ∂_A , by Lemma 13.2.4. Let \mathbf{D}_2 be the part that contains \mathbf{C}_2^A . The active switching function on \mathbf{D}_2 is $\chi_{A,0}$. The Fuller-Poincaré map F extends continuously from the interior of \mathbf{D}_2 to a continuous function F_2 with domain \mathbf{D}_2 , and the restriction of F_2 to \mathbf{C}_2^A is F_A . The part \mathbf{D}_2 is in self involution.

Let \mathbf{D}_3 be the other part of the partition of the second big cell. The active switching function on \mathbf{D}_3 is $\chi_{B,1}$, and F extends continuously to a function F_3 with domain \mathbf{D}_3 .

Let $\mathbf{D}_4 := \iota_{\tau F}(\mathbf{D}_3)$. It is a subset of the first big cell, that shares the boundary ∂_{res} (and part of the boundary ∂_A with \mathbf{D}_1). Finally, let \mathbf{D}_0 be the closure of the complement in the first big cell of the union of \mathbf{D}_1 and \mathbf{D}_4 . The boundary of \mathbf{D}_0 consists of $\partial_B := \iota_{\tau F}(\mathbf{C}_2^B)$ and a subset of ∂_A . Along ∂_B , the

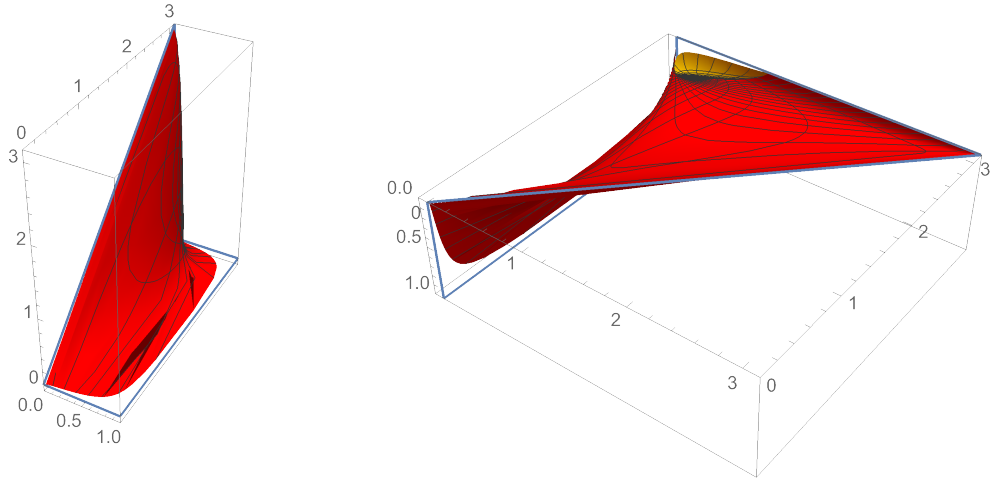


Figure 15.3.1: Geometric partition of the first big cell into parts $\mathbf{D}_0, \mathbf{D}_1, \mathbf{D}_4$. The two panels show two different views of the boundary separating \mathbf{D}_1 from $\mathbf{D}_0 \cup \mathbf{D}_4$ in the first big cell. On the red shaded part ∂_{res} of the boundary, the resultant vanishes. On the yellow shaded part ∂_A of the boundary, the discriminant $\Delta_{A,0}$ vanishes. These red and yellow boundaries extend to the blue perimeter, even if the displayed graphics stop short due to imperfect rendering. The blue perimeter is in involution with the perimeter of the red region in the first frame of Figure 15.1.1. The part \mathbf{D}_1 lies above and to the right of the boundary in the first panel and to the lower right of the boundary in the second panel. The parts \mathbf{D}_0 and \mathbf{D}_4 lie below the boundary in the first panel and to the upper left in the second panel. The boundary ∂_B between \mathbf{D}_0 and \mathbf{D}_4 is not shown. The part \mathbf{D}_0 is a very small bubble, which is attached to the yellow part ∂_A of the boundary.

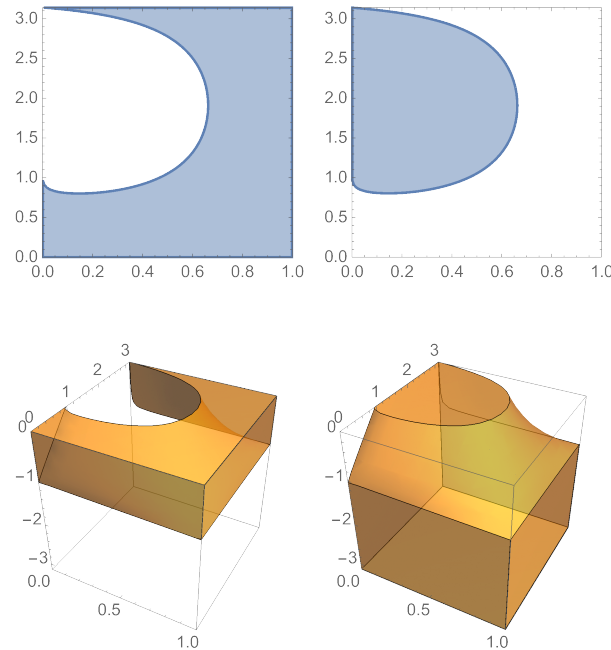


Figure 15.3.2: Geometric partition of the second big cell into parts \mathbf{D}_2 (lower left panel) and \mathbf{D}_3 (lower right panel). The top left panel \mathbf{C}_2^A and top right panel \mathbf{C}_2^B are given by $\Delta_{A,0} \geq 0$ and $\Delta_{A,0} < 0$, respectively in the top face $\theta_2 = 0$ of the second big cell. The lower left panel \mathbf{D}_2 and lower right panel \mathbf{D}_3 are separated by the discriminant locus $\Delta_{A,0} = 0$. The part \mathbf{D}_2 is in involution with itself, and the involution exchanges its top face \mathbf{C}_2^A with the locus separating \mathbf{D}_2 from \mathbf{D}_3 . The involution exchanges \mathbf{D}_3 and \mathbf{D}_4 , sending the top face \mathbf{C}_2^B of \mathbf{D}_3 to the boundary ∂_B separating \mathbf{D}_4 from \mathbf{D}_0 .

discriminant vanishes: $\Delta_{B,1} = 0$.

Remark 15.3.1. *The fixed point $q_{in} \in \mathbf{D}_1$ is given by coordinates*

$$(r_{2in}, \psi_{in}, \theta_{2in}) \approx (0.267949, 0.1705935, 2.91574).$$

The fixed point is remarkably close to the triple juncture of \mathbf{D}_0 , \mathbf{D}_1 , and \mathbf{D}_4 . In fact, the line segment

$$r_2 \mapsto (r_2, \psi_{in}, \theta_{2in}), \quad r_2 \in [0, 1]$$

meets the boundary ∂_B (separating D_4 from D_0) at $r_2 \approx 0.2677$, then meets the boundary ∂_A (separating D_0 from D_1) at $r_2 \approx 0.267905$, then reaches the fixed point at $r_2 \approx 0.267949$. The fixed point $q_{out} \in \mathbf{D}_1$ with coordinates $(r_2, \pi - \psi_{in}, \pi - \theta_{2in}) \in \mathbf{D}_1$ is far from the other parts $\mathbf{D}_0, \mathbf{D}_4$.

In summary, we have the following proposition.

Proposition 15.3.2. *Let \mathbf{D}_i , $i = 0, 1, 2, 3, 4$ be the geometric partition of the two big cells defined as above. The Fuller-Poincaré map extends continuously from the interiors of \mathbf{D}_i to functions F_i on the closures \mathbf{D}_i , for $i = 0, 1, 2, 3, 4$. The involution acts on the parts by $\mathbf{D}_3 \leftrightarrow \mathbf{D}_4$. Moreover, $\mathbf{D}_1, \mathbf{D}_2, \mathbf{D}_0$ are each in self involution.*

Proof. The proof is contained in the discussion leading up to the proposition. To briefly summarize the argument, any discontinuity in the interior of a big cell must appear along one of the loci $\text{res}_{AB} = 0$, $\Delta_{A0} = 0$, or $\Delta_{B1} = 0$. By Lemma 13.2.4, the involution maps the interior discontinuities to the boundary faces of the big cells.

The Fuller-Poincaré map is continuous on the boundary cells $\mathbf{C}_2(\zeta^{\pm 1}, 0, 2)$ and $\mathbf{C}_2(\zeta, 1, 1)$, again with exceptions where a resultant or discriminant vanishes. Analyzing cases on two-cells, the only discontinuity is given by $\Delta_{A0} = 0$ on $\mathbf{C}_2(\zeta^2, 0, 2)$. Using the involution to map these parts of the faces back into big cells, we obtain a complete description of the discontinuities. \square

Chapter 16

Global Basin of Attraction and Mahler's First

Throughout this chapter, dropping the subscript on F_{ang} , we let F denote the Poincaré map for the Fuller system on the two big cells. Also, F_i denotes the continuous extension of F to \mathbf{D}_i .

16.1 Main result on Basin of Attraction

Theorem 16.1.1 (Global Basin). *Let $q \neq q_{in}$ be a point in $\Xi_{W,0}/V_T$. Then the iterates $F^k q$ under the Fuller-Poincaré map tend to the fixed point q_{out} .*

Proof. The proof follows the strategy of *containment functions* from interval arithmetic. However, the proof is simple enough that it is not necessary to adopt the entire infrastructure of interval arithmetic.

We work with the representation of $\Xi_{W,0}/V_T$ as the union of two closed big cells $\mathbf{C}_3(\zeta^{\pm 1})$. Let $\mathbf{D}_0, \dots, \mathbf{D}_4$ be the geometric partition of the cells, and let F_i be the continuous extension of F from the interior of \mathbf{D}_i to \mathbf{D}_i .

We further partition \mathbf{D}_1 into 9 rectangles. Set

$$\begin{aligned}\mathbf{D}_{ij} &:= \{(r_2, \psi, \theta_2) \in \mathbf{C}_3(\zeta) \mid r_2 \in [0, 1], \psi \in [a_i, a_{i+1}], \theta_2 \in [b_{i+1}, b_i]\}, \\ \mathbf{D}_{1,ij} &:= \mathbf{D}_1 \cap \mathbf{D}_{ij}, \quad i = 0, 1, 2, \quad j = 0, 1, 2,\end{aligned}$$

where $(a_0, a_1, a_2, a_3) = (0, \pi/3, 2\pi/3, \pi)$ and $(b_0, b_1, b_2, b_3) = (\pi, \pi - 1.1, 1.1, 0)$. We have $q_{in} \in \mathbf{D}_{in} := \mathbf{D}_{1,22}$ and $q_{out} \in \mathbf{D}_{out} := \mathbf{D}_{1,00} = \mathbf{D}_{00}$.

	\mathbf{D}_{in}	\mathbf{D}_{out}	\mathbf{D}_4	\mathbf{D}_2	\mathbf{D}_0	\mathbf{D}_3	$\mathbf{D}_1 \setminus \mathbf{D}_{in}$
\mathbf{D}_{in}	*	*	*	*	*	*	*
\mathbf{D}_{out}		*					
\mathbf{D}_4			*			*	
\mathbf{D}_2				*		*	
\mathbf{D}_0					*		*
\mathbf{D}_3						*	
$\mathbf{D}_1 \setminus \mathbf{D}_{in}$							*

Table 16.1: Upper triangular structure of the Fuller-Poincaré map on the two big cells. The dots \cdot are placeholders along the diagonal. The nontrivial diagonal entries appear in the first, second, and last rows.

We claim that we have the following domain and range restrictions. Let \mathbf{D}, \mathbf{D}^* run over the sets in Table 16.1.

$$\mathbf{D}, \mathbf{D}^* \in \{\mathbf{D}_{in}, \mathbf{D}_{out}, \mathbf{D}_4, \mathbf{D}_2, \mathbf{D}_0, \mathbf{D}_3, \mathbf{D}_1 \setminus \mathbf{D}_{in}\}.$$

Assume $\mathbf{D} \subseteq \mathbf{D}_i$. We claim that $F_i(\mathbf{D}) \subset \cup_{(\mathbf{D}, \mathbf{D}^*) \sim *} \mathbf{D}^*$, where \mathbf{D}^* is included in the union whenever the row-column entry $(\mathbf{D}, \mathbf{D}^*)$ of Table 16.1 is marked with an asterisk. (The dots \cdot are placeholders along the diagonal of the table and do not indicate inclusion in the union.)

We justify the claim and the associated table as follows. Whenever $\mathbf{D} \subset \mathbf{D}_i$ is topologically a closed ball with boundary $\partial\mathbf{D}$, then in order to show that $F_i(\mathbf{D}) \subset \tilde{\mathbf{D}}$, where $\tilde{\mathbf{D}}$ is a closed convex subset of \mathbb{R}^3 , it is enough to show $F_i(\partial\mathbf{D}) \subset \tilde{\mathbf{D}}$. In practice, $\partial\mathbf{D}$ consists of a small number of analytic surfaces (such as the six faces of a cube), and the proof of the containment $F_i(\mathbf{D}) \subset \tilde{\mathbf{D}}$ reduces to the containment of the images of the faces, which we compute numerically without difficulty in Mathematica. We call this the *boundary method*. In fact, by using the involution $\iota_{\tau F}$, we can mostly avoid direct use of the Fuller-Poincaré map.

We start with the second row. We compute the interval containment $F_1(\mathbf{D}_{out}) \subset \mathbf{D}_{out}$ by the boundary method. The image $F_1(\mathbf{D}_{out})$ and the fixed point q_{out} are shown in Figure 16.1.1. The forward iterates $F_1^k(\mathbf{D}_{out})$ quickly

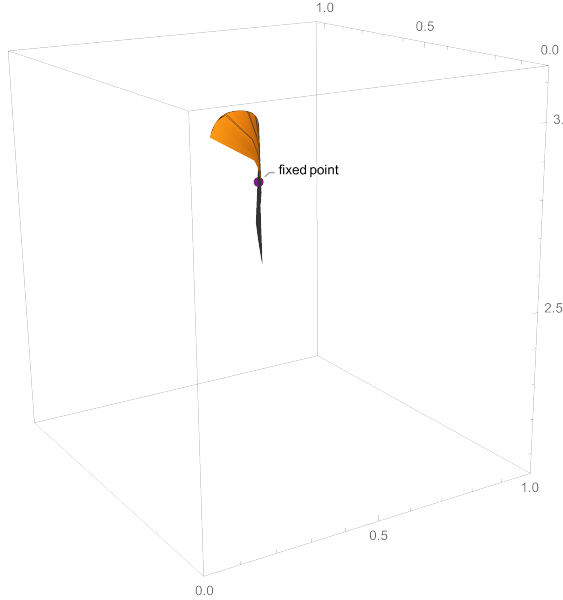


Figure 16.1.1: The bounding box is the set $\mathbf{D}_{out} \subset \mathbf{D}_1$ and the shaded region is the image $F_1(\mathbf{D}_{out})$, showing the contraction of \mathbf{D}_{out} toward the fixed point $q_{out} \in \mathbf{D}_{out}$.

shrink toward q_{out} . The Jacobian calculation at the fixed point (appearing earlier) shows that q_{out} is an asymptotically stable fixed point.

The first row asserts that the range of \mathbf{D}_{in} can be anything, and there is nothing to prove in this case. For the \mathbf{D}_4 row, the image satisfies $F_4(\mathbf{D}_4) = \tau(\iota_{\tau F}(\mathbf{D}_4)) = \tau(\mathbf{D}_3)$, which is contained in the second big cell, covered by $\mathbf{D}_2 \cup \mathbf{D}_3$. For the next row, $F_2(\mathbf{D}_2) = \tau(\iota_{\tau F}(\mathbf{D}_2)) = \tau(\mathbf{D}_2) \subset \mathbf{D}_3$. (Note that $\theta_2 \in [-\pi/3, 0]$ holds on \mathbf{D}_2 , so that $\theta_2 \in [-\pi, -2\pi/3]$ holds on $\tau(\mathbf{D}_2)$, to see the containment in \mathbf{D}_3 .)

Turning to the row for \mathbf{D}_0 , we note that $F_0(\mathbf{D}_0) = \tau(\iota_{\tau F}(\mathbf{D}_0)) = \tau(\mathbf{D}_0)$. The boundary of $\tau(\mathbf{D}_0)$ consists of $\tau\iota_{\tau F}(C_2^B)$ and a subset of $\tau(\partial_A)$. Both of these boundary components lie in \mathbf{D}_{out} , which is a subset of $\mathbf{D}_1 \setminus \mathbf{D}_{in}$. The containment $F_0(\mathbf{D}_0) \subset \mathbf{D}_1 \setminus \mathbf{D}_{in}$ follows by the boundary method.

Next consider the row \mathbf{D}_3 . We have $F_3(\mathbf{D}_3) = \tau(\iota_{\tau F}(\mathbf{D}_3)) = \tau(\mathbf{D}_4)$, which is a subset of the first cell. Recall that the first big cell is covered by the union of \mathbf{D}_0 , \mathbf{D}_1 , and \mathbf{D}_4 . The inequality $\theta_1 = \theta_2 - \psi \leq 0$ holds on \mathbf{D}_4 , \mathbf{D}_0 , and \mathbf{D}_{in} , but $\theta_1 = \theta_2 - \psi \geq 0$ holds on $\tau(\mathbf{D}_4)$. Hence by exclusion, $\tau(\mathbf{D}_4) \subset \mathbf{D}_1 \setminus \mathbf{D}_{in}$. (In the boundary case $\theta_2 = \psi$, the edge given by equations $r_2 = 0$, $\theta_2 = \psi$

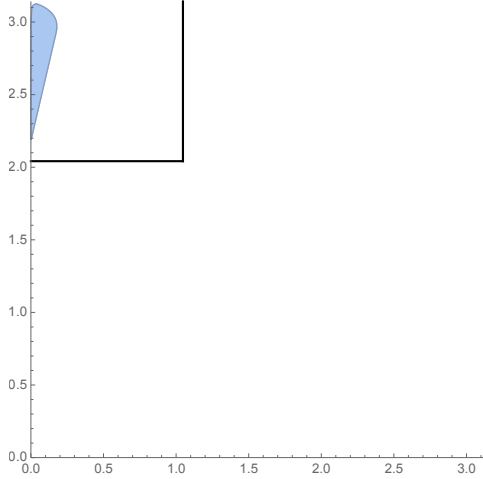


Figure 16.1.2: The shaded region is the convex hull of the projection to the (ψ, θ_2) -plane of the iterated image $F^2 \mathbf{D}_3$. The black lines show the boundary of the projection of \mathbf{D}_{out} . The conclusion is that $F^2 \mathbf{D}_3 \subset \mathbf{D}_{out}$.

belongs to both \mathbf{D}_1 and \mathbf{D}_4 , but we still have $\tau(\mathbf{D}_4) \subset \mathbf{D}_1 \setminus \mathbf{D}_{in}$.

We have that $F^2 \mathbf{D}_3 \subset \mathbf{D}_{00}$, as shown by the calculation in Figure 16.1.2. Applying the function $F \circ \tau$ to both sides of this inclusion, we obtain

$$\mathbf{D}_4 \subset F(\mathbf{D}_{22}), \quad (16.1.1)$$

because

$$\mathbf{D}_4 = \iota_{\tau F}(\mathbf{D}_3) = F\tau F^2 \mathbf{D}_3 \subset F\tau \mathbf{D}_{00} = F(\mathbf{D}_{22}).$$

The last row of the table is justified below by taking an interval refinement. We claim that $F_1(\mathbf{D}_1 \setminus \mathbf{D}_{in}) \subset \mathbf{C}_3(\zeta) \setminus \mathbf{D}_{in}$. (Note that if $q_1 \in \mathbf{D}_1 \setminus \mathbf{D}_{in}$ and $F_1(q_1) \in \mathbf{C}_3(\zeta) \setminus \mathbf{D}_{in}$, then using facts $\mathbf{C}_3(\zeta) = \mathbf{D}_0 \cup \mathbf{D}_1 \cup \mathbf{D}_4$ and $\mathbf{D}_0 \subset \mathbf{D}_{in}$ and $\mathbf{D}_4 \subset F\mathbf{D}_{22} \not\ni F(q_1)$, we get $F_1(q_1) \in \mathbf{D}_1 \setminus \mathbf{D}_{in}$ to complete the justification of the row.)

The cases $(i, j) = (0, 0), (2, 2)$ are the cases $\mathbf{D}_{in}, \mathbf{D}_{out}$, which are treated elsewhere. For $(i, j) \neq (0, 0), (2, 2)$, we break the claim into a series of subclaims. The domain $\mathbf{D}_1 \setminus \mathbf{D}_{in}$ is covered by the sets $\mathbf{D}_{1,ij}$, for $(i, j) \neq (2, 2)$. The subclaims are the following domain and range restrictions for $(i, j) \neq (0, 0), (2, 2)$; *subclaim_{ij}*: we have $F_1(\mathbf{D}_{1,ij}) \subset \cup_{k,\ell} \mathbf{D}_{k\ell}$, where the union runs over $(k, \ell) < (i, j)$. Here we use the lexicographic total order ($<$) on ordered pairs given by

$$(k, \ell) < (i, j) \iff (k < i) \text{ or } (k = i \text{ and } \ell < j).$$

These subclaims are established by the boundary method through direct computation, explained above. The convex hulls of planar projections of the images are shown in Figure 16.1.3. The domain and range restrictions follow by observing that the blue regions are subsets of the yellow regions. The three-dimensional images $F_1(D_{1,21})$ $F_1(D_{1,01})$ are shown in Figure 16.1.4. Their projections appears in panels (2, 1) and (0, 1) of Figure 16.1.3.

We are ready to prove that q_{out} has a global basin. Let $q \neq q_{in}$. Assume first that $q \in \mathbf{D}_{in}$. By time reversal symmetry, for every $q \in \mathbf{D}_{in}$, with $q \neq q_{in}$, the iterates $F^k q$ must eventually exit \mathbf{D}_{in} (because the iterates $F^{-k}(\tau q)$ exit \mathbf{D}_{out} for all sufficiently large k). Note the upper triangular structure of the first table, with diagonal entries only for \mathbf{D}_{in} and $\mathbf{D}_1 \setminus \mathbf{D}_{in}$. Hence, if $q \neq q_{in}$, the iterates $F^k q$ lie in $\mathbf{D}_1 \setminus \mathbf{D}_{in}$ for all sufficiently large k .

Note that the total order ($<$) gives a strict triangular structure with respect to domain and range interval containments. Hence, if $q \in \mathbf{D}_1 \setminus \mathbf{D}_{in}$, the forward iterates $F^k q$ must then eventually all lie in $\mathbf{D}_{1,00} = \mathbf{D}_{out}$. As already noted, once in the small rectangle \mathbf{D}_{out} containing q_{out} , the iterates rapidly converge to the fixed point q_{out} . \square

16.2 Classification of Outward Fuller Trajectories

In this section we return to the Fuller-Poincaré map $F : (\mathbb{C}^3 \setminus \mathbf{0}) \rightarrow (\mathbb{C}^3 \setminus \mathbf{0})$ (including the radial component) and restore the subscript F_{ang} when referring to the Fuller-Poincaré map on the angular component.

Theorem 16.2.1. *Consider the Fuller-Poincaré dynamical system F on $(\mathbb{C}^3 \setminus \mathbf{0})/V_T$. Every outward trajectory that emanates from the singular locus has all its switching points in the set $\mathbb{R}_{>0} \times \{q_{out}\}$ modulo V_T . Every inward trajectory to the singular locus has all its switching points in the set $\mathbb{R}_{>0} \times \{q_{in}\}$ modulo V_T .*

Proof. By time reversal symmetry, it is enough to prove the second statement of the lemma. Let $q \in \Xi_{\mathcal{W}}/V_T$ be any switching point of any trajectory. If $q = q_{in}$, then it is the inward spiral.

Otherwise, $q \neq q_{in}$. In this case, by the Fuller basin theorem and by the stability calculation near q_{in} , for large j , the iterates $F_{ang}^j(q)$ approach the outward spiral. For every $r > 0$, this implies that the angular component of

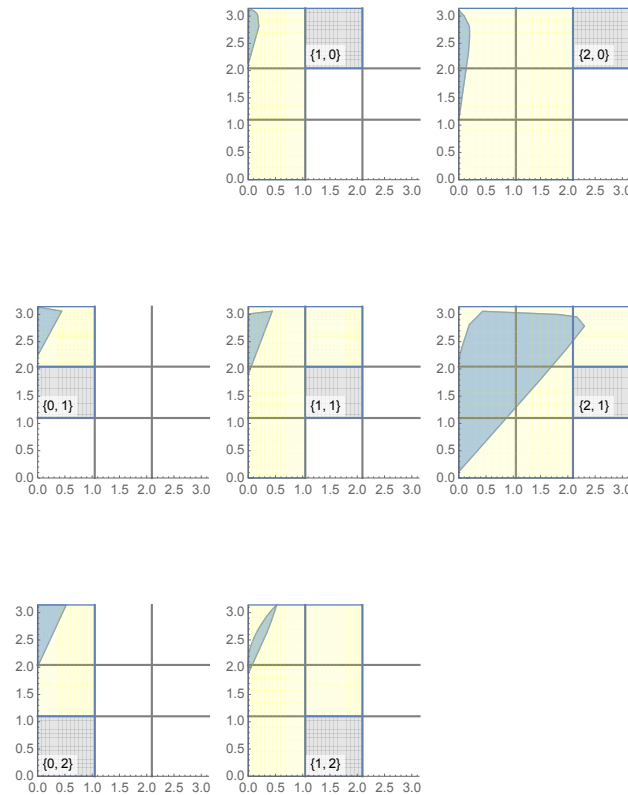


Figure 16.1.3: Projections of images $F_1(\mathbf{D}_{1,ij})$ in panel (i,j) . The coordinates are (ψ, θ_2) and projection map is $(r_2, \psi, \theta_2) \mapsto (\psi, \theta_2)$. The gray square labeled $\{i,j\}$ is the projection of \mathbf{D}_{ij} , containing the domain. The blue region is the convex hull of the projection of $F_1(\mathbf{D}_{1,ij})$. The yellow squares are the projections of \mathbf{D}_{kl} such that $(k,l) < (i,j)$. The subclaims follow from the observation that each blue region is contained in the corresponding yellow region.

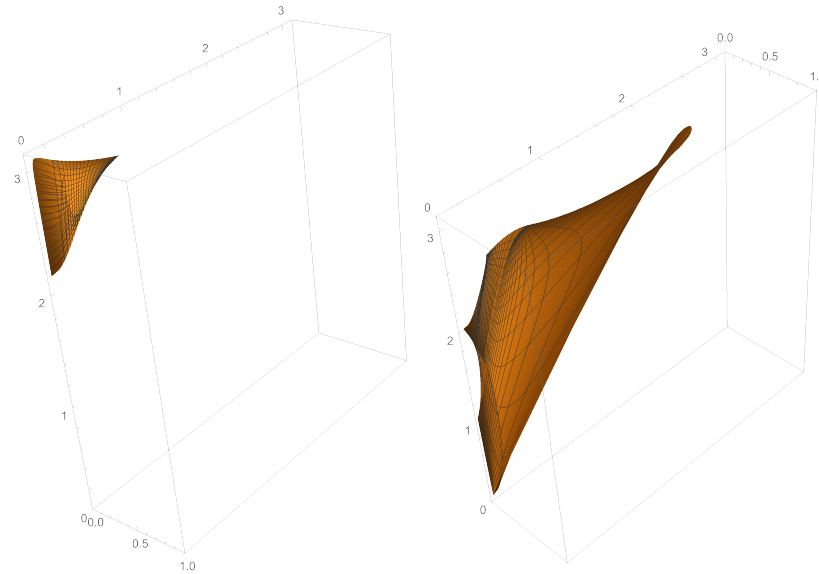


Figure 16.1.4: The right panel shows the image $F_1(\mathbf{D}_{1,21})$ in the first big cell. The projection of this region appears in panel (2, 1) of Figure 16.1.3. The left panel shows $F_1(\mathbf{D}_{1,01})$, corresponding to panel (0, 1) of Figure 16.1.3.

the Fuller trajectory $z(t)$ with initial conditions (r, q) approaches the outward spiral. The outward spiral moves away from the singular locus (because of the scaling factor $r_{\text{scale}} > 1$), and the Fuller trajectory must then also move away from the singular locus. In particular, (r, q) is not the initial condition of a forward trajectory that converges to the singular locus. \square

16.3 Mahler's First: Bang-bang with Finitely Many Switches

In this section, we return to the Reinhardt dynamical system, and F now denotes the Reinhardt-Poincaré map.

We prove Mahler's First conjecture from 1947. Theorem 16.3.1 is our main result.

Theorem 16.3.1 (Mahler's First conjecture). *The global minimizer of the Reinhardt optimal control problem is a bang-bang solution with finitely many switches. In particular, the minimizer K_{\min} of the Reinhardt problem is a*

finite-sided smoothed polygon with rounded hyperbolic arcs at each corner of the sort described by Reinhardt and Mahler.

By *the sort described by Reinhardt and Mahler*, we mean more precisely that the minimizer K_{min} has no corners and the boundary alternates between straight edge segments and hyperbolic arcs, whose asymptotes are lines extending the straight edge segments of the boundary, as in Figure 1.1.1.

Proof. A bang-bang trajectory with finitely many switches is a polygon with rounded corners of the sort described by Reinhardt, so the second statement of the theorem follows from the first.

By Proposition 8.1.3, any globally minimizing trajectory that avoids the singular locus is an extremal for the Reinhardt control problem and is also edge-extremal. By Theorem 8.3.2, such a trajectory is a bang-bang trajectory with finitely many switches. A trajectory cannot remain on the singular locus for any positive interval of time by Theorem 8.2.7. A trajectory cannot reach the singular locus with finitely many switches by Lemma 8.3.4.

The proof then reduces to the consideration of a trajectory such that the infinite sequence of switching points has a subsequence tending to the singular locus. Passing to the blow-up, which has a compact exceptional divisor, the sequence of switching points has a subsequence tending to a limit on the exceptional divisor in finite time. By Theorem 16.4.1, which appears below, the limit is q_{in} and the sequence approaches q_{in} along the stable curve $W^s(q_{in})$. By Theorem 14.4.1 and its time reversal, the stable curve $W^s(q_{in})$ did not come from the exceptional divisor at an earlier time. Thus, the trajectory is not periodic. This is contrary to the boundary conditions of the Reinhardt conjecture. \square

16.4 Cluster Point Theorem

The proof of Mahler's First relies on the following theorem.

Theorem 16.4.1. *If the sequence of switching points of a Pontryagin extremal Reinhardt trajectory has a cluster point on the exceptional divisor of the blow-up, reached in finite time, and if the switching points themselves are not on the exceptional divisor, then that cluster point is the fixed point q_{in} and the switching points lie on the stable curve $W^s(q_{in})$.*

The proof of Theorem 16.4.1 will be presented after some preparations.

16.4.1 Coordinates

We return to the hyperboloid coordinate system $(w, b, c) \in \mathbb{C}^3$ for the Reinhardt dynamical system. We use parameters

$$\rho = 2, \quad d_1 = 3/2, \quad \lambda_{cost} = -1, \quad \epsilon = 1,$$

We recall that we have rescaled variables

$$(z_1, z_2, z_3) = (w/\rho, -ib/(2\rho), c/6\rho), \quad (w, b, c) = (\rho z_1, 2\rho iz_2, 6\rho z_3), \quad \rho = 2,$$

that were introduced in Equation (11.2.4). We assume that $(z_1, z_2, z_3) \neq \mathbf{0}$. Formulas involving hyperboloid variables from previous chapters can be rewritten in terms of z . We do so without further comment.

Returning to earlier notation, we let r be the radial variable in the angular decomposition of $\mathbb{C}^3 \setminus \{\mathbf{0}\}$. As usual, we call r and ξ the radial and angular components of z . We have coordinates

$$z_k = r^k \xi_k, \quad \xi = (\xi_1, \xi_2, \xi_3) \in \mathbb{C}^3, \quad \phi(\xi) = 1, \quad r > 0.$$

The set

$$\{\xi \in \mathbb{C}^3 \mid \phi(\xi) = 1\}$$

is a compact manifold. This is the *angular component* in this context. For now, we do not impose the vanishing of the Hamiltonian. That will be reimposed later.

16.4.2 Reinhardt Switching functions as cubic polynomials

In Section 14.2, the asymptotic formulas in r_0 for the Reinhardt switching functions are functions of rescaled time s . These switching functions (and their derivatives with respect to s) are approximated as $r_0 \rightarrow 0$ by the Fuller switching functions, as functions of s . The Fuller switching functions are cubic polynomials, whose leading coefficients are nonzero constants. For r_0 sufficiently small, the third derivative of the Reinhardt switching functions are also nonzero. This implies that the Reinhardt switching functions behave qualitatively as cubic polynomials: the third derivative has fixed sign, the second derivative is monotonic with at most one zero, the first derivative is convex with at most two zeros, and the function itself has at most one

inflection point, has at most two local minima, and has at most three zeros. In summary, the Reinhardt switching function behaves qualitatively like a monic cubic polynomial.

We can make this polynomial behavior precise using Weierstrass preparation. Let $z(s)$ be the solution to the Reinhardt system in hyperboloid coordinates with initial condition (r, ξ^0) , rescaled time $t = sr$, and first control $u = \zeta^k$. We view the Reinhardt switching functions $\chi_{ij}^k(s)/r^3$ from ζ^i to ζ^j as analytic functions of the variables $s, r, \Re(\xi_k^0), \Im(\xi_k^0)$. By the earlier asymptotic formulas (adapted to this system of variables), the switching functions extend analytically to a neighborhood of $r = 0$. When $r = 0$, the Reinhardt switching function agrees with the Fuller switching function and is a cubic polynomial in s .

For a given initial condition ξ^0 on the angular component, the restriction of the switching function $\chi(s, r, \xi^0) = \chi_{ij}^k(s, r, \xi^0)$ to $r = 0$ is a cubic polynomial with roots s_1, s_2, \dots having algebraic multiplicities m_i , where $\sum_i m_i = 3$. Applying the Weierstrass preparation theorem centered at the point $(s, r, \xi) = (s_i, 0, \xi^0)$, we obtain a (monic) Weierstrass polynomial of degree m_i .

$$\chi_{W,i}(s, r, \xi) = \sum_{m=0}^{m_i} (s - s_i)^m b_m(r, \xi),$$

where $b_{m_i} = 1$. For $m < m_i$, the coefficients b_m are analytic functions of (r, ξ) near $(0, \xi^0)$ such that $b_m(0, \xi^0) = 0$. If $m_i = 1$, then $s_i - b_0(r, \xi)$ is simply the implicitly defined root of χ near $(s_i, 0, \xi^0)$. Set $\chi_W(s, r, \xi) = \prod_i \chi_{W,i}(s, r, \xi)$, which is defined for all s and for all (r, ξ) in some open neighborhood of $(0, \xi^0)$. Since χ is a *real* analytic function, the nonreal roots s_i come in complex conjugate pairs, and the corresponding Weierstrass polynomials come in pairs. By the uniqueness of the Weierstrass polynomials, $\chi_W(s, r, \xi)$ takes real values on real inputs. By Weierstrass division, and the continuous dependence of roots on their coefficients, the polynomial χ_W captures all real roots of χ for all (r, ξ) in some neighborhood of $(0, \xi^0)$. Thus χ_W can be used as the switching function.

Now we drop the subscript W , and take the switching function χ to be a cubic polynomial in s , whose coefficients are analytic in (r, ξ) . A monic polynomial switching function $\chi(s) = s^3 + b_2 s^2 + b_1 s + b_0$, determines complex analytic varieties for each $\ell \leq 3$ by the equations $b_i(r, \xi) = 0$ for $i < \ell$. We have truncations

$$\chi_\ell(s) = \sum_{m=\ell}^3 b_m s^{m-\ell}.$$

On this complex analytic variety, we have $\chi_\ell(s) = \chi(s)/s^\ell$.

We have defined cells \mathbf{C}_k for the Fuller system by conditions on the first control, multiplicities m_A, m_B of the zero at $s = 0$ of the switching functions χ_A, χ_B . We have defined a further geometric partition according to inequalities on the discriminants $\Delta_{A,m_A}, \Delta_{B,m_B}$, and the resultant $\text{res}(\Delta_{A,m_A}, \Delta_{B,m_B})$, and according to the active switching function. All of these defining conditions can be carried over to the Reinhardt dynamical system in terms of the switching functions of the Reinhardt system. We use the superscript R to designate an extension from the exceptional divisor to a neighborhood, according to Reinhardt dynamics. In this way, we extend the definitions of cells \mathbf{C}_k to a neighborhood \mathbf{C}_k^R of the exceptional division using the Reinhardt system dynamics. Upon restriction to $r = 0$, the cells agree with the cells defined for the Fuller system. There is a shift in dimension of each cell by one, because the Fuller system exceptional divisor has codimension one (if we restrict to the vanishing set of the Hamiltonian in both cases).

The rule for the first control for the Fuller system extends to give first control u on the two big cells $\mathbf{C}_3^R(u)$. We obtain a geometric partition of the two big cells into five regular closed sets $\mathbf{D}_i^R, i = 0, 1, 2, 3, 4$ and a continuous extension F_i of the Reinhardt-Poincaré map F from the interior of \mathbf{D}_i^R to all of \mathbf{D}_i^R . The restriction of each \mathbf{D}_i^R to the exceptional divisor $r = 0$ is the previously defined Fuller-system part \mathbf{D}_i .

Similarly, where we have refined the partition into smaller parts (such as $\mathbf{D}_{1,ij}$), we choose a corresponding refinement of the parts, such as \mathbf{D}_1^R into $\mathbf{D}_{1,ij}^R$. The precise definitions of these subparts will not matter as long as they agree with previously established subparts $\mathbf{D}_{1,ij}$ on the exceptional divisor $r = 0$.

16.4.3 Proof

Proof. We now turn to the proof of Theorem 16.4.1. Consider a sequence of switching points of a Pontryagin extremal trajectory that has a cluster point on the exceptional divisor. Assume that the switching points themselves are not on the exceptional divisor.

Note that a periodic set of switching points does not approach the exceptional divisor. Hence the sequence of switching points is injective, and the set of switching points is countably infinite.

We consider the various possibilities for the cluster points on the exceptional divisor. If q_{in} is a cluster point, then by the definition of the stable

manifold, the switching points lie on the stable manifold $W^s(q_{in})$. This case appears as a possibility in the statement of the theorem. In this case, q_{in} is the only cluster point of the trajectory. (If the sequence of switching points has q_{in} as a cluster point, then the finite time hypothesis implies that the limit of the sequence exists and equals q_{in} , because of the time required to travel from outside an ϵ -ball with center q_{in} to a point inside an ϵ/r_{scale} -ball with center q_{in} ; once entering an ϵ/r_{scale} -ball, a finite time sequence must eventually remain inside the ϵ -ball. Here time is measured with respect to the unscaled time parameter t .)

We now assume that q_{in} is not a cluster point of the trajectory. We assume for a contradiction that the trajectory has a cluster point other than q_{in} .

We claim that q_{out} is not a cluster point. Otherwise, for a contradiction, we find that the switching points lie on the stable manifold $W^s(q_{out})$. (Again, the finite time hypothesis is used to convert a cluster point to a limit.) However, this stable manifold is a subset of the exceptional divisor, which is contrary to the assumption that the switching points are not on the exceptional divisor.

Consider the set of cluster points on the exceptional divisor, viewed as a union of the two big cells $\mathbf{C}_3(u)$. If a cluster point q lies in two or more parts \mathbf{D}_i (where boundaries meet), then we can assign q to \mathbf{D}_i , if a convergent subsequence (q_{n_k}) of (q_n) has limit q , with $q_{n_k} \in \mathbf{D}_i^R$. Each cluster point q can be assigned to at least one part \mathbf{D}_i in this way.

We claim that with respect to the order on parts imposed by the upper triangular structure of containment relations in Table 16.1, if q is a cluster point in \mathbf{D} , then there is also a cluster point in some $\tilde{\mathbf{D}}$, which is smaller with respect this order. (Here $\mathbf{D}, \tilde{\mathbf{D}}$ are the parts \mathbf{D}_i or subparts $\mathbf{D}_{1,ij}$, etc. of the geometric partitions that appear in the proof of Theorem 16.1.1.) In fact, if $q_{n_k} \rightarrow q$, with $q_{n_k} \in \mathbf{D}_i^R$, then $F_i(q_{n_k})$ lies in a finite union of lesser parts $\tilde{\mathbf{D}}^R$ (extending $\tilde{\mathbf{D}}$ to $\tilde{\mathbf{D}}^R$). Passing again to a subsequence, we may assume that $F_i(q_{n_k}) \in \tilde{\mathbf{D}}^R$ converges to a limit in some lesser $\tilde{\mathbf{D}}$. Repeating the argument of Theorem 16.1.1, eventually we obtain a cluster point $q \in \mathbf{D}_{out}^R$.

However, a cluster point in the local stable manifold \mathbf{D}_{out}^R contradicts the local structure of the stable and unstable manifolds at q_{out} . (The dynamics are analytic on \mathbf{D}_{out}^R , and the set of cluster points being closed, we would find that q_{out} itself would be a cluster point, which has already been ruled out.) Thus, the cluster point q cannot exist. \square

Part VI

Appendices

Appendix A

Background Material

A.1 Gronwall inequality

We give two versions of Gronwall's inequality.

Lemma A.1.1 (Gronwall inequality). *Let $I \subset \mathbb{R}$ be an interval, $t_0 \in I$, and let ψ_1, ψ_2, x be continuous nonnegative functions on I . If*

$$x(t) \leq \psi_1(t) + \left| \int_{t_0}^t \psi_2(s)x(s)ds \right|, \quad \text{for all } t \in I,$$

then for all $t \in I$,

$$x(t) \leq \psi_1(t) + \left| \int_{t_0}^t \psi_1(s)\psi_2(s) \exp \left| \int_s^t \psi_2(\tau)d\tau \right| ds \right|.$$

Proof. See [2, p.90]. □

Here is the second version.

Lemma A.1.2. *Let $x : [t_0, t_1] \rightarrow \mathbb{R}^n$ be absolutely continuous and satisfy*

$$\|x'(t)\| \leq \psi_2(t)\|x(t)\| + \psi_1(t), \quad t \in [t_0, t_1] \text{ a.e.},$$

where $\psi_1, \psi_2 \in L^1(t_0, t_1)$, with ψ_2 nonnegative. Then, for all $t \in [t_0, t_1]$, we have

$$\|x(t) - x(t_0)\| \leq \int_{t_0}^t \exp \left(\int_s^t \psi_2(\tau)d\tau \right) (\psi_2(s)\|x(t_0)\| + \psi_1(s))ds$$

Proof. [5, Th.6.41]. □

Corollary A.1.3. *Let $x : [0, t_1] \rightarrow \mathbb{R}$ be a nonnegative continuous function, let n be positive integer, and let C, C_1 nonnegative real numbers. Assume*

$$x(t) \leq Ct^n + C_1 \int_0^t x(t)dt, \quad \text{for all } t \in [0, t_1].$$

Then $x(t) = O(t^n)$ for t nonnegative and sufficiently close to $t = 0$.

A.2 Functional derivative

Definition A.2.1 (functional derivative). *Consider a real finite-dimensional vector space V , and its linear dual V^* . Let $F : V \rightarrow \mathbb{R}$ be smooth. We define the functional derivative $\delta F / \delta \mathbf{v} \in V^*$ in terms of the directional derivative F' of F at $\mathbf{v} \in V$ by*

$$F'(\mathbf{v}; \mathbf{w}) := \lim_{t \rightarrow 0} \frac{1}{t} (F(\mathbf{v} + t\mathbf{w}) - F(\mathbf{v})) =: \left\langle \mathbf{w}, \frac{\delta F}{\delta \mathbf{v}} \right\rangle_* \quad (\text{A.2.1})$$

for all directions $\mathbf{w} \in V$, where $\langle \cdot, \cdot \rangle_$ is the natural pairing between a vector space and its dual.*

A.3 Stable and Unstable Manifolds

We review basic facts about stable and unstable manifolds at a hyperbolic fixed point [18, Chapter 6]. Let M be a manifold and let $f : M \rightarrow M$ be a diffeomorphism with fixed point $p = f(p)$. The *global stable set* at p is the set of all $q \in M$ such that $\lim_{n \rightarrow \infty} f^n(q) = p$. If $U \subseteq M$ is open, the *local stable set* at p is the set of all $q \in U$ such that $\lim_{n \rightarrow \infty} f^n(q) = p$.

A fixed point p is *hyperbolic* if the tangent map $T_p f : T_p M \rightarrow T_p M$ has no eigenvalues of absolute value 1. At a hyperbolic fixed point, the tangent space $T_p M$ is a direct sum of two summands, according to the factorization of the characteristic polynomial of $T_p f$ into two factors: the *stable* factor with eigenvalues $|\lambda| < 1$ and the *unstable* factor with eigenvalues $|\lambda| > 1$.

Theorem A.3.1 (Irwin [18]). *Let p be a hyperbolic fixed point of a C^r diffeomorphism ($r \geq 1$) of M . Then, for some open neighborhood U of p ,*

the local stable set $W^s(p)$ of $f|_U$ at p is a C^r embedded submanifold of M , tangent at p to the stable summand of $T_p f$. The global stable set at p is a C^r immersed submanifold of M , tangent at p to the stable summand of $T_p f$.

There are corresponding statements for local and global unstable manifolds $W^u(p)$. Unstable for f means stable for f^{-1} .

A.4 Classical Lie Groups and Lie Algebras

Let $\mathrm{GL}_n(\mathbb{C})$ be the general linear group, consisting of all invertible linear transformations $\mathbb{C}^n \rightarrow \mathbb{C}^n$. Let $\mathrm{SL}_n(\mathbb{C})$ be the special linear subgroup, consisting of all linear transformations of determinant 1. Let $\mathrm{GL}_n(\mathbb{R})$ and $\mathrm{SL}_n(\mathbb{R})$ be the general linear and special linear groups of linear transformations $\mathbb{R}^n \rightarrow \mathbb{R}^n$. All of the groups $\mathrm{GL}_n(\mathbb{C})$, $\mathrm{SL}_n(\mathbb{C})$, $\mathrm{GL}_n(\mathbb{R})$, and $\mathrm{SL}_n(\mathbb{R})$ are Lie groups.

The Lie algebras of these groups are $\mathfrak{gl}_n(\mathbb{C})$ ($n \times n$ matrices with complex entries), $\mathfrak{sl}_n(\mathbb{C})$ (complex entries and trace zero), $\mathfrak{gl}_n(\mathbb{R})$ (real entries), and $\mathfrak{sl}_n(\mathbb{R})$ (real entries and trace zero).

The unitary group $U(1, 1)$ of signature $(1, 1)$ is

$$U(1, 1) = \{g \in \mathrm{GL}_2(\mathbb{C}) \mid \bar{g}^{tr} J_{\mathfrak{su}} g = J_{\mathfrak{su}}\},$$

where $J_{\mathfrak{su}} = \mathrm{diag}(-i, i)$. The special unitary group $\mathrm{SU}(1, 1)$ is the determinant 1 subgroup of $U(1, 1)$. The Lie algebra $\mathfrak{su}(1, 1)$ of $\mathrm{SU}(1, 1)$ is given by

$$\{X \in \mathfrak{sl}_2(\mathbb{C}) \mid \bar{X}^{tr} J_{\mathfrak{su}} + J_{\mathfrak{su}} X = 0\} = \left\{ \begin{pmatrix} it & z \\ \bar{z} & -it \end{pmatrix} \mid t \in \mathbb{R}, z \in \mathbb{C} \right\}.$$

The special orthogonal group $\mathrm{SO}(m, n)$ is the subgroup of $\mathrm{SL}_{m+n}(\mathbb{R})$ preserving a symmetric matrix A of signature (m, n) :

$$\mathrm{SO}(m, n) = \{g \in \mathrm{SL}_{m+n}(\mathbb{R}) \mid g^{tr} A g = A\},$$

where $-^{tr}$ is the transpose. Different choices of matrices A of the same (m, n) or reversed (n, m) signature give isomorphic Lie groups. The Lie algebra is

$$\mathfrak{so}(m, n) = \{X \in \mathfrak{sl}_{m+n}(\mathbb{R}) \mid X^{tr} A + A X = 0\}.$$

For a general Lie group G , the Lie algebra \mathfrak{g} can be defined as the tangent space $T_e G$ at the neutral element $e \in G$. The group G acts as inner

automorphisms (conjugation) on itself. Passing to the tangent spaces, the differential of inner automorphism affords a representation $\text{Ad} : G \rightarrow \text{GL}(\mathfrak{g})$ on the Lie algebra \mathfrak{g} , called the adjoint representation. Again by taking derivatives, this in turn affords a representation of the Lie algebra $\text{ad} : \mathfrak{g} \rightarrow \mathfrak{gl}(\mathfrak{g})$, called the adjoint representation of the Lie algebra.

Let \mathfrak{g}^* be the linear dual of the Lie algebra \mathfrak{g} . The coadjoint representation $\text{Ad}^* : G \rightarrow \text{GL}(\mathfrak{g}^*)$ of G is defined by

$$\langle \text{Ad}_g^* Y, X \rangle_* = \langle Y, \text{Ad}_{g^{-1}} X \rangle_*,$$

for all $Y \in \mathfrak{g}^*$ and $X \in \mathfrak{g}$. The coadjoint representation $\text{ad}^* : \mathfrak{g} \rightarrow \mathfrak{gl}(\mathfrak{g}^*)$ of the Lie algebra \mathfrak{g} is defined by

$$\langle \text{ad}_Z^* Y, X \rangle_* = \langle Y, -\text{ad}_Z X \rangle_*,$$

for all $Y \in \mathfrak{g}^*$ and $X \in \mathfrak{g}$.

The *Cayley transform* of a 2×2 matrix X is defined as

$$\text{Cayley}(X) := A^{-1} X A, \quad \text{where } A = \frac{1}{\sqrt{2}} \begin{pmatrix} 1 & i \\ i & 1 \end{pmatrix} \in \text{SL}_2(\mathbb{C}).$$

A.5 Exceptional Isomorphisms in Rank One

Lemma A.5.1. • *There is an isomorphism of Lie groups:*

$$\text{SL}_2(\mathbb{R}) \cong \text{SU}(1, 1) \tag{A.5.1}$$

• *There are isomorphisms of Lie algebras:*

$$\mathfrak{sl}_2(\mathbb{R}) \cong \mathfrak{su}(1, 1) \cong \mathfrak{so}(2, 1) \tag{A.5.2}$$

Proof. The isomorphism between the special linear and special unitary group is provided by the Cayley transform. We have

$$\text{Cayley}(\text{SL}_2(\mathbb{R})) = A^{-1} \text{SL}_2(\mathbb{R}) A = \text{SU}(1, 1) \tag{A.5.3}$$

$$\text{Cayley}(\mathfrak{sl}_2(\mathbb{R})) = A^{-1} \mathfrak{sl}_2(\mathbb{R}) A = \mathfrak{su}(1, 1). \tag{A.5.4}$$

To establish the isomorphism with the special orthogonal Lie algebra consider the adjoint representation of $\mathfrak{g} = \mathfrak{sl}_2(\mathbb{R})$.

$$\text{ad} : \mathfrak{sl}_2(\mathbb{R}) \rightarrow \mathfrak{gl}(\mathfrak{g}).$$

We set $\langle X, Y \rangle = \text{trace}(XY)$, for $X, Y \in \mathfrak{sl}_2(\mathbb{R})$. This is a quadratic form of signature $(2, 1)$ on $\mathfrak{sl}_2(\mathbb{R})$. The linear transformation ad_X preserves the quadratic form in the sense that

$$\langle \text{ad}_X Y, Z \rangle + \langle Y, \text{ad}_X Z \rangle = 0.$$

This implies that the image of the adjoint representation is contained in a special orthogonal Lie subalgebra of $\mathfrak{gl}(\mathfrak{g})$ of signature $(2, 1)$. This is an isomorphism. \square

A.6 Matrix Identities

We collect the following properties of matrices in $\mathfrak{sl}_2(\mathbb{C})$.

Proposition A.6.1. *For matrices $X, Y \in \mathfrak{sl}_2(\mathbb{C})$ we have*

$$\begin{aligned} \text{ad}_X^2 Y &= [[Y, X], X] = -2 \det(X)Y - 2XYX \\ &= 2\langle X, X \rangle Y - 2\langle X, Y \rangle X. \end{aligned}$$

Proposition A.6.2. *For matrices $X, Y, Z, W \in \mathfrak{sl}_2(\mathbb{C})$, we have*

$$\langle X, Z \rangle \langle Y, W \rangle - \langle Y, Z \rangle \langle X, W \rangle = -\frac{1}{2} \langle [X, Y], [Z, W] \rangle$$

Proof. Compute. \square

Proposition A.6.3. *For matrices $X, Y, Z, W \in \mathfrak{sl}_2(\mathbb{C})$ such that $\langle Y, Z \rangle = 0$, we have*

$$\langle [X, Y], [Z, W] \rangle = -2\langle X, Z \rangle \langle Y, W \rangle$$

Proof. This is immediate from the previous proposition. \square

The matrix exponential is defined by the power series, which converges for all $n \times n$ matrices X :

$$\exp(X) = \sum_{k=0}^{\infty} \frac{X^k}{k!}.$$

Lemma A.6.4. *If $X \in \mathfrak{sl}_2(\mathbb{R})$ and $d = \det(X)$, then $\exp(X) \in \mathrm{SL}_2(\mathbb{R})$, and*

$$\begin{aligned}\exp(tX) &= \cosh(t\sqrt{-d})I_2 + \frac{\sinh(t\sqrt{-d})}{\sqrt{-d}}X, \quad (d < 0) \\ &= \cos(t\sqrt{d})I_2 + \frac{\sin(t\sqrt{d})}{\sqrt{d}}X, \quad (d > 0) \\ &= I_2 + tX, \quad (d = 0).\end{aligned}\tag{A.6.1}$$

Proof. By the Cayley-Hamilton theorem, for $X \in \mathfrak{sl}_2(\mathbb{R})$, the matrix exponential $\exp(tX)$ is a linear combination of I_2 and X . The lemma makes this linear combination explicit. The lemma is a variant of the classical Rodrigues formula, which holds for rotation matrices. The two sides of the identity are equal, both being the unique solution of the initial value problem

$$F'(t) = XF(t), \quad F(0) = I_2.$$

The determinant of $\exp(X)$ is given by the formula

$$\det(\exp(X)) = \exp(\mathrm{trace}(X)) = 1$$

since $\mathrm{trace}(X) = 0$. □

A.7 Symplectic Geometry

For any finite dimensional vector space V with dual V^* , we have a nondegenerate pairing between the exterior power $\Lambda^k(V^*)$ and $\Lambda^k V$ that sends

$$\mathbf{v}_1^* \wedge \mathbf{v}_2^* \cdots \wedge \mathbf{v}_k^* \in \Lambda^k(V^*), \quad \mathbf{w}_1 \wedge \mathbf{w}_2 \cdots \wedge \mathbf{w}_k \in \Lambda^k V$$

to $\det(\langle \mathbf{v}_i^*, \mathbf{w}_j \rangle_*)$. We can regard an element ω of the exterior power $\Lambda^k(V^*)$ as an alternating multilinear map on V^k by using this pairing.

$$\omega(\mathbf{w}_1, \dots, \mathbf{w}_k) = \langle \omega, \mathbf{w}_1 \wedge \mathbf{w}_2 \cdots \wedge \mathbf{w}_k \rangle_*.$$

Recall that the cotangent bundle T^*M of a smooth manifold carries the tautological one-form θ . Each element \mathbf{v} of $T(T^*M)$ defines both an element $\mathbf{v}^* \in T^*M$ (by projection) and an element $\mathbf{v}_* \in TM$ (by the tangent map of $T^*M \rightarrow M$). The tautological one-form is defined by the relation

$\langle \theta, \mathbf{v} \rangle_* = \langle \mathbf{v}^*, \mathbf{v}_* \rangle_*$. The exterior derivative $\omega = d\theta$ defines a canonical two-form on T^*M , giving the cotangent bundle the structure of a symplectic manifold.

Each differentiable function F on a symplectic manifold (M, ω) defines a vector field \vec{F} by

$$\omega_q(\vec{F}, \mathbf{v}_*) = \langle dF, \mathbf{v}_* \rangle_*,$$

for $\mathbf{v}_* \in T_q M$. The Poisson bracket is defined by $\{F, G\} = \omega(\vec{F}, \vec{G})$. Hamilton's equation corresponding to a Hamiltonian \mathcal{H} is the ODE

$$p' = \{p, \mathcal{H}\}.$$

A.8 Lie-Poisson Dynamics on the Lie Algebra

The dual vector space \mathfrak{g}^* can be equipped with a Poisson bracket called the \pm *Lie-Poisson bracket*: if F, G are two smooth functions on \mathfrak{g}^* , then the bracket is given by

$$\{F, G\}(X^*) = \pm \left\langle X^*, \left[\frac{\delta F}{\delta X^*}, \frac{\delta G}{\delta X^*} \right] \right\rangle_* \quad X^* \in \mathfrak{g}^*$$

Here we identify $\mathfrak{g} \cong \mathfrak{g}^{**}$.

Hamilton's equations with respect to this bracket are called *Lie-Poisson equations* and take the following form (Marsden and Ratiu [31, Proposition 10.7.1]).

Proposition A.8.1 (Lie-Poisson equations). *Let G be a Lie group. The equations of motion for a smooth Hamiltonian $\mathcal{H} : \mathfrak{g}^* \rightarrow \mathbb{R}$ with respect to the \pm Lie-Poisson brackets on \mathfrak{g}^* are*

$$\frac{dX^*}{dt} = \mp \text{ad}_{\delta \mathcal{H} / \delta X^*}^* X^* \quad X^* \in \mathfrak{g}^* \quad (\text{A.8.1})$$

Assume further that our Lie algebra \mathfrak{g} is semisimple: it can be equipped with a nondegenerate bilinear form, which we denote by $\langle \cdot, \cdot \rangle$. This bilinear form satisfies the following relation:

$$\langle X, [Y, Z] \rangle = \langle [X, Y], Z \rangle, \quad X, Y, Z \in \mathfrak{g} \quad (\text{A.8.2})$$

Using this bilinear form, we can identify \mathfrak{g}^* with \mathfrak{g} as follows:

$$X^*(Y) = \langle X, Y \rangle \quad X, Y \in \mathfrak{g}, \quad X^* \in \mathfrak{g}^*, \quad (\text{A.8.3})$$

where X^* maps to X , under this isomorphism.

This isomorphism maps the operator ad to ad^* and so equation (A.8.1) becomes

$$\frac{dX}{dt} = \mp \text{ad}_{\delta \mathcal{H}/\delta X} X = \mp \left[\frac{\delta \mathcal{H}}{\delta X}, X \right], \quad X \in \mathfrak{g}.$$

Armed with this background material, in this section we recast the dynamics for X in our system, as given in Lemma 4.5.2, as the Lie-Poisson equation of a control-dependent Hamiltonian on the vector space $\mathfrak{sl}_2(\mathbb{R})^*$. To do this we shall need to exhibit a Hamiltonian function. Recall that we have defined $\langle X, Y \rangle = \text{trace}(XY)$ for matrices $X, Y \in \mathfrak{sl}_2(\mathbb{R})$.

Proposition A.8.2. *If $\mathcal{H}(X) = -\frac{\langle X, X \rangle}{2} \ln \frac{\langle X, X \rangle}{\langle X, Z_0 \rangle}$ then*

$$X' = -\text{ad}_{\delta \mathcal{H}/\delta X} X = -\frac{\langle X, X \rangle}{2\langle X, Z_0 \rangle} [Z_0, X]$$

Proof. The function \mathcal{H} is well-defined since $\langle X, X \rangle = -2$ and on the star-domain, by Lemma 3.3.4, we have that $\langle X, Z_0 \rangle < 0$. Now we have that

$$\begin{aligned} \text{ad}_{\delta \mathcal{H}/\delta X} X &= \left[\frac{\delta \mathcal{H}}{\delta X}, X \right] \\ &= \left[\frac{\delta}{\delta X} \left(-\frac{\langle X, X \rangle}{2} \ln \frac{\langle X, X \rangle}{\langle X, Z_0 \rangle} \right), X \right] \\ &= \left[-X \ln \frac{\langle X, X \rangle}{\langle X, Z_0 \rangle} - \frac{\langle X, X \rangle}{2} \left(\frac{\langle X, Z_0 \rangle 2X \langle X, Z_0 \rangle - \langle X, X \rangle Z_0}{\langle X, X \rangle \langle X, Z_0 \rangle^2} \right), X \right] \\ &= \frac{\langle X, X \rangle}{2\langle X, Z_0 \rangle} [Z_0, X] = -X' \end{aligned}$$

Thus, we see that the dynamics for X is Lie-Poisson with respect to the Hamiltonian $\mathcal{H}(X) = -\frac{\langle X, X \rangle}{2} \ln \frac{\langle X, X \rangle}{\langle X, Z_0 \rangle}$. \square

Remark A.8.3. Note that, with the parameterization of Section 3.4, the Hamiltonian becomes $\mathcal{H}(X) = \ln(-\langle X, Z_0 \rangle)$.

A.9 Poisson Reduction of the Extended State Space

The Poisson manifold $T^*T\mathrm{SL}_2(\mathbb{R})$ can be Poisson-reduced by left-translation symmetries arising from the left-multiplication action of $\mathrm{SL}_2(\mathbb{R})$. This reduction results in a Poisson bracket on the reduced Poisson manifold, which we call the *extended space Poisson bracket*. For preliminaries on Poisson reduction, we refer to Chapter 10 of Marsden and Ratiu [31].

This reduction procedure also reduces a Hamiltonian system on $T^*T\mathrm{SL}_2(\mathbb{R})$ to a system on the quotient

$$T^*T\mathrm{SL}_2(\mathbb{R})/\mathrm{SL}_2(\mathbb{R}) \cong \mathfrak{sl}_2(\mathbb{R})^* \times \mathfrak{sl}_2(\mathbb{R}) \times \mathfrak{sl}_2(\mathbb{R})^* \cong \mathfrak{sl}_2(\mathbb{R}) \times \mathfrak{sl}_2(\mathbb{R}) \times \mathfrak{sl}_2(\mathbb{R}), \quad (\text{A.9.1})$$

by means of the invariant bilinear form on $\mathfrak{sl}_2(\mathbb{R})$. Thus, for example, the Hamiltonian system arising from the Pontryagin Maximum Principle gets reduced this way. We have already seen expressions for integral curves of the reduced Hamiltonian vector field in Section 6.5.

These ODEs for X, Λ_1, Λ_R on the quotient Poisson manifold can be written in Poisson bracket form with respect to the extended space Poisson bracket. We have the following expression for this bracket, which appears in multiple sources. See Jurdjevic [21], Gay-Balmaz et al. [12, pp. 34] and Esen et al. [10, pp. 13].

Theorem A.9.1. *If F and G are left-invariant smooth functions on $T^*(\mathrm{SL}_2(\mathbb{R}))$, then we can identify them with functions on the quotient (A.9.1), which is isomorphic to $\mathfrak{sl}_2(\mathbb{R})^3$. By using coordinates $(X, \Lambda_1, \Lambda_2)$ introduced in Section 6.2, their extended space Poisson bracket on the quotient Poisson manifold is given by*

$$\{F, G\}_{ex} := \left\langle \Lambda_1, \left[\frac{\delta F}{\delta \Lambda_1}, \frac{\delta G}{\delta \Lambda_1} \right] \right\rangle + \left\langle \frac{\delta F}{\delta X}, \frac{\delta G}{\delta \Lambda_2} \right\rangle - \left\langle \frac{\delta F}{\delta \Lambda_2}, \frac{\delta G}{\delta X} \right\rangle$$

which is the sum of the Lie-Poisson bracket on $\mathfrak{sl}_2(\mathbb{R})^$ and the canonical Poisson bracket on $T^*(\mathfrak{sl}_2(\mathbb{R}))$ (where $\mathfrak{sl}_2(\mathbb{R})$ is identified with the dual $\mathfrak{sl}_2(\mathbb{R})^*$ as needed). Here $\delta/\delta X$ denotes the functional derivative with respect to X .*

Using this bracket, we can deduce the following theorem.

Theorem A.9.2. *The Reinhardt system defined in problem 6.7.1 can be written in Poisson bracket form as follows.*

$$\begin{aligned} X' &= \{X, \mathcal{H}\}_{ex}, \\ \Lambda'_1 &= \{\Lambda_1, \mathcal{H}\}_{ex}, \\ \Lambda'_R &= \{\Lambda_R, \mathcal{H}\}_{ex}, \end{aligned}$$

where $\mathcal{H}(\Lambda_1, \Lambda_R, X; Z_u) = \left\langle \Lambda_1 - \frac{3}{2} \lambda_{cost} J, X \right\rangle - \frac{\langle \Lambda_R, Z_u \rangle}{\langle X, Z_u \rangle}$ and $\Lambda_R = [\Lambda_2, X]$ as usual.

In the theorem, the bracket is applied to each matrix entry, and we identify $\mathfrak{sl}_2(\mathbb{R})^* \cong \mathfrak{sl}_2(\mathbb{R})$ via the nondegenerate trace form.

Proof. This is a routine calculation. We show the derivation for X and omit the others. For an arbitrary constant $Y \in \mathfrak{sl}_2(\mathbb{R})$, we have

$$\begin{aligned} \{\langle X, Y \rangle, \mathcal{H}\}_{ex} &= \left\langle \frac{\delta}{\delta X} \langle X, Y \rangle, \frac{\delta \mathcal{H}}{\delta \Lambda_2} \right\rangle \\ &= \left\langle Y, \frac{\delta}{\delta \Lambda_2} \frac{\langle \Lambda_2, [Z_u, X] \rangle}{\langle Z_u, X \rangle} \right\rangle \\ &= \left\langle Y, \frac{[Z_u, X]}{\langle Z_u, X \rangle} \right\rangle \\ &= \langle X', Y \rangle. \end{aligned}$$

which proves the first equation. \square

A.10 Symplectic Structure of Coadjoint Orbits

On a Lie group G with Lie algebra \mathfrak{g} , Kirillov [22] has defined a symplectic structure on the coadjoint orbit $\mathcal{O}_{Z^*} := \{\text{Ad}_{g^{-1}}^* Z^* \mid g \in G\}$ through $Z^* \in \mathfrak{g}^*$ (the linear dual of the Lie algebra \mathfrak{g}). This two-form ω^K on \mathcal{O}_{Z^*} is given by

$$\omega_{Z^*}^K(\text{ad}_X^* W^*, \text{ad}_Y^* W^*) := \langle W^*, [X, Y] \rangle_*, \quad W^* \in \mathcal{O}_{Z^*}, \quad X, Y \in \mathfrak{g}$$

where $\text{ad}_X^* W^*, \text{ad}_Y^* W^* \in T_{W^*} \mathcal{O}_{Z^*}$. We specialize this general construction to our setting with $G = \text{SL}_2(\mathbb{R})$.

Since the Lie algebra $\mathfrak{sl}_2(\mathbb{R})$ carries with it the nondegenerate trace form: $\langle X, Y \rangle = \text{trace}(XY)$, this sets up a linear isomorphism $\mathfrak{sl}_2(\mathbb{R})^* \cong \mathfrak{sl}_2(\mathbb{R})$, which we use to transport the symplectic structure from coadjoint orbits to adjoint orbits.

In this section, we prove that the Kirillov symplectic structures on the adjoint orbit $\mathcal{O}_X \subset \mathfrak{sl}_2(\mathbb{R})$ and the symplectic structure on the Poincaré upper half-plane \mathfrak{h} are (anti)-equivalent. Recall that we have the following map.

$$\begin{aligned} \Phi : \mathfrak{h} &\rightarrow \mathcal{O}_J \\ z = x + iy &\mapsto \begin{pmatrix} x/y & -(x^2 + y^2)/y \\ 1/y & -x/y \end{pmatrix} =: \Phi(z), \end{aligned}$$

from the upper half-plane to adjoint orbit $\mathcal{O}_X = \mathcal{O}_J$ in $\mathfrak{sl}_2(\mathbb{R})$.

Lemma A.10.1. *The map Φ (defined in Lemma 4.2.1) is an anti-symplectomorphism.*

Proof. Let ω be the symplectic form of the upper half-plane.

$$\omega = \frac{dx \wedge dy}{y^2}$$

and let ω^K be the Kirillov two-form on the coadjoint orbit \mathcal{O}_X . We have to show ω^K pulls back to the two-form $-\omega$ on the upper half-plane by $\Phi : \mathfrak{h} \rightarrow \mathcal{O}_X$. So, at a point $z = x + iy \in \mathfrak{h}$ and tangent vectors $\mathbf{v}, \mathbf{w} \in T_z \mathfrak{h}$:

$$\begin{aligned} \Phi^* \omega_z^K(\mathbf{v}, \mathbf{w}) &= \omega_{\Phi(z)}^K(T_z \Phi(\mathbf{v}), T_z \Phi(\mathbf{w})) \\ &= \left\langle \Phi(z), \left[\begin{pmatrix} \frac{v_2}{2y} & \frac{v_1 y - v_2 x}{y} \\ 0 & \frac{v_2}{2y} \end{pmatrix}, \begin{pmatrix} \frac{w_2}{2y} & \frac{w_1 y - w_2 x}{y} \\ 0 & \frac{w_2}{2y} \end{pmatrix} \right] \right\rangle \\ &= -\frac{v_1 w_2 - v_2 w_1}{y^2} = -\omega_z(\mathbf{v}, \mathbf{w}) \end{aligned}$$

This proves that $\Phi^* \omega^K = -\omega$. □

A.11 Riemannian Metric on Coadjoint Orbits

Let $X \in \mathcal{O}_J$. Then X is regular semisimple, and $\mathbb{R}X$ is a rank one Cartan subalgebra of $\mathfrak{sl}_2(\mathbb{R})$, where $\mathbb{R}X$ is the span of X . There is a Cartan decomposition $\mathfrak{sl}_2(\mathbb{R}) = \mathbb{R}X \oplus \mathfrak{p}_X$ decomposition adapted to $\mathfrak{sl}_2(\mathbb{R})$, where

$\mathfrak{p}_X = X^\perp$ is the two-dimensional orthogonal complement of $\mathbb{R}X$ with respect to the trace form on $\mathfrak{sl}_2(\mathbb{R})$.

Explicitly,

$$\mathfrak{p}_X = \{[X, Y] \mid Y \in \mathfrak{sl}_2(\mathbb{R})\}.$$

From Lemma 4.2.3, \mathfrak{p}_X is the tangent space $T_X \mathcal{O}_J$, which is also identified with $T_z \mathfrak{h}$, where $X = \Phi(z)$.

By transport of structure, the trace form on $\mathfrak{sl}_2(\mathbb{R})$ restricts to \mathfrak{p}_X and defines a symmetric bilinear form on $T_z \mathfrak{h}$. By general theory, this quadratic form is positive definite on \mathfrak{p}_X .

Lemma A.11.1. *The symmetric bilinear form on $T_z \mathfrak{h}$ determined by the trace form on \mathfrak{p}_X is twice the usual invariant Riemannian metric on \mathfrak{h} :*

$$2 \frac{dx^2 + dy^2}{y^2}.$$

Proof. Set

$$\tilde{\mathbf{e}}_1 = \begin{pmatrix} 0 & 1 \\ 0 & 0 \end{pmatrix}, \quad \tilde{\mathbf{e}}_2 = \begin{pmatrix} 1/(2y) & -x/y \\ 0 & -1/(2y) \end{pmatrix}.$$

Under the map $T\Phi : T_z \mathfrak{h} \rightarrow T_X \mathcal{O}_J$ of Lemma 4.2.4, the preimage of $\tilde{\mathbf{e}}_1$ and $\tilde{\mathbf{e}}_2$ is the basis $\mathbf{e}_1 = \partial/\partial x$, $\mathbf{e}_2 = \partial/\partial y$ of $\mathbb{R}^2 = T_z \mathfrak{h}$. The isomorphism $\mathfrak{sl}_2(\mathbb{R})/\mathbb{R}X \rightarrow \mathfrak{p}_X = X^\perp$ is $Y \mapsto [Y, X]$. Thus, it is enough to check that

$$\langle [\tilde{\mathbf{e}}_i, \Phi(z)], [\tilde{\mathbf{e}}_j, \Phi(z)] \rangle = \frac{2\delta_{ij}}{y^2},$$

where δ_{ij} is the Kronecker delta. This is easily computed. \square

Appendix B

Extensions of the Theory

B.1 Hypotrochoids

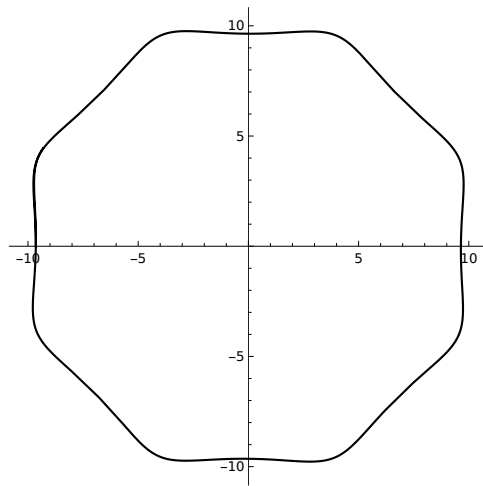


Figure B.1.1: A hypotrochoid resembling the smoothed octagon.

A hypotrochoid is a roulette curve which is traced by a point which is at a distance r_0 from the center of a circle of radius r_1 as it rolls without slipping on the inside of a circle of a fixed circle of radius r_2 . The parametric equation of a hypotrochoid in the complex plane \mathbb{C} is given by

$$z(t) = (r_2 - r_1) \exp(it) + r_0 \exp\left(-\frac{(r_2 - r_1)}{r_1}it\right).$$

This section was motivated by the striking figure in Figure B.1.1, which depicts a hypotrochoid with parameters $r_1 = 2.498$, $(r_2 - r_1)/r_1 = 1/7$, and $r_0 = -10$. As we can see, the Figure 1.1.1 resembles the smoothed octagon.

If ζ is a primitive cube root of unity, and n, j are integers, define

$$\sigma_{2j}(t) := r \exp(it)\zeta^j + r_0 \exp(-it/n)\zeta^{-j}, \quad (\text{B.1.1})$$

which is a closed curve of period $2\pi n$. We recover a hypotrochoid from σ_0 by setting $1/n = (r_2 - r_1)/r_1$ and $r = (r_2 - r_1)$.

The smoothed octagon is given by a bang-bang control and hence is not a real analytic curve. But the following proposition shows that the hypotrochoid is a multi-curve, realized by a curve in $\text{SL}_2(\mathbb{R})$.

Proposition B.1.1. *If $|r_0| \neq |r|$ and if $n \equiv 1 \pmod{3}$, then there exists a curve in $\text{SL}_2(\mathbb{R})$ which realizes the hypotrochoid σ_0 .*

Proof. We will prove the following identities of the curves $\sigma_{2j}(t)$:

$$\begin{aligned} \sigma_0(t) + \sigma_2(t) + \sigma_4(t) &= 0, \\ \Re(i\sigma_0(t), \sigma_2(t)) &= \text{constant}, \\ \sigma_{2j}(t + \frac{2\pi n}{3}) &= \sigma_{2j+2}(t). \end{aligned}$$

The first identity is a result of $1 + \zeta + \zeta^2 = 0$. The second identity follows from

$$\bar{\sigma}_0(t)\sigma_2(t) = r_0^2\zeta^2 + r^2\zeta + 2r_0r \Re(\zeta \exp(it + it/n))$$

The third follows from the definition of σ_{2j} . Identifying \mathbb{C} with \mathbb{R}^2 we get that

$$\Re(i\sigma_0(t), \sigma_2(t)) = \det(\sigma_0(t), \sigma_2(t)) = \text{constant}.$$

This means that there is a constant $s > 0$ such that the rescaled curves $s\sigma_{2j}$ (and their negations $-s\sigma_{2j}$) form a multi-curve as in Definition 2.4.1. We can go through the same construction now as in Section 3.1 to construct a curve $g : [0, t_f] \rightarrow \text{SL}_2(\mathbb{R})$ so that $s\sigma_{2j}(t) = g(t)\mathbf{e}_{2j}^*$. \square

Remark B.1.2. *This hypotrochoid result might allow us a further speculation. We can compute the curvatures $\kappa_j(t)$ of the curves $\sigma_{2j}(t)$ defined in that section and compute their normalization and label them as controls. This then shows that a hypotrochoid determines a control function in the control vector space $\{(u_0, u_1, u_2) \mid u_0 + u_1 + u_2 = 1\}$.*

We might then ask for an optimal control problem which has a particular hypotrochoid as a global optimizer and investigate how it might relate to the smoothed octagon.

B.2 Chaos in Numerical Experiments

This appendix describes some numerical experiments for the Reinhardt control problem with circular control set for various choices of parameters. Here we use the hyperboloid coordinates w, b, c introduced in Section 10.1 with fixed angular momentum \mathcal{A}_0 .

A numerical experiment suggests that for some values of the parameters, the trajectories might be chaotic. See Figure B.2.1. However, for other parameter values, the trajectories appear to be periodic. See Figure B.2.2. The only difference in parameter values for these two figures is $\mathcal{A}_0 = 3$ in the first figure and $\mathcal{A}_0 = 2.5$ in the second. We cannot guarantee the accuracy of these numerical solutions.

Much further numerical exploration of the solutions would be desirable, both for circular control sets and for triangular control sets.

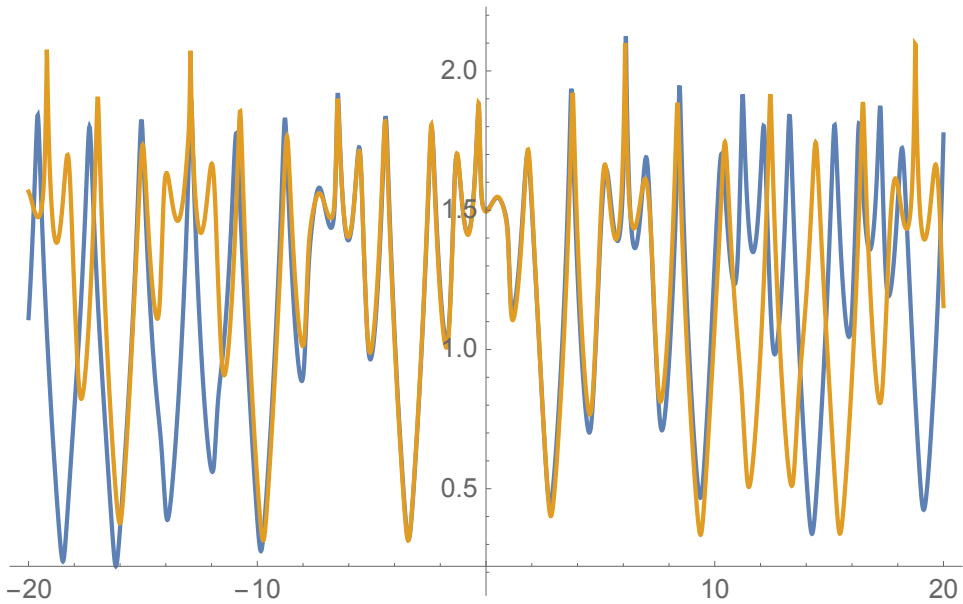


Figure B.2.1: The graph of $|w|$ as a function of time. For nearby initial conditions, the trajectories of $|w|$ drift apart in a way that suggests the onset of chaos. The parameter values are $\rho = 1.1$, $d_1 = 3/2$, $\epsilon = 1$, $\mathcal{A}_0 = 3$, and $\epsilon_b = 1$. The two solutions (in orange and blue) have initial values $(w_0, c_0) = (1.5, 0.5)$ and $(w_0, c_0) = (1.495, 0.5)$, respectively. The figure was produced using NDSolve, Mathematica's numerical ODE solver.

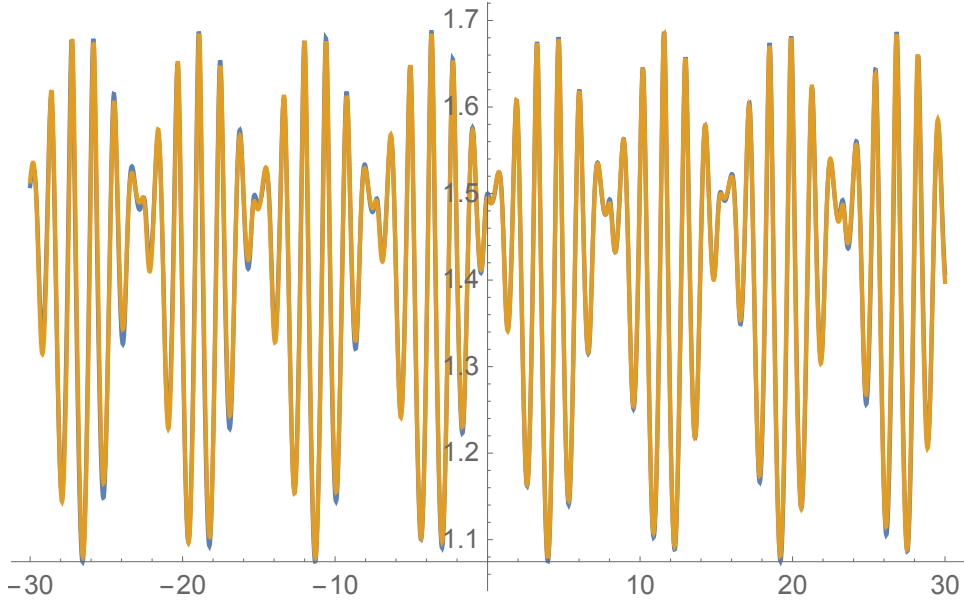


Figure B.2.2: The graph of $|w|$ as a function of time. For other nearby initial conditions, the trajectories of $|w|$ remain close to each other. The trajectories appear to be periodic. The parameter values are $\rho = 1.1$, $d_1 = 3/2$, $\epsilon = 1$, $\mathcal{A}_0 = 2.5$, and $\epsilon_b = 1$. The two solutions (in orange and blue) have initial values $(w_0, c_0) = (1.5, 0.5)$ and $(w_0, c_0) = (1.495, 0.5)$, respectively. The graphic was produced by the numerical solver NDSolve.

B.3 Kuperberg's Area Formula

Greg Kuperberg has given an area formula for centrally symmetric disks satisfying the minimality conditions of Reinhardt [23]. Write $g \in \text{SL}_2(\mathbb{R})$ as

$$g = \begin{pmatrix} 1 & x \\ 0 & 1 \end{pmatrix} \begin{pmatrix} y^{1/2} & 0 \\ 0 & y^{-1/2} \end{pmatrix} \begin{pmatrix} \cos \theta & -\sin \theta \\ \sin \theta & \cos \theta \end{pmatrix}, \quad y > 0.$$

Then $g \cdot i = x + iy$.

Let K be a balanced disk in the Euclidean plane, given by a path $g : [0, t_f] \rightarrow \text{SL}_2(\mathbb{R})$. Let $\tilde{g} : [0, t_f] \rightarrow \mathfrak{h}$ be the image $\tilde{g}(t) = g(t) \cdot i$ of the path in the upper-half plane. Note that with the usual boundary conditions on g , we have $g(t_f) = g(0)R$, and $\tilde{g}(t_f) = \tilde{g}(0)$, so that the curve in the upper-half plane is closed.

Based on the formula (3.2.2), there is a cost one-form, which expressed in

the coordinates (x, y, θ) gives

$$-\frac{3}{2} \text{trace}(Jg^{-1}dg) = 3d\theta - \frac{3dx}{2y}, \quad (\text{B.3.1})$$

where $g^{-1}dg$ is the Cartan-Maurer one-form on $\text{SL}_2(\mathbb{R})$, and J is the infinitesimal generator of the rotation group $\text{SO}_2(\mathbb{R})$. On any disk with hexagonal symmetry, $\theta(t_f) = \pi/3$. Also,

$$d(dx/y) = \frac{dx \wedge dy}{y^2},$$

which is the invariant two-form ω on \mathfrak{h} . Thus, the area is

$$\text{area}(K) = \pi - \frac{3}{2} \int \omega \quad (\text{B.3.2})$$

where the integral is the signed hyperbolic area of the region in the upper-half plane enclosed by the path \tilde{g} . The Reinhardt problem is asking for a maximization of the signed area given by the integral.

Note that the upper-half plane occurs in two contexts now: as the codomain of the path $\tilde{g} : [0, t_f] \rightarrow \mathfrak{h}$ and as the parameter space for the tangent $X = \Phi(z)$, $z \in \mathfrak{h}$. Roughly speaking, the derivative of the first \mathfrak{h} is the second \mathfrak{h} , according to the relation $g' = gX$.

Example. *If K is the circle, then $g(t) = i$ is constant, and the signed area $\int \omega = 0$. The area formula reads $\text{area}(K) = \pi$.*

Example. *We can imagine the proof of the local optimality of the smoothed octagon in Figure B.3.1 by the way that the smoothed octagon is approximately an area maximizing circle. Also shown are the smoothed 10-gon, 20-gon, and 62-gon. In general the smoothed $6k - 2$ -gon will have turning number $-k$ (and negative area), and the smoothed $6k + 2$ will have turning number $+k$ (and positive area).*

B.4 Research Problems

We begin with a few questions related to circular control sets.

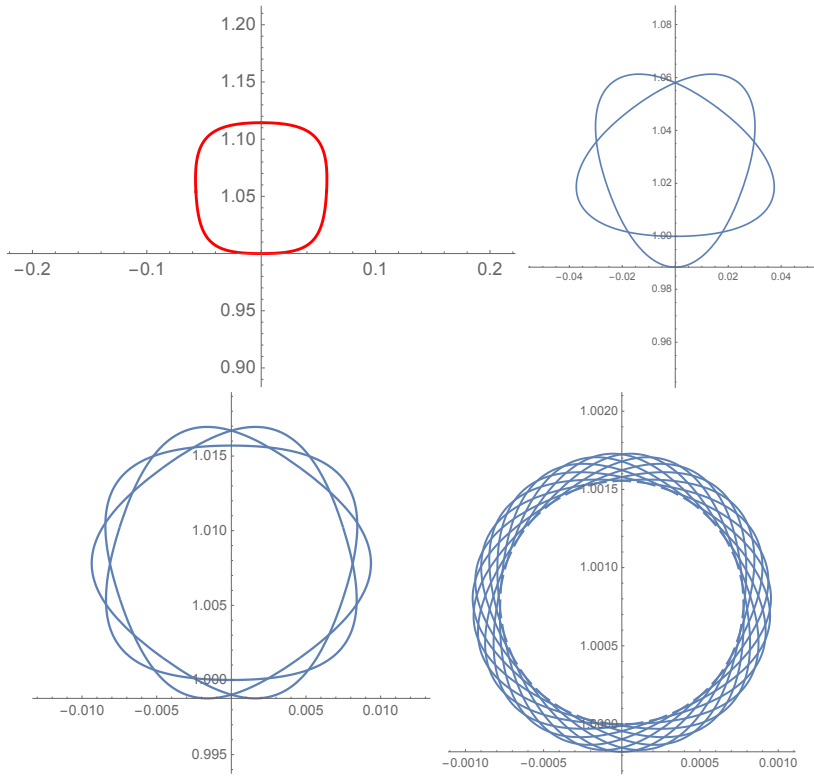


Figure B.3.1: Kuperberg representation of the smoothed octagon, 10-gon, 20-gon, 62-gon

1. In the context of a circular control set, determine numerically, the parameter regions that give chaos.
2. Give a comprehensive description of the global dynamics for circular control, building on the description of global dynamics for the Fuller system.

Here are some research questions related to triangular control U_T .

1. We do not give an upper bound on the number of edges in the smoothed polygon. It seems to us that an extension of the methods presented here might lead to an explicit upper bound on the number of edges. (In fact, we expect that our analysis of the singular locus completes the most difficult stage of the proof of the full Reinhardt conjecture.) To obtain a

bound on the number of edges, it would be useful to extend our analysis from trajectories that meet the singular locus to include trajectories that come within a small neighborhood of the singular locus. It might then be possible to obtain an upper bound on the number of control mode switches for trajectories that avoid a given small neighborhood of the singular locus.

2. We have a family of dynamical systems parameterized by $d = \det(\Lambda_1)$. For each d , the Poincaré section is a four-dimensional space. Short of giving the complete solution to the Reinhardt problem, the Reinhardt problem might be solved for particular d (such as $d = 0$).
3. In the particular case $d = \det(\Lambda_1) = d_1^2 = 9/4$, we might ask whether our analysis of the behavior of the dynamical system around the singular locus (the stable and unstable manifolds at the fixed points) gives the comprehensive picture. That is, do trajectories generally start at the boundary of the star domain, start to move inward toward the fixed point q_{in} , only to veer toward the other fixed point q_{out} , and finally move back out to the boundary of the star domain?
4. We have described the global behavior of trajectories that meet the singular locus, including the global behavior of the Fuller system. To what extent do the methods introduced there (such as the involution $\iota_{\tau F}$, the geometric partition of the domain, and a block triangular structure of the Poincaré map) generalize to the Reinhardt system? Are these ideas sufficient to give a full proof of the Reinhardt conjecture?

Bibliography

- [1] Ralph Abraham and Jerrold E Marsden. *Foundations of Mechanics*. Number 364 in AMS Chelsea. American Mathematical Soc., 2008.
- [2] Herbert Amann. *Ordinary differential equations: an introduction to nonlinear analysis*, volume 13. Walter de gruyter, 2011.
- [3] Olivier Babelon, Denis Bernard, and Michel Talon. *Introduction to Classical Integrable Systems*. Cambridge University Press, 2003.
- [4] Wilhelm Blaschke. Differentialgeometrie. *Berlin*, 1945.
- [5] Francis Clarke. *Functional analysis, calculus of variations and optimal control*, volume 264. Springer, 2013.
- [6] Henry Cohn. The work of Maryna Viazovska, 2022.
- [7] Leonardo Colombo and David De Diego. Higher-order variational problems on Lie groups and optimal control applications. *Journal of Geometric Mechanics*, 6(4), 2014.
- [8] Richard H. Cushman and Larry M. Bates. *Global aspects of Classical Integrable Systems*, volume 94. Springer, 1997.
- [9] V. Ennola. On the Lattice Constant of a Symmetric Convex Domain. *Journal of the London Mathematical Society*, 1(1):135–138, 1961.
- [10] Oğul Esen, Hasan Gümral, and Serkan Sütlü. Tulczyjew’s triplet for Lie groups III: Higher order dynamics and reductions for iterated bundles. *arXiv preprint arXiv:2102.10807*, 2021.
- [11] Anthony T. Fuller. Study of an Optimum Non-linear Control System. *International Journal of Electronics*, 15(1):63–71, 1963.

- [12] François Gay-Balmaz, Darryl D. Holm, David M. Meier, Tudor S. Ratiu, and François-Xavier Vialard. Invariant higher-order variational problems. *Communications in Mathematical Physics*, 309:413–458, 2012.
- [13] Peter M. Gruber. *Convex and Discrete Geometry*, volume 336. Springer, 2007.
- [14] Thomas C Hales. A proof of the Kepler conjecture. *Annals of mathematics*, pages 1065–1185, 2005.
- [15] Thomas C. Hales. On the Reinhardt Conjecture. *Vietnam Journal of Mathematics*, 39(3):287, 2011.
- [16] Thomas C. Hales. The Reinhardt Conjecture as an Optimal Control Problem, 2017.
- [17] Richard F Hartl, Suresh P Sethi, and Raymond G Vickson. A survey of the maximum principles for optimal control problems with state constraints. *SIAM review*, 37(2):181–218, 1995.
- [18] Michael C Irwin. *Smooth Dynamical Systems*. World Scientific, 2001.
- [19] Velimir Jurdjevic. *Geometric Control Theory*. Cambridge Studies in Advanced Mathematics. Cambridge University Press, 1996.
- [20] Velimir Jurdjevic. The Delaunay-Dubins Problem. In *Geometric Control Theory and Sub-Riemannian Geometry*, pages 219–239. Springer, 2014.
- [21] Velimir Jurdjevic. *Optimal control and Geometry: Integrable Systems*, volume 154. Cambridge University Press, 2016.
- [22] Aleksandr Aleksandrovich Kirillov. *Lectures on the Orbit Method*, volume 64. American Mathematical Soc., 2004.
- [23] G Kuperberg. Area formula. private communication, May 2018.
- [24] Ivan A.K. Kupka. The Ubiquity of Fuller’s Phenomenon. In *Nonlinear controllability and optimal control*, pages 313–350. Routledge, 2017.
- [25] Walter Ledermann and Kurt Mahler. On Lattice Points in a Convex Decagon. *Acta Mathematica*, 81(1):319–351, 1949.

- [26] R.M. Lewis. Definitions of Order and Junction Conditions in Singular Optimal Control Problems. *SIAM Journal on Control and Optimization*, 18(1):21–32, 1980.
- [27] Kurt Mahler. Lattice Points in n -dimensional Star Bodies. II. In *Proceedings of the Koninklijke Nederlandse Academie van Wetenschappen*, volume 49, pages 331–343, 1946.
- [28] Kurt Mahler. On the Area and the Densest Packing of Convex Domains. In *Proceedings of the Koninklijke Nederlandse Academie van Wetenschappen*, volume 50, page 108, 1947.
- [29] Kurt Mahler. On the Minimum Determinant and the Circumscribed Hexagons of a Convex Domain. In *Proc. Kon. Ned. Akad. Wet*, volume 50, pages 692–703, 1947.
- [30] Larisa Manita and Mariya Ronzhina. Optimal Spiral-like Solutions near a Singular Extremal in a Two-input Control Problem. *Discrete and Continuous Dynamical Systems-B*, 27(6):3325, 2022.
- [31] Jerrold E. Marsden and Tudor S. Ratiu. *Introduction to Mechanics and Symmetry*, volume 17. Springer Science & Business Media, 2013.
- [32] Hermann Minkowski. Dichteste gitterförmige Lagerung kongruenter Körper. *Nachrichten von der Gesellschaft der Wissenschaften zu Göttingen, Mathematisch-Physikalische Klasse*, 1904:311–355, 1904.
- [33] Hermann Minkowski. *Diophantische Approximationen: Eine Einführung in die Zahlentheorie*, volume 2. Teubner, 1907.
- [34] Hermann Minkowski. *Geometrie der Zahlen*. BG Teubner, 1910.
- [35] James Montaldi. Relative equilibria and conserved quantities. *Peyresq Lectures In Nonlinear Phenomena*, page 239, 2000.
- [36] F.L. Nazarov. Reinhhardt's Problem of Lattice Packings of Convex Domains: Local Extremality of the Reinhardt Octagon. *Journal of Soviet Mathematics*, 43(5):2687–2693, 1988.
- [37] Seyed Kamaleddin Yadavar Nikravesh. *Nonlinear systems stability analysis: Lyapunov-based approach*. CRC Press, 2018.

- [38] János Pach and Pankaj K. Agarwal. *Combinatorial Geometry*, volume 37. John Wiley & Sons, 2011.
- [39] Askold Mikhailovich Perelomov. *Integrable Systems of Classical Mechanics and Lie Algebras*. Birkhäuser, 1990.
- [40] Karl Reinhardt. Über die dichteste gitterförmige Lagerung kongruenter Bereiche in der Ebene und eine besondere Art konvexer Kurven. *Abhandlungen aus dem Mathematischen Seminar der Universität Hamburg*, 10(1):216–230, 1934.
- [41] Mariya Igorevna Ronzhina, Larisa Anatol'evna Manita, and Lev Vyacheslavovich Lokutsievskiy. Neighborhood of the Second-Order Singular Regime in Problems with Control in a Disk. *Proceedings of the Steklov Institute of Mathematics*, 315(1):209–222, 2021.
- [42] Theodore Shifrin. Differential Geometry: a First Course in Curves and Surfaces. *University of Georgia*, 2015.
- [43] Héctor Sussmann. Symmetries and Integrals of Motion in Optimal Control. *Banach Center Publications*, 32:379–393, 11 1996.
- [44] Paul P. Tammela. An Estimate of the Critical Determinant of a Two-Dimensional Convex Symmetric Domain. *Izvestiya Vysshikh Uchebnykh Zavedenii. Matematika*, 103(12):103–107, 1969.
- [45] L Fejes Tóth. Some packing and covering theorems. *Acta Sci. Math. Szeged*, 12(A):62–67, 1950.
- [46] L Fejes Tóth. *Lagerungen in der Ebene auf der Kugel und im Raum*. Springer-Verlag, first edition, 1953.
- [47] L Fejes Tóth, G Fejes Tóth, and Włodzimierz Kuperberg. *Lagerungen: Arrangements in the Plane, on the Sphere, and in Space*. Springer-Verlag, 2023.
- [48] Koundinya Vajjha. *On the Reinhardt Conjecture and Formal Foundations of Optimal Control*. PhD thesis, University of Pittsburgh, 7 2022. <https://arxiv.org/abs/2208.04443>.

- [49] M. I. Zelikin, Andrei A. Agrachev, Yuri Sachkov, and Yuri L. Sachkov. *Control theory from the geometric viewpoint*, volume 2. Springer Science & Business Media, 2004.
- [50] Mikhail Zelikin and Vladimir F. Borisov. *Theory of Chattering Control: with Applications to Astronautics, Robotics, Economics, and Engineering*. Springer Science & Business Media, 2012.
- [51] Mikhail Zelikin, Lev Lokutsievskii, and Roland Hildebrand. Typicality of Chaotic Fractal Behavior of Integral Vortices in Hamiltonian systems with Discontinuous Right Hand Side. *Journal of Mathematical Sciences*, 221(1):1–136, 2017.
- [52] Mikhail Zelikin, N. B. Melnikov, and Roland Hildebrand. The Topological Structure of the Phase Portrait of a Typical Fiber of Optimal Synthesis for Chattering Problems. *Proc. Steklov Inst. Math.*, 233(1):125–152, 2001.

Index

a.e. almost everywhere, 127

abnormal extremal, 21, 93, 125, 161

adjoint orbit, 65

adjoint representation

- Lie algebra, 245

- Lie group, 245

admissible, 37

analytic continuation, 215

angular component, 202

angular momentum, 146, 151

argmax, 111

attainable set, 89

balanced disk, 45, 140

balanced pair, 46

bang-bang, 20

- control, 111

- solution, 111

big cell, 220

Blaschke selection theorem, 33

Blaschke, Wilhelm, 16

blowing up, 202

blowup

- oriented weighted real, 202

body, convex, 27

boundary method, 230

calculus of variations, 16

canonical two-form, 249

Cartan decomposition, 253

Cartan subalgebra, 156

Cartan-Maurer one-form, 135, 258

Cartesian coordinates, 202

Cayley transform, 148, 155, 246

Cayley-Hamilton theorem, 248

cell

- first and second big, 220

centralizer, 68

chattering, 165

chattering arc, 140

circle representation, 46

circle, generalized, 107

coadjoint orbit, 19, 252

coadjoint representation, 246

compactification, 77

conformal equivalence, 69

conformal map, 179

conjecture

- Courant, 16, 29

- Mahler's First, 193

- Reinhardt, 15, 193

conjugacy class, 156

containment function, 229

control

- first, 198
- function, 70
- mode, 114
- most recent, 197
- parameter, 49
- variable, 59
- vector, 198
- convex body, 13
- cost functional, 49
- costate variables, 96
- covolume, 37
- critical lattice, 38
- density
 - greatest lattice packing, 28
 - greatest packing, 27
 - packing, 13, 27
- Descartes's rule of signs, 223
- determinant, minimal, 38
- dihedral group, 72
- directional derivative, 244
- disk
 - circular, 23
 - convex, 13, 27
- disk model of hyperbolic geometry, 72
- divisor
 - exceptional, 193
- edge
 - control problem, 21
- edge extremal, 127
- edge of control simplex, 125
- element
 - neutral, 63
- elliptic element of a Lie group, 116
- elliptic semisimple element of \mathfrak{sl}_2 , 156
- equilibrium point, 182
- equivalent (under virial group), 196
- Euler-Arnold equations, 97
- Euler-Lagrange equation, 16
- Euler-Manchin identity, 173
- exceptional divisor, 215
- exponential
 - matrix, 247
- extremal, 93
- face, 21, 110
- Fejes Tóth, Laszlo, 29
- Filippov's theorem, 89
- final submanifold, 99
- fixed point
 - hyperbolic, 244
- fixed points
 - q_{out}, q_{in} , 193
- Frenet-Serret formula, 19
- Fuller dynamical system, 193
- Fuller system, 165
 - multi-dimensional, 174
 - triangular control, 194
 - ubiquity, 175
- Fuller-Poincaré section, 203, 210
- functional derivative, 97, 98, 150, 244
- general linear group, 245
- generalized eigenspace, 244
- geometric partition, 225
- Green's theorem, 55
- Gronwall inequality, 90, 130, 138, 139
- Hamilton's equation, 249
- Hamiltonian
 - control-dependent, 20, 92

- cost-extended, 92
- Fuller system, 194
- maximized, 20, 92
- hexagon
 - critical, 40
 - inscribed, 38
- hexagon, critical, 31
- horoball, 77, 78
- horocycle, 77, 164
- hyperbolic
 - fixed point, 215
 - geometry, 19
 - metric, 69
- hyperbolic fixed point, 244
- hyperboloid
 - coordinate, 155, 156
 - model of hyperbolic geometry, 72
- hypotrochoid, 41, 255
- ideal triangle, 69
- infinitesimal group of symmetries, 145
- initial submanifold, 99
- inverse function theorem, 123
- involution, 224
- involution with respect to the bracket, 170
- irreducible disk, 38
- isospectral, 61
- isotropy algebra, 68
- Iwasawa decomposition, 65, 258
- Jacobi's formula, 54
- Kepler dynamical system, 171
- Kuperberg, Greg, 258
- Landau big oh, 129, 160, 167
- lattice, 28
 - admissible, 37
 - critical, 38
- Lax equation, 61
- level of ODE subsystem, 94
- lexicographic order, 198
- Lie algebra, 50, 63
- Lie group, 49, 63
- Lie-Poisson
 - bracket, 249
 - dynamics, 249
 - equations, 249
- Lie-Poisson structure, 61
- line, support, 32
- linear fractional transformation, 66
- Lipschitz
 - continuity, 42
- log spiral, 173
- Lyapunov function, 189
- Möbius transformation, 66
- Mahler's First conjecture, 18, 236
- Mahler, Kurt, 16, 193
- manifold
 - stable, unstable, 215
- Mathematica, 117, 131, 162, 163, 189, 206, 211, 216, 230
 - NDsolve, 257
- measurable, 89
- Minkowski sum, 35
- Minkowski, Hermann, 16
- momentum map, 145
- multi-curve, 18, 41
- multi-point, 33, 41
- nilpotent cone, 156
- Noether's theorem, 23, 144
- Noether-Sussmann theorem, 145

- norm
 - Euclidean, 130
 - natural matrix, 130, 138
- normal extremal, 93
- octagon
 - smoothed, 29
- odd function, 182
- orbit-stabilizer theorem, 66
- overloading, 179
- packing, 27
 - lattice, 28
- Pontryagin Maximum Principle, 20, 91
- PMP, Pontryagin Maximum Principle, 20, 91, 146
- Poincaré map, 204
 - first recurrence map, 193
 - Fuller-Poincaré F , 204
 - Reinhardt-Poincaré, 204
- Poincaré section, 122
- Poisson
 - bracket, 151, 170, 249
 - commuting, 151
 - descending bracket, 175
 - extended bracket, 251
 - structure, direct sum, 252
- Poisson bracket, 249
- Pontryagin extremal, 21, 93
- positive orientation, 41
- punctured neighborhood of singular locus, 167
- Rademacher's theorem, 43
- radial component, 202
- reduced costate, 98
- regular
 - nilpotent class, 156
- semisimple element of \mathfrak{sl}_2 , 156
- semisimple element of Lie algebra, 253
- regular closed set, 225
- Reinhardt
 - conjecture, 15
 - optimal control problem, 19
- Reinhardt dynamical system, 193
- Reinhardt problem
 - balanced, 55
- Reinhardt, Karl, 14
- Riemannian metric
 - invariant, 105
 - on \mathfrak{h} , 254
- Rodrigues formula for rotations, 248
- roulette curve, 255
- section of a bundle, 181
- semisimple Lie algebra, 249
- singular extremal, 21
- singular locus, 125, 134, 165, 193, 200
- singular subarc, 92, 93
- smoothed octagon, 17
- smoothed polygon, 113
- special Fuller trajectory, 187
- special linear group, 245
- special orthogonal group, 245
- special unitary group, 245
- sphere packing problem, 13
- split
 - semisimple element of \mathfrak{sl}_2 , 156
 - semisimple element of Lie algebra, 159
- stability at equilibrium point, 183
- stable manifold, 215

stable manifold, 244
star
 condition, 44
 domain, 69, 70
 inequality, 52
state equations, 19, 63
state space, 49
support, 32
symmetric, centrally, 27
symmetrization, 28
symplectic vector field \vec{F} , 249
symplectomorphism, 67
tautological one-form, 249
time reversal, τ , 171, 193
toy control problem, 143
trace, 51, 246
transversality, 99
trivial principal topological bundle,
 180
trivialization of a bundle, 181
unitary group, 245
unpackable, 14, 29
upper-half plane, 19, 66
Viazovska, Maryna, 13
virial
 action, 170
 group, 196
Von Mises iteration, 216
wall, 111, 198
Weierstrass
 polynomial, 238
 preparation, 238
weighted determinant, 152

Index of Notation

- \approx , approximate equality, 15, 29
- \cong , isomorphism, 246
- $<$, lexicographic order, 198, 232
- $(-, -)$, edge between endpoints, 35
- $(-, -)$, ordered pair, 27
- $(-, -) \subset \mathbb{R}$, open interval, 133
- $-'$, derivative, 42
 - directional, 244
- $-\bar{-}$, complex conjugate, 73
- $-\tilde{-}$, transformed quantity, 53, 72, 144
- $-\vec{-}$, vector field of function, 171, 248
- $-^*$, dual
 - isomorphism, 249
 - linear, 62, 145
- $-^*$, pullback of differential form, 55
- $-^*$, special value
 - optimizer, 157
 - spiral solution, 173
- $-^0$ or $-_0$, initial value, 194
- $-^0$, interior, 177, 220
- $-^\circ$, annihilator, 101
- $-^\perp$, orthogonal complement, 101
- $-^*$, star domain, 69
- $-^{**}$, truncated star domain, 77
- $-^{cr}$, crop, 30
- $-^{tr}$, transpose, 55, 245
- $-_F$, Fuller truncation, 169
- $-_X$, centralizer of X , 68
- $-_x$, partial derivative, 86
- $0.902414\dots$, smoothed octagon density, 30
- $[-, -]$, Lie bracket, 60
- $[-, -]$, linear segment between endpoints, 188
- $[-]$, line through $-$, 107
- $\llbracket - \rrbracket = \llbracket - \rrbracket_1$, 155
- $\llbracket - \rrbracket_\epsilon = \sqrt{\epsilon + -^2}$, 155
- $\bar{-}$, complex conjugation, 196
- $\langle -, - \rangle$, bilinear form
 - nondegenerate, 249
- trace form on Lie algebra, 59, 246, 250
- $\langle -, - \rangle_*$, canonical pairing, 92, 244
- \cdot , action
 - linear fractional on \mathfrak{h} , 66
 - of dihedral group on control, 74
 - virial, 170
- \circ , function composition, 78
- ∞ , boundary point of \mathfrak{h} , 107
- ∂ , boundary, 35, 148

∂ , boundary locus, 224
 ∂_A, ∂_B , discriminant locus, 224
 ∂_{res} , resultant locus, 224
 $\| - \|$, norm, 130, 166
 \wedge , wedge product of differential forms, 171, 253
 $\{-, -\}$, Poisson bracket, 249
 $-_F$, Fuller, 170
 $-_{ex}$, extended, 151, 251
 Lie-Poisson, 249
 Δ , triangle, 81

A , matrix or linear map, 54, 129
 3×4 system of ODEs, 158
 $A : \mathfrak{sl}_2(\mathbb{R}) \rightarrow \mathfrak{sl}_2(\mathbb{R})$, 137
 as bounded operator, 168
 Cayley transform matrix, 246
 in dihedral group, 72
 nonsingular, 166
 of eigenvectors, 107
 rotation, 69, 144

\mathcal{A} , angular momentum, 146, 151
 \mathcal{A}_F , truncated, 169
 \mathcal{A}_n , of length n Fuller, 172
 in hyperboloid coordinates, 158

a_i, b_i , real numbers, 229
 $a_j, b_j \in \mathbb{C}$, complex coefficients, 172
 a, b, c, d , matrix entries, 155
 of X , 51
 of linear fractional transformation, 66, 78

Ad , adjoint representation of Lie group, 50, 245
 Ad^* , coadjoint representation of the Lie group, 98, 246
 ad , adjoint representation of the Lie algebra, 67, 245

ad^* , coadjoint representation of the Lie algebra, 97, 246
 area
 area_i , area of a triangle, 83
 Lebesgue measure on \mathbb{R}^2 , 27

B , horoball at a cusp, 78
 B^n , unit ball, 13
 $\mathbf{b} \in \mathbb{R}^2$, vector, 129
 b, c , hyperboloid coordinates, 157
 b_F, c_F , truncated, 169

C, C_0, C_1, C_2 , local real constant, 109, 129–131, 138, 167, 168
 C^k , differentiability class, 41
 $\mathbf{C}_k(u, m_A, m_B)$ cell of dimension k , 220
 Cayley, Cayley transform, 148, 246
 $\cos_i \in \mathbb{R}$, cosine coordinate over Ω , 178
 cosh, hyperbolic cosine, 247
 cost, cost function, 113, 136

D , matrix, 54
 D_r , small disk, 189
 \mathbf{D}_j , parts of a geometric partition, 225
 $\mathbf{D}_{1,ij}$, geometric partition of \mathbf{D}_1 , 229
 Dih_6 , dihedral group of order 12, 72
 \mathbb{D} , disk model of hyperbolic geometry, 69
 diag, diagonal matrix, 156
 d , determinant
 $d = \det(\Lambda_1)$, a constant of motion, 117
 $d \in \mathbb{R}$, 122
 $d_1, \det(\Lambda_1) = d = \epsilon d_1^2$, 156, 207

$d_R = \langle \Lambda_R, \Lambda_R \rangle \in \mathbb{R}$, 163
 $d_{oct} = \det(\Lambda_1)$, for smoothed octagon, 122
 $\det(\mathbf{L})$, determinant of a lattice, 37
 $\det(\Lambda, \alpha, \beta)$, weighted determinant, 152
 $\det(\mathbf{v}_1, \mathbf{v}_2)$, 2×2 determinant, columns \mathbf{v}_i , 33
 \mathbf{e}_i , standard basis
 $\tilde{\mathbf{e}}_i$, image of standard basis., 254
of \mathbb{R}^2 , 254
extreme point of the control set, 90, 111, 112
 $e \in G$, neutral element, 63
 \exp , exponential and matrix exponential, 57, 247
solution to ODE, 145

F , Poincaré map, 203
 F_i extension to \mathbf{D}_i , 229
 F_{ang} , angular component, 203
first recurrence, 203

F , face of a convex set, 110

F, G , smooth functions, 151, 170, 171, 244, 248, 251

$\mathbb{F} = \mathbb{R}$ or \mathbb{C} , archimedean field, 166

f , function
 $f : \mathbb{R}^2 \rightarrow \mathbb{R}$, 117
 f_i , 129

f , term of an ODE, 168

f , vector field, 89, 145
 f_2 , component, 126
on M , 181

f_i , function, 167

G , Lie group, 63, 145, 245
 \mathfrak{g} , Lie algebra, 63, 145, 245

\mathcal{G} , virial group, 170, 196
 g , group element
 (g, X) , state variables, 93
 $g(\mathcal{I}, z, t) \in \text{SL}_2(\mathbb{R})$, trajectory with bang-bang control, 112
 $g(t)$, curve in SL_2 , 49
 g_i , trajectory in $\text{SL}_2(\mathbb{R})$, constant control, 112
 $g_{sw} \in \text{SL}_2$, at switching time, 118
 $g_s(t)$, deformed curve in SL_2 , 135
affine transformation, 29
in $\text{SL}_2(\mathbb{R})$, 65
in $\text{SU}(1, 1)$, 163

GL_n , general linear group, 54, 245
 \mathfrak{gl}_n , Lie algebra, 245

H , Euclidean region
 H, K , convex regions in the plane, 79
 $H^* \subset \mathbb{R}^4$, coordinate chart, 209
convex hull, 84

\mathcal{H} , Hamiltonian, 92
 \mathcal{H}^+ , maximized, 195
 \mathcal{H}_1 , Lie group level term, 95
 \mathcal{H}_2 , Lie algebra level term, 95
 \mathcal{H}_F , Fuller system, 169, 195
 \mathcal{H}_n , length n Fuller system, 172
 \mathcal{H}^+ , maximized, 92
in hyperboloid coordinates, 158
Lie-Poisson, 249, 250

\mathfrak{h} , upper-half plane, 66
 \mathfrak{h}^{**} , star domain
compactification, 77

\mathfrak{h}_i , subset of \mathfrak{h}^* , 83
 \mathfrak{h}^* , star domain, 69
 $h \in G$, element of Lie group, 94
 $h(t) \in \mathrm{SL}_2(\mathbb{R})$, 126
 component of Iwasawa decomposition, 65
 in $\mathrm{SL}_2(\mathbb{R})$, 116
 H_K , critical hexagon, 30, 40
 h_K , inscribed hexagon, 33, 38
 h , hexagon, 38

I , identity map, 123
 I , identity matrix, 54
 $I \subseteq \{1, 2, 3\}$, 111, 131
 I_2 , 2×2 identity matrix, 56
 \mathbf{I}_i , indicator function, 83
 \mathcal{I} , tuple of control data, 112
 $i = \sqrt{-1}$, 33, 173, 194
 i, j , integers, 33

J , infinitesimal generator of rotations, 51
 $J_{\mathfrak{su}} = \mathrm{diag}(-i, i)$, Cayley transform of J , 156, 245

\mathbf{J}^τ , momentum map, 145
 Jac , Jacobian matrix, 183

K , conserved matrix, 161
 $K_{12} \in \mathbb{C}$, matrix entry, 161

K , convex disk, 27
 $K(g, X)$, attached to data (g, X) , 140
 K_{\min} , minimax optimizer, 29, 236
 K_{oct} , smoothed octagon, 119
 K_{sym} , symmetrization, 28
 body, 13
 compact convex set in \mathbb{R}^n , 110

k , integer, 49, 112

\mathfrak{K} , set of convex disks, 13
 $\mathfrak{K}_{\text{bal}}$, balanced, 45
 $\mathfrak{K}_{\text{ccs}}$, centrally symmetric convex, 13, 27

L , affine function, 90, 148
 L , matrix, 54
 L_g , left multiplication by g , 63
 \mathbf{L} , lattice, 28
 l , lattice element, 30
 ℓ_i , support line, 39
 $\ell(y_0) \in \mathbb{R}$, 116
 l_{ij} , matrix coefficients of Λ , 152
 lhs , left-hand side, 162
 \ln , natural log, 250

M , manifold
 M_d , for smoothed octagon, 122
 for Fuller system dynamics, 177
 for Noether-Sussmann, 145
 optimal control on, 99

m , integer dimension, 89, 166
 multiplicity of root, 220

N_d , Poincaré section, 122
 n , length of Fuller system, 166

O , Landau big oh, 129, 167, 210
 O_2 , orthogonal group, 72
 \mathcal{O}_- , adjoint or coadjoint orbit, 65, 252

$\mathbf{0}$, origin, 27, 37, 79

P , normalized control matrix, 96, 137
 P^* , optimal, 150, 152
 P_0 , constant, 106
 $P_{i,j}$, at mixed controls $\mathbf{e}_j, \mathbf{e}_i$, 115

Lax equation, 61
 P_K , parallelogram, 53
 \mathcal{P} packing, 13
 $\mathfrak{p}_X = X^\perp$, component of Cartan decomposition, 253
 $\mathbf{p}_i, \mathbf{q}_i, \mathbf{r}_i$, points in the plane, 79
 p , point in bundle
 $\tilde{p} \in T_g^*G$, cotangent vector, 95
 lifted controlled trajectory, 146
 lifted extremal trajectory, 99
 value of section ψ , 185
 vector in cotangent space, 92

 Q , quadratic polynomial, 159, 160
 \mathcal{Q} , optimal control system, 145
 q , point on manifold, 89, 145
 q_0 , in submanifold, 122
 q_\pm^* , image of the log-spiral, 182
 q_c , arrival point on boundary, 188
 q_i , 122
 $q_{2,2}$, equilibrium point, 187
 q_{in}, q_{out}, q_{fix} , fixed points, 204

 R , rotation by $\pi/3$, 51
 $\Re(-, -)$, sesquilinear form, 155
 $\mathbb{R}X$, span of X , 67
 \mathbb{R}^2_Ω , topological plane, 179
 \mathbf{r} , point in the plane, 79
 r , real number, 27, 82, 117
 $r = \langle [\Lambda_R, X], K \rangle$, 163
 r_i , hypotrochoid parameter, 255
 r_i , scalar, 68
 r_j , subexpression in vector field, 181
 $r_{scale} \approx 6.27$, scaling factor, 204

 homothety, 30
 polar coordinate, 186
 radial component of ODE, 159
 radius, 78, 148
 scalar, 161, 164
 slope of ODE solution, 109, 131
 trace, 116
 rhs , right-hand side, 162
 \mathbb{RP}^1 , real projective line, 73

 $S \in \mathfrak{sl}_2(\mathbb{R})$, reflection matrix, 73
 \mathcal{S}_{sing} , singular locus, 134, 165
 \mathbf{s}_i , multi-point, 33, 79
 \mathbf{s}_j^* , sixth roots of unity, 33
 s , real parameter
 $s(t)$, reparameterization, 126
 $s = t/r$, rescaled time, 211
 $s \in (0, 2)$, local parameter, 185
 $s \in \mathbb{R}$, deformation parameter, 135
 arclength, 43
 dummy integration variable, 106
 speed, 42
 $\sin_i \in \mathbb{R}$, sine coordinate over Ω , 178
 \sinh , hyperbolic sine, 247
 SL_n , special linear group, 19, 49, 245
 \mathfrak{sl}_n , Lie algebra, 50, 245
 SO , special orthogonal group
 \mathfrak{so} , Lie algebra, 245
 O_n , orthogonal group, 72
 SO_n , compact orthogonal, 51
 $\text{SU}(1, 1)$, special unitary group, 163, 245
 $\text{U}(1, 1)$, full unitary group, 245

$\mathfrak{su}(1, 1)$, Lie algebra, 148, 245
 T , triangle, 33, 79, 117
 T^{ext} , exterior triangle, 79
 T_q^*M , cotangent space at q , 63
 T_qM , tangent space at $q \in M$, 67
 $Tf : T_qM \rightarrow T_{f(q)}N$, tangent map of f , 63
 t , real number, 110, 155
 t_0, t_1 , scalars, 35
matrix entry, 245
scalar, 178
 $t \in \mathbb{R}$, time, 41
 \tilde{t}_i , time parameter, 112
 t_0, t_1 , 167
 t_1 , 129
 t_2 , 130
 t_c , arrival time at boundary, 188
 t_{sw} , switching time, 114, 122, 197
 U , control set, 145
 $(U_T)_I$, face, 111
 U_C , circumscribed, 143
 U_I , inscribed, 143
 U_T , triangular, 59
 U_r , intermediate, 143, 148
 \mathbf{u} , arbitrary multi-point, 35
 \mathbf{u} , vector
 $\mathbf{u}_0, \mathbf{u}_1 \in \mathbb{R}^2$, 37
in \mathbb{R}^2 , 33, 55, 56
normal, 185
unit tangent, 42
 u , control
 u_{edge} , on edge, 126
 $u, v \in U$, 110
 $u \in [-1, 1]$, classical Fuller control, 174
 $u \in V_T$, 194
 u^* , optimal, 92
 $u_i \in U$, 145
 u_j , j th component of control, 58
 V , vector space, 244, 248
 $V_T = \{1, \zeta, \zeta^2\}$, vertices of control set, 194
 $V_i \subset M$, open neighborhood of a manifold, 145
 \mathbf{v} , vector
 (v_2, v_3) , vector field, 181
 $\mathbf{v}(z, u)$, control vector, 198
 \mathbf{v}, \mathbf{w} , vectors, 244
 $\mathbf{v}, \mathbf{w} \in T_z \mathfrak{h}$, tangent, 253
 $\mathbf{v}^* \in T^*M$, 248
 $\mathbf{v}_* \in TM$, 248
 \mathbf{v}_\pm , eigenvectors, 107
 $\mathbf{v}_i \in \mathbb{R}^2$, 37
 $v_i, w_i \in \mathbb{R}$, components of \mathbf{v}, \mathbf{w} , 253
components v_i , 129
in $T(T^*M)$, 248
tangent vector, 99
 $W \in \mathfrak{sl}_2(\mathbb{R})$, 101
 $W^*, Z^* \in \mathfrak{g}^*$, 252
 $W^s(q), W^u(q)$, stable and unstable manifolds, 207
 $\mathcal{W}, \mathcal{W}_i$, wall, 198
 \mathbf{w} , vector
in \mathbb{R}^2 , 55
 w path in the hyperbolic disk, 69
 w , hyperboloid coordinate
 $\tilde{w} = \bar{c}w/|c|$, 159
 w, b, c coordinates, 156
 w_F , truncated, 169

in \mathbb{C} , 157

X , Lie algebra element

- $X, Y, Z, W \in \mathfrak{sl}_2$, 60, 105, 152, 155, 247
- $X, Y, Z \in \mathfrak{g}$, 145, 249
- $X = g^{-1}g'$, curve in Lie algebra, 50
- $X \in \mathfrak{sl}_2$, 50
- $X^* \in \mathfrak{g}^*$, 249
- X_0 , initial condition for $X(t)$, 62
- $X(\mathcal{I}, z, t)$, Lie algebra trajectory with bang-bang control, 112
- $\tilde{x}_{21}^*(r) = \sqrt{3} - 1/r$, star domain boundary curve, 209
- x , function of time, 244
- x , real part of z , 65
- x, y , coordinates of the classical Fuller problem, 174
- x_i , coordinates (x_2, x_3) of Ω , 177
- $Y \in \mathfrak{g}$, Lie algebra element, 249
 - in \mathfrak{sl}_2 , 56, 68, 137, 214
- y , imaginary part of z , 65
- $y \in \mathbb{R}$, local variable, 117
- $y_0, 0 + iy_0$, smoothed polygon initial condition, 114, 122
- Z_u , control matrix, 59, 209
 - Z_0 , constant, 250
 - Z_u , constant, 106
 - Z_u^* , optimal, 131
- z , optimal control, 148, 153
 - $\tilde{z} = \bar{c}z/|c|$, 159
 - z^* , 157
- $z \in \mathbb{C}$, 155, 245
- $z \in \mathfrak{h}$

\bar{z} , complex conjugate, 73

\tilde{z}_0 , 107

$z = x + iy$, 66

z_i , Fuller system

- $z = (z_1, z_2, z_3) \in \mathbb{C}^3$, 177, 194
- z_{spec} , special trajectory, 187
- component, 166, 169

α, β , control matrix parameters, 149, 152, 166

Γ^∞ , smooth sections of a vector bundle, 145

γ , planar curve, 55, 189

- γ_s , hyperbolic arc, 43

$\gamma \in \mathbb{C}^\times$, Fuller system multiplier, 166

Δ , discriminant, 160, 220

$\Delta(K)$, minimal determinant, 38

δ , density

- $\delta(K)$, greatest, 13
- $\delta(K, \mathbf{L})$, of lattice packing, 28
- $\delta(K, \mathcal{P})$, packing, 13, 28
- $\delta(z)$ density bound, 85
- $\delta_0(z)$, density bound, 87
- $\delta_L(K)$, greatest lattice, 28
- δ_{\min} , minimax, 29
- δ_{oct} , of smoothed octagon, 85

$\delta/\delta X$, functional derivative, 97, 150, 244

δ_{ij} , Kronecker delta, 254

$\epsilon \in \{-1, 0, 1\}$, sign

- $\epsilon \in \{-1, 0, 1\}$, sign $\det(\Lambda_1)$, 155, 207
- ϵ_A , determinant of A , 72
- $\epsilon_i \in \mathbb{R}$, sign coordinate over Ω , 178

$\zeta = \exp(2\pi i/3)$, cube root of unity, 148, 194, 256

θ , angle, 73, 146, 159, 170, 186, 196
 $\theta_k = \pi k/(3k+1)$, 118
 θ , differential one-form, 55, 248
 $\iota_{\tau F} = \tau \circ F$, involution, 224
 κ , curvature
 $\kappa = \kappa_1 + \kappa_2 + \kappa_3$, 60
 κ_j , state-dependent curvature, 58
planar, 43
 Λ , costate
 $\Lambda \in \mathfrak{sl}_2(\mathbb{C})$, 152
 $\Lambda_R \in \mathfrak{sl}_2$, reduced, 96
 $\Lambda_i \in \mathfrak{sl}_2$, 93
 $\Lambda_{1,cost} = \Lambda_1 - 3\lambda_{cost}J/2$, 133, 137
 $\Lambda_{10} \in \mathfrak{sl}_2(\mathbb{R})$, 116
 λ_1, λ_R , multiplier, 116
 λ_i , on edge, 127
 λ_{cost} , cost multiplier, 92, 207
 $\tilde{\Lambda}_R$, solution specification for
 Λ_R , 106
 $\tilde{\lambda}$, approximation to costate on
edge, 129
 λ , eigenvalue, 54, 106, 118
 $\mu : \mathbb{C}^2 \rightarrow \mathbb{R}$, star denominator, 157
 $\mu^* = \mu(w, z^*)$, 158
 $\nu \in T_z^*\mathfrak{h}$, cotangent variable, 102, 132
 ν_1, ν_2 , components of ν , 102
 Ξ , 202
 $\Xi_{\mathcal{W}}, \Xi_{\mathcal{W},0}$, Poincaré section, 203, 210
 ξ_i , quadratic control equation
coefficients
 $\xi_0 = 2 + |\tilde{w}|^2 - \tilde{w}^2$, 159
 $\xi_0 = 2 + |w|^2 - (w\bar{c}/|c|)^2$, 157
 $\xi_1 = 2\rho(\tilde{w} - \tilde{\bar{w}})\llbracket \tilde{w} \rrbracket$, 159
 ξ , angular component, 202
 Π , affine plane, 148
 Π_i^+ , open half-plane, 78
 π , projection
 π_{rad}, π_{ang} , radial and angular
projections, 202
 $\pi : M \rightarrow \mathbb{R}^2$, function, 177
 $\pi = 3.14\dots$, 16
 $\rho = \beta/\alpha > 0$, control parameter, 149, 156, 207
 ρ_j , star function, 51, 59
 $\rho_j(z) := \rho_j(\Phi(z))$, 81
 $\tilde{\rho}_j$, 52
 σ_i , multi-curve, 41, 256
 τ , dummy variable of integration, 129, 130
 τ , infinitesimal group of
symmetries, 145
 τ , time reversal involution, 171, 196
 $\Phi : \mathfrak{h} \rightarrow \mathfrak{sl}_2(\mathbb{R})$, 65, 66
 ϕ , cost integrand, 89, 145
 $\phi_{edge} = x^2/y$, on edge, 126
 ϕ , weighted norm, 202
 χ_{ij} , switching function, 115, 137, 196
 $\chi_{A,m_A}, \chi_{B,m_B}$, reduced
switching, 220
 $\chi_{\mathcal{W}}$, Weierstrass polynomial of, 238
 Ψ , auxiliary function in ODE
solution of Λ_R , 106
 $\Psi_s(t) = \exp(s(-))$, deformation of
identity matrix, 135
 ψ , local auxiliary function or
integral, 243
 ψ , section of a bundle, 181
 ψ , solution specification for
 Λ_R , 106

$\psi : V_1 \rightarrow V_2$, diffeomorphism of
 open neighborhoods, 145
 $\psi : \mathfrak{h}^* \rightarrow \mathbb{R}$, cutoff function, 90
 ψ_i , compactly supported
 functions, 135
 $\psi = \theta_2 - \theta_1$, phase difference, 219
 $\Omega \subset [0, 2]^2$, 177
 $\Omega_{\epsilon_i, \epsilon_j}$, copies of Ω , 179
 $\Omega_{spec+} \subset \Omega_{-+}$, subregion, 188
 $\Omega_{spec-} \subset \Omega_{+-}$, sign reversal of
 Ω_{spec+} , 189

$\partial\Omega_{\pm, \pm}^+ = \partial_{\pm, \pm}^+$, upper boundary
 curve of $\Omega_{\pm, \pm}$, 179
 $\partial\Omega_{\pm, \pm}^- = \partial_{\pm, \pm}^-$, lower boundary
 curve of $\Omega_{\pm, \pm}$, 179
 ω , two-form
 ω^K , Kirillov, 252, 253
 ω_n , for length n Fuller system,
 172
 on \mathbb{C}^3 , 171
 on \mathfrak{h} , 253, 259
 on symplectic manifold, 248